

**ASSESSING NUTRIENT RETENTION AND REMOVAL MEASUREMENTS  
AMONG RESTORED FLOODPLAIN WETLANDS**

---

A Dissertation

Presented to

the Faculty of the College of Graduate Studies

Tennessee Technological University

by

Robert S. Brown

---

In Partial Fulfillment

of the Requirements of the Degree

Doctor of Philosophy

Environmental Science

---

July 2023

## AN ABSTRACT OF A DISSERTATION

### ASSESSING NUTRIENT RETENTION AND REMOVAL MEASUREMENTS AMONG RESTORED FLOODPLAIN WETLANDS

Robert S. Brown

Doctor of Philosophy in Environmental Science

Floodplain wetland restoration can improve nutrient retention capacity in agricultural landscapes. The United States Department of Agriculture has implemented the Wetlands Reserve Program (WRP) to improve wetland ecosystem services on previously marginal cropland. The goal of my dissertation was to account for variability of nutrient flux measurements derived from flow-through core incubations of restored floodplain wetland soils enrolled in WRP. Methodological constraints of fieldwork explained up to 16% of variation in nutrient flux rates. Use of water column control cores to account for nutrient processing effects not attributable to the soil sample resulted in substantial changes in nutrient uptake. Extrapolation of soil core measurements to represented wetland habitat areas provided a more robust method of accounting for variability in nutrient flux, compared with interpolated predictions at unsampled locations between soil cores. Floodwater was sampled across one easement using automated water samplers. Changes in floodwater nitrogen and phosphorus concentrations across the easement qualified it as a net nutrient sink, and phosphorus retention capacity was higher than nitrogen. Soil core incubations also qualified the easement as a net nutrient sink, but nitrogen retention capacity was higher than phosphorus, likely due to differences in water residence times and relative nutrient concentrations between *in situ* floodwater and incubated soil cores. Flow-through soil core incubations provide valuable insights into nutrient retention capacity of restored wetlands. However, my research shows that variability introduced throughout the process of soil collection, incubation design, and data processing must be considered by researchers and managers employing these techniques.

©Robert S. Brown 2023

# TABLE OF CONTENTS

	Page
CERTIFICATE OF APPROVAL OF DISSERTATION .....	viii
ACKNOWLEDEGMENTS .....	ix
LIST OF FIGURES .....	x
LIST OF TABLES .....	xvi
CHAPTER 1: INTRODUCTION .....	1
CHAPTER 2: EVALUATING FLOW-THROUGH SOIL CORE INCUBATIONS FOR MEASURING NUTRIENT UPTAKE, NITROGEN REMOVAL, AND SOIL OXYGEN DEMAND IN RESTORED FLOODPLAIN WETLANDS .....	6
Abstract .....	6
Introduction .....	7
Methods .....	10
Flow-through incubation design choices .....	10
Soil core collection and transport .....	11
Continuous flow-through incubation: Water sources .....	12
Dissolved nutrient analyses .....	17
Dissolved gas analyses .....	17
Flux calculations .....	20
Control core comparison .....	20
Flow rate measurement comparison .....	21
Data processing and analyses .....	21
Assessing fieldwork constraints .....	21
Control core effects .....	23
Flow rate effects .....	24
Results .....	24
Fieldwork constraints .....	24
Explanatory variables .....	24
Nitrate (NO <sub>3</sub> ) flux .....	25
Phosphate (PO <sub>4</sub> ) flux .....	28

Dinitrogen (N <sub>2</sub> ) flux .....	33
Soil oxygen demand (O <sub>2</sub> flux) .....	37
Flow rate effects.....	39
Control core effects.....	41
Discussion.....	47
Fieldwork constraints.....	47
Julian day .....	47
Core depth.....	50
Hold time .....	53
Soil moisture .....	55
Flow rate effects.....	56
Control core effects.....	56
Conclusions and recommendations.....	58
CHAPTER 3: NUTRIENT STORAGE AND FLUX IN SURFICIAL SOILS OF FLOODPLAIN WETLANDS: SCALING UP FROM SOIL CORES TO WRP MANAGEMENT AREAS.....	61
Abstract.....	61
Introduction.....	62
Methods.....	66
Easement selection.....	66
Soil core collection and transport .....	67
Soil property analyses .....	68
Flow-through soil core incubations .....	69
Dissolved nutrient analyses.....	70
Topographical analyses.....	71
Data processing and analyses.....	71
Extrapolation.....	71
Interpolation.....	73
Results.....	76
Variability of measurements.....	76
Inverse distance weighted (IDW) model comparisons .....	77
Factors influencing IDW model error.....	78
Soil C .....	78

Soil N .....	80
Soil P .....	81
Nitrate flux .....	83
Phosphate flux.....	84
Soil pH .....	86
Soil moisture .....	87
Bulk density .....	88
Extrapolation vs. interpolation.....	90
Influence of tree planting age and elevation.....	93
Influence of elevation in remnant forests.....	95
Comparison of tree plantings and remnant forest.....	97
Discussion.....	99
Interpolation error for local-scale predictions.....	99
Extrapolation of nutrient retention estimates.....	101
Restoration age.....	102
Topography.....	105
Conclusion .....	108
CHAPTER 4: NUTRIENT DELIVERY, RETENTION, AND PROCESSING IN A RECONNECTED FLOODPLAIN FOREST: INSIGHTS FROM FLOODWATER MONITORING AND FLOW-THROUGH SOIL CORE INCUBATIONS .....	110
Abstract.....	110
Introduction.....	111
Methods.....	114
Study site.....	114
Floodwater sampling.....	115
Sample processing .....	117
Particulates.....	117
Total nutrient concentrations .....	118
Soil core collection and processing.....	118
Soil core incubation .....	119
Nutrient analyses.....	120
Dissolved gas analyses.....	121
Flux rate calculations .....	122

Data processing and analyses.....	122
Nutrient concentrations .....	122
Nutrient flux at the soil-water interface .....	124
Results.....	125
Floodwater nutrients and hydrology .....	125
240 m from levee .....	127
490 m from levee .....	127
950 m from levee .....	128
Floodwater N:P stoichiometry .....	131
Longitudinal changes among floods .....	131
Temporal changes during floods.....	133
Dissolved nutrients in the July flood .....	137
Total nutrients and particulates.....	140
Soil N:P stoichiometry .....	141
Nutrient flux at the soil-water interface .....	143
Redundancy analysis.....	145
Discussion .....	148
Floodplain nutrient retention capacity .....	148
N:P stoichiometry .....	149
Spatial patterns in floodwater .....	149
Flood duration.....	150
Soil N:P stoichiometry .....	152
Nutrient fractions in floodwater.....	154
Soil nutrient processing.....	156
Comparing flow-through incubation with flooding in July .....	156
Fates of nitrate and N <sub>2</sub> production .....	158
Greenhouse gas production.....	159
Conclusion .....	161
CHAPTER 5: SUMMARY AND FUTURE WORK.....	163
BIBLIOGRAPHY.....	167

**CERTIFICATE OF APPROVAL OF DISSERTATION**

**ASSESSING NUTRIENT RETENTION AND REMOVAL MEASUREMENTS  
ACROSS RESTORED FLOODPLAIN WETLANDS**

by

Robert S. Brown

Graduate Advisory Committee:

---

Justin Murdock, Chair Date

---

Brad Cook Date

---

Kit Wheeler Date

---

Jeannette Luna Date

---

Tania Datta Date

---

Alfred Kalyanapu Date

Approved for the Faculty:

---

Mark Stephens, Dean Date  
College of Graduate Studies

## ACKNOWLEDGMENTS

I would like to thank Dr. Justin Murdock for offering me an opportunity to work as a graduate student in his lab, for encouraging me to pursue outside research interests amidst a sea of 1000 soil cores and supporting me over the past four and half years. Many thanks to my committee members: Dr. Brad Cook, Dr. Kit Wheeler, Dr. Jeannette Luna, Dr. Tania Datta, and Dr. Alfred Kalyanapu for your support and guidance. Spencer Womble and Shrijana Duwadi, thank you for your friendship and collaboration through it all. I could not have done it without you both. Thanks to Jordan Evans and Ryan Wigner who helped me lift this project off the ground, and thanks to David Hobbs for his constant support and technical expertise. Thanks to all of my fellow graduate students who assisted with field and lab work over the years: Peter Blum, Ryan Hanscom, Trevor Crawford, Andy Rosson, Reed Alexander and Morgan Michael. Thanks to Stephanie Driscoll for keeping us afloat into our final lap. Many thanks to the dozens of undergraduates who helped in this endeavor.

This work would not be possible without funding from the United States Department of Agriculture (USDA) Natural Resources Conservation Service and The Nature Conservancy, support from the Tennessee Tech Center for the Management, Utilization, and Protection of Water Resources, and a grant award from the Tennessee Water Resources Research Center (Award No. 78201920). Data can be requested from the USDA.

Thank you to my family and friends for your love and support, close by and far away.

## LIST OF FIGURES

Figure 1.1. Locations of WRP easements included in this study.....	5
Figure 2.1. Pictures of soil core collection and incubation. Soil core collection from unsubmerged (top left, top middle) and submerged (top right) environments. Synthetic source water for incubations with recirculating pump and air stones (bottom left). Flow-through incubation setup (bottom middle). Soil core filling during incubation (bottom right).....	12
Figure 2.2. Diagram of flow-through core incubation setup. Drawing not to scale. ....	15
Figure 2.3. Main effects of Julian day, core depth, hold time, and soil moisture on flux rates. NO <sub>3</sub> flux from soil cores after initial (6h) inundation (a, b, c), 24 hours inundation (d, e, f), and 48 hours inundation (g, h). Each point represents a soil core that was either submerged (blue) or not submerged (red) at the time of field collection. Binary submergence categories are represented visually but not statistically because of collinearity with soil moisture. ....	28
Figure 2.4. Responses of PO <sub>4</sub> flux to fieldwork constraint-soil moisture interactions. Interactions between hold time and soil moisture (panels a, c, e), core depth and soil moisture (panel b) and Julian Day and soil moisture (panel d) that influence PO <sub>4</sub> flux where flux is regressed against hold time for constant soil moisture values at 0, 25, 50, 75, and 97.5 percentiles corresponding to the range of soil moisture values shown visually in the legend above (0.07, 0.27, 0.39, 0.55, 1.40 g g <sup>-1</sup> ) with 95% confidence intervals for regression lines at each soil moisture level.....	32
Figure 2.5. Response of PO <sub>4</sub> flux to core depth. Main effect of core depth on 24 h PO <sub>4</sub> flux regardless of soil moisture level. Core depth was the only field collection factor influencing PO <sub>4</sub> flux regardless of soil moisture (Table 2.3). Each point represents a soil core that was either submerged (blue) or not submerged (red) at the time of field collection. Binary submergence categories are represented visually but not statistically because of collinearity with soil moisture. ....	33
Figure 2.6. Response of N <sub>2</sub> flux to fieldwork constraint-soil moisture interactions. Two-way interactions between core depth and soil moisture (a, c) and hold time and soil moisture (b, d) that influence N <sub>2</sub> flux after 24 h (a, b) and 48 h (c, d) inundation. N <sub>2</sub> flux is regressed against hold time for constant soil moisture values at 0, 25, 50, 75, and 97.5 percentiles corresponding to the range of soil moisture values shown visually in the legend above (0.07, 0.27, 0.39, 0.55, 1.40 g g <sup>-1</sup> ) with 95% confidence intervals for regression lines at each soil moisture level. ....	36
Figure 2.7. Relationship between the main effect of Julian day and N <sub>2</sub> flux after 24 hours inundation. Julian day was the only significant main effect influencing N <sub>2</sub> flux without an interaction with soil moisture (Table 2.4). Each point represents a soil core that was either submerged (blue) or not submerged (red) at the time of field collection. Binary submergence categories are represented visually but not statistically because of collinearity with soil moisture. ....	37

- Figure 2.8. Response of soil oxygen demand (SOD) to fieldwork constraints. Effect of core depth on SOD after 48 h inundation (a) and interactive effects of hold time and soil moisture on SOD after 48 h inundation (b). O<sub>2</sub> flux (negative flux represents SOD) is regressed against hold time for constant soil moisture values at 0, 25, 50, 75, and 97.5 percentiles corresponding to the range of soil moisture values shown visually in the legend above (0.07, 0.27, 0.39, 0.55, 1.40 g g<sup>-1</sup>) with 95% confidence intervals for regression lines at each soil moisture level. .... 39
- Figure 2.9. Nutrient flux rates calculated with individual outflow values for each core (x-axis) compared to flux calculated with average inflow rate from source water (y-axis). Each point represents a soil core (n = 594 in panels a and b and n = 595 in panels c and d). The black line in each panel represents a 1:1 ratio where all points would fall if there were no difference in flux due to use of average vs. individual flow rates. Largest effect sizes of average inflow use were observed after 48 hours incubation for soil oxygen demand (panel a - 1.82% median decrease) and N<sub>2</sub> flux (panel b - 1.86% median decrease), and after initial inundation for NO<sub>3</sub> (panel c - 1.81% median increase) and PO<sub>4</sub> flux (panel d - 2.133% median increase)..... 41
- Figure 2.10. Nutrient flux rates calculated without (x-axis) and with (y-axis) control cores. Each point represents a soil core to visualize control core effects across the scale that each flux rate was measured. Paired Wilcoxon t-tests were conducted for each incubation (n =20) because control core effects were constant for all cores in each incubation. The black line in each panel represents a 1:1 ratio where all points would fall if there were no difference in flux due to use of control cores in flux calculations. .... 44
- Figure 2.11. Relationships between N<sub>2</sub> flux and soil oxygen demand with and without control cores. With water control cores after 24 h (panel a); 48 h incubation (panel b) and without water control cores after 24 h (panel c) and 48 h incubation (panel d). Second order (panels a and c) and third order (panels b and d) polynomial regressions were used to model relationships after selecting the linear model with the lowest AIC for each flux rate at each time point. .... 46
- Figure 3.1. Root mean squared error (RMSE) of IDW interpolation predictions for soil C. Soil C RMSE regressed against coefficient of variation (CV) for easement slope (a), elevation change over each easement (b), CV for soil C measurements within each easement (c), and CV for distance between 30 core collection locations at each easement. Values for each easement are symbolized according the IDW power with the lowest RMSE used in these regressions..... 80
- Figure 3.2. Root mean squared error (RMSE) of IDW interpolation predictions for soil N. Soil N RMSE regressed against coefficient of variation (CV) for easement slope (a), elevation change over each easement (b), CV for soil N measurements within each easement (c), and CV for distance between 30 core collection locations at each easement. Values for each easement are symbolized according the IDW power with the lowest RMSE used in these regressions..... 81
- Figure 3.3. Root mean squared error (RMSE) of IDW interpolation predictions for soil P. Soil P RMSE regressed against coefficient of variation (CV) for easement slope (a),

	elevation change over each easement (b), CV for soil P measurements within each easement (c), and CV for distance between 30 core collection locations at each easement. Values for each easement are symbolized according the IDW power with the lowest RMSE used in these regressions.....	82
Figure 3.4.	Root mean squared error (RMSE) of IDW interpolation predictions for NO <sub>3</sub> flux. NO <sub>3</sub> flux RMSE regressed against coefficient of variation (CV) for easement slope (a), elevation change over each easement (b), CV for NO <sub>3</sub> flux measurements within each easement (c), and CV for distance between 30 core collection locations at each easement. Values for each easement are symbolized according the IDW power with the lowest RMSE used in these regressions. ....	84
Figure 3.5.	Root mean squared error (RMSE) of IDW interpolation predictions for PO <sub>4</sub> flux. PO <sub>4</sub> flux RMSE regressed against coefficient of variation (CV) for easement slope (a), elevation change over each easement (b), CV for PO <sub>4</sub> flux measurements within each easement (c), and CV for distance between 30 core collection locations at each easement. Values for each easement are symbolized according the IDW power with the lowest RMSE used in these regressions. ....	85
Figure 3.6.	Root mean squared error (RMSE) of IDW interpolation predictions for soil pH. Soil pH RMSE regressed against coefficient of variation (CV) for easement slope (a), elevation change over each easement (b), CV for soil pH measurements within each easement (c), and CV for distance between 30 core collection locations at each easement. Values for each easement are symbolized according the IDW power with the lowest RMSE used in these regressions. ....	87
Figure 3.7.	Root mean squared error (RMSE) of IDW interpolation predictions for soil moisture. Soil moisture RMSE regressed against coefficient of variation (CV) for easement slope (a), elevation change over each easement (b), CV for soil moisture measurements within each easement (c), and CV for distance between 30 core collection locations at each easement. Values for each easement are symbolized according the IDW power with the lowest RMSE used in these regressions.....	88
Figure 3.8.	Root mean squared error (RMSE) of IDW interpolation predictions for soil bulk density. Soil bulk density RMSE regressed against coefficient of variation (CV) for easement slope (a), elevation change over each easement (b), CV for soil bulk density measurements within each easement (c), and CV for distance between 30 core collection locations at each easement. Values for each easement are symbolized according the IDW power with the lowest RMSE used in these regressions.....	89
Figure 3.9.	Comparison of IDW interpolated estimates and extrapolated 95% confidence intervals for surficial soil carbon (a), nitrogen (b), and phosphorus (c) storage. Mean extrapolated estimates for each nutrient are indicated by a dark blue X for each easement, bounded by 95% confidence intervals in black. Interpolated IDW estimates of nutrient storage are shown as red circles (1 <sup>st</sup> order IDW) and light blue triangles (2 <sup>nd</sup> order IDW).....	91
Figure 3.10.	Comparison of IDW interpolated estimates and extrapolated 95% confidence intervals for initial NO <sub>3</sub> (a) and PO <sub>4</sub> (b) flux. Mean extrapolated estimates for each dissolved nutrient are indicated by a dark blue X for each easement, bounded by	

95% confidence intervals in black. Interpolated IDW estimates of nutrient storage are shown as red circles (1<sup>st</sup> order IDW) and light blue triangles (2<sup>nd</sup> order IDW).. 92

Figure 3.11. Relationships of soil nutrient measurements to tree planting age and elevation. Meters above sea level and surficial soil C (a) and N (b) storage, and initial PO<sub>4</sub> flux (e). Tree planting age and surficial soil P storage (c), and initial flux of NO<sub>3</sub> (d) at the soil-water interface. Panels display the stronger relationship (tree planting age vs. elevation) derived from corresponding statistics in Table 3.2..... 95

Figure 3.12. Relationships between elevation (m) above sea level and remnant forest soil C (a), N (b), and P (c) storage, initial NO<sub>3</sub> (d) and PO<sub>4</sub> (e) flux. Corresponding statistics in Table 3.3..... 97

Figure 3.13. Comparison of surficial soil C (a), N (b), and P (c) storage, and initial NO<sub>3</sub> (d) and PO<sub>4</sub> (e) flux between remnant forest and tree planting habitats. Error bars represent 95% confidence intervals or means. Non-significant differences are denoted by “NS”. ..... 98

Figure 4.1. Mayfield Creek watershed landcover and proximity to Mississippi River. Screenshot modified from Stroud Water Research Center “Model My Watershed” tool. .... 115

Figure 4.2. Floodwater flow direction (blue arrows), sampling locations (yellow ellipses) and distances from levee break. .... 116

Figure 4.3. Hydrographs from USGS gauge (# 07024000) on Bayou de Chien, Kentucky, comparing relative size and duration of three floods between January 11-14th, July 1- 4th, and October 19-22nd 2020. The y-axis scale is identical for each hydrograph and ranges from approximately 6 feet to 16 feet, including the minimum and maximum water levels during the 72-hour window (x-axis) shown for each flood. Boxplots below hydrographs summarize the range of TN (blue) and TP (orange) concentrations over the duration of sample collection (24 h) for each flood. .... 126

Figure 4.4. Percentage decrease in total nitrogen and total phosphorus concentrations between the levee sampling station and the forest sampling station 240 m downstream. Error bars represent 95 % confidence intervals calculated by Wilcoxon non-parametric paired t-tests..... 129

Figure 4.5. Percentage decrease in total nitrogen and total phosphorus concentrations between the levee sampling station and the backwater sampling station 490 m downstream. Error bars represent 95 % confidence intervals calculated by Wilcoxon non-parametric paired t-tests..... 130

Figure 4.6. Percentage decrease in total nitrogen and total phosphorus concentrations between the levee sampling station and the furthest sampling station 950 m downstream. Error bars represent 95 % confidence intervals calculated by Wilcoxon non-parametric paired t-tests..... 131

Figure 4.7. Relationships between floodwater TN:TP ratios and distance from levee. Interaction between distance from levee and flood was not statistically significant, so an additive model was used. Non-overlapping 95% confidence intervals for each regression line at the intercept indicate that the ratio of N:P delivery to the

floodplain differed between floods, with the July flood delivering the most N relative to P. ....	132
Figure 4.8. Simple linear regressions of January floodwater molar TN:TP ratios against flood duration for each sampling station. Relationships are regressed across the time that all four ISCOs were collecting samples (n = 16). The dashed blue line represents the intercept (8.03), indicative of floodwater TN:TP ratio at the time when water first breached the levee. Corresponding statistics are in Table 4.4. ....	135
Figure 4.9. Simple linear regressions of July floodwater molar TN:TP ratios against flood duration for each sampling station. Relationships are regressed across the time that all four ISCOs were collecting samples (n = 14). The dashed blue line represents the intercept (14.01), indicative of floodwater TN:TP ratio at the time when water first breached the levee. Corresponding statistics are in Table 4.4. ....	136
Figure 4.10. Simple linear regressions of October floodwater molar TN:TP ratios against flood duration for each sampling station. Relationships are regressed across the time that all four ISCOs were collecting samples (n = 7). The dashed blue line represents the intercept (13.15), indicative of floodwater TN:TP ratio at the time when water first breached the levee. Corresponding statistics are in Table 4.4. ....	137
Figure 4.11. Relationship of July floodwater dissolved inorganic nitrogen DIN:PO <sub>4</sub> ratio with distance from levee. Intercept = 7.796, slope = 0.025, $F_{(1,29)} = 152.4$ , $R^2 = 0.83$ , $p < 0.001$ ). ....	138
Figure 4.12. Boxplots comparing July NH <sub>4</sub> , NO <sub>3</sub> , and PO <sub>4</sub> , concentrations with distance from levee. Comparison of percent change in each nutrient concentration is relative to mean concentration at the levee (dashed line). Blue arrows indicate the direction of change. Comparisons were made by Welch t-test accounting for unequal variances in MS Excel. Non statistically significant differences from levee concentrations are shown by “NS”. ....	139
Figure 4.13. Regression of ammonium (NH <sub>4</sub> ) concentration against particulate organic matter (POM) at 950 m from the levee in July 2020. $R^2 = 0.60$ , $p < 0.001$ . ....	140
Figure 4.14. Regression with ANCOVA results of TN and TP concentrations regressed against TSS and POM, accounting for differences in TN and TP concentrations between floods. ....	141
Figure 4.15. Molar ratios of soil total nitrogen to extractable phosphorus (TN:eP) and dissolved inorganic nitrogen to extractable phosphorus ratios (DIN:eP) in the top 10 cm of soil regressed against distance (m) from levee. Molar soil TN:eP ratios are inflated compared with ISCO TN:TP ratios due to lack of soil TP data. Molar DIN:eP ratios are compressed because eP makes up a larger proportion of TP than DIN does for TN. ....	142
Figure 4.16. Variation in PO <sub>4</sub> , NH <sub>4</sub> , NO <sub>2</sub> , N <sub>2</sub> , and NO <sub>3</sub> flux rates for 30 soil cores collected across the floodplain and incubated in a flow-through system. The dashed line represents zero flux. Means are indicated by x and medians by horizontal line in boxplots. Boxes represent one standard deviation from the mean and whiskers represent two standard deviations. ....	144

Figure 4.17. Variation in N<sub>2</sub>O and CH<sub>4</sub> flux rates for 30 soil cores collected across the floodplain and incubated in a flow-through system. The dashed line represents zero flux. Means are indicated by x and medians by horizontal line in boxplots. Boxes represent one standard deviation from the mean and whiskers represent two standard deviations. Methane flux was < 1 µg/m<sup>2</sup>/h in 28 of 30 soil cores..... 145

Figure 4.18. Redundancy analysis of flux rate responses to soil structural properties and distance from levee. Explanatory variables are shown with blue rays. Soil total nitrogen is represented by Soil TN, soil total carbon by Soil TC. And soil extractable phosphorus by Soil eP. Flux rate responses for each nutrient/gas species are color coded as in Fig. 4.16. Rays are pointed in the direction of release of release for CH<sub>4</sub>, N<sub>2</sub>O and N<sub>2</sub>; and uptake for PO<sub>4</sub>, NH<sub>4</sub>, NO<sub>2</sub>, and NO<sub>3</sub>. Smaller acute angles between rays represent positive correlations between variables; 90 ° angles between variables indicate no relationship; 180 ° angles between variables represent negative correlations..... 147

## LIST OF TABLES

Table 2.1. Concentrations of dry chemical compounds added to 135 L of deionized (DI) water in a clean and sterile trashcan (reservoir). Mineral solutions were dissolved in DI water as individual solutions in ziplock baggies and added to the trashcan in the order listed below (1-13) to achieve each concentration listed in the 135 L trashcan. Trace metals were prepared in concentrated 1 L solutions ahead of incubations.....	14
Table 2.2. Final model results of field work constraints influencing NO <sub>3</sub> flux (mg m <sup>-2</sup> h <sup>-1</sup> ) at each incubation time point. Effect size represents percent difference from mean NO <sub>3</sub> flux attributable to per unit change in each field work constraint. ....	27
Table 2.3. Final model results of field work constraints influencing PO <sub>4</sub> flux (mg m <sup>-2</sup> h <sup>-1</sup> ) at each incubation time point. Effect size represents percent difference from mean PO <sub>4</sub> flux attributable to per unit change in each field work constraint. ....	31
Table 2.4. Final model results of field work constraints influencing N <sub>2</sub> flux (mg m <sup>-2</sup> h <sup>-1</sup> ) at each incubation time point. Effect size represents percent difference from mean N <sub>2</sub> flux attributable to per unit change in each field work constraint. ....	35
Table 2.5. Final model results of field work constraints influencing O <sub>2</sub> flux (mg m <sup>-2</sup> h <sup>-1</sup> ) at each incubation time point. Effect size represents percent difference from mean O <sub>2</sub> flux attributable to per unit change in each field work constraint. ....	38
Table 2.6. Results of paired Wilcoxon t-tests showing differences in flux rates attributable to use of average inflow rates in flux calculations. ....	40
Table 2.7. Results of one-sample Wilcoxon t-test for effects of control core use in flux calculations. ....	43
Table 2.8. Polynomial regression results of relationships between N <sub>2</sub> flux (mg m <sup>-2</sup> h <sup>-1</sup> ) and O <sub>2</sub> (mg m <sup>-2</sup> h <sup>-1</sup> ) at 24 and 48h incubation times with and without control core included in calculations.....	45
Table 3.1. Root mean squared error (RMSE) for 1st, 2nd, and 3rd order IDW models for each soil parameter for each easement (column). Values in bold denote lower RMSE for the three different models for each soil parameter for each easement, indicating the most parsimonious model. ....	78
Table 3.2. Results of additive multiple regression models evaluating relationships between tree planting age (y) and elevation (m) above sea level for soil C (kg C ha <sup>-1</sup> ), soil N (kg N ha <sup>-1</sup> ), soil P (kg P ha <sup>-1</sup> ), NO <sub>3</sub> flux (g NO <sub>3</sub> -N ha <sup>-1</sup> h <sup>-1</sup> ), and PO <sub>4</sub> flux (g PO <sub>4</sub> -P ha <sup>-1</sup> h <sup>-1</sup> ). ....	94
Table 3.3. Results of simple linear regression models evaluating relationships between tree planting age (y) and elevation (m) above sea level for soil C (kg C ha <sup>-1</sup> ), soil P (kg P ha <sup>-1</sup> ), NO <sub>3</sub> flux (g NO <sub>3</sub> -N ha <sup>-1</sup> h <sup>-1</sup> ), and PO <sub>4</sub> flux (g PO <sub>4</sub> -P ha <sup>-1</sup> h <sup>-1</sup> ). Quadratic regression for soil N (kg N ha <sup>-1</sup> ) improved model fit. ....	96
Table 4.1. Minimum, median, and maximum TN (mg N L <sup>-1</sup> ) and TP (mg P L <sup>-1</sup> ) concentrations for each sampling location (as meters downstream of levee break) in each month. ....	126
Table 4.2. Results of Wilcoxon non-parametric paired t-tests. Difference of medians is reported in units of mg L <sup>-1</sup> . Percent decrease refers to change in each downstream	

median estimate compared with median estimates at the levee; essentially, a measure of relative TN or TP retention between sampling stations. ....	128
Table 4.3. Results of regression with ANCOVA for the relationship of floodwater TN:TP ratio with distance from levee, controlling for starting concentrations of TN and TP in each flood. The estimate for the intercept shows predicted TN:TP ratio as water first entered the levee break in January. Estimates for July and October floods show predicted differences in TN:TP ratios as water first entered levee breaks in each flood compared with the January (intercept) estimate. ....	132
Table 4.4. Simple linear regression results of molar N:P ratios against flood duration. Flood duration (hours) is representative of the length of time that all ISCOs were simultaneously collecting floodwater. Sampling stations are demoted by distance (m) downstream from levee. ....	134
Table 4.5. Simple linear regression results of soil N:P ratios of 30 soil cores against distance (m) from levee. Soil total nitrogen to extractable phosphorus ratio (TN:eP) and dissolved inorganic nitrogen to extractable phosphorus ratios (DIN:eP) at 0-10 cm soil depth. ....	142
Table 4.6. Summary statistics for NH <sub>4</sub> , NO <sub>2</sub> , NO <sub>3</sub> , and N <sub>2</sub> (mg N L <sup>-1</sup> ), PO <sub>4</sub> (mg P L <sup>-1</sup> ), O <sub>2</sub> (mg O L <sup>-1</sup> ), N <sub>2</sub> O (μg N L <sup>-1</sup> ), and CH <sub>4</sub> (μg C L <sup>-1</sup> ) for 30 soil cores incubated in a flow-through system simulating a 48 h flood. Coefficient of variation (CV) is the ratio of standard deviation of the mean. Negative median and mean values represent uptake from the water column by the soil. Positive values represent release from the soil to the water column. ....	144

## CHAPTER 1: INTRODUCTION

Wetlands function as landscape filters that retain water, nutrients, and contaminants from rapid delivery to downstream ecosystems. Historical drainage of wetlands and channelization of streams in the Mississippi River Basin facilitated agricultural production by limiting localized flood risks to crops, but cumulative effects of upstream alterations enhance downstream risks of floods and exposure to pollutants (Junk et al., 1989). Development of the Haber-Bosch process enabled mass production of nitrogen (N) fertilizers which further enhanced crop production and global food supplies in the 20<sup>th</sup> century (Galloway, 1998; Glibert et al., 2014; Vitousek et al., 1997). However, the economic efficiency of modern agriculture comes at an ecological cost, where the supply of nutrients to downstream ecosystems is amplified by rapid drainage of tributary watersheds feeding larger river basins like the Mississippi, which feeds the Gulf of Mexico. “Dead Zones” form near the mouths of human-impacted river systems because of cultural eutrophication, where excess nutrient pulses from anthropogenic runoff promote excessive autotrophic and heterotrophic microbial growth (Dodds, 2006; Dodds & Cole, 2007). Algae and other microbes at the base of food webs die-off rapidly after nutrient pulses and their decomposition creates hypoxic zones across large coastal areas that negatively impact food web dynamics and fisheries production (Diaz & Rosenberg, 2008). Thus, there is widely recognized and critical need to reduce nutrient export from diffuse non-point sources in agricultural regions (Carpenter et al., 1998; Glibert, 2017, 2020).

Wetland restoration has been touted as a beneficial practice to mitigate non-point source nutrient runoff (Mitsch et al., 2001; Mitsch & Day, 2006; Zedler, 2003). Targeted placement of wetland restoration projects within watersheds with high nutrient loads can enhance overall nutrient retention capacity and reduce downstream eutrophication (Cheng et al., 2020; Hansen et al., 2018). Wetlands with longer water residence times tend to enhance nutrient retention as contact time between the water and soil is increased, allowing more time for biotic and abiotic nutrient transformations to occur across the soil-water interface (James et al., 2008; Winikoff & Finlay, 2023). However, differences in inundation frequency and duration can influence tradeoffs between nitrogen (N) and phosphorus (P) retention, and greenhouse gas (GHG) production in wetland soils (Baldwin & Mitchell, 2000; Burgin et al., 2013; Groffman & Tiedje, 1988; Hansson et al., 2005). Inundation differences can be especially pronounced among floodplain wetlands. Further, the physiochemical structure of wetland soils and their associated microbial communities can influence nutrient cycling processes at small scales (Bruland & Richardson, 2004; Duncan et al., 2013; Kuzyakov & Blagodatskaya, 2015) which poses a challenge when developing regional-scale nutrient budgets from limited field measurements. A combination of local-scale mechanistic studies and large-scale field observations are needed to develop accurate descriptions of wetland nutrient retention capacity.

The USDA Natural Resources Conservation Service (NRCS) has implemented the Wetlands Reserve Program (WRP) to compensate landowners for taking marginally productive cropland out of production in favor of restoration to bottomland hardwood forests that historically covered the Mississippi River Alluvial Valley (King et al., 2006).

Wetland restoration through WRP has multifaceted goals to restore ecosystem services including nutrient retention, flood mitigation, and biodiversity enhancement (Brinson & Eckles, 2011; Faulkner et al., 2011a). Monitoring of WRP nutrient retention capacity has occurred (Brinson & Eckles, 2011) but comprehensive regional scale estimates are missing.

My dissertation research stems from a monitoring project funded by the Natural Resources Conservation Service (NRCS) and implemented by The Nature Conservancy to monitor 20 WRP easements in west Tennessee and Kentucky for their nutrient retention capacity as restored floodplain wetlands (Fig. 1.1). We chose to measure nutrient retention capacity using a space-for-time substitution approach where a variety of WRP easements with different times since restoration (0-25 years) were sampled over the duration of three growing seasons (May-August 2020, 2021, 2022). We employed soil core collection and flow-through incubations within the space-for-time approach because this allows more consistent treatment of soils among diverse wetland ecosystems encountered across our study region. Whole wetland measurements of nutrient inflows and outflows are useful for quantifying nutrient retention patterns at the ecosystem scale (Gillespie et al., 2018; Noe & Hupp, 2007) but are limited in their ability to identify mechanisms of nutrient cycling processes. Both methods can contribute to accurate nutrient budgets.

Flow-through soil core incubations have been used to study nutrient cycling processes among diverse aquatic systems (Grantz et al., 2012; Kana et al., 1994; McCarthy et al., 2007; Smyth et al., 2013; Speir et al., 2017) but no previous study has employed flow-through incubations at the spatial scale of the current WRP monitoring

project. Therefore, my second dissertation chapter focuses on evaluation of experimental artifacts that can influence nutrient flux measurements from flow-through incubations in terms of field collection constraints and methodological decisions in the laboratory. This chapter is targeted for publication in the journal *Limnology and Oceanography: Methods* and should be a useful guide for many research groups who are beginning to apply flow-through incubations to understand wetland nutrient retention capacity. My third dissertation chapter stems from a need to scale our uniquely large spatial dataset from individual soil cores to whole WRP management areas so that we derive the best possible estimates of nutrient retention capacities from our data. Results from this chapter will be helpful for developing a decision tool that NRCS can use to identify floodplain areas where wetland restoration through WRP will provide optimal benefits in terms of nutrient retention. This chapter is targeted for publication in the journal *Ecological Applications*. My fourth dissertation chapter focuses on one WRP easement and provides a case study highlighting the benefits of combining flow-through core incubations with *in situ* floodwater monitoring to identify floodplain wetland features that improve nutrient retention capacity. This chapter is targeted for publication in the journal *Freshwater Science*. Together, these three chapters highlight essential considerations for interpreting and contextualizing nutrient retention capacity estimates derived from flow-through soil core incubations.

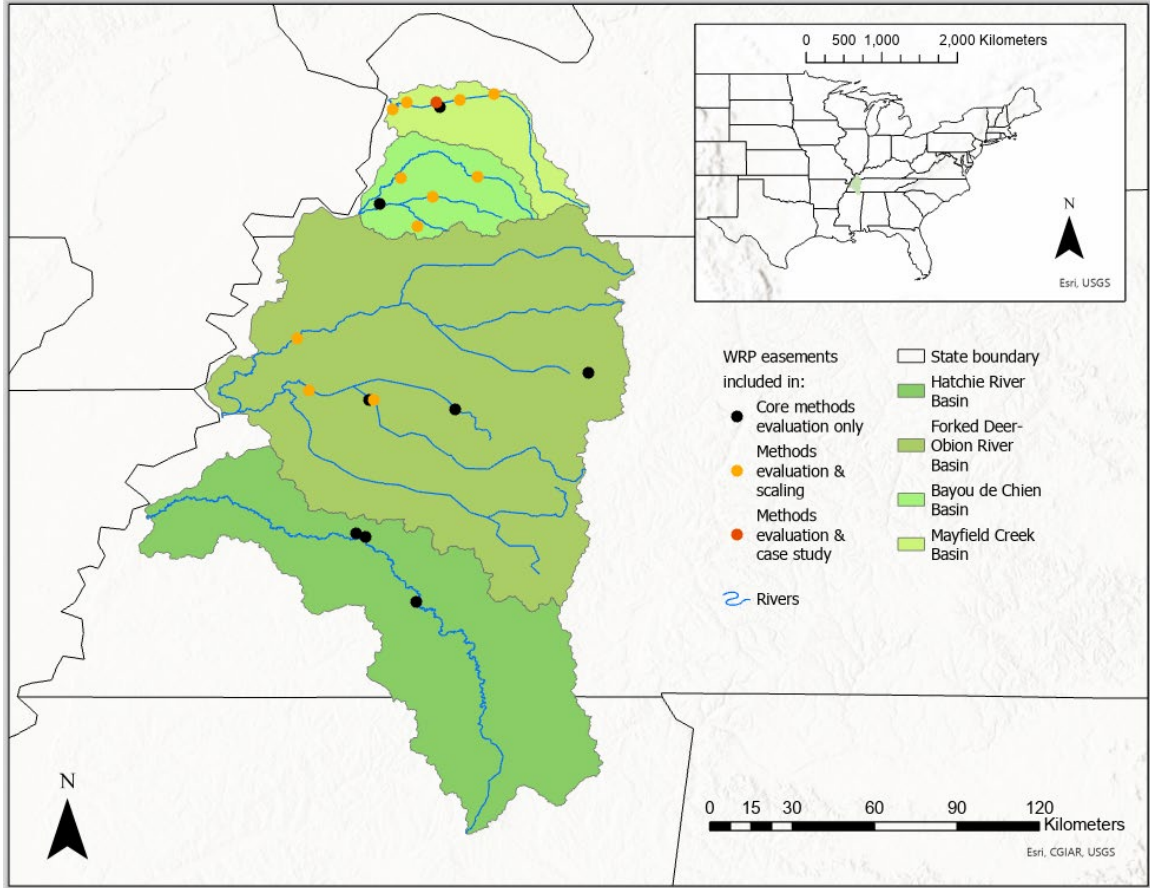


Figure 1.1. Locations of WRP easements included in this study.

## **CHAPTER 2: EVALUATING FLOW-THROUGH SOIL CORE INCUBATIONS FOR MEASURING NUTRIENT UPTAKE, NITROGEN REMOVAL, AND SOIL OXYGEN DEMAND IN RESTORED FLOODPLAIN WETLANDS**

### **Abstract**

Flow-through core incubations are becoming a common method to assess nutrient flux rates in soils and sediments. However, the influence of core collection, transport, and incubation methods on these measurements have not yet been evaluated with large sample sizes. I examined the influence of methodological decisions using 600 soil cores from 20 easements enrolled in the USDA Natural Resources Conservation's Wetlands Reserve Program (WRP). I show that field collection constraints can influence nutrient flux measurements and interact with each other, but this influence is generally small compared to observed natural variation. Soil moisture during collection affected (1) the influence of core depth, hold time, and collection date on  $\text{PO}_4$  flux; (2) the influence of core depth and hold time on nitrogen gas ( $\text{N}_2$ ) flux; (3) the influence of hold time on soil oxygen demand. Nitrate flux was influenced by collection date, core depth, hold time, and initial soil moisture, with no interactions among these variables. Incubation factors had varying effects on nutrient flux calculations. Water flow rate measurements caused relatively small changes in flux rate estimates for  $\text{NO}_3$ ,  $\text{PO}_4$ ,  $\text{N}_2$  and  $\text{O}_2$ , while the use of blank water column control cores to account for potential changes not caused by the soil sample resulted in considerable changes to the estimates of uptake for all nutrients. More investigation is needed into uptake mechanisms of blank cores and interactive effects of

field collection constraints on nutrient uptake measurements. Design and analyses of future flow-through core incubations should strive to account for interactions between soil moisture during collection, collection date, core depth, and hold time that influence nutrient flux responses.

## **Introduction**

Flow-through core incubations have been employed in a variety of aquatic ecosystems to measure nutrient cycling rates for decades, and were critical in early applications of nitrogen isotope pairing (Rysgaard et al., 1993) and the N<sub>2</sub>:Ar ratio method (Kana et al., 1994). This method has greatly improved our mechanistic understanding of nitrogen (N) cycling processes in estuarine (An et al., 2001; An & Gardner, 2002; Gardner et al., 2006; Kana et al., 1998; Smyth et al., 2013), lake (Evans et al., 2021; Grantz et al., 2012; McCarthy et al., 2007; Nifong & Taylor, 2022), stream (Kröger et al., 2014; Nifong et al., 2019; Smith et al., 2006; Speir et al., 2017), and wetland/pond environments (Hohman et al., 2021; Scott et al., 2008; Smith et al., 2000). These studies highlight the interdependence of N cycling processes on physical, chemical, and biological characteristics at the sediment-water interface. Flow-through incubation studies focus on soil phosphorus (P) flux less often, but valuable work has been done (Gibbs & Özkundakci, 2011; Hamdan et al., 2010). Recent flow-through incubations have focused on N and P dynamics in aquatic agroecosystems (Evans et al., 2021; Nifong et al., 2019; Nifong & Taylor, 2022) with the goal of guiding management practices that simultaneously reduce N and P inputs to the Gulf of Mexico.

Expanding the suite of nutrient flux measurements obtained from flow-through core incubations promotes understanding of interactive biogeochemical processes in submerged sediments and soils. However, flux of  $\text{NO}_3$ ,  $\text{PO}_4$ , and other aqueous chemicals can be influenced by collection and incubation methods for flow-through and static incubations systems (Kana et al., 1998; Miller-Way & Twilley, 1996; Noe, 2011). Most flow-through core studies report a range of core depths collected (i.e. 15 – 20 cm), a timeframe for transport from the field to the laboratory (i.e. within 24 hours) and a set flow rate for the flow-through system (i.e.  $\sim 1$  mL/min). However, effects of these logistical constraints/decisions are not commonly discussed in the literature, except for flow rate which controls water residence time in the system (Miller-Way & Twilley, 1996). Cores are often allowed to equilibrate for hours (McCarthy et al., 2007) or days (Rysgaard et al., 1993) once connected to a flow-through system before measurements begin. Miller-way and Twilley (1996) suggest that twice the water column residence time within cores is sufficient pre-incubation time for nutrient flux rates to equilibrate to ambient conditions, but this depends on the objectives of a study. Residence times of flow-through incubations can be optimized based on the nutrient of interest, expected pathways of production/consumption, and soil porosity (Miller-Way & Twilley, 1996). Such a targeted design is best for replicating ambient nutrient flux rates and requires knowledge of study-site characteristics well ahead of the start of core incubations. Essentially, core depths and flow-through residence times can be optimized for specific studies, such as those focused on seasonal nutrient dynamics in individual restored wetlands (Scott et al., 2008; Smith et al., 2000), or agricultural ditches with relatively homogenous soils (Kröger et al., 2014; Nifong et al., 2019; Speir et al., 2017)

Large-scale studies of nutrient flux across variable soil or sediment types must employ alternative methods of describing variation in nutrient flux rates introduced by sampling and incubation design. In addition to spatial variability, seasonal influence on nutrient flux rates can be a primary concern. Some studies address seasonality categorically in their study design (e.g., Kröger et al., 2014; Scott et al., 2008; Speir et al., 2017). Others are influenced by logistical constraints that necessitate sampling over a wider than ideal seasonal timeframe (Smith et al., 2000).

This study analyzes methodological influences of core collection and incubation procedures on nutrient flux measurements taken across a diversity of floodplain soils to evaluate nutrient retention capacity of restored floodplain wetlands enrolled in the United States Department of Agriculture's Wetlands Reserve Program (WRP). The USDA National Resources Conservation Service implements WRP by compensating landowners for taking frequently flooded cropland out of production to restore ecosystem services of nutrient retention, flood mitigation, and biodiversity enhancement (Brinson & Eckles, 2011; Faulkner et al., 2011b). I focus analysis here on intact soil cores collected from 20 WRP easements adjacent to Mississippi River Tributaries in west Kentucky and Tennessee, USA. Soil cores were collected across three growing seasons, across a spatial scale of approximately 21,500 km<sup>2</sup>, encompassing Mayfield Creek, Bayou de Chien, Obion River, Forked Deer River, and Hatchie River watersheds, to provide a gradient of diverse soil characteristics.

The objectives for this study were: (1) assess responses of nutrient flux rates from WRP soil cores to four different fieldwork constraints: calendar day of core collection (Julian day), core depth, time elapsed between field collection and that start of incubation

(hereafter hold time), and soil moisture during collection; (2) compare flux rates calculated with the use of water column blank “control” cores containing synthetic water only and flux rates calculated without use of water column blank “control” cores; and (3) compare nutrient flux rates calculated with average inflow rates of source water delivery to cores (hereafter average inflow rate) to flux calculated with individual outflow rates of water from each core (hereafter individual outflow rate) to assess whether core specific outflow measurements affected flow rates in a quantifiable way.

## **Methods**

### **Flow-through incubation design choices**

We chose to use flow-through core incubations in our assessment of WRP nutrient retention capacity because they allow direct comparisons of inundated microcosms through multi-day incubations across 20 different easements (Groffman et al., 2006; Miller-Way & Twilley, 1996). Most intact core incubations of permanently inundated sediments are plumbed to receive water collected from the study site. One or more “blank” cores are incubated with site water only to control for water column nutrient uptake. This enables measurement of ambient flux rates attributable directly to soil when site water is readily available. Intermittent inundation of agricultural floodplain wetlands necessitates an alternative water source for flow-through incubations, as many cores are not submerged at the time of field collection. We chose to prepare incubation water in the laboratory as others have done when collecting cores from sparsely inundated environments (Nifong et al., 2019; Speir et al., 2017). Aquatic substrata can

rapidly increase uptake rates in response to increased nutrient delivery (Hohman et al., 2021; Kana et al., 1998) but responses can differ for sporadically inundated floodplains (Richardson et al., 2019; Welti, Bondar-Kunze, Singer, et al., 2012). We were specifically interested in maximum  $\text{NO}_3$  and  $\text{PO}_4$  flux at the soil-water interface as inundation occurred, so we prepared incubation water with elevated  $\text{NO}_3$  and  $\text{PO}_4$  concentrations and did not allow for pre-incubation equilibration before sample collection.

### **Soil core collection and transport**

We collected soil cores from a total of 20 WRP easements, visiting each site once between May and August in 2020, 2021, and 2022. We selected 30 core locations within each easement to evaluate soil nutrient retention capacity across a variety of management practices and successional stages. All cores were collected in 7.62 x 30 cm acrylic tubes by hand or placed within a steel housing and hammered into the soil, depending on soil density and logistical needs (Fig. 2.1). Duplicate soil cores were collected at each location (within 30  $\text{cm}^2$ ) to a target depth of 15 cm, resulting in 30 pairs, or 60 cores per easement. Time of collection was noted for each core and exact depth was measured for each core in the laboratory. One core from each pair was used in flow-through incubations to derive biogeochemical flux rates, and the other was analyzed for soil properties including soil moisture. Soil moisture is the only soil property included in the current study as this property could change quickly with rainfall or flooding and be accounted for by the researcher by deciding when to collect a core after the introduction of water. Soil moisture was measured gravimetrically for the top 10 cm of soil in each core (Evelt et al., 2009). Cores collected from submerged locations were filled with

overlying water during transport. Incubation cores were transported on ice to Cookeville, Tennessee, and stored overnight in an environmental chamber at 24 C until the start of incubation at 08:00 the following morning. Hold time was calculated for each core from the difference between collection time in the field and incubation start time. Overlying water was syphoned off submerged cores immediately after placing them in the environmental chamber before attaching them to the flow-through setup.



Figure 2.1. Pictures of soil core collection and incubation. Soil core collection from unsubmerged (top left, top middle) and submerged (top right) environments. Synthetic source water for incubations with recirculating pump and air stones (bottom left). Flow-through incubation setup (bottom middle). Soil core filling during incubation (bottom right).

### **Continuous flow-through incubation: Water sources**

Collection of natural water at each easement over the duration of a multi-year flow-through incubation project introduces variability between incubations in terms of water macronutrient and micronutrient content, suspended solids, and microbes present at

the time of water collection. Synthetic laboratory water was used for all incubations to maintain more consistent water quality and attribute biogeochemical rates measured from cores directly to the soil. The water supply for flow through incubations was prepared in the laboratory according to historical average concentrations of micronutrients in the Obion River and Bayou de Chien, USA, and elevated concentrations of  $\text{NO}_3$  (~10 mg  $\text{NO}_3\text{-N/L}$ ) and  $\text{PO}_4$  (~1 mg  $\text{PO}_4\text{-P/L}$ ) added to DI water (hereafter synthetic water) to saturate nutrient uptake potential across all soils. Micronutrient concentrations added to synthetic water are shown in Table 2.1.

Table 2.1. Concentrations of dry chemical compounds added to 135 L of deionized (DI) water in a clean and sterile trashcan (reservoir). Mineral solutions were dissolved in DI water as individual solutions in ziplock baggies and added to the trashcan in the order listed below (**1-13**) to achieve each concentration listed in the 135 L trashcan. Trace metals were prepared in concentrated 1 L solutions ahead of incubations.

<b>Compound</b>	<b>Concentration</b>	<b>Final mg/L in reservoir</b>	<b>g added to 135 L reservoir</b>
<b>Mineral Solution</b>			
1.	NaHCO <sub>3</sub>	70	9.45
2.	KCl	3	0.405
3.	KH <sub>2</sub> PO <sub>4</sub>	4.4	0.594
4.	MgSO <sub>4</sub> *7H <sub>2</sub> O	27	3.645
5.	CaCl <sub>2</sub>	20	2.7
6.	NaNO <sub>3</sub>	60	8.1
13.	Fe(NH <sub>4</sub> ) <sub>2</sub> (SO <sub>4</sub> ) <sub>2</sub> *6H <sub>2</sub> O	3	0.405
<b>Dissolved organic Carbon</b>			
12.	C <sub>6</sub> H <sub>12</sub> O <sub>6</sub>	1	0.135
<b>Trace Metal Solution</b>			
7.	MnCl <sub>2</sub>	0.5	6.76
8.	CoCl <sub>2</sub> *6H <sub>2</sub> O	0.1	1.35
9.	ZnSO <sub>4</sub> *7H <sub>2</sub> O	0.05	0.675
10.	CuCl <sub>2</sub> *2H <sub>2</sub> O	0.02	0.27
11.	NaMoO <sub>4</sub> *2H <sub>2</sub> O	0.03	0.405

Flow-through incubation setup diagram is shown in Fig. 2.2. Synthetic water was pumped at ~1.8 mL/min from a clean and sterile trashcan via PFTE standard wall tubing with 0.86 mm inner diameter (Component Supply, Sparta, Tennessee, part number SWTT-20) connected to a Cole-Parmer Masterflex L/S peristaltic pump via PhthalateFree<sup>®</sup> PVC pump tubes with 1.52 mm inner diameter (ISMATEC, part number 95625-36). Inflow tubing fit tightly inside PVC pump tubes with no leaks. PVC pump tubes were connected to additional inflow tubes leading to each core, connected to

custom-made acrylic lids using a 1/16 inch white flangeless male nut (IDEX Health and Science part number P-203) with a 1/16 inch flangeless ferrule (IDEX Health and Science part number P-200x). Inflow tubing was extended through the flangeless fitting to ~ 1 cm above soil surface in each core. Water flowed out of each core through Tygon E-3603 Lab Tubing with 1/16 inch inner diameter, 1/8 inch outer diameter, and 1/32 inch wall (Component Supply, Sparta, Tennessee, part number TET-062A) connected to custom made acrylic lids with a 1/8 inch black flangeless male nut (IDEX Health and Science part number P-301X) and 3mm flangeless ferrule (IDEX Health and Science part number P-343X).

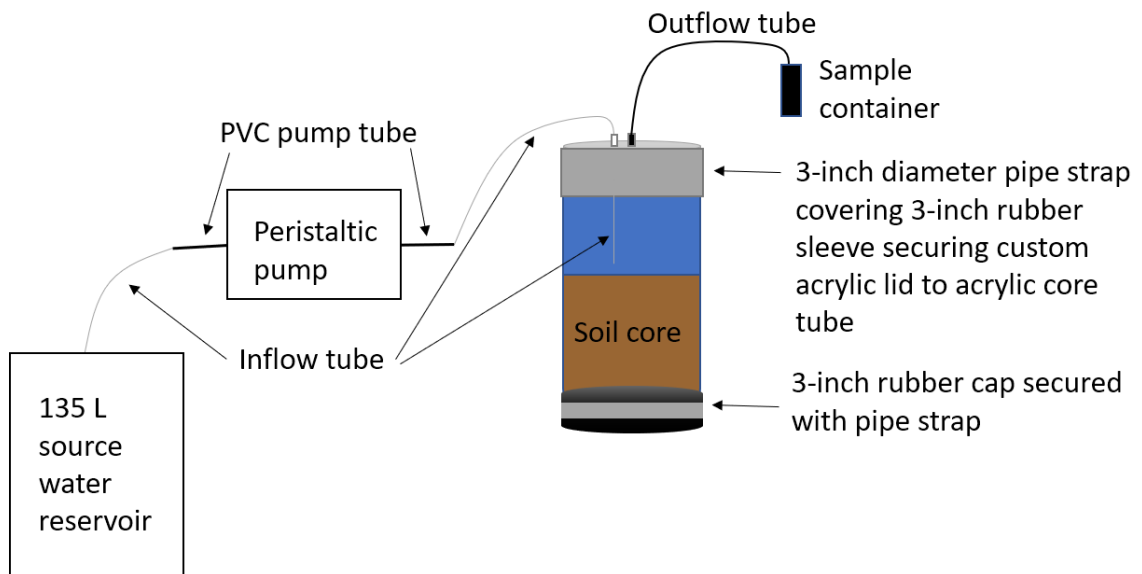


Figure 2.2. Diagram of flow-through core incubation setup. Drawing not to scale.

Water residence time within cores was approximately 6 h but varied with exact core depth and soil porosity. Approximately 15 mL was filtered with 0.45 (2021) or 0.7  $\mu\text{m}$  (2020 and 2022) glass fiber filters, stored in 20 mL Nalgene bottles, refrigerated, and

analyzed within 48 hours, or immediately placed on ice and frozen until analysis of  $\text{NO}_3$  and  $\text{PO}_4$  (see Nutrient analyses below). Outflow tubes were then placed in 12 mL exetainers so that exetainers filled from the bottom and overflowed at least three volumes before tubes were carefully removed. 157  $\mu\text{L}$  of  $\text{ZnCl}_2$  (50 % w:v) was added to stop microbial activity, and exetainers were immediately sealed and stored under water at  $4^\circ\text{C}$  until analysis via Membrane Inlet Mass Spectrometry (MIMS) for  $\text{N}_2$  and  $\text{O}_2$  using the Ar ratio method (Kana et al., 1994). Triplicate samples were taken at approximately 24 and 48h after incubation began.

Three water control cores were incubated per easement alongside sample cores. All acrylic control core materials were washed with soap and water, DI rinsed, soaked in 0.1 M HCl for one hour, and triple rinsed with DI water between incubations. Rubber core materials were similarly cleaned but skipped the HCl soak to preserve integrity of the rubber. Control cores consisted of synthetic water only to account for any physical processes occurring in the water column or through interaction with core materials that influence  $\text{NO}_3$ ,  $\text{PO}_4$ ,  $\text{N}_2$ , or  $\text{O}_2$  flux. Outflow samples from the three control cores were averaged to obtain one number representative of control core influences for each incubation sampling time point (approximately 6h, 24h, and 48h after incubation start time). Nutrient flux rates at 6h time points are referred to as initial flux below because outflow water was collected immediately after cores filled. Control core effects ( $[\text{Control}]_{out}$ ) are represented in equations 2 and 4 below. Full size water control cores (7.62 x 30 cm) were used in 2020 and half size cores (7.62 x 15 cm) were used in 2021 and 2022 to better represent the volume of water overlying soil cores. Flow rates through the cores were measured in two ways. First, flow rates were measured in triplicate inflow

tubes being pumped from the source water tub, but not through a core. These triplicate rates were averaged to give one inflow rate to all cores at each sampling time point. The second method was measuring the outflow rates for each soil core and water column control core at each sampling time point. This method accounted for any changes in flow within individual cores but was more labor intensive.

### **Dissolved nutrient analyses**

Nutrient concentrations were analyzed for filtered inflow water, water control core outflows, and soil core outflows using a Seal AQ400 discrete nutrient autoanalyzer and standard colorimetric methods provided by Seal, referencing EPA methods for each dissolved nutrient analysis. Nitrate and  $\text{NO}_2$  were measured using the cadmium reduction method, and  $\text{PO}_4$  was measured using the molybdate method. Nitrite concentrations were subtracted from  $\text{NO}_3 + \text{NO}_2$  analyses to yield  $\text{NO}_3$  only concentrations. Coefficients of variation (standard deviation divided by mean) were calculated for each triplicate set of water control core nutrient concentrations and inflow nutrient concentrations. Outlier concentrations of  $\text{NO}_3$  and  $\text{PO}_4$  were identified and removed from flux calculations if CVs were greater than 10 percent.

### **Dissolved gas analyses**

Triplicate exetainers were analyzed via MIMS in sequence for samples collected from each soil core, water control core, and inflow at 24 and 48h. Bubble formation and ebullition from soil prevented accurate dissolved gas measurements earlier in the incubation. Each gas was analyzed according to its atomic mass as follows:  $\text{N}_2$  at  $m/z$  28,

O<sub>2</sub> at  $m/z$  32 and Ar at  $m/z$  40. Samples analyzed for N<sub>2</sub>, O<sub>2</sub>, and Ar utilized the MIMS Faraday detector in 2020 and 2021. Samples were preserved with 180  $\mu$ L each of ZnCl<sub>2</sub> and NaOH (each 50 % w:v) in 2022 for simultaneous analysis of N<sub>2</sub>, O<sub>2</sub>, Ar, N<sub>2</sub>O, and CH<sub>4</sub> using the MIMS Secondary Electron Multiplier (SEM). Results of N<sub>2</sub>O, and CH<sub>4</sub> are not discussed, but prior tests show no difference in N<sub>2</sub>, O<sub>2</sub>, or Ar concentration measurements between the two methods. Dissolved gas standards for MIMS analysis consisted of deionized water continuously stirred to equilibrate gas concentrations with the atmosphere, held in a round 1L flask in a water bath at the sample collection temperature (24°C). Standard preparation in 2022 followed methods of Speir et al. (in review). Standards were measured in triplicate after every six samples to calculate calibration factors and correct for drift in MIMS signal over time. For each gas, thermodynamically expected concentration at 24°C corrected for atmospheric pressure (Weiss, 1970) was divided by the average  $m/z$  signal of triplicate standard measurements. The slope between each set of standards was used as a calibration factor to adjust  $m/z$  signal of N<sub>2</sub>, O<sub>2</sub>, and Ar in each sample before calculating concentrations for each gas. Gas concentrations ( $uncorrected[BG]_{sample}$  in Eq. 1) were corrected for physical effects using the Ar ratio method. All N<sub>2</sub> and O<sub>2</sub> concentration calculations were made with Ar correction using the *mimsy* package in R (Kelly, 2020).

Argon is increasingly used as a conservative gas tracer in aquatic systems (Hall & Madinger, 2018) as it responds to only physical process during analysis. Other gases (i.e. N<sub>2</sub> and O<sub>2</sub>) respond to physical and biological processes. Thus, physical effects on measured gas concentrations can be corrected using Ar ratios in the equation:

$$[BG]_{sample} = \left( \frac{uncorrected[BG]_{sample}}{[Ar]_{sample}} \times [Ar]_{expected} \right) \left( \frac{[BG]_{expected}/[Ar]_{expected}}{[BG]_{standard}/[Ar]_{standard}} \right) \quad \text{Eq. 1}$$

Where  $[BG]_{sample}$  is the corrected concentration of a biologically active gas ( $N_2$  or  $O_2$ );  $uncorrected[BG]_{sample}$  is the concentration of a biologically active gas before Ar ratio correction;  $[Ar]_{sample}$  is the Ar concentration in the same sample;  $[Ar]_{expected}$  is the thermodynamically Ar concentration at 24°C.  $[BG]_{expected}/[Ar]_{expected}$  is the thermodynamically expected ratio of a biologically reactive gas to Ar at 24°C.  $[BG]_{standard}/[Ar]_{standard}$  is the measured ratio of a biologically reactive gas to argon averaged over three triplicate standards.

All triplicate concentrations from each inflow, and core outflow sampling point were evaluated for outliers due to atmospheric gas contamination from direct exposure and bubble formation during sample collection. Careful efforts were made to minimize atmospheric contamination by triple filling exetainers and sealing immediately after preservative addition without headspace. Outliers were identified and removed if one triplicate concentration of  $N_2$  was  $> 0.5\%$  from the triplicate mean, or if one triplicate concentration of  $O_2$  was  $> 10\%$  from the triplicate mean. Differences in concentration thresholds for outlier identification reflect relatively higher concentration of  $N_2$  and less variability across samples compared with  $O_2$ . Outlier thresholds have not been previously described for triplicate MIMS gas concentration measurements from flow-through core incubations and those described here are somewhat arbitrary. I believe these thresholds greatly reduce the risk of including measurements where atmospheric contamination is likely (i.e. visual presence of bubbles). Some variation between triplicates is expected

because gas concentrations change during approximately one-hour triplicate sample collection time nested within approximately six-hour water column residence times.

## Flux calculations

### *Control core comparison*

Flux of dissolved nutrients (NO<sub>3</sub> and PO<sub>4</sub>) and gases (N<sub>2</sub> and O<sub>2</sub>) was calculated with (Eq. 2) and without (Eq. 3) water control cores in equations to identify net changes in each flux rate due to effects of physiochemical reactions within the synthetic water column and/or interactions with incubation materials:

$$F_{i,c} = \frac{([Core]_{out} - [IN]) Q_{core} - ([Control]_{out} - [IN]) Q_{control}}{A} \quad \text{Eq. 2}$$

$$F_{i,nc} = \frac{([Core]_{out} - [IN]) Q_{core}}{A} \quad \text{Eq. 3}$$

$F_{i,c}$  is the flux rate (mg m<sup>-2</sup> h<sup>-1</sup>) calculated using individual outflow rates (L h<sup>-1</sup>) from each soil core ( $Q_{core}$ ) and an average of triplicate outflow rates (L h<sup>-1</sup>) from water control cores ( $Q_{control}$ ) using Eq. 2.  $F_{i,nc}$  was calculated with individual outflow rates and without subtracting control core effects from soil core flux using Eq. 3. Nutrient concentration (mg L<sup>-1</sup>) in the outflow of each soil core at each sampling timepoint is shown by  $[Core]_{out}$ . Average outflow concentration (mg L<sup>-1</sup>) from triplicate water control cores is shown by  $[Control]_{out}$ . Average of triplicate inflow nutrient concentration (mg L<sup>-1</sup>) from source water is shown by  $[IN]$ . Soil surface area (m<sup>2</sup>) is shown by  $A$ .

### ***Flow rate measurement comparison***

Two additional paired measurements for each soil core nutrient flux were calculated as follows to compare flux calculated with average inflow rates vs. individual outflow rates for each core:

$$F_{a,c} = \frac{([Core]_{out-[IN]} Q_{in} - [Control]_{out-[IN]} Q_{in})}{A} \quad \text{Eq. 4}$$

$$F_{a,nc} = \frac{([Core]_{out-[IN]} Q_{in})}{A} \quad \text{Eq. 5}$$

$F_{a,c}$  (Eq. 4) and  $F_{a,nc}$  (Eq. 5) are identical to  $F_{i,c}$  and  $F_{i,nc}$  respectively, except for the use of average triplicate inflow rates ( $Q_{in}$ ) for each incubation round instead of individual core outflow rates. Comparison of results from these paired equations during 20 flow-through core incubations using 600 soil cores enables the influence of methodological decisions regarding flow-rate measurements to be quantified at a uniquely large scale. Specifically, we assessed control core effects by comparing results of equations 2 and 3, accounting differing flow rates for each core. We assessed flow rate effects by comparing results of equations 3 and 5. Equation 4 was not directly used in quantitative comparisons because it does not account for differences in flow rates through each core.

### **Data processing and analyses**

#### ***Assessing fieldwork constraints***

Multiple regression with stepwise (forward and backward) model selection was conducted using the stepAIC function, direction = “both” in the MASS package in R.

Akaike Information Criteria (AIC) measures information loss in a model. The model with the lowest AIC value after stepwise selection was interpreted as the most parsimonious (final) model to explain effects of logistical constraints on each flux rate measurement at each incubation timepoint. The response of each flux rate (calculated using equation 3, i.e., no control cores and individual core flow rates) at each incubation timepoint was regressed against Julian Calendar day of field collection, core depth (cm), hold time (h) between collection and the start of incubation, and initial soil moisture ( $\text{g g}^{-1}$ ), with two-way interaction terms included for soil moisture and each fieldwork constraint. Due to the hotspot/moment nature of nutrient uptake and removal in floodplain wetland soils, extreme flux values were removed from data used in these analyses. Nitrate and  $\text{PO}_4$  flux outside of 2.5 and 97.5 percentiles of our dataset were excluded because we observed some cases of extreme release and uptake of both nutrients using boxplots.  $\text{N}_2$  flux outside of 0 and 97.5 percentiles were excluded because we only observed extreme values at the high end (more positive) of  $\text{N}_2$  flux.  $\text{O}_2$  flux outside 2.5 and 100 percentiles were excluded because we only observed extreme values at the high end (more negative) of  $\text{O}_2$  flux (i.e. soil oxygen demand). Outliers may represent real hotspots in soil nutrient flux. However, the goal of this analysis is to accurately assess field work constraints that influence nutrient flux measurements across a range most applicable to current and future studies. Because core incubations were designed to maximize nutrient uptake potentials, extreme values in this study are less likely to be applicable to studies of ambient nutrient flux. Additionally, a few nutrient flux hotspots can disproportionately influence parameter estimates for the effects of field work constraints influencing the bulk of our nutrient flux measurements. All analyses were conducted in R version 4.2.2 (R core Team 2022).

Results were plotted using ggplot2 (Wickham 2016) and ggeffects (Lüdtke, 2022) packages in R. Results were considered significant with  $\alpha < 0.05$  and marginally significant with  $\alpha$  between 0.05 and 0.10.

### ***Control core effects***

Subtracting paired flux rates ( $F_{i,c} - F_{i,nc}$ ) results in uniform values for all cores at each incubation timepoint for each easement because the same average control core flux is subtracted from each soil core flux. A positive result from this subtraction suggests that control cores were removing a given nutrient from the water column. A negative result suggests that control cores were adding a given nutrient to the water column. Zero difference suggests that a given nutrient concentration was not affected by processes occurring in control cores. One-sample Wilcoxon t-tests were used to assess median difference from zero of all water control core effects calculated with individual outflow rates for each core (i.e. result from Eq.2 minus result from Eq. 3). The statistical sample size for this analysis is the number of incubations at a given timepoint ( $n = 20$ ), not the total number of cores, for each nutrient in the present study. Results are presented graphically for each nutrient for the incubation timepoint where control core effect size was largest. Flux rates from all cores would fall along a 1:1 line if there was no difference attributable to control core effects for each incubation at each timepoint. Nonparametric analysis enabled the inclusion of all flux rates without the need for outlier removal thresholds applied across paired rate calculation methods.

### ***Flow rate effects***

Paired Wilcoxon rank t-tests were used to test for differences in medians between flux rates calculated with average inflow rate ( $F_{a,nc}$ ) and individual outflow rates ( $F_{i,nc}$ ) for each soil core. Results are presented graphically for each nutrient at the incubation time point where the effect size of flow rate on nutrient flux was largest, where flux rates from all cores would fall along a 1:1 line if there was no difference attributable to flow rate type. Nonparametric analysis enabled the inclusion of all flux rates without the need for outlier removal thresholds applied across paired rate calculation methods.

## **Results**

### **Fieldwork constraints**

#### ***Explanatory variables***

Julian day of core collection ranged over 92 calendar days from 131 (May 11<sup>th</sup>) to 223 (August 11<sup>th</sup>) across 2020, 2021, and 2022. Target core depth was 15 cm, averaged 14.95 cm, and ranged from 9.5 to 22.5 cm. Core hold times between field collection and the start of incubation ranged from 16.98 to 26.08 hours. Cores were collected roughly between 06:00 and 15:00 the day before incubations, with incubations beginning at 08:00 the following morning. Soil moisture values averaged 0.495 g g<sup>-1</sup> in the top 10 cm and ranged from 0.07 to 4.99 g g<sup>-1</sup>. Soil moisture values above the 97.5 percentile (1.41 to 4.99 g g<sup>-1</sup>) were excluded from analyses reported below. Ranges of explanatory variables included in analyses below were 131-223 (Julian day), 9.5-22.5 cm (core depth), 16.98-26.08 hours (hold time), and 0.07-1.40 g g<sup>-1</sup> (soil moisture). Mean residence time of the

water column among all 600 cores was approximately 6.4h but ranged from approximately 3.2 to 8.7h due to variable core depths and flow rates (mean outflow rate 1.80 mL/min). Soil porosity was not measured but likely varied among soil cores and influenced water column residence time beyond the approximations reported above.

### *Nitrate (NO<sub>3</sub>) flux*

Nitrate flux was influenced differently by fieldwork constraints among 6h, 24h, and 48h incubation times. Nitrate was the only nutrient measured that its responses to Julian day, core depth, and hold time were not dependent on soil moisture. Rather, each fieldwork constraint, including soil moisture, influenced NO<sub>3</sub> flux independently.

Fieldwork constraints explained 13.1% of the variation in initial (6h) NO<sub>3</sub> flux after inundation (Table 2.2, Fig. 2.3,  $F_{(3, 453)} = 23.9$ ,  $R^2 = 0.131$ ,  $p < 0.001$ ). The best model for relating 6h NO<sub>3</sub> flux to fieldwork constraints included core depth, hold time, and soil moisture, and no interactive terms were included in the final model. Nitrate flux was 0.925 mg m<sup>-2</sup> h<sup>-1</sup> more negative (i.e., more NO<sub>3</sub> removal from the water) for each cm increase in core depth (Table 2.2, Fig. 2.3a,  $p = 0.008$ ). Nitrate flux was 0.678 mg m<sup>-2</sup> h<sup>-1</sup> more negative for every hour increase in holding time (Table 2.2, Fig. 2.3b,  $p = 0.023$ ). Nitrate flux was 16.404 mg m<sup>-2</sup> h<sup>-1</sup> more negative for each g g<sup>-1</sup> increase soil moisture (Table 2.2, Fig. 2.3c,  $p < 0.001$ ). This equates to a 10.859%, 7.963% and 192.580% increase in mean NO<sub>3</sub> uptake for each unit change in core depth (cm), hold time (h), and soil moisture (g g<sup>-1</sup>), respectively.

Fieldwork constraints explained 5.4% of the variation in NO<sub>3</sub> flux after 24 hours inundation (Table 2.2, Fig. 2.3,  $F_{(3, 456)} = 9.794$ ,  $R^2 = 0.054$ ,  $p < 0.001$ ). The best model for effects of fieldwork constraints on NO<sub>3</sub> flux after 24 hours inundation included Julian

day, core depth, and soil moisture with no interactive terms in the final model. Nitrate flux was  $0.058 \text{ mg m}^{-2} \text{ h}^{-1}$  more positive per Julian calendar day of field collection (Table 2.2, Fig. 2.3d,  $p = 0.011$ ). Nitrate flux was  $1.121 \text{ mg m}^{-2} \text{ h}^{-1}$  more negative for each cm increase in core depth (Table 2.2, Fig. 2.3e,  $p = 0.003$ ). Nitrate flux was  $7.840 \text{ mg m}^{-2} \text{ h}^{-1}$  more negative for each  $\text{g g}^{-1}$  increase in soil moisture (Table 2.2, Fig. 2.3f,  $p = 0.002$ ). This equates to a 0.510% decrease in mean 24h  $\text{NO}_3$  uptake for each day later in the growing season that cores were collected, 9.858% increase in 24h  $\text{NO}_3$  uptake for each unit change in core depth, and a 68.947% increase in 24h  $\text{NO}_3$  uptake for each unit change in soil moisture.

Fieldwork constraints explained 7.0% of the variation in  $\text{NO}_3$  flux after 48 hours inundation (Table 2.2, Fig. 2.3,  $F_{(2, 448)} = 18.03$ ,  $R^2 = 0.070$ ,  $p < 0.001$ ). The best model for effects of fieldwork constraints on  $\text{NO}_3$  flux after 48 h inundation included Julian day and soil moisture with no interactive terms in the final model. Nitrate flux was  $0.137 \text{ mg m}^{-2} \text{ h}^{-1}$  more negative for each day later in the growing season that cores were collected (Table 2.2, Fig. 2.3g,  $p < 0.001$ ). Nitrate flux was  $6.688 \text{ mg m}^{-2} \text{ h}^{-1}$  more negative for each  $\text{g g}^{-1}$  increase in soil moisture (Table 2.2, Fig. 2.3h,  $p = 0.012$ ). This equates to a 0.718% and increase in 48h  $\text{NO}_3$  uptake for each Julian calendar day and a 35.034% increase in 48h  $\text{NO}_3$  uptake for each  $\text{g g}^{-1}$  increase in soil moisture.

Table 2.2. Final model results of field work constraints influencing NO<sub>3</sub> flux (mg m<sup>-2</sup> h<sup>-1</sup>) at each incubation time point. Effect size represents percent difference from mean NO<sub>3</sub> flux attributable to per unit change in each field work constraint.

Incubation time	Parameter	Estimate	Effect size	Std. error	p-value	F-value	Adjusted R <sup>2</sup>
6h	intercept	27.884	NA	8.187	< 0.001	23.9 <sub>(3, 453)</sub>	0.131
	core depth (cm)	-0.925	-10.859	0.349	0.008		
	hold time (h)	-0.678	-7.963	0.298	0.023		
	soil moisture (g/g)	-16.404	-192.580	2.391	< 0.001		
24h	intercept	-2.268	NA	6.466	0.726	9.794 <sub>(3, 456)</sub>	0.054
	Julian day	0.058	0.510	0.023	0.011		
	core depth (cm)	-1.121	-9.858	0.372	0.003		
	soil moisture (g/g)	-7.840	-68.947	2.521	0.002		
48h	intercept	9.872	NA	4.922	0.046	18.03 <sub>(2, 448)</sub>	0.070
	Julian day	-0.137	-0.718	0.025	< 0.001		
	soil moisture (g/g)	-6.688	-35.034	2.649	0.012		

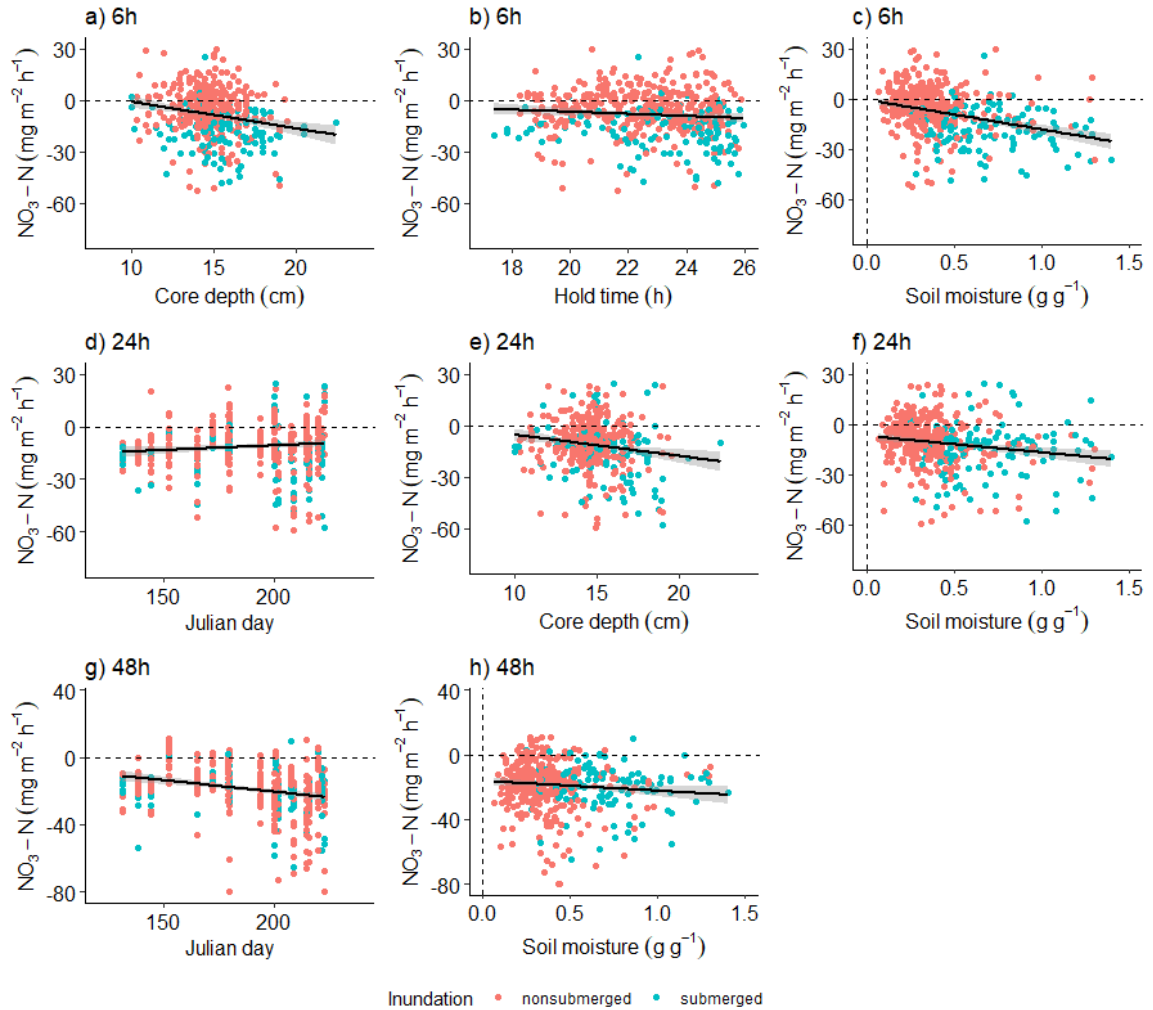


Figure 2.3. Main effects of Julian day, core depth, hold time, and soil moisture on flux rates.  $\text{NO}_3$  flux from soil cores after initial (6h) inundation (a, b, c), 24 hours inundation (d, e, f), and 48 hours inundation (g, h). Each point represents a soil core that was either submerged (blue) or not submerged (red) at the time of field collection. Binary submergence categories are represented visually but not statistically because of collinearity with soil moisture.

### ***Phosphate ( $\text{PO}_4$ ) flux***

Phosphate flux was influenced by different factors throughout incubation sampling times. Phosphate flux at all incubation sampling times was influenced by interaction of hold time and soil moisture but the strength of this interaction varied between incubation sampling times (Fig. 2.4a, c, e). Soil moisture influenced the

relationship between 48h PO<sub>4</sub> flux and Julian day, but Julian day was not an important driver of PO<sub>4</sub> flux earlier in incubations. Visually, a parabolic relationship between 48 h PO<sub>4</sub> flux and Julian day seems apparent (Fig. 2.4d), but inclusion of a quadratic term in the model for 48h flux was not statistically significant and resulted in similar parameter estimates for the non-quadratic model presented here. Phosphate flux was 0.141 mg m<sup>-2</sup> h<sup>-1</sup> more negative for each cm increase in core depth (Table 2.3, Fig. 2.5, p = 0.006) regardless of soil moisture. This equates to a 7.642% increase in mean 24h PO<sub>4</sub> uptake for each cm increase in core depth.

Fieldwork constraints explained 7.5% of the variation in initial (6h) PO<sub>4</sub> flux after inundation (Table 2.3, Figs. 2.4a, b,  $F_{(5, 447)} = 8.289$ ,  $R^2 = 0.075$ ,  $p < 0.001$ ). The best model for fieldwork constraint effects on initial (6h) PO<sub>4</sub> flux after inundation included core depth, hold time, and soil moisture. Including the interaction between hold time and soil moisture improved the final model (Table 2.3,  $p < 0.001$ ), indicating the relationship between 6h PO<sub>4</sub> flux and hold time depended on soil moisture. Slopes of the relationship between 6h PO<sub>4</sub> flux and hold time were -0.288 at zero percentile soil moisture, -0.115 at 25<sup>th</sup> percentile soil moisture, -0.011 at 50<sup>th</sup> percentile soil moisture, 0.128 at 75<sup>th</sup> percentile soil moisture, and 0.861 at 97.5<sup>th</sup> percentile soil moisture (Fig. 2.4a). Inclusion of the core depth and soil moisture interaction term improved the model, even though the interaction term itself was not statistically significant (Table 2.3,  $p = 0.108$ ). Slopes of the relationship between 6h PO<sub>4</sub> flux and core depth were -0.187 at zero percentile soil moisture, -0.105 at 25<sup>th</sup> percentile soil moisture, -0.056 at 50<sup>th</sup> percentile soil moisture, 0.009 at 75<sup>th</sup> percentile soil moisture, and 0.358 at 97.5<sup>th</sup> percentile soil moisture (Fig. 4b).

Fieldwork constraints explained 13.0% of the variation in PO<sub>4</sub> flux after 24 hours inundation (Table 2.3, Fig. 2.4c, Fig 5,  $F_{(4, 451)} = 17.98$ ,  $R^2 = 0.130$ ,  $p < 0.001$ ). The best model for fieldwork constraint effects on PO<sub>4</sub> flux after 24 hours included core depth, hold time, and soil moisture. The interaction between hold time and soil moisture was marginally statistically significant (Table 2.3.  $p = 0.072$ ), indicating a weaker influence of soil moisture on the relationship between hold time and PO<sub>4</sub> flux after 24h inundation compared to initial (6h) PO<sub>4</sub> flux (Fig. 2.4). Slopes of the relationship between 24h PO<sub>4</sub> flux and hold time were -0.100 at zero percentile soil moisture, -0.046 at 25<sup>th</sup> percentile soil moisture, -0.012 at 50<sup>th</sup> percentile soil moisture, 0.031 at 75<sup>th</sup> percentile soil moisture, and 0.263 at 97.5<sup>th</sup> percentile soil moisture (Fig. 2.4c).

Fieldwork constraints explained 12.3% of the variation in PO<sub>4</sub> flux after 48h inundation (Table 2.3, Fig. 2.4d, e,  $F_{(5, 447)} = 13.62$ ,  $R^2 = 0.123$ ,  $p < 0.001$ ). The best model for effects of fieldwork constraints on PO<sub>4</sub> flux after 48 h inundation included Julian day, hold time, and soil moisture. The interaction between Julian day and soil moisture was marginally statistically significant (Table 2.3,  $p = 0.051$ ), indicating that the effect of Julian day on 48h PO<sub>4</sub> flux depended on soil moisture. Slopes of the relationship between Julian day and 48h PO<sub>4</sub> flux were -0.018 at zero percentile soil moisture, -0.013 at 25<sup>th</sup> percentile soil moisture, -0.009 at 50<sup>th</sup> percentile soil moisture, -0.005 at 75<sup>th</sup> percentile soil moisture, and 0.019 at 97.5<sup>th</sup> percentile soil moisture (Fig. 2.4d). There was a statistically significant interaction between hold time and soil moisture (Table 2.3,  $p < 0.001$ ), indicating that the effect of hold time on 48h PO<sub>4</sub> flux depends on soil moisture. Slopes of the relationship between hold time and 48 h PO<sub>4</sub> flux were -0.126 at zero percentile soil moisture, -0.01 at 25<sup>th</sup> percentile soil moisture, 0.06 at 50<sup>th</sup> percentile

soil moisture, 0.152 at 75<sup>th</sup> percentile soil moisture, and 0.643 at 97.5<sup>th</sup> percentile soil moisture (Fig. 2.4e).

Table 2.3. Final model results of field work constraints influencing PO<sub>4</sub> flux (mg m<sup>-2</sup> h<sup>-1</sup>) at each incubation time point. Effect size represents percent difference from mean PO<sub>4</sub> flux attributable to per unit change in each field work constraint.

Incubation time	Parameter	Estimate	Effect size	Std. error	p-value	F-value	Adjusted R <sup>2</sup>
6h	intercept	10.215	NA	3.545	0.004	8.289 (5, 447)	0.075
	core depth (cm)	-0.216	-11.607	0.147	0.140		
	hold time (h)	-0.348	-18.700	0.118	0.003		
	soil moisture (g/g)	-27.906	-1499.516	6.219	< 0.001		
	core depth:soil moisture	0.410	22.047	0.255	0.108		
	hold time:soil moisture	0.864	46.443	0.207	< 0.001		
24h	intercept	4.054	NA	2.132	0.058	17.98 (4, 451)	0.130
	core depth (cm)	-0.141	-7.642	0.051	0.006		
	hold time (h)	-0.119	-6.450	0.087	0.174		
	soil moisture (g/g)	-8.653	-468.997	3.465	0.013		
	hold time:soil moisture	0.274	14.851	0.152	0.072		
48h	intercept	7.290	NA	2.353	0.002	13.62 (5, 447)	0.123
	Julian day	-0.020	-1.453	0.007	0.007		
	hold time (h)	-0.166	-12.064	0.093	0.077		
	soil moisture (g/g)	-20.780	-1510.174	4.200	< 0.001		
	Julian day:soil moisture	0.028	2.035	0.014	0.051		
	hold time:soil moisture	0.578	42.006	0.167	< 0.001		

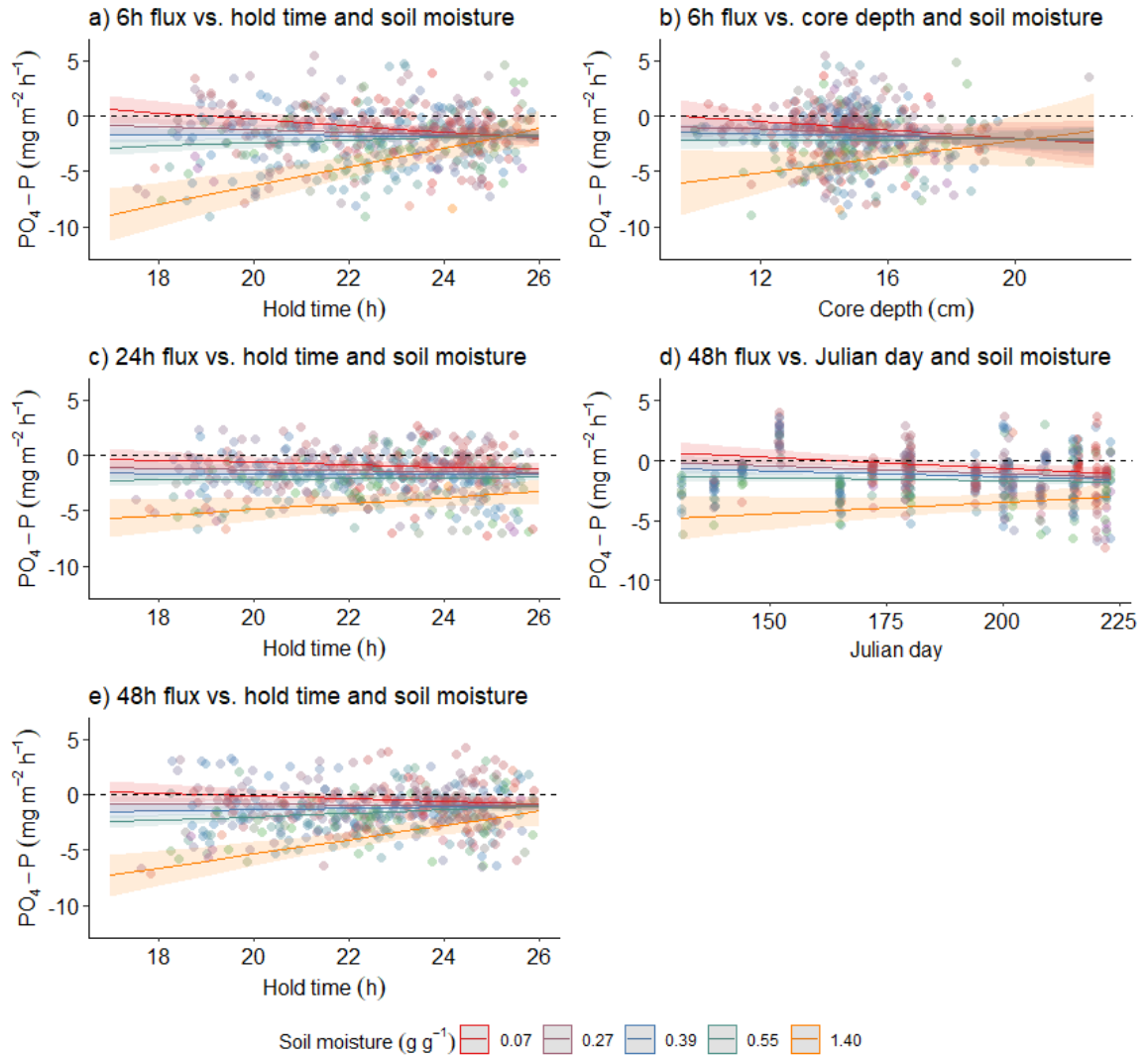


Figure 2.4. Responses of  $\text{PO}_4$  flux to fieldwork constraint-soil moisture interactions. Interactions between hold time and soil moisture (panels a, c, e), core depth and soil moisture (panel b) and Julian Day and soil moisture (panel d) that influence  $\text{PO}_4$  flux where flux is regressed against hold time for constant soil moisture values at 0, 25, 50, 75, and 97.5 percentiles corresponding to the range of soil moisture values shown visually in the legend above (0.07, 0.27, 0.39, 0.55, 1.40  $\text{g g}^{-1}$ ) with 95% confidence intervals for regression lines at each soil moisture level.

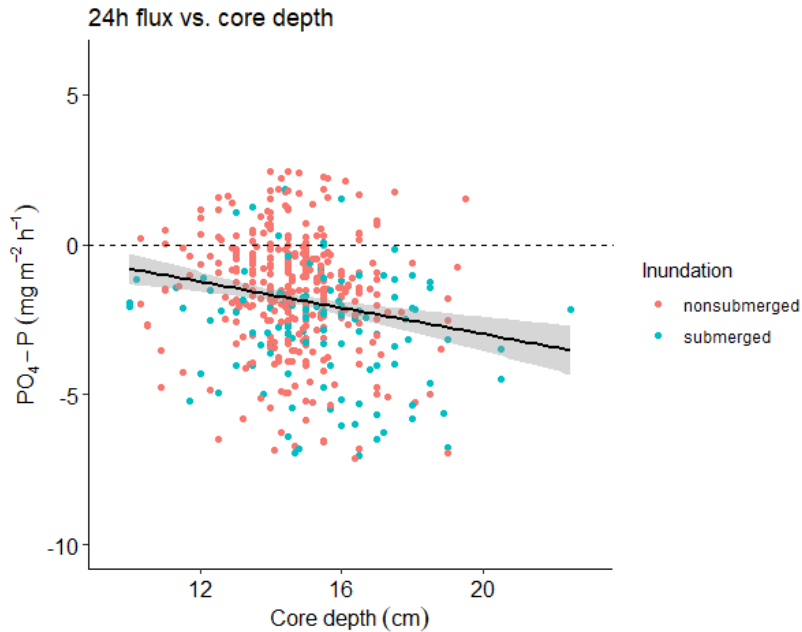


Figure 2.5. Response of  $\text{PO}_4$  flux to core depth. Main effect of core depth on 24 h  $\text{PO}_4$  flux regardless of soil moisture level. Core depth was the only field collection factor influencing  $\text{PO}_4$  flux regardless of soil moisture (Table 2.3). Each point represents a soil core that was either submerged (blue) or not submerged (red) at the time of field collection. Binary submergence categories are represented visually but not statistically because of collinearity with soil moisture.

### ***Dinitrogen ( $\text{N}_2$ ) flux***

$\text{N}_2$  flux at 24 and 48 h incubation was most strongly and positively influenced by core depth and hold time at soil moisture above the 97.5<sup>th</sup> percentile in this study (Fig. 2.6), but  $\text{N}_2$  flux at 24h decreased with Julian day regardless of soil moisture (Fig. 2.7).  $\text{N}_2$  flux at 24 h was  $0.011 \text{ mg m}^{-2} \text{ h}^{-1}$  more negative for each additional day collected later in the growing season (Table 2.4, Fig. 27,  $p = 0.014$ ), or a  $1.012 \text{ mg m}^{-2} \text{ h}^{-1}$  decrease in  $\text{N}_2$  flux over the duration of the growing season (92 days) represented in this study. This equates to a 0.230% decrease in N removal for each day later in the growing season that cores were collected.

Fieldwork constraints explained 15.6% of the variation in N<sub>2</sub> flux after 24h (Table 2.4, Figs. 2.6 and 7,  $F_{(6, 459)} = 15.29$ ,  $R^2 = 0.156$ ,  $p < 0.001$ ) and 9.0% of the variation in N<sub>2</sub> flux after 48 h (Table 2.4, Figs. 2.6 and 2.7,  $F_{(5, 458)} = 10.12$ ,  $R^2 = 0.090$ ,  $p < 0.001$ ). The best model for effects of fieldwork constraints on N<sub>2</sub> flux after 24 hours inundation included Julian day, core depth, hold time, and soil moisture. The best model for 48 h N<sub>2</sub> flux was similar but Julian day did not improve the model and was removed via AIC selection.

The effect of core depth on N<sub>2</sub> flux depended on soil moisture at both 24 (Table 2.4, Fig. 2.6a,  $p = 0.019$ ) and 48 h (Table 2.4, Fig. 2.6c,  $p = 0.044$ ). Deeper cores were associated with more negative N<sub>2</sub> flux in relatively dry soils (less than or equal to 75<sup>th</sup> percentile soil moisture values) but deeper cores were associated with more positive N<sub>2</sub> flux in relatively wet soils (97.5 percentile of soil moisture, Fig. 2.6a, c). Slopes of the relationship between 24h N<sub>2</sub> flux and core depth were -0.313 at zero percentile soil moisture, -0.189 at 25<sup>th</sup> percentile soil moisture, -0.115 at 50<sup>th</sup> percentile soil moisture, -0.016 at 75<sup>th</sup> percentile soil moisture, and 0.508 at 97.5<sup>th</sup> percentile soil moisture (Fig. 2.6a). Similarly, slopes of the relationship between 48h N<sub>2</sub> flux and core depth were -0.378 at zero percentile soil moisture, -0.256 at 25<sup>th</sup> percentile soil moisture, -0.183 at 50<sup>th</sup> percentile soil moisture, -0.085 at 75<sup>th</sup> percentile soil moisture, and 0.435 at 97.5<sup>th</sup> percentile soil moisture (Fig. 2.6c).

The effect of hold time on N<sub>2</sub> flux depended on soil moisture at 24 (Table 2.4, Fig. 2.6b,  $p < 0.001$ ) and 48 h (Table 2.4, Fig. 2.6d,  $p < 0.001$ ). Longer hold times were associated with more positive N<sub>2</sub> flux in relatively dry soils (below 75<sup>th</sup> percentile soil moisture) but longer hold times were associated with more negative N<sub>2</sub> flux in relatively

wet soils (97.5 percentile soil moisture). Slopes of the relationship between 24h N<sub>2</sub> flux and hold time were 0.381 at zero percentile soil moisture, 0.213 at 25<sup>th</sup> percentile soil moisture, 0.112 at 50<sup>th</sup> percentile soil moisture, -0.021 at 75<sup>th</sup> percentile soil moisture, -0.734 at 97.5<sup>th</sup> percentile soil moisture (Fig. 2.6b). Slopes of the relationship between 48h N<sub>2</sub> flux and hold time were 0.536 at zero percentile soil moisture, 0.268 at 25<sup>th</sup> percentile soil moisture, 0.107 at 50<sup>th</sup> percentile soil moisture, -0.109 at 75<sup>th</sup> percentile soil moisture, and 1.252 at 97.5<sup>th</sup> percentile soil moisture (Fig. 2.6d). The steeper relationship between N<sub>2</sub> flux and hold time at 97.5<sup>th</sup> percentile soil moisture indicates a stronger interactive effect of soil moisture and hold time at 48h compared to 24h inundation. However, more overall variation in 24h N<sub>2</sub> flux is explained by fieldwork constraints compared with 48h N<sub>2</sub> flux.

Table 2.4. Final model results of field work constraints influencing N<sub>2</sub> flux (mg m<sup>-2</sup> h<sup>-1</sup>) at each incubation time point. Effect size represents percent difference from mean N<sub>2</sub> flux attributable to per unit change in each field work constraint.

Incubation time	Parameter	Estimate	Effect size	Std. error	p-value	F-value	Adjusted R <sup>2</sup>
24h	intercept	3.917	NA	3.671	0.286	15.29 (6, 459)	0.156
	Julian day	-0.011	-0.230	0.005	0.014		
	core depth (cm)	-0.356	-7.454	0.152	0.019		
	hold time (h)	0.440	9.213	0.124	< 0.001		
	soil moisture (g/g)	5.964	124.874	6.272	0.342		
	core depth:soil moisture	0.618	12.940	0.263	0.019		
	hold time:soil moisture	-0.838	-17.546	0.218	< 0.001		
48h	intercept	-1.735	NA	4.148	0.676	10.12 (5, 458)	0.090
	core depth (cm)	-0.421	-7.695	0.172	0.015		
	hold time (h)	0.630	11.515	0.143	< 0.001		
	soil moisture (g/g)	19.392	354.451	7.200	0.007		
	core depth:soil moisture	0.611	11.168	0.303	0.044		
	hold time:soil moisture	-1.344	-24.566	0.254	< 0.001		

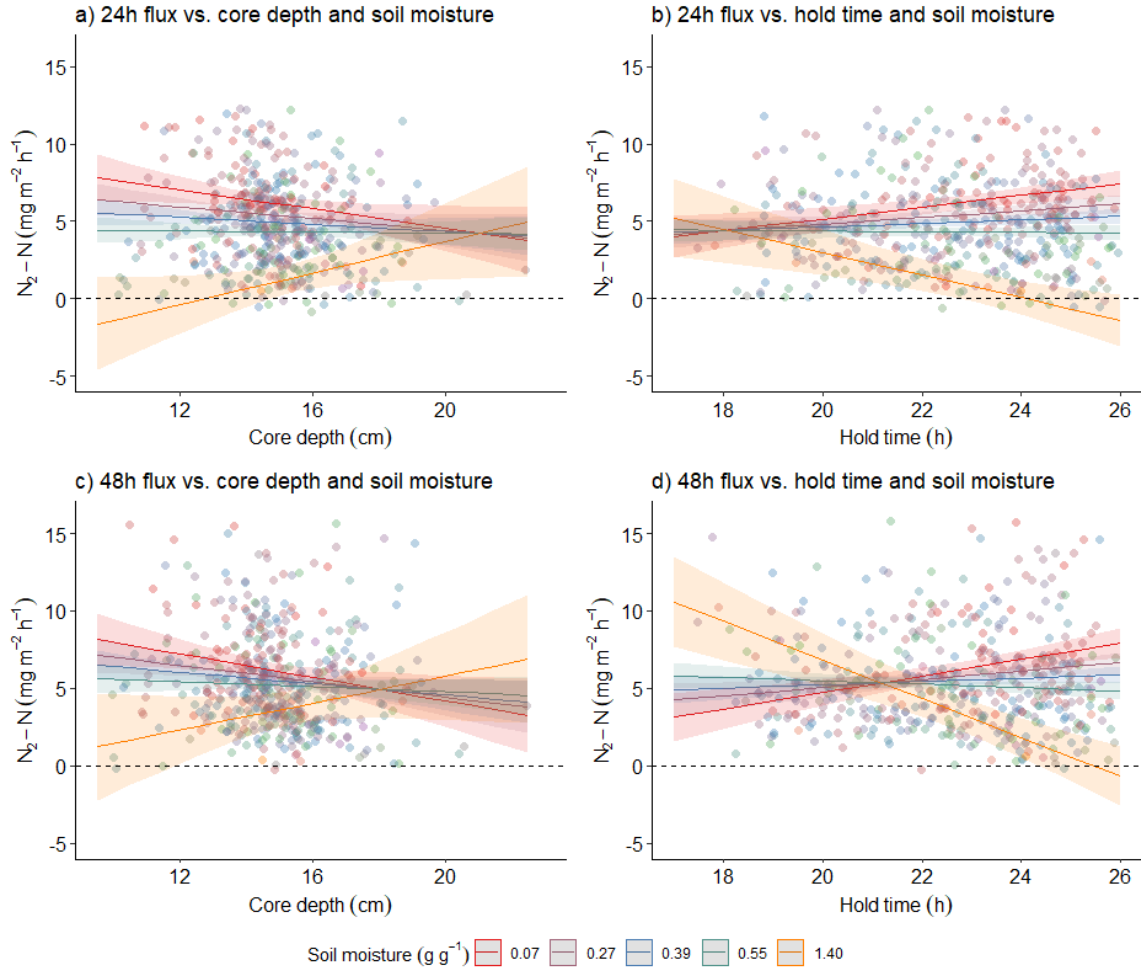


Figure 2.6. Response of  $N_2$  flux to fieldwork constraint-soil moisture interactions. Two-way interactions between core depth and soil moisture (a, c) and hold time and soil moisture (b, d) that influence  $N_2$  flux after 24 h (a, b) and 48 h (c, d) inundation.  $N_2$  flux is regressed against hold time for constant soil moisture values at 0, 25, 50, 75, and 97.5 percentiles corresponding to the range of soil moisture values shown visually in the legend above (0.07, 0.27, 0.39, 0.55, 1.40  $\text{g g}^{-1}$ ) with 95% confidence intervals for regression lines at each soil moisture level.

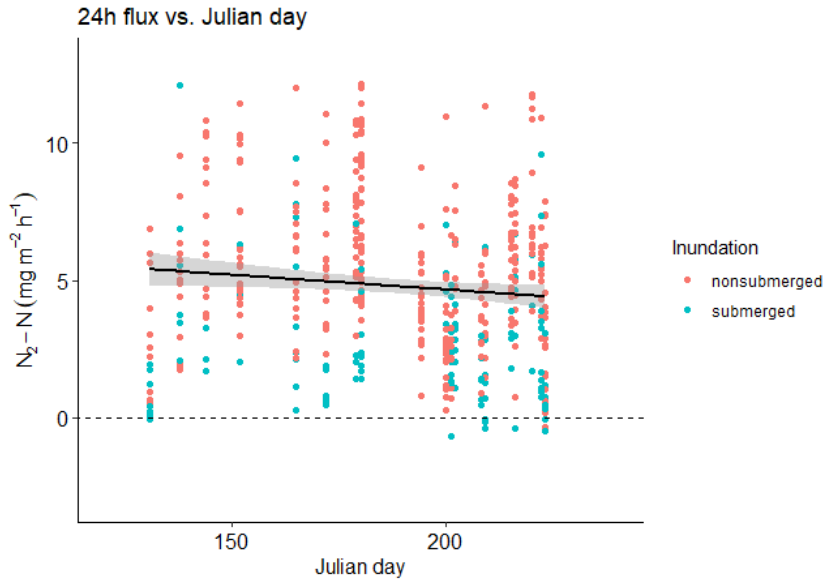


Figure 2.7. Relationship between the main effect of Julian day and  $N_2$  flux after 24 hours inundation. Julian day was the only significant main effect influencing  $N_2$  flux without an interaction with soil moisture (Table 2.4). Each point represents a soil core that was either submerged (blue) or not submerged (red) at the time of field collection. Binary submergence categories are represented visually but not statistically because of collinearity with soil moisture.

### ***Soil oxygen demand ( $O_2$ flux)***

The best model for the fieldwork constraint effects on  $O_2$  flux after 24 hours inundation included Julian day, core depth, hold time, and soil moisture. Field work constraints explained less than one percent of variation in  $O_2$  flux after 24 hours. The final model was not statistically significant (Table 2.5,  $F_{(6, 461)} = 1.563$ ,  $R^2 = 0.007$ ,  $p = 0.156$ ) and is not considered further.

Fieldwork constraints explained 3.4% of the variation in  $O_2$  flux after 48 hours inundation (Table 2.5, Fig. 2.8,  $F_{(5, 459)} = 4.26$ ,  $R^2 = 0.034$ ,  $p < 0.001$ ). The best model for the effects of fieldwork constraints on  $O_2$  flux after 48 hours inundation included Julian day, core depth, hold time, and soil moisture.  $O_2$  flux was  $0.960 \text{ mg m}^{-2} \text{ h}^{-1}$  more negative for each cm increase in core depth (Table 2.5, Fig 2.8a,  $p = 0.031$ ). This equates to a

1.017% increase in soil oxygen demand per cm increase in core depth. The influence of hold time on 48 h O<sub>2</sub> flux depended on soil moisture (Table 2.5, Fig 2.8b, p = 0.002). Slopes of the relationship between hold time and O<sub>2</sub> flux were -0.936 for zero percentile soil moisture, -0.122 for 25<sup>th</sup> percentile soil moisture, 0.364 for 50<sup>th</sup> percentile soil moisture, 1.014 for 75<sup>th</sup> percentile soil moisture, and 4.467 for 97.5<sup>th</sup> percentile (Fig. 2.8b). Longer hold time for cores with high soil moisture resulted in decreased (less negative) measurements of soil oxygen demand (SOD) after 48h incubation.

Table 2.5. Final model results of field work constraints influencing O<sub>2</sub> flux (mg m<sup>-2</sup> h<sup>-1</sup>) at each incubation time point. Effect size represents percent difference from mean O<sub>2</sub> flux attributable to per unit change in each field work constraint.

Incubation time	Parameter	Estimate	Effect size	Std. error	p-value	F-value	Adjusted R <sup>2</sup>
24h	intercept	1.814	NA	29.062	0.950	1.563 (6, 461)	0.007
	Julian day	-0.099	-0.164	0.088	0.263		
	core depth (cm)	-1.033	-1.708	0.620	0.097		
	hold time (h)	-1.329	-2.197	1.086	0.222		
	soil moisture (g/g)	-111.058	-183.597	49.108	0.024		
	Julian day:soil moisture	0.267	0.441	0.175	0.129		
	hold time:soil moisture	2.855	4.720	1.977	0.149		
48h	intercept	-42.411	NA	18.828	0.025	4.26 (5, 459)	0.034
	Julian day	-0.045	-0.048	0.028	0.109		
	core depth (cm)	-0.960	-1.017	0.442	0.031		
	hold time (h)	-1.219	-1.292	0.767	0.113		
	soil moisture (g/g)	-95.259	-100.931	30.496	0.002		
	hold time:soil moisture	4.061	4.303	1.334	0.002		

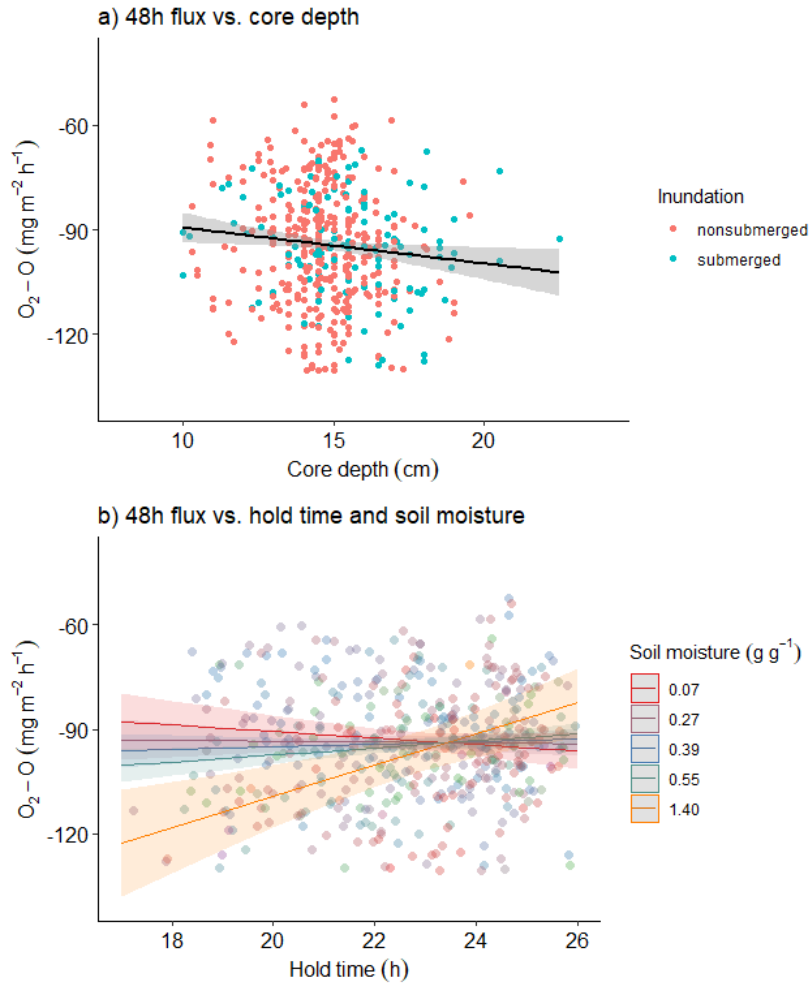


Figure 2.8. Response of soil oxygen demand (SOD) to fieldwork constraints. Effect of core depth on SOD after 48 h inundation (a) and interactive effects of hold time and soil moisture on SOD after 48 h inundation (b).  $O_2$  flux (negative flux represents SOD) is regressed against hold time for constant soil moisture values at 0, 25, 50, 75, and 97.5 percentiles corresponding to the range of soil moisture values shown visually in the legend above ( $0.07, 0.27, 0.39, 0.55, 1.40\ g\ g^{-1}$ ) with 95% confidence intervals for regression lines at each soil moisture level.

### Flow rate effects

Differences in flux due to average inflow vs. individual core outflow rates used in calculations were largest at 48h for  $O_2$  and  $N_2$  flux. Median  $O_2$  flux calculated with average inflow rates was  $1.708\ mg\ m^{-2}\ h^{-1}$  more positive than flux calculated with

individual outflow rates for each core (Table 2.6, Fig 2.9a.  $p < 0.001$ ). This equates to a 1.815% decrease in median SOD after 48h. Median  $N_2$  flux was  $0.089 \text{ mg m}^{-2} \text{ h}^{-1}$  more negative when average flow rates were used compared to individual outflow rates (Table 2.6, Fig 2.9b.  $p < 0.001$ ). This equates to a 1.855% decrease in  $N_2$  removal after 48h when average inflow rates were used.

Differences in  $NO_3$  and  $PO_4$  flux due to average inflow vs. individual outflow rates used in calculations were largest after initial (6h) measurements. Median  $NO_3$  flux was  $0.143 \text{ mg m}^{-2} \text{ h}^{-1}$  more positive when average inflow rates were used than flux calculated with individual outflow rates for each core (Table 2.6, Fig 2.9c.  $p < 0.001$ ). This equates to a 1.810% decrease in median initial (6h)  $NO_3$  uptake. Median  $PO_4$  flux was  $0.032 \text{ mg m}^{-2} \text{ h}^{-1}$  more positive when average flow rates were used (Table 2.6, Fig 2.9d.  $p < 0.001$ ). This equates to a 2.133% decrease in median initial (6h)  $PO_4$  uptake.

Table 2.6. Results of paired Wilcoxon t-tests showing differences in flux rates attributable to use of average inflow rates in flux calculations.

Flux rate	Time (h)	median effect of average inflow rate ( $\text{mg m}^{-2} \text{ h}^{-1}$ )	95% CI ( $\text{mg m}^{-2} \text{ h}^{-1}$ )	% difference from median flux with individual outflow rate	p-value	cores included	flow rate effect min, max ( $\text{mg m}^{-2} \text{ h}^{-1}$ )
$O_2$	24	1.025	0.802, 1.250	1.796	<0.001	599	-31.829, 9.718
	48	1.708	1.295, 2.079	1.815	<0.001	594	-35.125, 19.237
$N_2$	24	-0.073	-0.091, -0.057	-1.656	<0.001	599	-0.968, 3.807
	48	-0.089	-0.109, -0.068	-1.855	<0.001	594	-3.647, 2.838
$NO_3$	6	0.143	0.096, 0.194	1.810	<0.001	594	-34.857, 23.222
	24	0.058	0.007, 0.108	0.529	0.024	597	-22.679, 11.374
	48	0.203	0.134, 0.272	1.281	<0.001	595	-12.037, 4.490
$PO_4$	6	0.032	0.022, 0.043	2.133	<0.001	593	-1.368, 3.512
	24	0.013	0.006, 0.020	0.773	<0.001	597	-2.607, 0.526
	48	0.014	0.003, 0.018	1.026	0.005	595	-1.489, 0.581

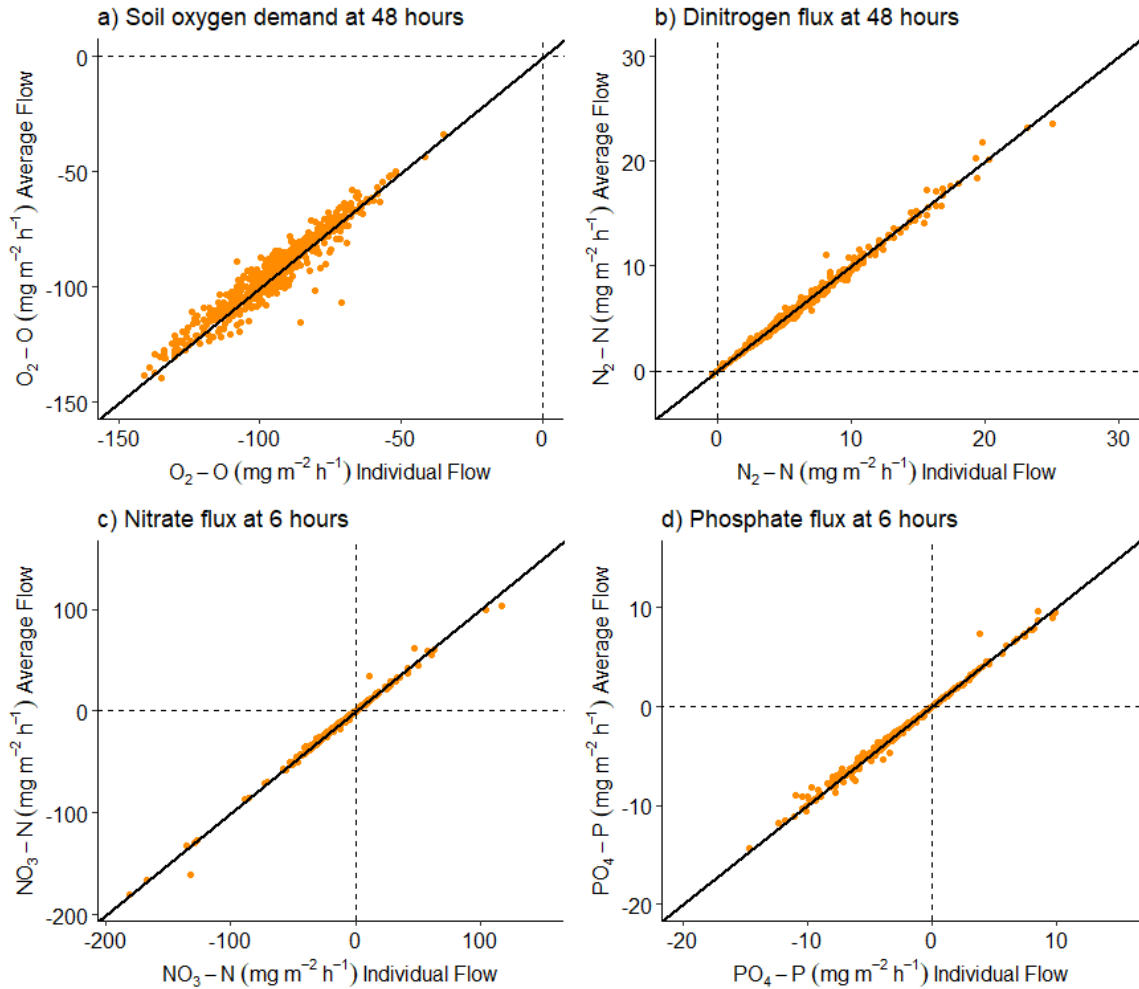


Figure 2.9. Nutrient flux rates calculated with individual outflow values for each core (x-axis) compared to flux calculated with average inflow rate from source water (y-axis). Each point represents a soil core (n = 594 in panels a and b and n = 595 in panels c and d). The black line in each panel represents a 1:1 ratio where all points would fall if there were no difference in flux due to use of average vs. individual flow rates. Largest effect sizes of average inflow use were observed after 48 hours incubation for soil oxygen demand (panel a - 1.82% median decrease) and N<sub>2</sub> flux (panel b - 1.86% median decrease), and after initial inundation for NO<sub>3</sub> (panel c - 1.81% median increase) and PO<sub>4</sub> flux (panel d - 2.133% median increase).

### Control core effects

Effects of control cores were largest after 48h for SOD, N<sub>2</sub>, NO<sub>3</sub>, and PO<sub>4</sub> flux.

Median SOD was 61.315 mg m<sup>-2</sup> h<sup>-1</sup> more positive (Table 2.7, Fig. 2.10a. p < 0.001), and

median  $\text{N}_2$  flux was  $0.741 \text{ mg m}^{-2} \text{ h}^{-1}$  more negative (Table 2.7, Fig. 2.10b.  $p = 0.026$ ) when control cores were used in calculations. Median  $\text{NO}_3$  flux was  $4.769 \text{ mg m}^{-2} \text{ h}^{-1}$  more positive (Table 2.7, Fig. 2.10c.  $p = 0.003$ ), and median  $\text{PO}_4$  flux was  $0.478 \text{ mg m}^{-2} \text{ h}^{-1}$  more positive (Table 2.7, Fig. 2.10d.  $p = 0.045$ ) when control cores were used in calculations. This equates to a 65.15% decrease in median SOD, a 15.44% decrease in median  $\text{N}_2$ -N removal, a 30.11% decrease in median  $\text{NO}_3$  uptake, and a 35.04% decrease in median  $\text{PO}_4$  uptake after 48 hours inundation when including control cores in the calculations.

Use of control cores in flux calculations affected relationships between  $\text{N}_2$  removal and SOD differently after 24 and 48h inundation. Quadratic polynomial regression showed similar trends in  $\text{N}_2$  flux and SOD relationships after 24h for both flux rates including (Table 2.8, Fig. 2.11a,  $F_{(2, 596)} = 149.4$ ,  $R^2 = 0.332$ ,  $p < 0.001$ ) and excluding (Table 2.8, Fig. 2.11c,  $F_{(2, 596)} = 166$ ,  $R^2 = 0.356$ ,  $p < 0.001$ ) control cores. Cubic polynomial regression showed more variable trends in 48h  $\text{N}_2$  flux and SOD relationships between flux rates including (Table 2.8, Fig 2.11b,  $F_{(3, 590)} = 44.9$ ,  $R^2 = 0.182$ ,  $p < 0.001$ ) and excluding (Table 2.8, Fig 2.11d,  $F_{(3, 590)} = 104.9$ ,  $R^2 = 0.345$ ,  $p < 0.001$ ) control cores after 48 hours inundation. Control cores were excluded from all other analyses in the present study, given raw effect sizes (Table 2.7, Fig. 2.10) and influence on biogeochemical relationships (Table 2.8, Fig. 2.11).

Table 2.7. Results of one-sample Wilcoxon t-test for effects of control core use in flux calculations.

Flux rate	Time (h)	median control core effect (mg m <sup>-2</sup> h <sup>-1</sup> )	95% CI (mg m <sup>-2</sup> h <sup>-1</sup> )	% difference from flux without control core	p-value	control core effect min, max (mg m <sup>-2</sup> h <sup>-1</sup> )
O <sub>2</sub>	24	27.556	23.737, 32.284	48.28	<0.001	1.36, 45.19
	48	61.315	54.022, 67.231	65.15	<0.001	-0.6815, 88.373
N <sub>2</sub>	24	-0.001	-0.235, 0.3583	-0.02	0.941	-1.098, 2.587
	48	-0.741	-1.182, -0.114	-15.44	0.026	-2.115, 1.836
NO <sub>3</sub>	6	-1.233	-4.444, 1.943	-15.61	0.409	-27.904, 18.652
	24	0.712	-3.664, 3.248	6.49	0.452	-46.896, 25.048
	48	4.769	1.709, 8.572	30.11	0.003	-3.693, 23.033
PO <sub>4</sub>	6	0.093	-0.251, 0.427	6.20	0.546	-4.992, 11.117
	24	0.089	-0.506, 0.500	5.29	0.709	-3.925, 2.379
	48	0.478	0.017, 0.783	35.04	0.045	-1.327, 1.609

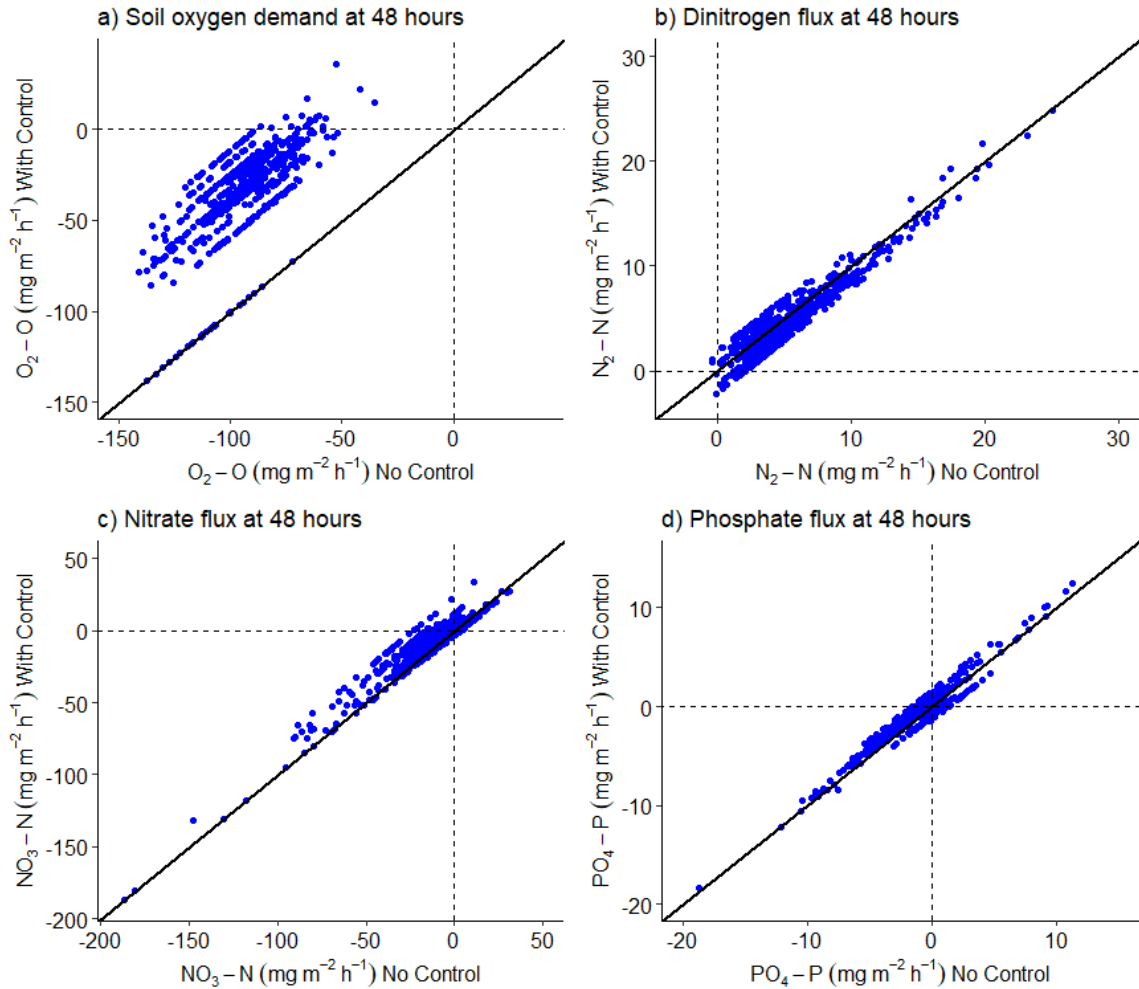


Figure 2.10. Nutrient flux rates calculated without (x-axis) and with (y-axis) control cores. Each point represents a soil core to visualize control core effects across the scale that each flux rate was measured. Paired Wilcoxon t-tests were conducted for each incubation ( $n=20$ ) because control core effects were constant for all cores in each incubation. The black line in each panel represents a 1:1 ratio where all points would fall if there were no difference in flux due to use of control cores in flux calculations.

Table 2.8. Polynomial regression results of relationships between N<sub>2</sub> flux (mg m<sup>-2</sup> h<sup>-1</sup>) and O<sub>2</sub> (mg m<sup>-2</sup> h<sup>-1</sup>) at 24 and 48h incubation times with and without control core included in calculations.

Incubation time	Control core	parameter	Estimate	Std. error	p-value	F-value	Adjusted R <sup>2</sup>
24h	yes	Intercept	4.944	0.109	< 0.001	149.4 (2, 596)	0.332
		O <sub>2</sub>	-45.595	2.670	< 0.001		
		(O <sub>2</sub> ) <sup>2</sup>	7.110	2.670	0.008		
	no	Intercept	4.944	0.107	< 0.001	166 (2, 596)	0.356
		O <sub>2</sub>	-46.695	2.620	< 0.001		
		(O <sub>2</sub> ) <sup>2</sup>	10.256	2.620	< 0.001		
48h	yes	Intercept	5.133	0.151	< 0.001	44.9 (3, 590)	0.182
		O <sub>2</sub>	-39.875	3.674	< 0.001		
		(O <sub>2</sub> ) <sup>2</sup>	-9.147	3.674	0.013		
		(O <sub>2</sub> ) <sup>3</sup>	12.030	3.674	0.001		
	no	Intercept	5.641	0.135	< 0.001	104.9 (3, 590)	0.345
		O <sub>2</sub>	-45.295	3.281	< 0.001		
		(O <sub>2</sub> ) <sup>2</sup>	33.589	3.281	< 0.001		
		(O <sub>2</sub> ) <sup>3</sup>	-14.420	3.281	< 0.001		

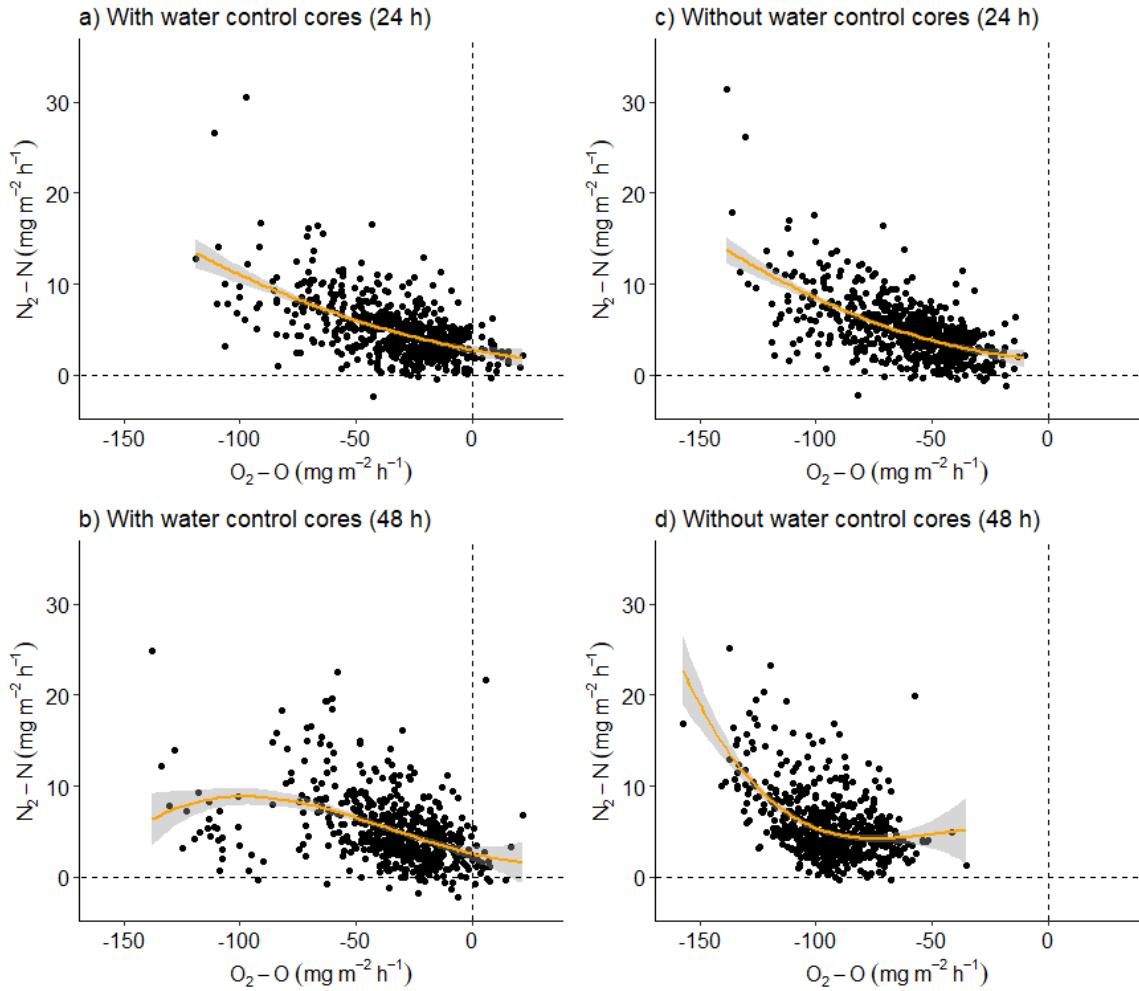


Figure 2.11. Relationships between  $N_2$  flux and soil oxygen demand with and without control cores. With water control cores after 24 h (panel a); 48 h incubation (panel b) and without water control cores after 24 h (panel c) and 48 h incubation (panel d). Second order (panels a and c) and third order (panels b and d) polynomial regressions were used to model relationships after selecting the linear model with the lowest AIC for each flux rate at each time point.

## Discussion

### Fieldwork constraints

Nutrient flux rates were influenced by Julian day, core depth, hold time, and soil moisture, but less than 16% of variation in flux rates was explained by these factors and differed between  $\text{NO}_3$ ,  $\text{PO}_4$ ,  $\text{N}_2$  flux, and SOD throughout incubations. Our flow-through incubation system was designed to maximize N and P uptake potential by saturating soils with synthetic water rich in  $\text{NO}_3$  and  $\text{PO}_4$ . This resulted in large variation in flux potential across the wide geographic range of incubated floodplain soils. Effect sizes, reported as percent change from mean flux ( $\text{mg m}^{-2} \text{h}^{-1}$ ) per unit change in each fieldwork constraint, must be interpreted within the context of the range of each fieldwork constraint included in this study. For example, effect sizes of soil moisture were generally large because a one-unit change in soil moisture covers most of the range included in this study, given soil moisture measurements from 0.07 to 1.40  $\text{g g}^{-1}$ . Effect sizes of Julian Day were comparatively small as the study included soil core collections over a range of 92 days. Core depth ranged over 13 cm and hold time ranged over 9 h in the current study. The range of these fieldwork constraints varies among flow-through core studies and potentially influences interpretation of results. The discussion below focuses on each fieldwork constraint as they influence multiple flux rates.

### *Julian day*

To the best of my knowledge, the current study compares nutrient flux rates across a wider geographic range with a larger sample size than any previous study employing flow-through soil/sediment incubation systems. Seasonal comparisons of

nutrient flux have been made (Scott et al., 2008; Smyth et al., 2013; Speir et al., 2017) and these studies were designed for comparison of seasonal differences. Soil cores were collected for the current study over a range of 92 days to constrain field collection to the growing season, assuming seasonal effects over this time would be minimal with the addition of  $\text{NO}_3$  and  $\text{PO}_4$  to source water. Significant relationships between Julian Day of field collection and nutrient flux need to be considered even though the amount of variation in flux rates explained by these relationships is relatively small.

The relationship between  $\text{NO}_3$  uptake (negative flux) and Julian Day differed between 24 and 48h inundation. There was a slight negative relationship after 24h inundation and a stronger positive relationship after 48h inundation. A positive relationship between 48h  $\text{NO}_3$  uptake and Julian day makes sense because microbial assimilation of  $\text{NO}_3$  is likely to increase over the course of the growing season where plant biomass and microbial growth are positively correlated (Wang et al., 2016). Wang et al. measured increases in microbial biomass N which positively correlated with plant biomass later in the growing season. If increased microbial biomass later in the growing season is driving  $\text{NO}_3$  uptake through assimilation, positive relationships between  $\text{NO}_3$  uptake and Julian day should be observed at 24 and 48 h. Interestingly, both  $\text{NO}_3$  uptake and  $\text{N}_2$  flux had slightly negative relationships with Julian Day after 24h incubation, indicating that an influence of Julian Day on  $\text{NO}_3$  uptake may negatively influence dissimilatory pathways leading to  $\text{N}_2$  production. There is a lack of research describing causal relationships between microbial growth and nutrient assimilation patterns during the growing season but there is evidence that dissimilatory  $\text{NO}_3$  uptake and denitrification increases later in the growing season in agricultural systems (Speir et al., 2017).

Combining isotopic labeling experiments (Glibert et al., 2019; Robertson et al., 2019) with flow-through incubations could improve quantification of relationships between nutrient retention, nutrient assimilation through microbial growth (McCarthy et al., 2007), and dissimilatory N reduction pathways in floodplain soils (Masta et al., 2022).

Accounting for seasonal influences of sample collection constraints is likely to improve estimates of ambient nutrient retention derived from flow-through incubations as flux rates are scaled up to areas of interest (Nifong & Taylor, 2022) and used to determine success of restoration trajectories (Smith et al., 2000). Smith et al. 2000 measured ambient denitrification (as N<sub>2</sub> flux) before and after a treatment wetland in southern California was reconfigured to minimize internal N loading to replace dense emergent vegetation with more deep open water. However, their pre-reconfiguration study period spanned January-March 1998 and their post-reconfiguration study period was in May 1999, with higher denitrification rates measured in May. Smith et al. 2000 carried out both March and May flow-through core incubations at 18°C but warmer *in situ* temperatures and agricultural runoff in May could have enhanced development of soil microbial denitrifying communities and subsequent denitrification rates (Cross et al., 2015; Evans et al., 2021), confounding interpretation of wetland reconfiguration benefits to denitrification. Future work that focuses on disentangling seasonal effects of temperature and nutrient delivery patterns affecting nutrient processing rates could improve understanding of ambient nutrient retention mechanisms. Such work will likely require more intensive experimental treatments of flow-through core incubations and repeated sampling of fewer study sites (i.e. Smith et al., 2000) than the current study.

### ***Core depth***

Collecting intact soil/sediment cores to a consistent depth is often impossible, especially in submerged environments (Nifong & Taylor, 2022). Core depth measurements are often reported and range over 10-15 cm (Kana et al., 1994) to 10-30 cm (Deek et al., 2012), 18-33 cm (Nifong & Taylor, 2022), and 25-40 cm (Kröger et al., 2014). The current study is the first, to the best of my knowledge, to quantify influence of intact soil core depth on  $\text{NO}_3$ ,  $\text{PO}_4$ ,  $\text{N}_2$  flux, and SOD over a depth range of 9.5 to 22.5 cm. Core depth was positively correlated with  $\text{NO}_3$  uptake at 6h and 24h inundation and influenced  $\text{N}_2$  flux differentially depending on soil moisture. The influence of core depth on  $\text{PO}_4$  uptake depended on soil moisture at 6h inundation but was directly positively correlated with  $\text{PO}_4$  uptake at 24h inundation. Soil oxygen demand was positively related to core depth at 48h inundation.

Smaller overlying water volumes associated with deeper cores should decrease water column residence times but residence times could be lengthened in deep cores if soils are porous and water flows through soil pore spaces (Rutherford & Nguyen, 2004). Increasing residence time is generally thought to improve  $\text{NO}_3$  uptake (James et al., 2008; Wollheim et al., 2014) but longer residence times are not always associated with increased nutrient uptake (Nifong & Taylor, 2021). Essentially, longer residence times allow nutrient molecules more time to interact with biotic and abiotic uptake mechanisms in a system. Presence of vegetation (Nifong & Taylor, 2021) or other potential uptake mechanisms in a system (i.e. soil core) can overshadow the influence of residence time on nutrient uptake rates. If longer residence times were facilitated by deeper cores with

porous soils in the current study and these factors increased  $\text{NO}_3$  uptake at 6 and 24 h, the effect did not continue through 48h inundation.

The influence of core depth on  $\text{N}_2$  flux was more consistent throughout incubations such that the relationship depended similarly on soil moisture at both 24 and 48h inundation. Core depth was positively correlated with  $\text{N}_2$  flux in cores with high soil moisture ( $1.4 \text{ g g}^{-1}$ ). Denitrification is typically the dominant  $\text{N}_2$  production pathway in wetlands but see (Burgin & Hamilton, 2007; Hoagland et al., 2019). Denitrification rates generally increase with soil moisture (Almaraz et al., 2020; Olde Venterink et al., 2002) but hysteresis responses of denitrification have been measured as soils wet and dry (Groffman & Tiedje, 1988). Essentially, denitrification rates can be different at the same soil moisture content depending on whether soils are in the process of wetting or drying (Groffman & Tiedje, 1988). Soil cores in the current study were always in the wetting process but future flow-through core studies that focus on nutrient flux responses to wetting and drying are likely to improve floodplain nutrient retention estimates (Baldwin & Mitchell, 2000; Peng et al., 2019) as flood regimes change (Schramm et al., 2009). Deeper soil cores with high moisture content may be more conducive to denitrification because of increased soil volume where stepwise N reduction processes can occur throughout inundation. Interaction depth of the water column with the soil likely varies with soil type/porosity but was not measured for the diversity of soils encountered in the current study. Dye tracing is often used to measure hyporheic flow paths in rivers (Fernald et al., 2001) and similar methods can be used to determine interaction depth of water columns and sediments in flow-through core incubations. This information is often gained through pilot studies but does not appear to be included in any publications of

flow-through core incubations. Water column interactions with sandy lake sediments typically reach 5 cm in flow through incubations with flow rates  $\sim 2$  mL/min (Murdock et al. unpublished data). Future flow-through incubation studies should include estimates of core depth, residence times, and water column mixing depth within diverse sediments/soils.

Different responses of  $\text{NO}_3$  uptake and  $\text{N}_2$  flux to core depth over the course of incubations show that these N cycling processes are not coupled to experimental artifacts caused by differences in core depth, as would be expected if  $\text{NO}_3$  uptake were driving  $\text{N}_2$  flux across a gradient of core depths. This decoupling indicates that core depth influences biotic assimilation and alternative dissimilatory pathways (Burgin & Hamilton, 2007) as mechanisms of N retention and removal among soil cores in the current study.

Phosphate uptake after 24h inundation was positively correlated with deeper soil cores regardless of soil moisture. These results corroborate the positive relationship measured between  $\text{NO}_3$  uptake and core depth by showing an expected positive relationship between  $\text{PO}_4$  uptake and residence time (Lu et al., 2009; Skinner, 2022; Woltemade, 2000). Essentially, deeper cores may result in longer water column residence times within the first 24h of incubation if soils are porous enough to facilitate flow of nutrients beyond 10 cm soil depth. Cores with soil moisture less than  $0.55 \text{ g g}^{-1}$  support this trend for  $\text{PO}_4$  uptake at the earliest measurements (6h) after inundation, showing a slightly positive relationship with 6h  $\text{PO}_4$  uptake. However, the negative relationship between 6h  $\text{PO}_4$  uptake and core depth for cores with soil moisture at  $1.4 \text{ g g}^{-1}$  contrasts with the trend measured at 24h. Phosphorus release is often attributed to abiotic desorption from cations upon rewetting (Kinsman-Costello et al., 2014; Peng et al., 2019)

but heterotrophic P mineralization may also play a role. Deeper cores with high soil moisture ( $\sim 1.4 \text{ g g}^{-1}$ ) likely contain more heterotrophic biomass (Urakawa & Bernhard, 2017) which could potentially mineralize organic P during initial inundation (Cotner et al., 2000), leading to the observed negative relationship between 6h  $\text{PO}_4$  uptake and core depth at high soil moisture content.

An investigation of P flux dynamics in two forested floodplain wetlands with similar inundation regimes revealed different spatial patterns in P sorption potentials, but soil aluminum content was an important driver in both wetlands (Bruland & Richardson, 2004). Bruland and Richardson's 2004 study exemplifies that variation in nutrient flux between two similar wetlands can be driven by specific soil parameters (i.e. aluminum content) that are not often measured in flow-through incubation studies. Potential variation in nutrient flux is amplified in the analysis I present here due to the wide geographic range of soil collection and differences in post-restoration successional stage among WRP easements. This natural variation underlies differences in nutrient flux attributed to soil core depth in the discussion above. Future flow-through core incubation studies should consider soil properties that vary with depth and influence spatially heterogeneous patterns of floodplain nutrient flux (Appling et al., 2014; Wohl, 2021).

### ***Hold time***

Flow-through core incubation studies often report that soil was collected in the field and transported on ice to the laboratory incubation setup within 24h. Variation in sample collection and transport time (i.e. hold time) is unavoidable in field ecology. However, results of the current study show that variations in intact soil core hold time between 17 and 26 hours can influence nutrient flux measurements.

Effects of hold time depended on soil moisture for N<sub>2</sub>, PO<sub>4</sub>, and O<sub>2</sub> flux, but not NO<sub>3</sub> flux. The relationship of N<sub>2</sub> flux to hold time shifts from slightly positive at soil moisture below 0.55 g g<sup>-1</sup> to clearly negative at soil moisture at 1.4 g g<sup>-1</sup>. While soil cores were placed on ice during transport to limit microbial activity, lowering the temperature relative to field conditions may have inadvertently increased dissolved oxygen concentrations in cores with high soil moisture. The final step of denitrification (N<sub>2</sub>O → N<sub>2</sub>) is inhibited in the presence of oxygen (Knowles, 1982; Seitzinger, 1988). Longer times on ice may have altered the redox environment in cores with high soil moisture so that N<sub>2</sub> production declined with hold time. However, the negative relationship between N<sub>2</sub> flux and hold time for cores with high soil moisture was stronger after 48h inundation when redox should have lowered to the point of promoting N<sub>2</sub> production (Dee & Tank, 2020). Interestingly, there was a strong negative relationship observed between 48h SOD and hold time at 1.4 g g<sup>-1</sup> soil moisture, while relationships between 48h SOD and hold time were more positive or only slightly negative at lower soil moisture values. Complementary results between 48h N<sub>2</sub> flux and 48h SOD indicate a likely effect of hold time on redox conditions for high moisture soils, possibly related to transport on ice. Further work is needed to determine mechanisms that inhibit N<sub>2</sub> production and SOD in high moisture soils with longer hold times.

Loss of PO<sub>4</sub> uptake capacity with longer hold times was observed for cores with higher soil moisture and this relationship was strongest after 6h inundation. This result is unexpected, given the negative relationships of both N<sub>2</sub> flux and SOD with longer hold times in cores with high soil moisture. Phosphate uptake should be promoted under oxidizing conditions that inhibit N<sub>2</sub> flux (Ardón et al., 2010; Skinner, 2022) but PO<sub>4</sub>

uptake was generally higher for soil cores with high moisture content ( $\sim 1.4 \text{ g g}^{-1}$ ) and negatively associated with hold time. Consistently moist soils have been shown to release less P upon rewetting than drier soils (Aldous et al., 2005). Results from the current study indicate that the positive relationship between P retention and soil moisture is negatively influenced by hold time. Mechanisms by which hold time and soil moisture interact to influence P retention and release in soil need further investigation.

### ***Soil moisture***

Soil moisture has not been measured for previous flow-through core incubations because most soils are already submerged at the time of field collection. However, soil moisture measurements are frequently used to investigate soil nutrient cycling processes (Burgin et al., 2010; Burgin & Groffman, 2012; McMillan & Noe, 2017; Ruser et al., 2006). Results of the current study show that interactions between soil moisture during sample collection and other fieldwork constraints influence nutrient flux measurements, especially  $\text{N}_2$  and  $\text{PO}_4$  flux. Soil moisture was positively related to  $\text{NO}_3$  uptake (negative flux) independent of other fieldwork constraints throughout the incubation. Studies of denitrification in terrestrial ecosystems often measure soil moisture as it positively influences N reduction processes (Almaraz et al., 2020). Flow-through incubations are increasingly being used to quantify nutrient retention processes among restored wetlands that vary in soil inundation, such as WRP monitoring efforts in the current study and the H2Ohio program (Ohio Departments of Natural Resources, 2023). Soil moisture measurements during field collection can be integrated with topographical analyses and nutrient flux measurements over time (Duncan et al., 2013) to model (Mostovoy &

Anantharaj, 2008) and improve understanding of the influences of drying and rewetting on nutrient retention processes.

### **Flow rate effects**

The method of measuring flow rate through continuous core incubation systems can influence nutrient flux rates derived from these incubations. However, the effect size is very small relative to median flux rates of  $\text{NO}_3$ ,  $\text{PO}_4$ ,  $\text{N}_2$  and  $\text{O}_2$ . Median SOD (negative  $\text{O}_2$  flux),  $\text{N}_2$ ,  $\text{NO}_3$ , and  $\text{PO}_4$  flux rates were compressed by use of average inflow rates compared to individual outflow rates from individual cores, meaning that flux was slightly closer to zero for all gas/nutrient species. Flux rates decreased less than 2.2% for all gases/nutrients relative to median flux. Generally, these effects represent a slight measurement error within incubation flux rate calculations due to slightly shorter residence times (faster flow rates) in of the majority of core water columns than would be expected by measuring average inflow rates to cores set to a target rate (i.e. 1.8 mL/min). Future studies that systematically vary flow rates using a peristaltic pump to test the effect of residence time on nutrient flux rates (Miller-Way & Twilley, 1996) should account for variation in flow for each core to improve accuracy of effect size estimates of residence time on nutrient flux.

### **Control core effects**

Control core effects observed in this study were unexpectedly large. Substantial amounts of  $\text{O}_2$  (65% of median flux in soil cores) can be consumed within water control cores. The effect size is smaller for  $\text{N}_2$ , which can be consumed in control cores at 15% of the median  $\text{N}_2$  production rate from soil cores. Control cores can consume up to 30%

median  $\text{NO}_3$  and 35% of median  $\text{PO}_4$  uptake observed in soil cores. Control core effect sizes do appear to be smaller than biological processes expected from natural water. Previous flow-through incubations measuring denitrification in lakes showed that water column control cores can consume  $\text{NO}_3$  at 40% of the rate of lake sediments, but the range of water column effects spanned from -6 to 125% of sediment  $\text{NO}_3$  uptake (Grantz et al., 2012). We dosed filtered (1  $\mu\text{m}$  pore size) river water to elevate  $\text{NO}_3$  and  $\text{PO}_4$  concentrations to 10 mg  $\text{NO}_3\text{-N/L}$  and 1 mg  $\text{PO}_4\text{-P/L}$  in preliminary core incubations in 2019. Control cores with filtered river water consumed 85% of soil core  $\text{O}_2$  consumption and 40% of soil core  $\text{N}_2$  production. Phosphate and  $\text{NO}_3$  consumption in river water control cores was greater than that attributable directly to the soil. However, this biological activity should not occur in synthetic water. It is unlikely that enough microbial life was present on any core materials to account for the rates of nutrient consumption measured in control cores. Physical sorption processes involving oxidation of rubber caps on core bottoms are more likely (Li & Koenig, 2005). More experiments testing effects of different core incubation materials are needed to identify potential mechanisms of control core effects.

We elected to exclude control cores from all other flux calculations analyzed in this project for two reasons. First, negative  $\text{O}_2$  flux is expected as a measure of SOD as these were incubated in the dark, but we demonstrate  $\text{O}_2$  production attributed to some inundated soils when control cores are included in flux calculation. Second, robust directional relationships are expected between  $\text{N}_2$  flux and SOD, as  $\text{N}_2$  flux is driven by anaerobic processes (i.e. denitrification and anammox) but this was not the case for our data when control cores were included in flux calculations, especially after 48 hours

inundation. Use of control cores flux calculations in the current study would have resulted in a conclusion that 48h N<sub>2</sub> flux had a muted response to high rates of SOD, while the strongest relationship between N<sub>2</sub> flux and SOD occurred when SOD is near zero. Without control cores included, 48h N<sub>2</sub> flux showed a strong positive relationship with high rates of SOD but the relationship was muted at lower rates of SOD, as observed in the literature. If effects of control cores are influenced by rubber caps on core bottoms, these core materials (buried under 10-20 cm of soil) are less likely to influence whole soil core flux calculated without blank control cores.

### **Conclusions and recommendations**

The relatively large effects sizes of Julian day, core depth, hold time, and soil moisture explain relatively little variation in PO<sub>4</sub>, NO<sub>3</sub>, N<sub>2</sub> flux, and SOD. This highlights the variability in nutrient cycling processes and potential maximum rates across restored floodplain wetlands. The geographic scale of our study necessitated core collection across a broader seasonal gradient than would have been ideal for strictly controlled comparisons. Nutrient flux from soils of a given wetland likely behave differently in May compared with August. However, our large sample size provides a robust dataset to assess those differences within the context of the wide variation in flux rates observed across WRP easements.

Variation in hold times for cores was unavoidable given the time required to collect 30 soil cores from across large wetlands and transport them several hours to the laboratory for incubation. The mechanisms causing the interactive effects of hold time and soil moisture on PO<sub>4</sub>, N<sub>2</sub> flux are unclear biogeochemically, and pose a problem for ensuring all soil cores are treated consistently between collection and incubation.

Methods of core transport, such as temperature regulation with ice and the decision to transport submerged cores with full water columns or siphoning in the field, should be evaluated in future studies. The question posed in this study is primarily methodological, so I describe these interactive effects such that the relationship between flux rates and hold time is influenced by soil moisture. Conversely, studies focused on ecological predictors of nutrient flux may describe the relationship between soil moisture and nutrient flux being influenced by hold time.

Variation in soil core depth from the 15 cm target was not ideal, but sometimes essential to ensure that intact soil cores remained intact after collection (Nifong & Taylor, 2022). Some cores required multiple attempts to collect intact. Some root structures were so integrated with soil structure (sometimes unconsolidated muck) that we were unable to extrude bottom portions of deep cores to remove excess deep soil without tearing apart the 15 cm of soil we intended to collect. Some dry soils were so impenetrable that we were unable to hammer our steel coring apparatus 15 cm into the ground. Variation in core depth is a necessary artifact of an attempt to consistently sample soils of highly variable structural characteristics. Inclusion of soil structural metrics (i.e. Peng et al. 2019) that vary with soil depth (Appling et al., 2014) in future flow-through core incubation studies should enable more predictive comparisons of nutrient flux across lake (Grantz et al., 2012), stream (Smith et al., 2006), wetland (Smyth et al., 2013), and pond (Hohman et al., 2021) environments.

Soil moisture measurements in our study represented an ecological starting point for cores at the time of collection. Floodplain soils experience different moisture regimes over time as floods advance and recede at increasingly variable rates in the Mississippi

River Valley (Schramm et al., 2009). Our study is the first I know of to systematically measure flux rates of 600 soil cores from a broad range of floodplain soil moisture regimes. Studies using flow-through incubations for nutrient flux measurements almost always collect soil/sediment cores from submerged environments. Soil moisture values at the low end for our study and their influence on nutrient flux patterns discussed above may not be directly relevant for flow-through incubations of permanently submerged soils. However, increasing drought and flood frequencies suggest less predictable inundation regimes in the future, especially for floodplain wetlands (Poff, 2002). Understanding soil moisture as a strong interactive driver of nutrient cycling processes will likely increase in relevance with less predictable climate patterns.

Taken together, field work constraints of Julian day, core depth, hold time, and soil moisture have relatively strong but variable influence on nutrient flux rates over the ranges we measured. Quantitatively correcting for these influences is unlikely to be helpful in improving nutrient flux measurements, given variability in our data. Rather, relationships described in this study will be helpful for informing design of large-scale soil core studies and facilitate qualitative discussion of individual wetland features that inform and constrain our ability to comprehensively sample any site.

# **CHAPTER 3: NUTRIENT STORAGE AND FLUX IN SURFICIAL SOILS OF FLOODPLAIN WETLANDS: SCALING UP FROM SOIL CORES TO WRP MANAGEMENT AREAS**

## **Abstract**

Comprehensive regional-scale monitoring of nutrient retention capacity in restored floodplain wetlands is rarely conducted due to financial and logistical constraints. Scaling a few localized measurements across floodplain landscapes to represent regional patterns can introduce and compound biases that influence ecosystem level estimates. I focus this chapter on evaluation of soil nutrient storage and flux measurements made using flow-through core incubations during monitoring of 11 wetland easements enrolled in the USDA Natural Resources Conservation Service's Wetlands Reserve Program (WRP). Specifically, I compare interpolated and extrapolated estimates of soil measurements to understand how floodplain nutrient processing estimates are influenced by topographical variation within sampling areas. I found that inverse distance weighted (IDW) interpolation made good predictions for soil pH (< 10 % error), made relatively poor predictions of soil nutrient storage, moisture, and bulk density (between 20 and 65% error), and was particularly error prone in predicting dissolved nutrient flux (> 100% error) within easements. Topographical variation was not significantly related to interpolation error for any soil measurements. At the whole easement scale, all IDW interpolated predictions of soil nutrient storage and flux fell within 95% confidence intervals of extrapolated estimates. However, extrapolation

should be preferred to interpolation for the current dataset so that variation of nutrient measurements within and between individual WRP habitats (i.e. tree plantings as they mature to forests) can be more precisely quantified. Remnant forests stored 21% more nitrogen (N) in surficial soils than tree plantings. Remnant forest soil carbon (C) tended to be higher than tree plantings, but the difference was not statistically significant. Surficial soil phosphorus (P) storage, initial nitrate (NO<sub>3</sub>) flux, and phosphate (PO<sub>4</sub>) flux did not differ between remnant forests and tree plantings among easements. Differences in elevation between soil core locations within tree planting restorations among easements explained more variation in surficial soil C storage and initial PO<sub>4</sub> flux, but tree planting age explained more variation in surficial soil P storage and initial NO<sub>3</sub> flux. Soil core elevation among remnant forest habitats was correlated with surficial soil C and N storage and initial PO<sub>4</sub> flux, but not initial NO<sub>3</sub> flux or P storage in surficial soils. Overall, variation in soil nutrient measurements between easements was greater than variation between remnant forest and tree planting habitats. Continuing work should seek to identify landscape-scale features, in addition to topography within easements, that influence soil nutrient storage and flux so that measurements made within current WRP easements can be used to identify floodplain areas most likely to yield nutrient retention benefits through future WRP enrollment.

## **Introduction**

How do discrete functional measurements represent ecosystem processes at different scales? The issue of scale in ecology has been widely recognized (Chave, 2013; Wiens, 1989) and many solutions to scaling issues focus on relationships between

biodiversity and ecosystem functions within theoretical frameworks of community ecology and food webs (Gonzalez et al., 2020). There is a growing need to accurately scale nutrient flux measurements in localized agricultural areas that influence cultural eutrophication (Glibert, 2020; Peñuelas & Sardans, 2022), especially in the Mississippi River Basin (Alexander et al., 2008; Mitsch et al., 2001; Schramm et al., 2009; White et al., 2014). Financial and logistical constraints of field work necessitate that nutrient retention measurements made at local scales be extrapolated across represented areas (Pollard, 2022) or interpolated between measured locations (Dolph et al., 2022) to represent regional and/or global trends and inform nutrient management decisions outside of areas where nutrients were directly measured. Experimental and spatial errors associated with local scale estimates of nutrient storage and flux are compounded when scaled across landscapes (Groffman et al., 2009; Orr et al., 2014). Thus, it is imperative to investigate sources of error and sampling bias that exist within datasets to be extrapolated and/or interpolated. Such investigations will help determine how different scaling methods affect estimates and interpretation of increased spatial-scale assessments.

Wetland restoration has been adopted by managers as an effective way of improving ecosystem services of nutrient retention, flood control, and biodiversity enhancement (Hefting et al., 2013; Mitsch & Gosselink, 2000; Zedler, 2003). Re-establishment of bottomland hardwood forests (Gordon et al., 2020; Lowrance et al., 1984) and hydrological connections between rivers and floodplains (Hurst et al., 2016; Noe et al., 2013) improve wetland nutrient retention rates through sediment deposition, abiotic sorption, and assimilatory and dissimilatory biotic nutrient uptake. Nitrogen (N) and phosphorus (P) cycling rates within floodplain soils are infamously heterogeneous

(Bruland & Richardson, 2004; Duncan et al., 2013; Groffman et al., 2009; Orr et al., 2014; Peng et al., 2019) and tradeoffs between N and P retention goals can limit effectiveness of wetland restoration practices (Hansson et al., 2005). Nitrate ( $\text{NO}_3$ ) removal from floodwater is promoted in inundated, anaerobic environments that facilitate denitrification (Groffman & Tiedje, 1988), but phosphate ( $\text{PO}_4$ ) release from soil to the water column is promoted when dry soils become anoxic after inundation (Aldous et al., 2005).

Microtopographical features within floodplains are slight depressional (hollows) and elevated (hummocks) areas that differentially retain water, microbiota, and nutrients over time. These physical, chemical, and biological differences can lead to hot spots and hot moments of microbial nutrient processing and abiotic sorption (Kuzyakov & Blagodatskaya, 2015; McClain et al., 2003). Distributions of nutrient processing hotspots create a mosaic of nutrient transformations across floodplains (Appling et al., 2014) that occur at the soil-water interface when soils are inundated (i.e. hot moments). Duncan et al. (2013) found that 99% of denitrification activity in the top 10 cm of soil occurred in less than 1% of riparian floodplain area due to the distribution of sparse but biogeochemically significant low-lying (hollow) areas.

Increased flooding frequency and lower predictability has led to less reliable agricultural harvests in the Lower Mississippi River Valley, especially for croplands in low-lying areas. Landowners often enroll marginally productive farmland in the Wetlands Reserve Program (WRP), now the Wetlands Reserve Enhancement Partnership (WREP), implemented by the USDA's Natural Resources Conservation Service, where they are compensated for lost agricultural value and croplands are converted to

bottomland hardwood forests over time (King et al., 2006). Restoration practices within WRP are diverse but can be generally categorized as tree plantings, altering site topography to create shallow water areas, and allowing the return of natural vegetation and hydrology. Most WRP easements include sections of remnant bottomland hardwood forests that were detectable via satellite imagery before restorations began. The diversity of wetland easements enrolled in WRP provides an excellent setting to assess methods of scaling up nutrient retention measurements over topographically variable floodplains.

The current study is derived from a dataset generated as part of a large-scale monitoring project aimed at estimating nutrient retention capacity of WRP easements in west Tennessee and Kentucky, USA. Whole wetland inflow-outflow measurements of nutrient concentrations facilitate understanding of ambient nutrient flux through the system. However, whole wetland measurements preclude identification of habitat/restoration-specific nutrient retention rates, nutrient cycling hotspots and associated soil properties, and limit a mechanistic understanding of observed changes in water nutrient concentrations. We chose to focus monitoring efforts on nutrient cycling processes at the soil-water interface using continuous flow-through soil core incubations with consistent inflowing water nutrient concentrations for soil samples collected across WRP easements. This approach facilitates mechanistic understanding of soil structural properties in relation to soil nutrient flux but limits the ability to scale these point measurements back up to whole easements, or areas within easements (i.e. tree plantings), if experimental error is introduced during the soil collection and incubation process. Extrapolation provides a simpler method of scaling up, but interpolation

facilitates consideration of spatial relationships between measurements at different sampled locations.

The objectives of this study were: (1) compare interpolated estimates of soil nutrient content, pH, moisture, bulk density, and initial NO<sub>3</sub> and PO<sub>4</sub> flux rates among each of eight easements where available digital elevation model (DEM) units were consistent (2) quantify the influence of easement topography, variation in distance between core collection locations within each easement, and measurement variation of nutrient metrics on precision of interpolated estimates of soil nutrient content, moisture, pH, bulk density, and initial NO<sub>3</sub> and PO<sub>4</sub> flux rates after inundation (3) compare interpolated estimates of nutrient storage and flux with extrapolated estimates in terms of nutrient mass retained per hectare, (4) assess relationships between extrapolated estimates of nutrient storage/flux among tree planting and remnant forest habitats in consideration of tree planting restoration age and elevation above sea level. I focus on tree planting restorations in objective 4 because this was the most consistently implemented restoration practice among easements, and tree plantings are more ecologically comparable to remnant forest “reference” habitats, which were also consistently sampled among easements, more so than excavated shallow water or naturally regenerated areas.

## **Methods**

### **Easement selection**

I selected eight WRP easements with consistently collected soil parameters and digital elevation model (DEM) units covering all core locations to address objectives 1-3.

Restoration age for 6/8 of these easements ranged from 3-6 years, and 2/8 restorations were 18-20 years old. I included an additional easement with 8 years since restoration, and two easements with 12 years since restoration, in analyses for objective 4 focused on tree planting age (n = 11). These three additional easements had 1 m vertical DEM resolution, lower than the eight easements used in objectives 1-3, which had 0.3048 m vertical resolution (see Topographical analyses below).

### **Soil core collection and transport**

We collected 30 pairs of intact soil cores from each of the 11 WRP easements included in the current study, resulting in 60 total cores per easement. Each pair of cores was collected within 30 cm<sup>2</sup> using 7.62 x 30 cm acrylic tubes. Cores were either collected by hand or acrylic tubes were placed in steel housing and hammered into the soil, depending on soil rigidity and logistical needs. Cores were collected to a target depth of 15 cm but some variation in core depth was unavoidable (see chapter 2). Cores collected from submerged locations were filled with overlying water during transport to limit further soil disturbance. All intact soil cores were placed on ice as soon as possible after collection and transported to the laboratory to begin incubation within 17-26 hours post field collection time. All incubation cores were stored in an environmental chamber at 24°C overnight before incubation beginning at 08:00 the following morning. The second core from each pair was refrigerated at 4°C until processing for total carbon (soil C), total nitrogen (soil N), available phosphorus (soil P), soil pH, moisture content, and bulk density within the top 5 cm. We focused on the top 5 cm for analyses of soil properties because this soil volume is prone to respond to nutrient loading (Morris & Bradley, 1999)

and wetland soil studies often subsection deeper samples by 5 cm increments (Hinson et al., 2017).

### **Soil property analyses**

Soil from each core was homogenized by hand mixing with a putty scraper until visual homogenization was achieved. Soil moisture was measured gravimetrically following (Evelt et al., 2009) by weighing a 30 g subsample of soil for each core, then drying each subsample at 105°C to a constant weight. Soil moisture ( $\text{g g}^{-1}$ ) was reported as weight lost after drying divided by the dry weight of each soil sample. Soil bulk density ( $\text{g cm}^{-3}$ ) was calculated by dividing the dry weight of each soil subsample (g) by the soil volume in the top 5 cm of each core ( $228.02 \text{ cm}^3$ ). Soil pH was measured by mixing a 10 g subsample from each core with 20 mL deionized water with neutral pH, stirred for approximately 10 seconds every five minutes for 30 minutes, and allowed to settle for 30 minutes before measuring pH of the solutions with an electrode (Reddy et al., 2013). A subsample from each dried soil core was weighed and shipped to the Soil Testing Laboratory at Kansas State University where total carbon (C) and total nitrogen (N) was measured for each sample using catalytic combustion to  $\text{CO}_2$  and  $\text{N}_2$ , respectively. Soil available phosphorus (P) was measured by Mehlich-3 extraction procedures (Mehlich, 1984).

Soil nutrients were reported as  $\text{mg g}^{-1}$  soil within each core and scaled to  $\text{g m}^{-2}$  to represent grams of each nutrient in the top 5 cm of soil over one square meter, accounting for bulk density of each soil core. Essentially, each pair of soil cores were assumed to be structurally and functionally representative of one square meter of surficial soil at each of

the 30 collection locations within each WRP easement, acknowledging that hotspots of soil biogeochemical activity can occur at smaller scales (Groffman et al., 2009; Kuzyakov & Blagodatskaya, 2015; McClain et al., 2003; Vidon et al., 2010). I describe further extrapolation and interpolation of soil properties below (see Data processing and analyses). Importantly, our sample size for each easement was limited, compared with other studies focused only on evaluation of soil structure using geostatistics (Oliver & Webster, 2014), because of labor intensive flow-through incubations that accompanied each pair of soil cores.

### **Flow-through soil core incubations**

Overlying water was siphoned off submerged cores immediately after placing them in the incubation chamber held at 24°C before attaching each core to the flow-through system. Nitrate ( $\text{NO}_3$ ) and phosphate ( $\text{PO}_4$ ) concentrations of inflowing water were elevated to  $\sim 10$  mg  $\text{NO}_3\text{-N/L}$  and  $\sim 1$  mg  $\text{PO}_4\text{-P/L}$ , so that nutrient flux rates from soil cores approximated maximum uptake capacity for agricultural soils (Speir et al., 2017). Our flow-through incubation setup is discussed in further detail in chapter 2. Briefly, water was delivered to each soil core via peristaltic pump and flowed through cores at an average rate of 1.8 mL/min, though individual outflow rates for each core were used in nutrient flux calculations at the soil-water interface. Outflowing water samples were collected as soon as each core filled. It took an average of 6.4 h for cores to fill but this time varied from 3.2 to 8.7 h depending on core depth and soil porosity. Triplicate water samples were collected from source water pumped from the 135 L reservoir through inflow tubing, but not through a soil core, as soon as the first soil core

filled with water in each incubation. Water samples were filtered via 0.7  $\mu\text{m}$  glass fiber filters and frozen until analyses of dissolved  $\text{NO}_3$  and  $\text{PO}_4$ . Flux rates of  $\text{NO}_3$  and  $\text{PO}_4$  were calculated using equation 3 from chapter 2 shown below:

$$F_{i,nc} = \frac{([Core]_{out} - [IN]) Q_{core}}{A}$$

Where  $F_{i,nc}$  is the flux rate ( $\text{mg m}^{-2} \text{h}^{-1}$ ).  $[Core]_{out}$  is the dissolved nutrient concentration ( $\text{mg L}^{-1}$ ) in outflowing water for each core.  $[IN]$  is the inflow concentration of dissolved nutrient ( $\text{mg L}^{-1}$ ).  $Q_{core}$  is the outflow rate ( $\text{L h}^{-1}$ ) measured for each core.  $A$  is the core surface area ( $0.0045604 \text{ m}^2$ ). Flux rates are representative of initial  $\text{NO}_3$  and  $\text{PO}_4$  flux from WRP soils after inundation, with the caveat that flux rates were measured between 3.2 and 8.7 h after nutrient rich “floodwater” first contacted the soil.

### **Dissolved nutrient analyses**

Dissolved nutrient concentrations were analyzed for filtered inflowing water and soil core outflows using a Seal AQ400 auto analyzer and standard colorimetric methods provided by Seal with minimum detection limits of 0.012 mg  $\text{NO}_3\text{-N/L}$  and 0.003 mg  $\text{PO}_4\text{-P/L}$ . Nitrate was measured using cadmium reduction to nitrite ( $\text{NO}_2$ ). Nitrite concentrations were subtracted from  $\text{NO}_3 + \text{NO}_2$  concentrations to yield  $\text{NO}_3$  only. Nitrite concentrations were measured by color development after addition of sulfanilamide with N-(1-naphthyl)-ethylenediamine dihydrochloride (NEDD) to each sample. Absorbance was measured at 520 nm. Phosphate was measured via reaction of acid molybdate with antimony and reduced by ascorbic acid for color development. Absorbance was measured at 880 nm. Coefficients of variation (standard deviation divided by mean) were calculated for each triplicate set of inflowing nutrient concentrations. Outlier concentrations of

inflowing  $\text{NO}_3$  and  $\text{PO}_4$  were identified and removed from flux calculations if CVs were greater than 10 percent.

### **Topographical analyses**

Digital elevation models (DEM) from LiDAR data covering the eight Kentucky easements used for interpolation analyses with 1 m linear resolution and 0.3048 m vertical resolution were used to measure elevation change (maximum elevation minus minimum elevation) across the core collection area within each easement in ArcGIS Pro version 3.0.0. Average percent slope and standard deviation of percent slope for each easement were derived from DEMs using the “Surface Parameters” tool in the Spatial Analyst toolbox and used to compute the coefficient of variation (CV) for slope across each easement. These measures of topographical variability may influence precision of interpolated predictions across space in a way that is not effectively captured by distance-decay relationships (see data processing and analyses below). Three additional easements in Tennessee were included in analyses focused on nutrient responses to tree planting age, but DEMs for these easements had 1 m linear resolution and 1 m vertical resolution.

### **Data processing and analyses**

#### ***Extrapolation***

Gram per  $\text{m}^2$  measurements for soil C, N, and P content to 5 cm depth in each core were further extrapolated to kilograms per hectare of surficial nutrient storage. Given that our area of collection for 30 soil cores within each WRP easement ranged

from 8 to 33 ha for the 11 easements in the current study, extrapolation of soil properties from a single core to one hectare is reasonable. Some regional WRP easements are much larger (~ 280 ha). Comprehensive, even spaced, direct measurements of nutrient flux across entire easements were generally not possible but core locations within the 11 easements selected for analyses below were as evenly spaced as was logistically feasible. We were able to collect cores across most of the area of our smallest easement (~8 of 11 ha).

Measurements of initial  $\text{NO}_3\text{-N}$  and  $\text{PO}_4\text{-P}$  flux ( $\text{mg m}^{-2} \text{h}^{-1}$ ) for each core were extrapolated to represent dissolved nutrient flux in terms of  $\text{g NO}_3\text{-N ha}^{-1} \text{h}^{-1}$  and  $\text{g PO}_4\text{-P ha}^{-1} \text{h}^{-1}$  across each easement within the first few hours of inundation. Mean extrapolated rates and 95% confidence intervals for each easement were generated from all 30 cores within each easement. I focus the current study on scaling up initial (6h) dissolved nutrient flux at the soil-water interface to more closely approximate biogeochemical reactions of the soil to delivery of nutrient rich water early in a flood. This initial function of WRP soils (in terms of  $\text{NO}_3$  and  $\text{PO}_4$  uptake potential) within a given easement is informative of nutrient cycling processes that may occur during short-term inundation events (a few hours), which could occur more frequently than long term inundation in relatively small stream systems (Noe & Hupp, 2007). Estimating error associated with scaled up soil nutrient flux measurements during short-term inundation events will inform understanding of variability among WRP N and P budgets where information on inundation frequency is available.

## *Interpolation*

Spatial interpolation methods account for autocorrelation between locations where a given variable was measured (i.e. soil C content) to predict the value of that variable at unmeasured locations (Myers, 1994). Geostatistical methods such as kriging can be used to model variation in spatial autocorrelation patterns at each sampled location, provide location-specific estimates of interpolation error, and are more accurate than inverse distance weighting (IDW) for studies with large sample sizes (Li & Heap, 2014; Zimmerman et al., 1999). However, computationally intensive kriging methods require sample sizes of 100 or more for reliable results (Oliver & Webster, 2014). Inverse distance weighting (IDW) uses a power function to assign greater weights to variables measured at locations close to each other. A power of 1 assumes linear distance-decay relationships. Spatial autocorrelation is assumed by distance-decay relationships in IDW models such that a larger power function (i.e. 2 or 3) implies stronger spatial dependence of a variable on itself at smaller scales (Lu & Wong, 2008; Myers, 1994). Inverse distance weighted interpolations are commonly applied in geography because of their relative simplicity and accuracy with smaller datasets compared to kriging methods (Li & Heap, 2014; Lu & Wong, 2008). Recent case studies have shown improvements made to IDW models can rival accuracy of kriging predictions (Li, 2021; Li et al., 2020). Essentially, these improvements can optimize IDW power functions and interpolation neighborhoods for large samples sizes. I chose to use a traditional fixed power function ( $P = 1, 2, 3$ ) approach to IDW in the current study because of often improved results for datasets with smaller sample sizes compared to more computationally intensive

geostatistical models (Li & Heap, 2014; Lu & Wong, 2008; Wang et al., 2021). I applied this comparative approach to 8 soil characteristics across 8 easements.

Soil structural (C, N, P, moisture content, bulk density, and pH) and functional characteristics (NO<sub>3</sub> and PO<sub>4</sub> flux) were interpolated for each WRP easement using the inverse distance weighting (IDW) tool in the Spatial Analyst toolbox in ArcGIS Pro version 3.0.0. The search neighborhood default (n=12) for the IDW tool was left in place so that all predicted values were derived from the 12 closest core locations within an easement, allowing distance between the 12 cores used in prediction to vary. Optimizing the search neighborhood and power function of IDW is possible in ArcGIS Pro Geostatistical Analyst toolbox, but such precise optimization was not possible for 64 interpolations (8 soil parameters for 8 WRP easements) with relatively small within easement sample size (each n= 30). Therefore, three models were compared for each soil parameter in each easement to identify the fixed power IDW model (P = 1, 2, 3) that minimized variation of root mean square error (RMSE) during model cross-validation (Lu & Wong, 2008; Wang et al., 2021) comparing predictions to measured values for each set of soil parameters at all 30 core locations in each easement. The simpler (lower power) model was chosen if RMSE between two models was equal.

Interpolation error (RMSE) for each easement was regressed against each of four variables that potentially influence model accuracy of within easement soil parameter predictions: (1) the coefficient of variation (CV) in easement slope, (2) total elevation change across each easement, (3) CV for each soil parameter measurement, and (4) CV for distance between cores within each WRP easement. Essentially, variation in slope and easement elevation change within each sampled area provide metrics of topographical

variation that could influence spatial dependence of soil structure and nutrient cycling processes (Duncan et al., 2013). This type of stochastic spatial dependence (i.e. hot spots) likely contributes to error of IDW predictions as they are not accounted for in deterministic distance-decay relationships (Myers, 1994). Higher CVs for soil parameters are indicative of hot spots within easements that likely increase IDW prediction error at individual core locations. Higher CVs for distance between cores are indicative of uneven spacing and could contribute to IDW prediction error caused by variation in the distance between the 12 cores used to interpolate each unknown location. Simple linear regressions were used to model relationships between IDW error (RMSE) and potential contributing factors because each easement was an observation ( $n = 8$ ), leaving few degrees of freedom to model potential interactions.

The sum of interpolated 5 m<sup>2</sup> raster cells for each soil property (surficial soil C, N, an P storage, and initial NO<sub>3</sub> and PO<sub>4</sub> flux) in each easement was calculated using the “Zonal Statistics as Table” tool in the Spatial Analyst toolbox for 1<sup>st</sup> and 2<sup>nd</sup> order IDW models. This number was standardized for each model to represent kg of nutrient stored or g dissolved nutrient flux per hectare. Results of IDW scaling were visually compared to 95% confidence intervals of extrapolated estimates of nutrient storage/retention for each easement.

Multiple linear regressions were used to assess potential influence of tree planting restoration age (the most widespread WRP restoration practice) and elevation above sea level on surficial soil C, N, and P storage, and initial NO<sub>3</sub> and PO<sub>4</sub> flux. For remnant forest habitats, simple linear regressions were used to assess relationships between elevation and surficial soil C, N, and P storage, and initial NO<sub>3</sub> and PO<sub>4</sub> flux. Welch t-

tests were used to compare surficial soil C, N, and P storage, and initial NO<sub>3</sub> and PO<sub>4</sub> flux, averaged within habitats for each easement, between remnant forest and tree planting habitats. Results were considered significant with  $\alpha < 0.05$  and marginally significant with  $\alpha$  between 0.05 and 0.10.

## Results

### Variability of measurements

Dissolved nutrient flux rates were generally more variable among the 11 study easements than surficial nutrient content and physiochemical parameters, notably, because of the occurrence of both positive (release) and negative (uptake) NO<sub>3</sub> and PO<sub>4</sub> flux rates. Surficial soil C among easements was  $1002.6 \pm 408.4$  g C m<sup>-2</sup> (mean  $\pm$  standard deviation) and ranged from 178.8 to 2883.6 g C m<sup>-2</sup>. Surficial soil N among easements was  $89.27 \pm 30.75$  g N m<sup>-2</sup> and ranged from 21.45 to 215.80 g N m<sup>-2</sup>. Surficial soil P among easements was  $2.20 \pm 1.42$  g P m<sup>-2</sup> and ranged from 0.05 to 10.91 g P m<sup>-2</sup>. Nitrate flux at the soil-water interface among easements was  $-10.03 \pm 43.16$  mg NO<sub>3</sub>-N m<sup>-2</sup> h<sup>-1</sup> and ranged from -219.77 to 226.57 mg NO<sub>3</sub>-N m<sup>-2</sup> h<sup>-1</sup>. Phosphate flux at the soil-water interface among easements was  $-0.75 \pm 4.11$  mg PO<sub>4</sub>-P m<sup>-2</sup> h<sup>-1</sup> and ranged from -11.47 to 26.84 mg PO<sub>4</sub>-P m<sup>-2</sup> h<sup>-1</sup>. Soil pH among easements ranged from 3.76 to 7.56. Soil moisture among easements was  $0.61 \pm 0.50$  g g<sup>-1</sup> and ranged from 0.09 to 4.44 g g<sup>-1</sup>. Soil bulk density was  $0.90 \pm 0.27$  g cm<sup>-3</sup> and ranged from 0.13 to 1.56 g cm<sup>-3</sup>.

### **Inverse distance weighted (IDW) model comparisons**

For the eight easements included in IDW analyses, surficial soil C, N, and P storage were best modeled by linear (1<sup>st</sup> order) IDW distance-decay relationships in 75% of easements. Initial NO<sub>3</sub> flux was best modeled by 1<sup>st</sup> order distance-decay relationships in 87.5% of easements. Initial PO<sub>4</sub> flux was best modeled by 1<sup>st</sup> order distance-decay relationships in 62.5% of easements. Soil physiochemical properties (pH, moisture content, and bulk density) were best modeled by 1<sup>st</sup> order distance-decay relationships in 50% or fewer easements. Overall, non-linear distance-decay relationships were more prevalent for soil physiochemical properties and initial PO<sub>4</sub> flux than surficial soil nutrient storage and initial NO<sub>3</sub> flux. Model comparisons of IDW power functions for each easement are shown in Table 3.1.

Root mean square error (RMSE) of local-scale IDW predictions as a percentage of mean measured values (hereafter percent error) were generally much higher for dissolved nutrient flux, especially PO<sub>4</sub>, compared with surficial nutrient storage and soil physiochemical parameters. Mean NO<sub>3</sub> and PO<sub>4</sub> flux rates for individual easements were often low because both negative (uptake) and positive (release) fluxes occurred within easements, resulting in high variation relative to the mean. Percent error was  $7.3 \pm 2.5$  for soil pH,  $24.9 \pm 4.2$  for soil bulk density,  $28.3 \pm 6.3$  for soil N,  $32.6 \pm 19.2$  for soil C,  $50.3 \pm 24.0$  for soil P,  $63.8 \pm 36.7$  for soil moisture,  $185.0 \pm 133.4$  for NO<sub>3</sub>-N flux, and  $775.1 \pm 1195.7$  for PO<sub>4</sub>-P flux.

Table 3.1. Root mean squared error (RMSE) for 1st, 2nd, and 3rd order IDW models for each soil parameter for each easement (column). Values in **bold** denote lower RMSE for the three different models for each soil parameter for each easement, indicating the most parsimonious model.

Soil parameter	IDW power	CX RMSE	GW RMSE	MS RMSE	BT RMSE	JS RMSE	GK RMSE	HS RMSE	HN RMSE
Soil C	1	<b>262.356</b>	<b>314.191</b>	<b>263.909</b>	<b>324.769</b>	<b>322.406</b>	406.664	233.820	<b>475.697</b>
	2	272.483	354.775	265.754	344.708	326.462	391.988	<b>227.283</b>	498.244
	3	287.393	386.608	272.849	349.83	342.486	<b>388.037</b>	232.108	528.574
Soil N	1	<b>21.070</b>	<b>24.188</b>	<b>24.984</b>	<b>25.119</b>	<b>23.107</b>	30.800	19.159	<b>34.335</b>
	2	21.510	27.271	25.073	26.353	23.107	29.252	<b>18.512</b>	35.104
	3	22.137	29.658	25.554	26.993	23.107	<b>28.936</b>	18.709	37.154
Soil P	1	<b>0.856</b>	<b>0.941</b>	<b>0.544</b>	<b>1.427</b>	<b>0.758</b>	<b>1.427</b>	0.725	1.700
	2	0.886	0.973	0.545	1.472	0.789	1.444	<b>0.698</b>	1.593
	3	0.918	1.003	0.552	1.502	0.83	1.458	0.712	<b>1.565</b>
NO <sub>3</sub> flux	1	<b>7.714</b>	57.979	<b>28.622</b>	<b>15.198</b>	<b>6.832</b>	<b>6.365</b>	<b>60.085</b>	<b>49.749</b>
	2	7.825	<b>56.958</b>	28.875	16.960	7.271	6.614	60.263	50.685
	3	8.098	57.378	29.652	18.339	7.676	6.897	61.026	52.313
PO <sub>4</sub> flux	1	<b>2.286</b>	2.211	<b>2.029</b>	<b>5.700</b>	1.390	<b>1.731</b>	5.449	<b>3.064</b>
	2	2.441	<b>2.208</b>	2.113	5.700	<b>1.358</b>	1.735	4.987	3.174
	3	2.617	2.244	2.16	5.7	1.384	1.766	<b>4.903</b>	3.306
Soil pH	1	<b>0.556</b>	<b>0.582</b>	0.404	0.326	0.489	<b>0.559</b>	<b>0.225</b>	0.210
	2	0.595	0.642	0.357	<b>0.305</b>	<b>0.477</b>	0.559	0.228	<b>0.204</b>
	3	0.631	0.691	<b>0.356</b>	0.313	0.491	0.573	0.237	0.212
Soil moisture	1	<b>0.221</b>	0.318	0.290	<b>0.532</b>	0.377	0.760	0.351	<b>0.243</b>
	2	0.230	0.295	0.252	0.599	0.352	<b>0.756</b>	<b>0.336</b>	0.264
	3	0.242	<b>0.294</b>	<b>0.233</b>	0.664	<b>0.348</b>	0.771	0.338	0.29
Bulk density	1	<b>0.206</b>	0.211	0.186	0.274	0.257	<b>0.300</b>	0.207	<b>0.216</b>
	2	0.211	0.200	0.166	<b>0.266</b>	0.242	0.304	<b>0.206</b>	0.226
	3	0.219	<b>0.195</b>	<b>0.159</b>	0.275	<b>0.239</b>	0.317	0.219	0.236

## Factors influencing IDW model error

### *Soil C*

Prediction error from IDW models (RMSE) of soil C was roughly positively correlated with variation in easement topography, variation in soil C measurements, and

variation in distance between soil core locations (Fig. 3.1) but strength of these relationships was variable. Variation in easement slope was not significantly correlated with soil C RMSE (Fig. 3.1a,  $F_{(1,6)} = 1.914$ ,  $p = 0.216$ ,  $R^2 = 0.12$ ). The correlation was slightly stronger between easement elevation change and soil C RMSE but not significant at  $\alpha = 0.1$  (Fig. 3.1b,  $F_{(1,6)} = 3.382$ ,  $p = 0.116$ ,  $R^2 = 0.25$ ). However, soil C interpolation error had the strongest correlation with topographical variation of all soil characteristics reported in the current study. Variation in soil C measurements for each easement was strongly positively correlated with soil C RMSE (Fig. 3.1c,  $F_{(1,6)} = 23.85$ ,  $p = 0.003$ ,  $R^2 = 0.77$ ). Variation in distance between soil core locations for each easement was not significantly correlated with soil C RMSE (Fig. 3.1d,  $F_{(1,6)} = 1.641$ ,  $p = 0.248$ ,  $R^2 = 0.08$ ).

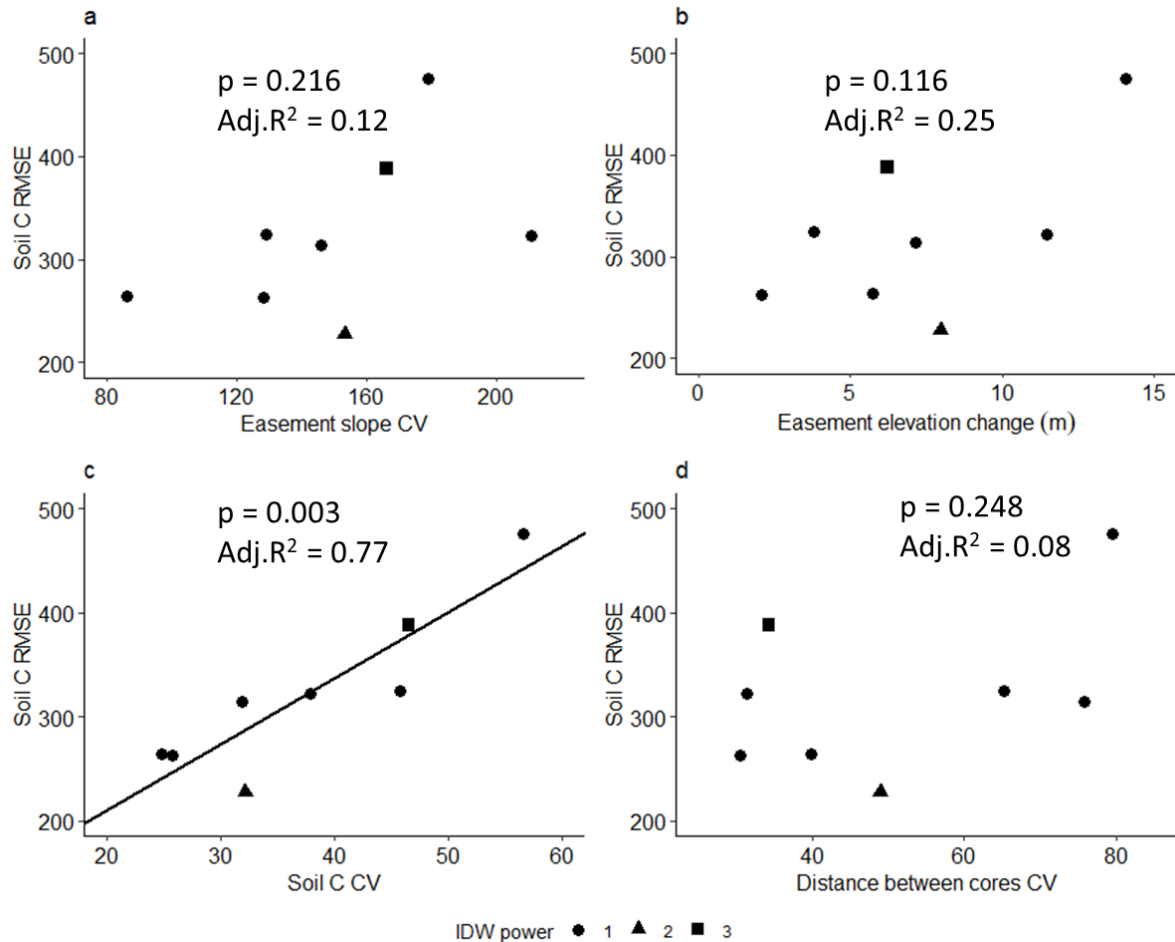


Figure 3.1. Root mean squared error (RMSE) of IDW interpolation predictions for soil C. Soil C RMSE regressed against coefficient of variation (CV) for easement slope (a), elevation change over each easement (b), CV for soil C measurements within each easement (c), and CV for distance between 30 core collection locations at each easement. Values for each easement are symbolized according the IDW power with the lowest RMSE used in these regressions.

### ***Soil N***

Prediction error from IDW models (RMSE) of soil N was not correlated with variation in easement slope (Fig. 3.2b,  $F_{(1,6)} = 2.062$ ,  $p = 0.201$ ,  $R^2 = 0.13$ ), or variation distance between core locations (Fig. 3.2d,  $F_{(1,6)} = 1.591$ ,  $p = 0.254$ ,  $R^2 = 0.08$ ). Soil N RMSE was positively correlated with variation in soil N measurements (Fig. 3.2c,  $F_{(1,6)} = 13.38$ ,  $p = 0.011$ ,  $R^2 = 0.64$ ), similar to the relationship of soil C RMSE.

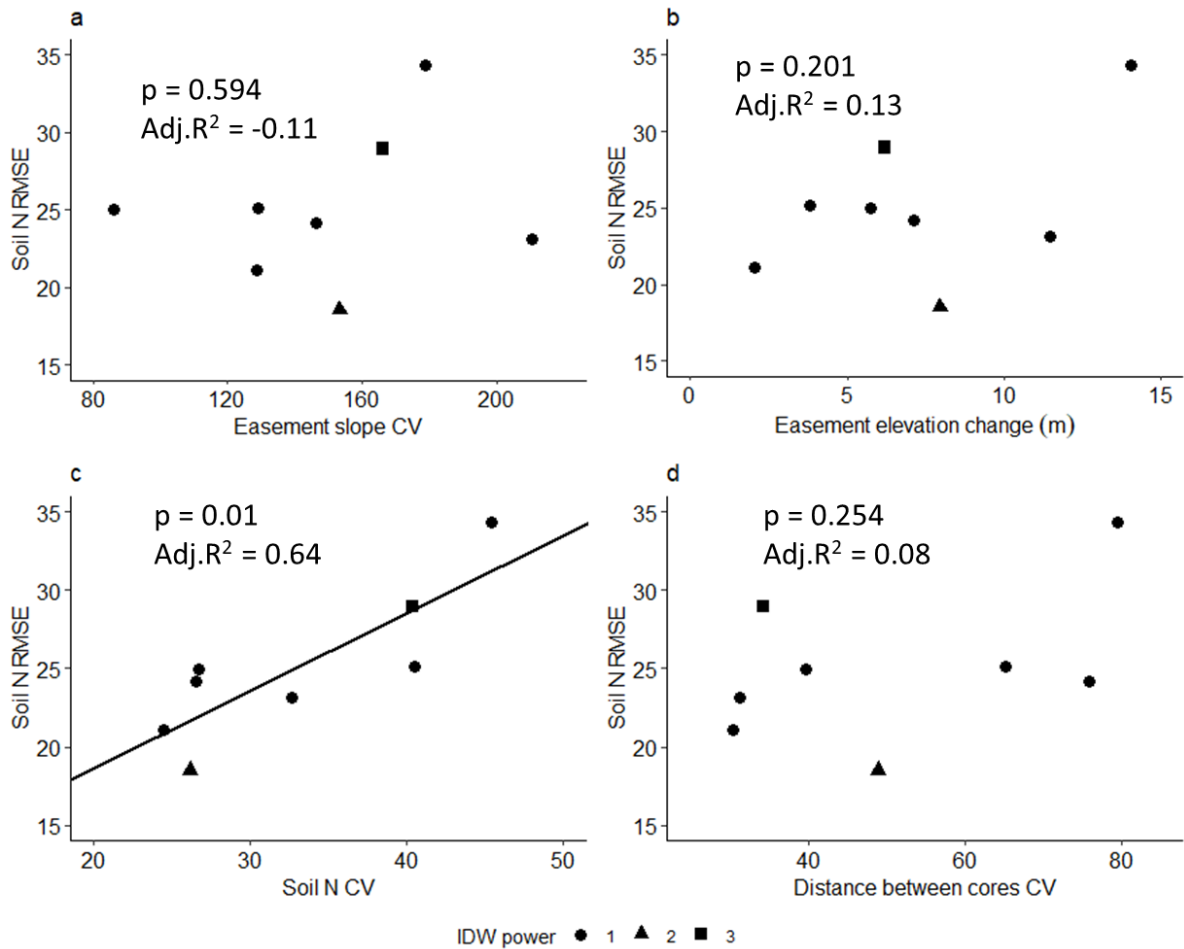


Figure 3.2. Root mean squared error (RMSE) of IDW interpolation predictions for soil N. Soil N RMSE regressed against coefficient of variation (CV) for easement slope (a), elevation change over each easement (b), CV for soil N measurements within each easement (c), and CV for distance between 30 core collection locations at each easement. Values for each easement are symbolized according the IDW power with the lowest RMSE used in these regressions.

### ***Soil P***

There was no relationship between soil P RMSE and metrics of topographic (variation in easement slope, Fig. 3.3a,  $F_{(1,6)} = 0.636$ ,  $p = 0.456$ ,  $R^2 = -0.05$ ; easement elevation change, Fig. 3.3b,  $F_{(1,6)} = 0.289$ ,  $p = 0.610$ ,  $R^2 = -0.11$ ). Variation in soil P measurements for each easement was strongly positively correlated with soil P RMSE (Fig. 3.3c,  $F_{(1,6)} = 14.44$ ,  $p = 0.009$ ,  $R^2 = 0.66$ ). Variation in distance between soil core

locations for each easement was poorly correlated with soil P RMSE (Fig. 3.3d,  $F_{(1,6)} = 2.006$ ,  $p = 0.206$ ,  $R^2 = 0.13$ ).

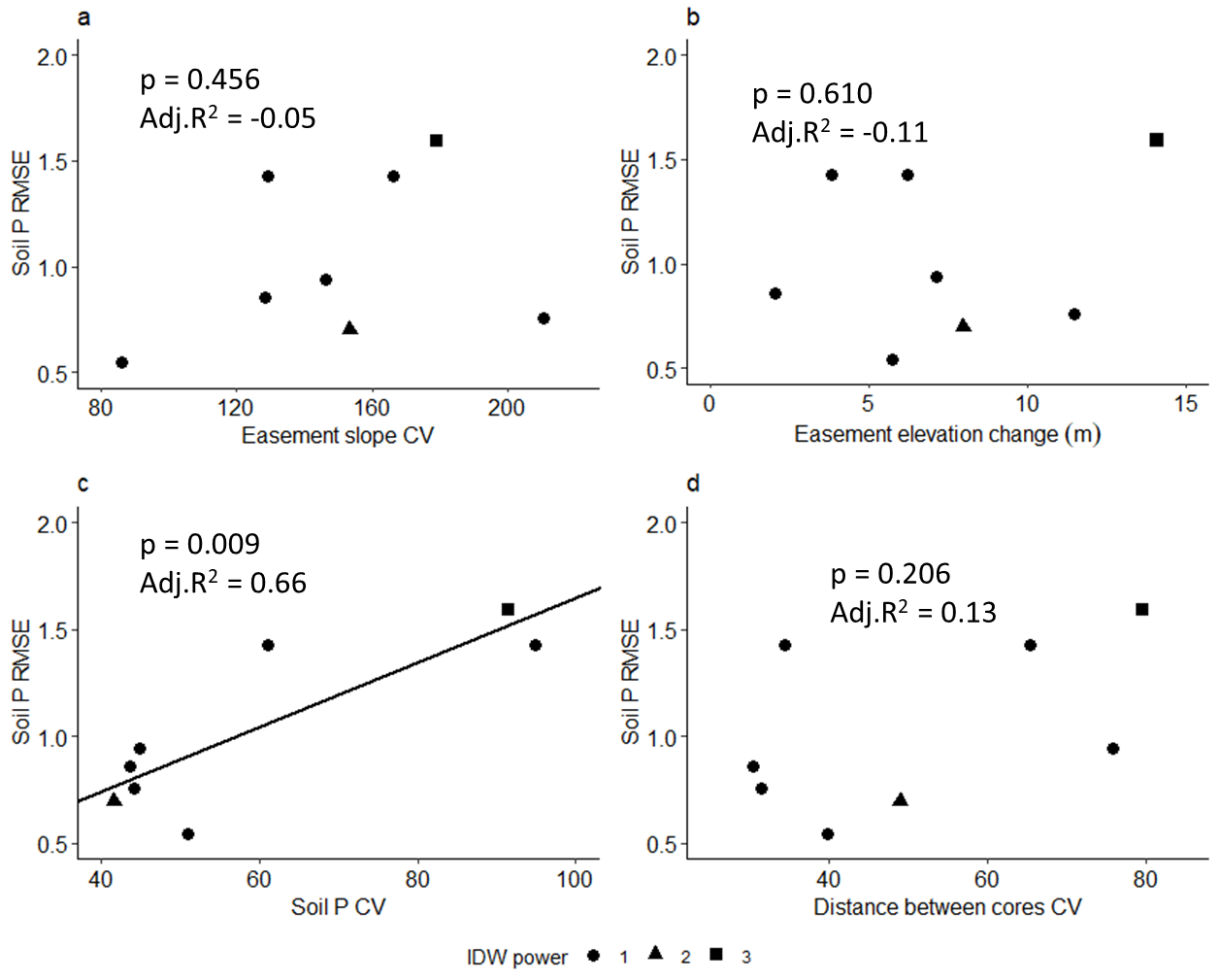


Figure 3.3. Root mean squared error (RMSE) of IDW interpolation predictions for soil P. Soil P RMSE regressed against coefficient of variation (CV) for easement slope (a), elevation change over each easement (b), CV for soil P measurements within each easement (c), and CV for distance between 30 core collection locations at each easement. Values for each easement are symbolized according the IDW power with the lowest RMSE used in these regressions.

### *Nitrate flux*

Prediction error from IDW models (RMSE) of NO<sub>3</sub> flux at the soil-water interface had poor correlations between NO<sub>3</sub> flux RMSE and variation in easement slope (Fig. 3.4a,  $F_{(1,6)} = 0.019$ ,  $p = 0.894$ ,  $R^2 = -0.16$ ) and easement elevation change (Fig. 3.4b,  $F_{(1,6)} = 1.071$ ,  $p = 0.341$ ,  $R^2 = 0.01$ ). Unlike soil nutrient interpolations, there was no correlation between NO<sub>3</sub> flux RMSE and variation in NO<sub>3</sub> flux measurements (Fig. 3.4c,  $F_{(1,6)} = 0.003$ ,  $p = 0.956$ ,  $R^2 = -0.17$ ) but there was a relatively strong positive correlation between variation in distance between soil core locations for each easement and NO<sub>3</sub> flux RMSE (Fig. 3.4d,  $F_{(1,6)} = 5.477$ ,  $p = 0.058$ ,  $R^2 = 0.39$ ).

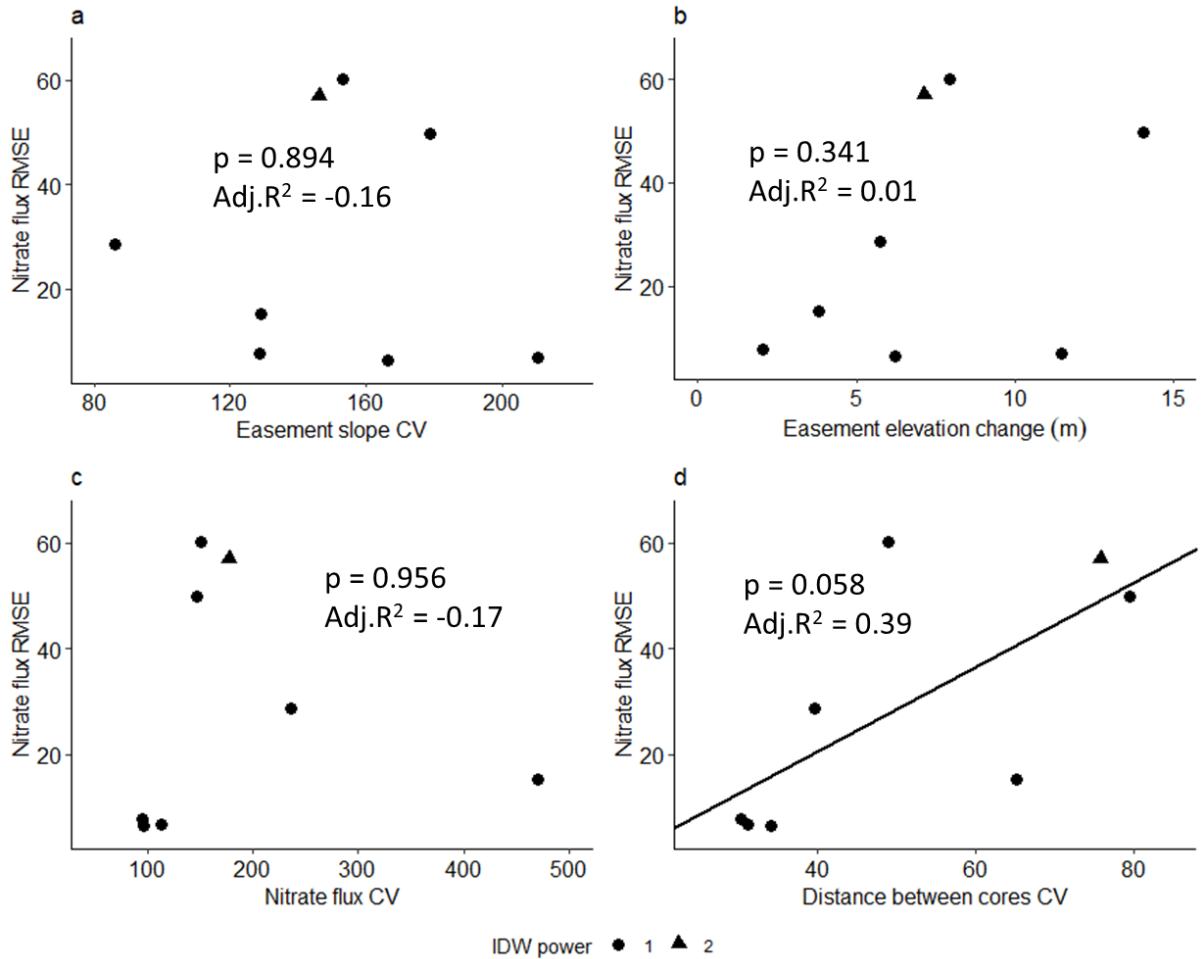


Figure 3.4. Root mean squared error (RMSE) of IDW interpolation predictions for NO<sub>3</sub> flux. NO<sub>3</sub> flux RMSE regressed against coefficient of variation (CV) for easement slope (a), elevation change over each easement (b), CV for NO<sub>3</sub> flux measurements within each easement (c), and CV for distance between 30 core collection locations at each easement. Values for each easement are symbolized according the IDW power with the lowest RMSE used in these regressions.

### ***Phosphate flux***

Prediction error from IDW models (RMSE) of PO<sub>4</sub> flux at the soil-water interface were poorly correlated with variation in easement slope (Fig. 3.5a,  $F_{(1,6)} = 0.291$ ,  $p = 0.609$ ,  $R^2 = -0.11$ ), easement elevation change (Fig. 3.5b,  $F_{(1,6)} = 0.207$ ,  $p = 0.665$ ,  $R^2 = -0.13$ ), variation in PO<sub>4</sub> flux measurements (Fig. 3.5c,  $F_{(1,6)} = 0.075$ ,  $p = 0.794$ ,  $R^2 = -$

0.15), and variation in distance between core collection locations (Fig. 3.5d,  $F_{(1,6)} = 1.369$ ,  $p = 0.286$ ,  $R^2 = 0.05$ ).

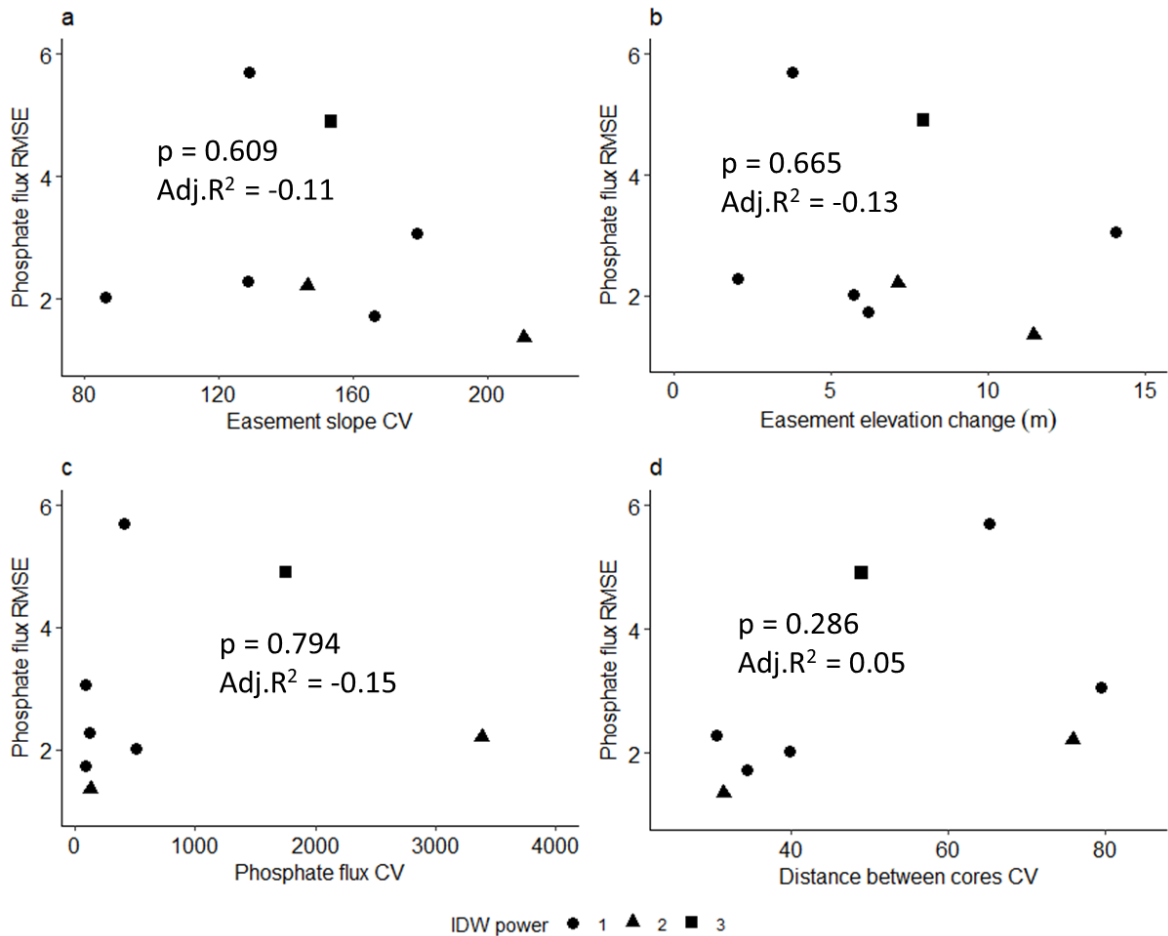


Figure 3.5. Root mean squared error (RMSE) of IDW interpolation predictions for  $PO_4$  flux.  $PO_4$  flux RMSE regressed against coefficient of variation (CV) for easement slope (a), elevation change over each easement (b), CV for  $PO_4$  flux measurements within each easement (c), and CV for distance between 30 core collection locations at each easement. Values for each easement are symbolized according to the IDW power with the lowest RMSE used in these regressions.

### ***Soil pH***

Prediction error for IDW models (RMSE) of soil pH was poorly correlated with variation in easement slope (Fig. 3.6a,  $F_{(1,6)} = 0.011$ ,  $p = 0.918$ ,  $R^2 = -0.16$ ), easement elevation change (Fig. 3.6b,  $F_{(1,6)} = 1.216$ ,  $p = 0.312$ ,  $R^2 = 0.03$ ), and variation in distance between soil core locations (Fig. 3.6d,  $F_{(1,6)} = 1.196$ ,  $p = 0.316$ ,  $R^2 = 0.03$ ). Soil pH RMSE for IDW models was positively correlated with variation in soil pH measurement (Fig. 3.6c,  $F_{(1,6)} = 9.643$ ,  $p = 0.021$ ,  $R^2 = 0.55$ ), similar to results of soil nutrient content (Figs. 3.1c, 3.2c, and 3.3c).

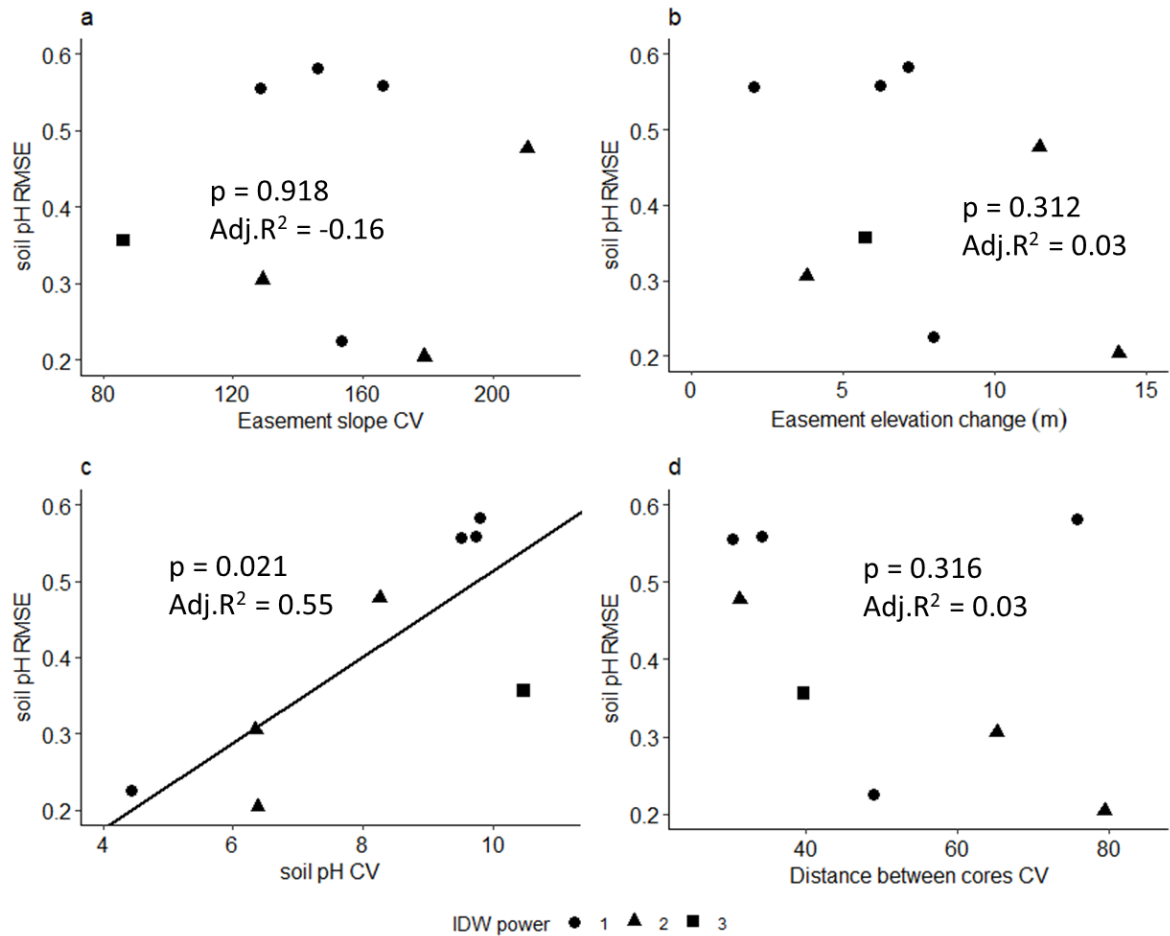


Figure 3.6. Root mean squared error (RMSE) of IDW interpolation predictions for soil pH. Soil pH RMSE regressed against coefficient of variation (CV) for easement slope (a), elevation change over each easement (b), CV for soil pH measurements within each easement (c), and CV for distance between 30 core collection locations at each easement. Values for each easement are symbolized according to the IDW power with the lowest RMSE used in these regressions.

### ***Soil moisture***

Prediction error for IDW models (RMSE) of soil moisture was poorly correlated with variation in easement slope (Fig. 3.7a,  $F_{(1,6)} = 0.269$ ,  $p = 0.623$ ,  $R^2 = -0.12$ ), easement elevation change (Fig. 3.7b,  $F_{(1,6)} = 0.221$ ,  $p = 0.655$ ,  $R^2 = -0.13$ ), and variation in distance between soil core locations (Fig. 3.7d,  $F_{(1,6)} = 0.187$ ,  $p = 0.680$ ,  $R^2 = -0.13$ ). Soil moisture RMSE for IDW models was strongly positively correlated with variation in

soil moisture measurements (Fig. 3.7c,  $F_{(1,6)} = 16.48$ ,  $p = 0.007$ ,  $R^2 = 0.69$ ), similar to results of soil nutrient content and pH (Figs. 3.1c, 3.2c, 3.3c, 3.6c).

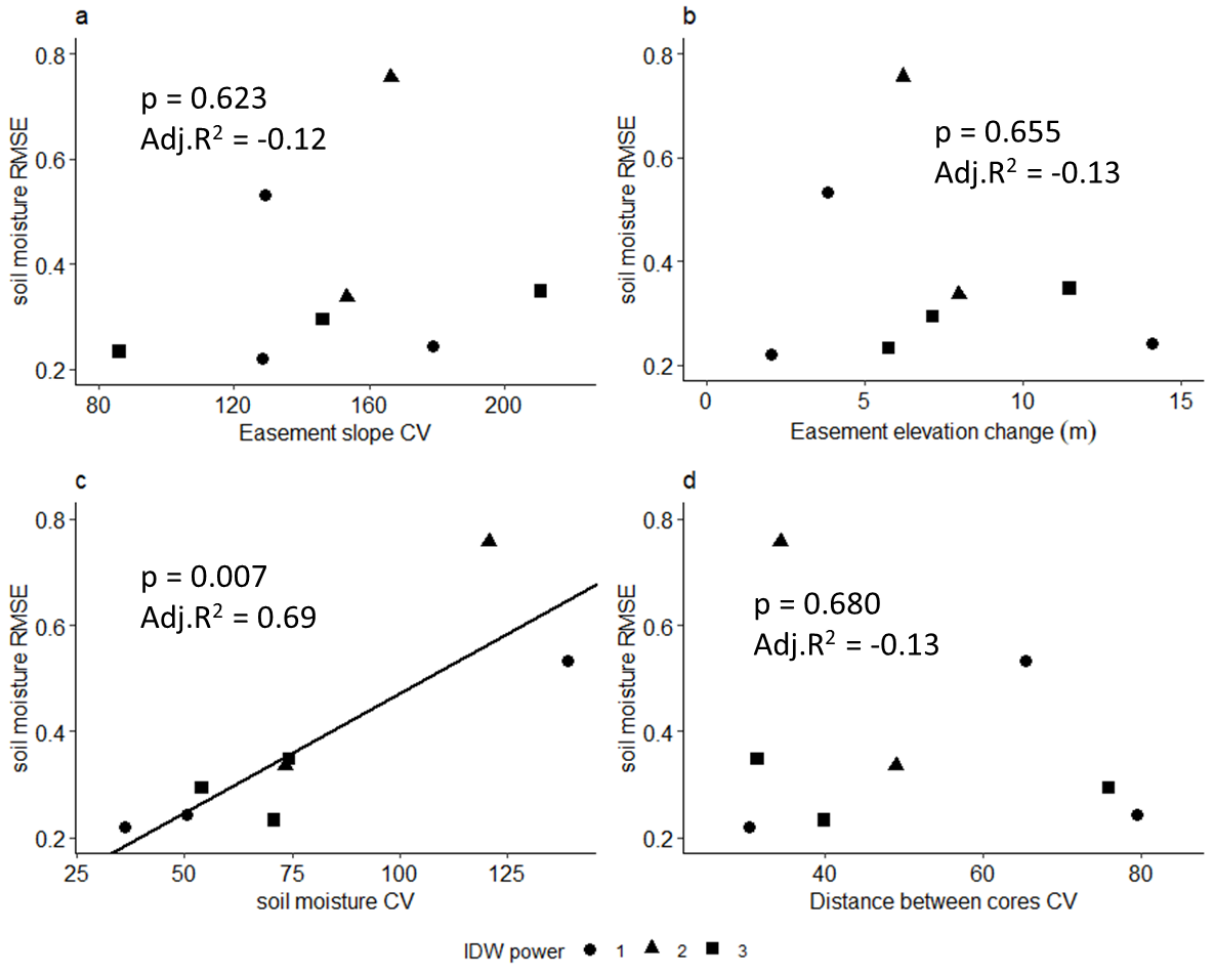


Figure 3.7. Root mean squared error (RMSE) of IDW interpolation predictions for soil moisture. Soil moisture RMSE regressed against coefficient of variation (CV) for easement slope (a), elevation change over each easement (b), CV for soil moisture measurements within each easement (c), and CV for distance between 30 core collection locations at each easement. Values for each easement are symbolized according the IDW power with the lowest RMSE used in these regressions.

### ***Bulk density***

Prediction error for IDW models (RMSE) of soil bulk density was poorly correlated with variation in easement slope (Fig. 3.8a,  $F_{(1,6)} = 1.885$ ,  $p = 0.219$ ,  $R^2 = 0.11$ ), easement elevation change (Fig. 3.8b,  $F_{(1,6)} = 0.005$ ,  $p = 0.948$ ,  $R^2 = -0.17$ ),

variation in soil bulk density measurements (Fig. 3.8c,  $F_{(1,6)} = 1.319$ ,  $p = 0.294$ ,  $R^2 = 0.05$ ), and variation in distance between soil core locations within each easement (Fig. 3.8d,  $F_{(1,6)} = 0.096$ ,  $p = 0.767$ ,  $R^2 = -0.15$ ). Bulk density was the only soil structural property where RMSE was not significantly correlated with measurement variation.

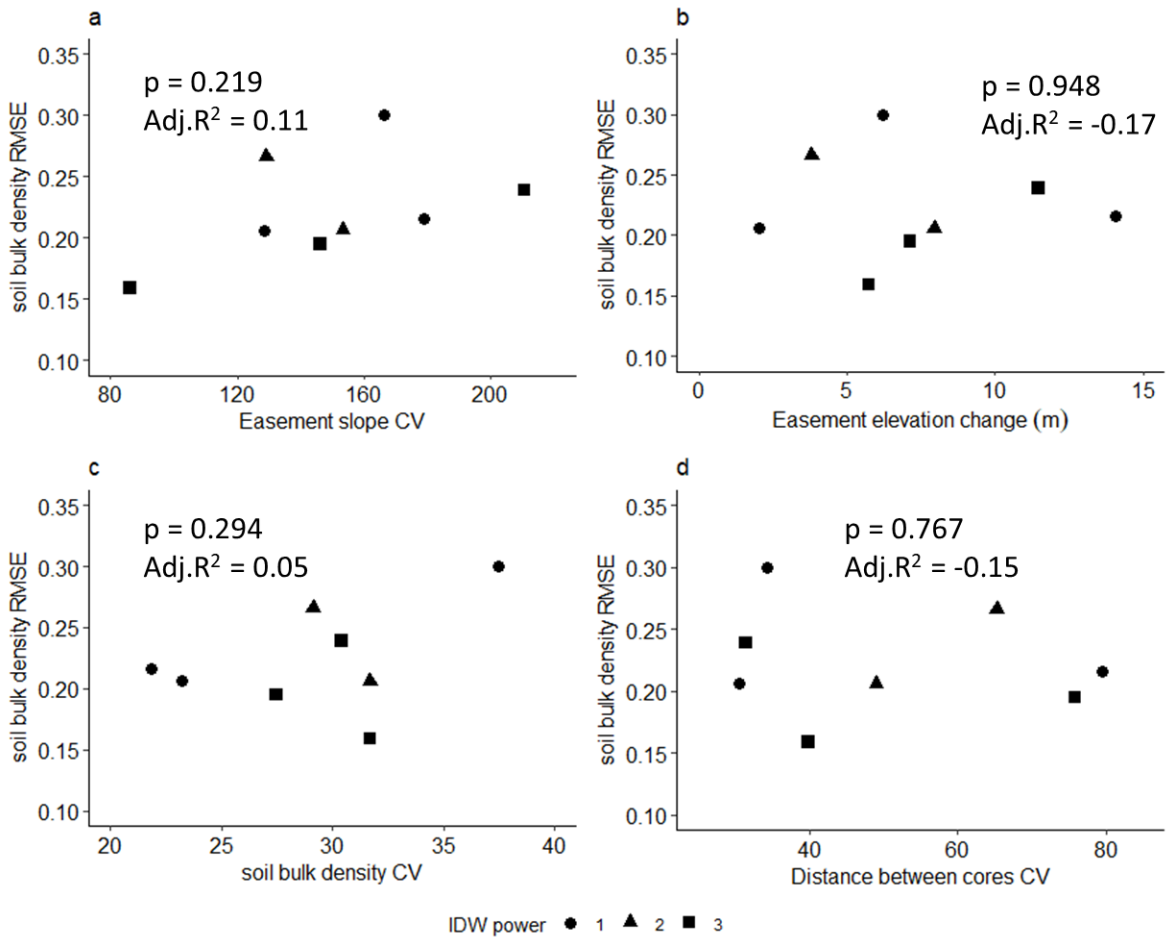


Figure 3.8. Root mean squared error (RMSE) of IDW interpolation predictions for soil bulk density. Soil bulk density RMSE regressed against coefficient of variation (CV) for easement slope (a), elevation change over each easement (b), CV for soil bulk density measurements within each easement (c), and CV for distance between 30 core collection locations at each easement. Values for each easement are symbolized according the IDW power with the lowest RMSE used in these regressions.

### **Extrapolation vs. interpolation**

All interpolated estimates of surficial nutrient storage (Fig. 3.9) and initial dissolved nutrient flux (Fig. 3.10) fell within 95% confidence intervals of extrapolated estimates. Both 1<sup>st</sup> and 2<sup>nd</sup> order IDW estimates were similar to each other for each nutrient in each easement and generally close to extrapolated means. Though increasing IDW power functions were optimal for some nutrient metrics in some easements, it is unlikely that application of different IDW power functions would cause easement-scale estimates of surficial nutrient storage and initial dissolved nutrient flux to fall outside of extrapolated 95% confidence intervals. Further, IDW interpolated estimates of surficial nutrient storage and initial flux at the soil-water interface appear not to vary significantly from each other, regardless of the power function used with IDW predictions.

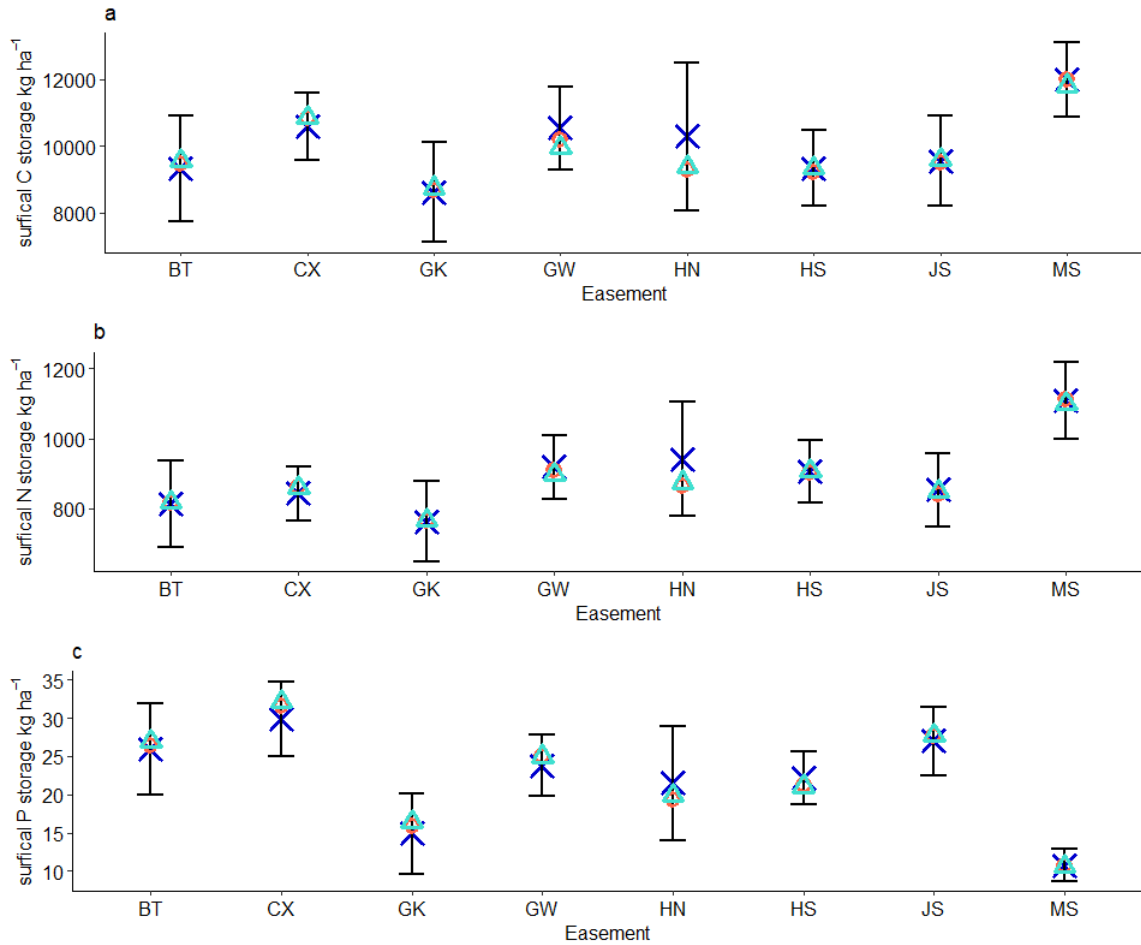


Figure 3.9. Comparison of IDW interpolated estimates and extrapolated 95% confidence intervals for surficial soil carbon (a), nitrogen (b), and phosphorus (c) storage. Mean extrapolated estimates for each nutrient are indicated by a dark blue X for each easement, bounded by 95% confidence intervals in black. Interpolated IDW estimates of nutrient storage are shown as red circles (1<sup>st</sup> order IDW) and light blue triangles (2<sup>nd</sup> order IDW).

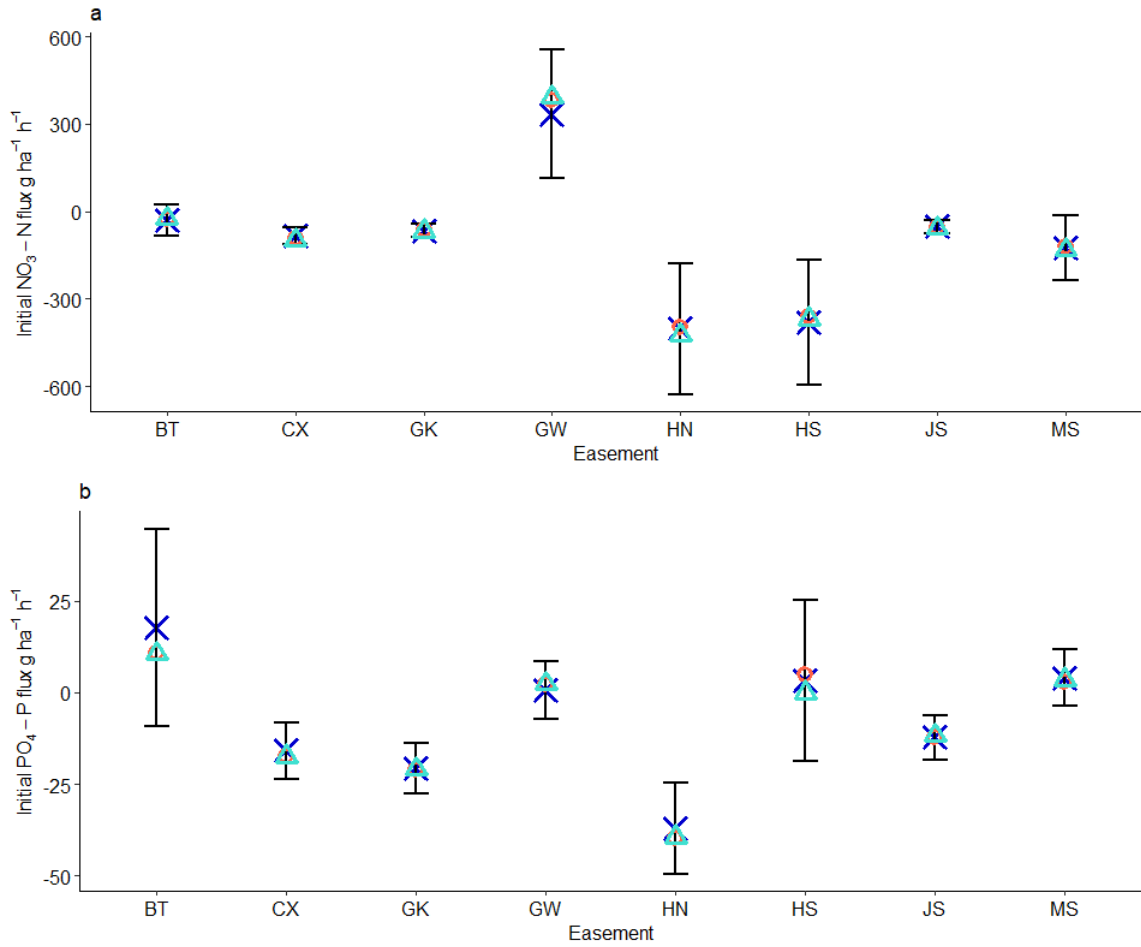


Figure 3.10. Comparison of IDW interpolated estimates and extrapolated 95% confidence intervals for initial NO<sub>3</sub> (a) and PO<sub>4</sub> (b) flux. Mean extrapolated estimates for each dissolved nutrient are indicated by a dark blue X for each easement, bounded by 95% confidence intervals in black. Interpolated IDW estimates of nutrient storage are shown as red circles (1<sup>st</sup> order IDW) and light blue triangles (2<sup>nd</sup> order IDW).

## **Influence of tree planting age and elevation**

Interaction terms between tree planting age and elevation were not significant for any models (all  $p > 0.1$ ) and were excluded from further analyses. Additive regression models of tree planting age and elevation above sea level explained little overall variation in surficial nutrient storage or initial dissolved nutrient flux (all adjusted  $R^2 < 0.12$ ). However, significant correlations with tree planting age and elevation were identified and varied among soil nutrient metrics. Extrapolated estimates of surficial soil C storage were positively correlated with elevation (m) above sea level (Fig. 3.11a, Table 3.2,  $F_{(2, 108)} = 3.366$ ,  $p = 0.019$ ,  $R^2 = 0.04$ ) but not tree planting age (Table 3.2,  $p = 0.117$ ). Surficial storage of soil N was poorly correlated with both elevation and tree planting age (Fig. 3.11b, Table 3.2,  $F_{(2, 108)} = 1.662$ ,  $p = 0.195$ ,  $R^2 = 0.01$ ). Surficial storage of soil P was positively correlated with tree planting age (Fig. 3.11c, Table 3.2,  $F_{(2, 108)} = 8.316$ ,  $p < 0.001$ ,  $R^2 = 0.12$ ) but not elevation (Table 3.2,  $p = 0.556$ ). Initial  $\text{NO}_3$  flux at the soil-water interface was positively correlated with tree planting age (Fig. 3.11d, Table 3.2,  $F_{(2, 102)} = 2.18$ ,  $p = 0.039$ ,  $R^2 = 0.02$ ) but not elevation (Table 3.2,  $p = 0.590$ ). Statistical outliers violate assumptions of equal variance and normality for the analysis of  $\text{NO}_3$  flux in Fig. 3.11d, but these point measurements represent real hotspots of  $\text{NO}_3$  uptake and are included in the figure to illustrate heterogeneity in initial  $\text{NO}_3$  uptake among new tree plantings. I defined statistical outliers as below the 5<sup>th</sup> percentile for tree planting  $\text{NO}_3$  flux (less than  $-784.20 \text{ g NO}_3\text{-N ha}^{-1} \text{ h}^{-1}$ ) and removed these highly negative values for statistical analyses of  $\text{NO}_3$  flux in Table 3.2. Initial  $\text{PO}_4$  flux was positively correlated with elevation (Fig. 3.11e, Table 3.2,  $F_{(2, 108)} = 2.82$ ,  $p = 0.024$ ,  $R^2 = 0.03$ ) but did not vary with tree planting age (Table 3.2,  $p = 0.987$ ).

Table 3.2. Results of additive multiple regression models evaluating relationships between tree planting age (y) and elevation (m) above sea level for soil C (kg C ha<sup>-1</sup>), soil N (kg N ha<sup>-1</sup>), soil P (kg P ha<sup>-1</sup>), NO<sub>3</sub> flux (g NO<sub>3</sub>-N ha<sup>-1</sup> h<sup>-1</sup>), and PO<sub>4</sub> flux (g PO<sub>4</sub>-P ha<sup>-1</sup> h<sup>-1</sup>).

Soil property	Parameter	estimate	Std. error	t-value	p-value parameter	F-value	Adj. R <sup>2</sup>	p-value model
Soil C	intercept	4724.75	2344.6	2.015	0.046	3.366 (2, 108)	0.041	0.038
	age	70.58	44.72	1.578	0.117			
	elevation	54.81	22.98	2.385	0.019			
Soil N	intercept	668.501	190.892	3.502	< 0.001	1.662 (2, 108)	0.012	0.195
	age	-2.151	3.641	-0.591	0.556			
	elevation	2.855	1.871	1.526	0.13			
Soil P	intercept	23.61651	10.49756	2.25	0.026	8.316 (2, 108)	0.117	< 0.001
	age	0.75359	0.20024	3.763	< 0.001			
	elevation	-0.06114	0.1029	-0.594	0.554			
NO <sub>3</sub> flux	intercept	-193.982	124.338	-1.560	0.122	2.18 (2, 102)	0.022	0.118
	age	5.02	2.406	2.086	0.039			
	elevation	0.678	1.223	0.555	0.580			
PO <sub>4</sub> flux	intercept	-85.2231	32.64842	-2.61	0.01	2.82 (2, 108)	0.032	0.064
	age	-0.01022	0.62276	-0.016	0.987			
	elevation	0.73521	0.32002	2.297	0.024			

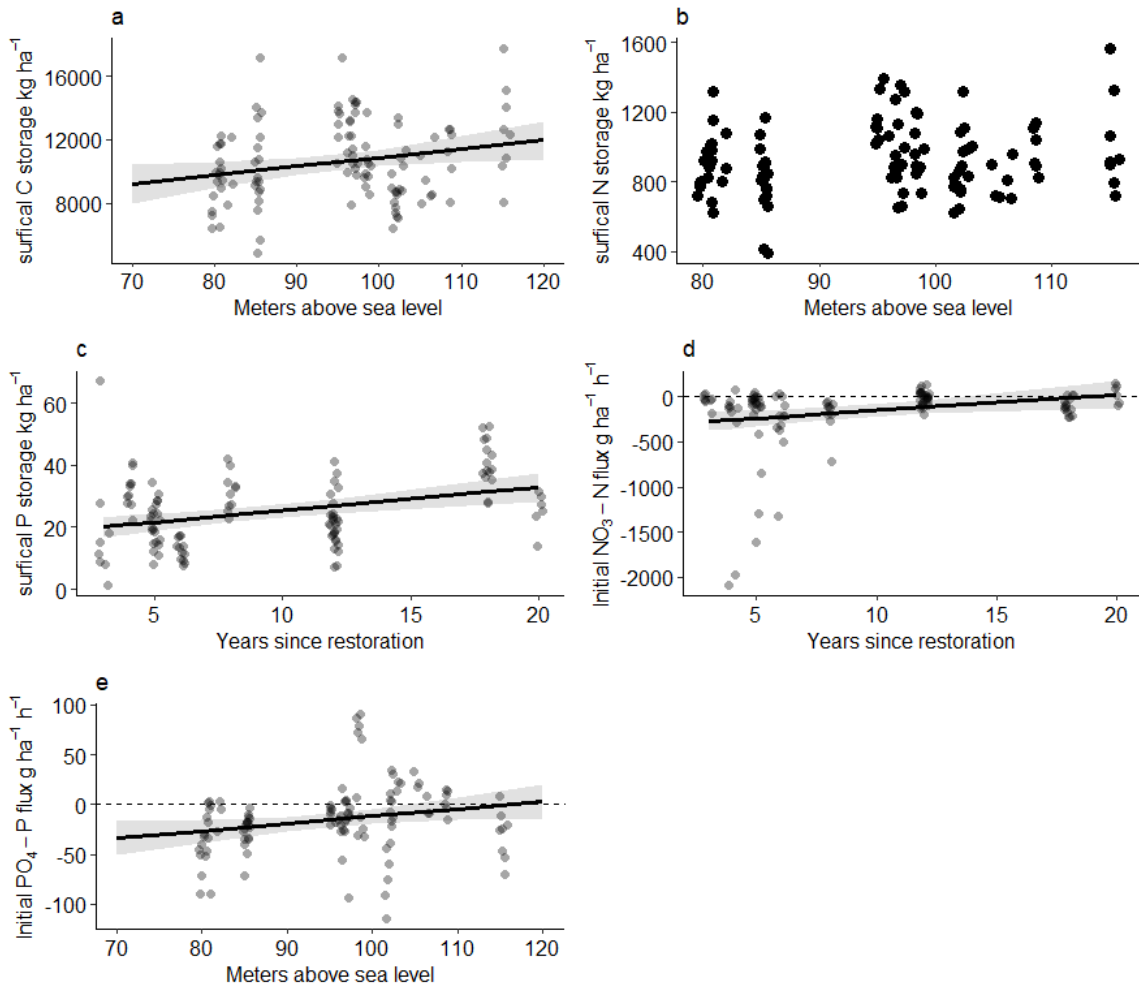


Figure 3.11. Relationships of soil nutrient measurements to tree planting age and elevation. Meters above sea level and surficial soil C (a) and N (b) storage, and initial  $\text{PO}_4$  flux (e). Tree planting age and surficial soil P storage (c), and initial flux of  $\text{NO}_3$  (d) at the soil-water interface. Panels display the stronger relationship (tree planting age vs. elevation) derived from corresponding statistics in Table 3.2.

### Influence of elevation in remnant forests

Surficial soil C storage in remnant forest habitats was positively correlated with elevation (m) above sea level (Fig. 3.12a, Table 3.3,  $F_{(1, 74)} = 4.446$ ,  $p = 0.038$ ,  $R^2 = 0.04$ ). Surficial soil N storage in forests showed a positive quadratic relationship with elevation (Fig. 3.12b, Table 3.3,  $F_{(2, 73)} = 5.155$ ,  $p = 0.002$ ,  $R^2 = 0.10$ ). Surficial soil P storage was not significantly related to elevation (Table 3.3,  $F_{(1, 74)} = 2.158$ ,  $p = 0.146$ ,  $R^2 = 0.02$ ), but

more variation was apparent at higher elevations (Fig. 3.12c). Initial NO<sub>3</sub> flux from forest soils was not correlated with elevation (Fig. 3.12d, Table 3.3,  $F_{(1, 70)} = 1.148$ ,  $p = 0.228$ ,  $R^2 = 0.002$ ) and this relationship was modeled after removal of NO<sub>3</sub> uptake hotspots (bottom 5<sup>th</sup> percentile of flux) in forests adjacent to young tree plantings. Hotspots of NO<sub>3</sub> uptake are plotted in Fig. 3.12d for visual comparison. Initial PO<sub>4</sub> flux from forest soils was positively related to elevation (Fig. 3.12e, Table 3.3,  $F_{(1, 74)} = 7.823$ ,  $p = 0.007$ ,  $R^2 = 0.08$ ).

Table 3.3. Results of simple linear regression models evaluating relationships between tree planting age (y) and elevation (m) above sea level for soil C (kg C ha<sup>-1</sup>), soil P (kg P ha<sup>-1</sup>), NO<sub>3</sub> flux (g NO<sub>3</sub>-N ha<sup>-1</sup> h<sup>-1</sup>), and PO<sub>4</sub> flux (g PO<sub>4</sub>-P ha<sup>-1</sup> h<sup>-1</sup>). Quadratic regression for soil N (kg N ha<sup>-1</sup>) improved model fit.

Soil property	Parameter	estimate	Std. error	t-value	p-value parameter	F-value	Adj. R <sup>2</sup>	p-value model																																																									
Soil C	intercept	2343.91	4691.23	0.5	0.619	4.446 <sub>(1, 74)</sub>	0.043	0.038																																																									
	elevation	105.88	50.21	2.109	0.038				Soil N	intercept	1117.83	37.58	29.746	< 0.001	5.155 <sub>(2, 73)</sub>	0.099	0.008	elevation	-30.49	327.61	-0.093	0.926	elevation <sup>2</sup>	1051.52	327.61	3.21	0.002	Soil P	intercept	6.0908	12.3889	0.492	0.624	2.158 <sub>(1, 74)</sub>	0.015	0.146	elevation	0.1951	0.1328	1.469	0.146	NO <sub>3</sub> flux	intercept	172.857	206.884	0.836	0.406	1.148 <sub>(1, 70)</sub>	0.002	0.288	elevation	-2.383	2.224	-1.072	0.228	PO <sub>4</sub> flux	intercept	-126.69	38.1877	-3.318	0.001	7.823 <sub>(1, 74)</sub>	0.083	0.007	elevation
Soil N	intercept	1117.83	37.58	29.746	< 0.001	5.155 <sub>(2, 73)</sub>	0.099	0.008																																																									
	elevation	-30.49	327.61	-0.093	0.926																																																												
	elevation <sup>2</sup>	1051.52	327.61	3.21	0.002																																																												
Soil P	intercept	6.0908	12.3889	0.492	0.624	2.158 <sub>(1, 74)</sub>	0.015	0.146																																																									
	elevation	0.1951	0.1328	1.469	0.146																																																												
NO <sub>3</sub> flux	intercept	172.857	206.884	0.836	0.406	1.148 <sub>(1, 70)</sub>	0.002	0.288																																																									
	elevation	-2.383	2.224	-1.072	0.228																																																												
PO <sub>4</sub> flux	intercept	-126.69	38.1877	-3.318	0.001	7.823 <sub>(1, 74)</sub>	0.083	0.007																																																									
	elevation	1.1432	0.4088	2.797	0.007																																																												

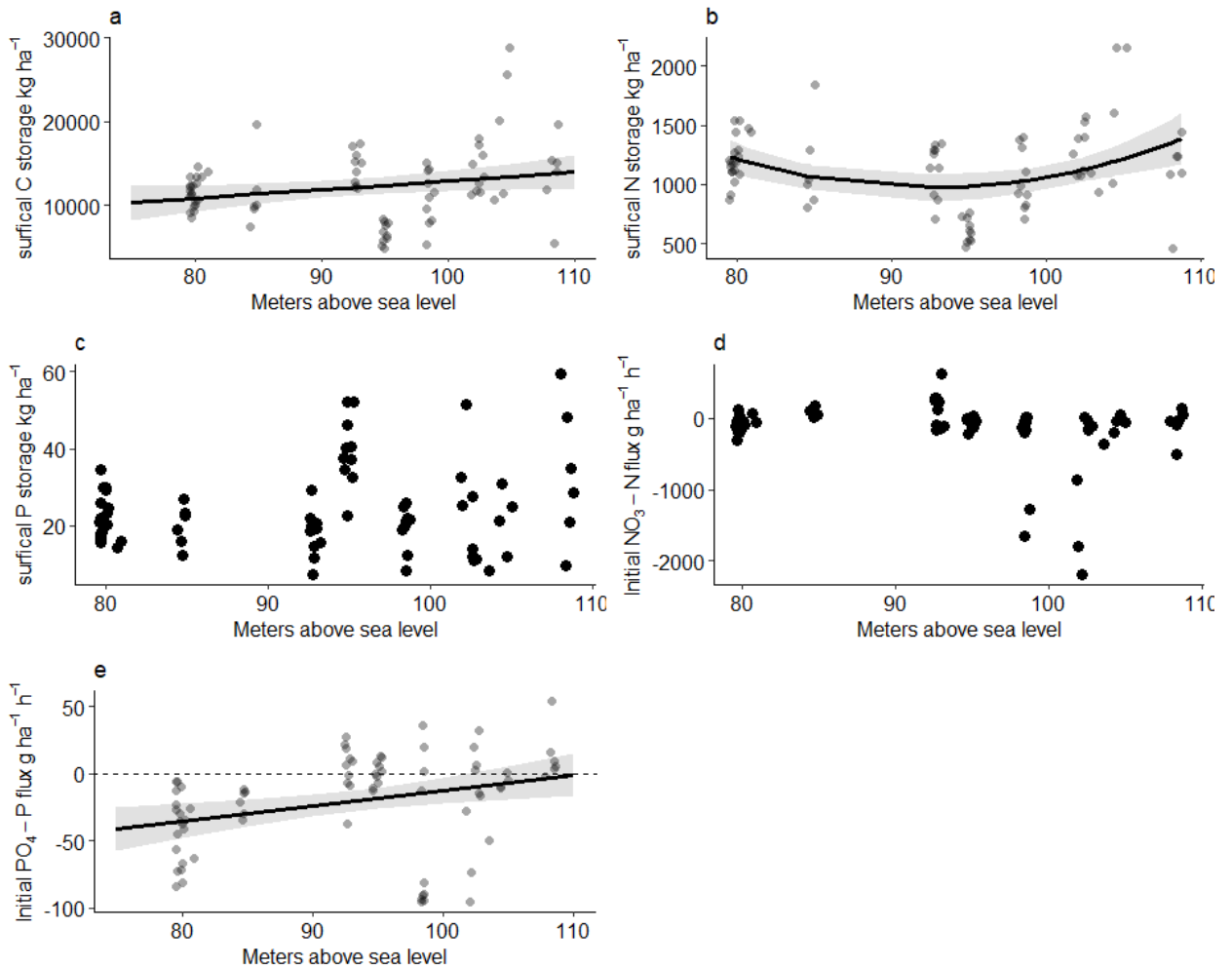


Figure 3.12. Relationships between elevation (m) above sea level and remnant forest soil C (a), N (b), and P (c) storage, initial NO<sub>3</sub> (d) and PO<sub>4</sub> (e) flux. Corresponding statistics in Table 3.3.

### Comparison of tree plantings and remnant forest

Extrapolated estimates of surficial soil C storage tended to be higher in remnant forest compared to tree plantings, but the estimated increase was not significantly different from zero (Fig. 3.13a, 95% CI: -672.00 to 4109.25 kg C ha<sup>-1</sup>,  $t = 1.570$ ,  $p = 0.143$ ). Surficial soil N storage was 20.8% higher in remnant forest compared to tree plantings (Fig. 3.13b, 95% CI: 2.42 to 387.85 kg N ha<sup>-1</sup>,  $t = 2.237$ ,  $p = 0.048$ ). There was

no difference between remnant forest and tree planting habitats on surficial soil P storage (Fig. 3.13c, 95% CI: -7.93 to 9.32 kg P ha<sup>-1</sup>, t = 0.171, p = 0.866), initial NO<sub>3</sub> flux (Fig. 3.13d, 95% CI: -184.13 to 228.25 g NO<sub>3</sub> ha<sup>-1</sup> h<sup>-1</sup>, t = 0.228, p = 0.823), or initial PO<sub>4</sub> flux (Fig. 3.13e, 95% CI: -28.54 to 19.45g PO<sub>4</sub> ha<sup>-1</sup> h<sup>-1</sup>, t = -0.399, p = 0.695).

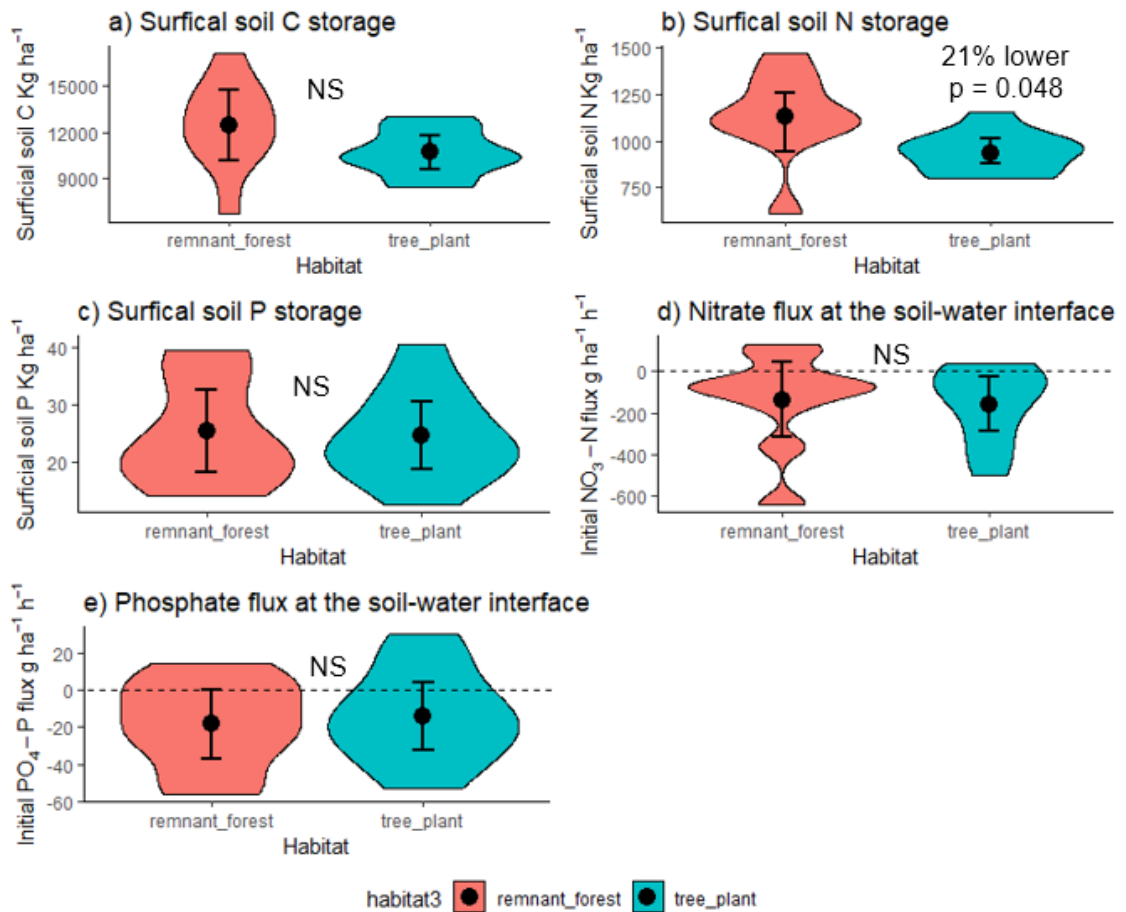


Figure 3.13. Comparison of surficial soil C (a), N (b), and P (c) storage, and initial NO<sub>3</sub> (d) and PO<sub>4</sub> (e) flux between remnant forest and tree planting habitats. Error bars represent 95% confidence intervals or means. Non-significant differences are denoted by “NS”.

## Discussion

### Interpolation error for local-scale predictions

Interpolation of soil characteristics measured in this study using fixed power IDW methods provides similar mean estimates of nutrient storage and flux compared to extrapolated measurements over the same area. However, IDW only provides estimates of prediction error (RMSE) for entire models, not specific prediction locations. IDW prediction error for most soil nutrients and physiochemical measurements was most associated with parameter measurement variability within an easement. However, prediction error of initial NO<sub>3</sub> flux was most strongly associated with variation in distance between core collection locations within each easement. This suggests that initial NO<sub>3</sub> flux at locations close to each other within an easement may be quite different compared to locations further away within the same easement (i.e. hot spots and hot moments).

The hot spot/moment nature of soil microbial activity (Kuzyakov & Blagodatskaya, 2015) and nutrient cycling processes (Groffman et al., 2009; McClain et al., 2003; Vidon et al., 2010) is well documented and has recently been further developed (Bernhardt et al., 2017). Bernhardt et al. (2017) argue that the term “ecosystem control points” facilitates a more nuanced framework for discussing gradients of ecosystem functional responses (i.e. nutrient retention) that vary over space and time. Essentially, soil within a specified location in a restored wetland may have high NO<sub>3</sub> retention capacity but that capacity is not fully realized until high concentrations of NO<sub>3</sub> are delivered to the soil during a flood. Natural variation in initial NO<sub>3</sub> uptake capacity from soils in the current study was probably enhanced relative to ambient NO<sub>3</sub> uptake rates by addition of NO<sub>3</sub> concentrations to flow-through core incubations that were higher than

natural concentrations in floodwater. Ancillary measurements of dissolved nutrient concentrations from floodwater collected from one Kentucky stream feeding several WRP easements in July, October, and March showed  $\text{NO}_3 + \text{NO}_2$  concentrations were  $1.332 \pm 0.694$  mg/L (mean  $\pm$  standard deviation) and  $\text{PO}_4$  concentrations were  $0.534 \pm 0.323$  mg/L. While both  $\text{NO}_3\text{-N}$  ( $\sim 10$  mg/L) and  $\text{PO}_4\text{-P}$  ( $\sim 1$  mg/L) were higher in flow-through incubations compared to ambient floodwater concentrations, the difference in  $\text{NO}_3$  is much greater. Increased variability in  $\text{NO}_3$  flux with increasing N supply has been found in previous studies of inundated agricultural soils (Speir et al., 2017). Our nutrient rich flow-through incubations likely enhanced ecosystem control points of  $\text{NO}_3$  retention in soil collected from some, but not all, locations within an easement. Quantification of factors influencing ecosystem control points (Bernhardt et al., 2017), in terms of differentially enhanced soil  $\text{NO}_3$  and  $\text{PO}_4$  flux at specific locations within easements could reduce local-scale interpolation error (Dolph et al., 2022) and promote more robust understanding of WRP easements as nutrient sinks.

The lack of relationship between easement topography (variation in slope; overall easement elevation change) and IDW prediction error was unexpected. Topographical variation should influence spatial relationships between soil variables in riparian ecosystems (Robertson, 1987), resulting in different N cycling capacities between depressional and elevated areas (Bannister et al., 2015; Duncan et al., 2013). While there was a positive trend between WRP easement topography and soil C IDW prediction error, topographical influence on IDW prediction error was generally weak or absent for all soil structural and functional parameters measured here. Low samples size ( $n = 8$  easements) reduced statistical power to detect these trends with reasonably high

confidence (i.e. p-values less than 0.1); however, the spatial scale of the data set in the current study ( $n = 30$  for each WRP easement) is unique in its application to connections between soil structure and nutrient processing capacity. Notably, IDW interpolations were made spanning several habitats within any given easement. The influence of topographical variation on IDW error may be obscured by soil biogeochemical changes that occur across habitat boundaries within easements.

### **Extrapolation of nutrient retention estimates**

Extrapolation likely provides a better method than IDW for scaling up measurements of nutrient storage and flux to estimate soil structural and functional properties across representative WRP management areas because IDW lacks location specific estimates of prediction error. Additionally, non-overlapping 95% confidence intervals suggest differences in extrapolated nutrient storage (Fig. 3.9) and processing capacity (Fig. 3.10) between WRP easements, potentially due to restoration age or position within the landscape. Extrapolation allows for error estimates (95 % CIs in the current study) for any restoration/management areas of interest (i.e. tree planting and remnant forest) with replicated measurements. Our relatively small sample size within each easement precluded use of more computationally intensive interpolation methods (Krivoruchko & Gribov, 2019; Li, 2021; Sekulić et al., 2020) that require larger sample sizes (Oliver & Webster, 2014). However, geostatistical methods such as kriging may be useful for intensively sampled WRP easements when much higher replication can be achieved (Michael 2021).

Extrapolation of soil nutrient metrics from our dataset allows for a two-pronged approach to assessing nutrient retention capacity of wetlands restored through WRP. First, extrapolated estimates of soil nutrient storage and flux from the current study can be compared with published estimates of restored floodplain wetland nutrient retention capacity and interpreted within the context of restoration age, elevation, and geographic location. Second, paired measurements of soil structural and functional properties enable correlative analyses between soil structure and nutrient cycling functions among WRP easements. Informative hypotheses can be generated from this large dataset and applied to future study designs to evaluate trajectories of different wetland restoration practices (Mitsch et al., 2005; Winikoff & Finlay, 2023). Importantly, restoration age and elevation of soil core collection locations explain relatively little variation (12% at most) in soil nutrient storage and flux among tree planting and remnant forest habitats. This amount of variation is roughly similar to the amount explained by effects of fieldwork constraints (Chapter 2). However, discussion of soil nutrient trends within the ecological context of restoration age and elevation can generate hypotheses that may be valuable to WRP easement managers.

### ***Restoration age***

Older tree plantings tended to have more positive NO<sub>3</sub> flux (i.e., lower retention rates). Relatively recent agricultural land use associated with new tree plantings may have positively influenced the occurrence of NO<sub>3</sub> uptake hotspots if landowners applied micronutrients (i.e. calcium, magnesium, sulfur) to maximize N use efficiency by crops (Grzebisz et al., 2023). Essentially, soils at some locations within WRP easements may function as NO<sub>3</sub> uptake control points (Bernhardt et al., 2017) when NO<sub>3</sub> rich floodwater

is introduced, only if recent farming practices supplied those soils with optimal levels of micronutrients such that soil uptake capacity for  $\text{NO}_3$  was maximized. The magnitude and spatial frequency of these effects should dissipate over time as micronutrients are consumed and soils undergo succession during tree growth. Figure 3.11d anecdotally supports this hypothesis as the most extreme  $\text{NO}_3$  uptake hotspots are observed for the newest tree plantings, but pre-restoration records of farm fertilizer application practices, and information regarding plant species and root structure within each soil core (Grzebisz et al., 2023), could lend further support. Interestingly, I did not observe  $\text{PO}_4$  uptake hotspots for newly restored WRP easements, suggesting  $\text{NO}_3$  limitation may occur in newly restored soils during floods, at least for tree plantings. More work is needed to assess how  $\text{NO}_3$  uptake control points in new restored easements are influenced by biotic assimilation (Grzebisz et al., 2023; Kuzyakov & Blagodatskaya, 2015), dissimilatory  $\text{NO}_3$  reduction pathways (Almaraz et al., 2020; Groffman et al., 2009), and the degree to which  $\text{NO}_3$  reduction depends on micronutrient concentration (Petersen et al., 2020). The frequency and distribution of  $\text{NO}_3$  uptake control points interpreted in conjunction with knowledge of pre-restoration farming practices and soil root structure at specific locations could lead to more nuanced understanding of  $\text{NO}_3$  retention capacity in WRP soils and improve our ability to accurately extrapolate N cycling process rates to unsampled areas.

Soil P storage tended to be higher in older tree plantings but there was no difference in soil P storage between tree plantings and remnant forest habitats in the current study. There are few monitoring or experimental studies of the relationships between bottomland hardwood forest succession and P retention (Niswander' & Mitsch,

1995). More recent studies have focused on the importance of macrophytes (Mitsch et al., 2005), inundation time (Aldous et al., 2005; Aldous et al., 2007; Kröger et al., 2012), and abiotic sorption (Bruland & Richardson, 2004; Peng et al., 2019) for P retention during succession after wetland restoration. Inundation time, P delivery during floods, and P sorption capacity of soils likely vary among the wide geographic distribution of WRP easements and contribute to the variation in soil P availability observed in relation to tree planting age (Fig. 3.11c). Additionally, upstream agricultural and urban land use likely contribute to P accumulation and storage via nutrient delivery and sediment deposition during floods (Dolph et al., 2022; Noe & Hupp, 2005). Floodplain vegetation can slow floodwater and increase sediment deposition, but this effect was lower for woodlands (i.e. tree plantings) compared to grasslands in tributaries of the Rhine River (Olde Venterink et al., 2006). Continued monitoring of tree planting restorations through successional stages is needed to accurately scale-up the role of this restoration practice in floodplain P retention and storage beyond WRP boundaries, especially as some tree plantings prone to long duration flooding near the Mississippi River often have low survival rates and succession favors herbaceous plant communities (personal observation). Importantly, our measure of soil P was made by Mehlich 3 extraction. Mehlich 3 procedures are typically used in agricultural studies to provide an estimate of P available for plant uptake (Richardson & Reddy, 2013), but does not provide an estimate of total soil P, unlike our data for soil C and N. Soil total P has been predicted for the Upper Mississippi River Basin using spatial simulation interpolation from a large national dataset (Dolph et al., 2022) but such a comprehensive analysis is lacking for soil total P in the Lower Mississippi River Basin.

The significant 21% increase in soil N and marginal 16% increase in soil C storage in remnant forests compared to tree plantings, regardless of age, is indicative of a slow buildup of soil organic matter in older forests that is apparently not detectable within the first 20 years of tree growth. Accumulation of mineral deposits in floodplain soils generally decreases with distance from river channels (Bannister et al., 2015) but organic matter often shows the opposite pattern with distance (Kroes et al. 2007). It is likely that organic matter accumulation in forest soils contributed to observed increases in soil C and N compared to tree plantings, but additional analyses of runoff patterns and route of water delivery to WRP soils (overland flow vs river flooding) are needed. Forest soils are known reservoirs of organic matter and organic matter content tends to increase with soil moisture (Błońska & Lasota, 2017). Our measurements of total C and N in soil were not limited to organic fractions, but inorganic C in a representative subset of our samples was less than 1% (Duwadi et al. unpublished data). Total soil C is likely representative of organic C content in the current study. Unlike total soil C, total soil N probably included larger amounts of inorganic N. Measurements of specific N fractions were not made for all WRP easements discussed here, but increased inorganic and organic N fractions in forest soils likely contributed to the observed increase compared to soil N for tree plantings.

### ***Topography***

Soil C storage tended to be higher for tree plantings and remnant forests at higher elevations, but elevation only explained about 4 % of the variance in soil C for each habitat. This slightly positive trend contrasts somewhat with findings of (Bannister et al., 2015) who found that elevation was not related to soil C accumulation in an alluvial

floodplain. However, the scale of elevation change between our two studies was quite different. Bannister et al. focused on a gradient of alluvial habitats near sea level with relatively small elevation change (11.3 to 12.3 m). I focused on elevation change among WRP easements covering a much wider geographic area with relatively “steep” changes in elevation (79 to 117 m). The geographical range of my analysis likely contributed to variability around the predicted increase in soil C storage as a function of elevation. The consistent trend in the relationship between soil C and elevation for both tree plantings and remnant forests supports the idea that soil C storage is more related to elevation than age of forest succession. Studies of soil C storage along floodplain elevational gradients is generally limited to a one or two meter change in elevation across the study area (Bannister et al., 2015; Drouin et al., 2011; Gallardo, 2003) and focus on a wide range of soil depths from 10 cm (Gallardo, 2003), 30 cm (Bannister et al., 2015), to 100 cm (Drouin et al., 2011) – all deeper than the 5 cm focus in the current study. Increased soil C storage at higher elevations ranging over 1000 m has been documented for mountain ranges due to lower temperatures depressing organic C mineralization rates (Garten & Hanson, 2006; Griffiths et al., 2009). This climatic influence on temperature is unlikely to affect soil C mineralization at the scale of 30 to 40 m elevational differences measured in the current study. More research is needed to understand how elevation and topography (Duncan et al., 2013) influence soil organic matter processing and nutrient cycling across moderate elevational changes.

Initial PO<sub>4</sub> flux tended to be more positive (i.e., lower retention rates) for tree plantings and remnant forests at higher elevations. Tendency toward PO<sub>4</sub> release could be caused by more extreme variation in soil moisture at higher elevations if soil is inundated

less frequently and drains more quickly than lower elevations. Phosphate retention is maximized in soils where moisture is maintained at moderate levels between floods (Aldous et al., 2005). Increased soil PO<sub>4</sub> release from inundation of previously drained wetlands has been demonstrated repeatedly (Ardón et al., 2010; Kinsman-Costello et al., 2014; Kröger et al., 2012) but factors controlling PO<sub>4</sub> release rates differ at local spatial scales (Bruland & Richardson, 2004) depending on abiotic sorption capacity of soil and associated vegetation communities (Peng et al., 2019).

Phosphate release from remnant forest soils appears to have a slightly stronger positive relationship with elevation than PO<sub>4</sub> release from tree plantings in the current study, even though overall PO<sub>4</sub> flux between the two habitats is very similar. The slight difference in PO<sub>4</sub> flux response to elevation between habitats is likely due to greater PO<sub>4</sub> uptake by tree planting soils for one relatively high elevation easement where remnant forests were apparently cleared (i.e. not included in this study) between 2008 and 2010, according to satellite imagery from Google Earth. Much of the easement was cultivated after forests were cleared but before enrollment in WRP. Trees were subsequently planted in one section of the easement in 2015 that had not been cropped between 2008-2015 but allowed to regenerate naturally after forest clearing. This sequence of management practices is unusual among WRP easements included in the current study, which typically exist as either bottomland hardwood forests or agricultural land for decades prior to WRP enrollment and restoration. Legacy effects of management practices implemented before enrollment in WRP likely influence soil properties and subsequent relationships with nutrient cycling during floods (Land et al., 2016; Skinner, 2022). Future studies of nutrient retention capacity of WRP soils will benefit from

explicitly incorporating pre-restoration land use history and topography into predictive models of nutrient storage and flux. For example, causative linkages between land use history, soil characteristics, and nutrient flux after inundation could be further explored using structural equation models, which account for indirect and direct relationships between predictive variables and nutrient cycling responses (Elrys et al., 2022; Kreiling et al., 2020) across diverse ecosystems (Hall et al., 2009). Enhanced predictive understanding of landscape processes influencing soil nutrient storage and flux will improve accuracy of scaled-up measurements of wetland nutrient retention.

## **Conclusion**

Inverse distance weighted interpolation models have poor prediction accuracy for soil parameters at the local scale (individual soil core locations within easements) and error associated with IDW predictions of soil nutrient storage/flux was not significantly correlated with topographical variation over the sampled areas. However, IDW predictions align with extrapolated mean estimates of nutrient storage and flux at the easement scale, regardless of the power function ( $P = 1, 2, \text{ or } 3$ ) used. Extrapolation should be preferred to IDW interpolation for the current dataset because the lack of localized error estimates associated with IDW predictions. Extrapolation allows more precise quantification of measurement variation within WRP management areas of interest (i.e. tree plantings) when sample size is relatively low (30 or fewer sampling locations) as is necessary for labor intensive flow-through incubations for functional measurements of soil nutrient flux. Extrapolated estimates revealed higher surficial soil N storage in remnant forest habitats compared with tree plantings, but significant differences in soil C and P storage, and initial  $\text{NO}_3$  and  $\text{PO}_4$  flux were not observed

between remnant forest and tree plantings. Overall, elevational changes among easements explained more variation in soil nutrient storage and flux than tree planting age. However, younger tree plantings were associated with  $\text{NO}_3$  uptake hotspots and lower P storage in soils. Variation in nutrient storage/flux estimates within a study area should be accounted for before extrapolating measurements beyond the region directly measured. Additionally, our flow-through incubations maximized nutrient uptake rates by continuously introducing high dissolved  $\text{NO}_3$  and  $\text{PO}_4$  concentrations to soils, likely influencing the magnitude of nutrient flux hot spots/control points among WRP easements, especially  $\text{NO}_3$  uptake in younger tree planting soils and adjacent remnant forest soils. Our measurements of soil nutrient content are directly representative of surficial storage of C and N, and availability of P during the growing season, but  $\text{NO}_3$  and  $\text{PO}_4$  flux rates are only representative of initial inundation during a single flood. Further work is needed to model inundation frequency and duration and approximate annual nutrient flux potential for WRP easements as a function of riverine nutrient loads.

**CHAPTER 4: NUTRIENT DELIVERY, RETENTION, AND PROCESSING IN A RECONNECTED FLOODPLAIN FOREST: INSIGHTS FROM FLOODWATER MONITORING AND FLOW-THROUGH SOIL CORE INCUBATIONS**

**Abstract**

Levee breaks along historically channelized rivers can restore floodplain dynamics that promote nutrient retention. In this case study, I evaluate nutrient retention capacity of a forested floodplain WRP easement reconnected to its river via levee breaks. Specifically, I compare results of floodwater monitoring and flow-through soil core incubations to assess differences in ambient and maximum nutrient retention rates. The floodplain was a net sink for total nitrogen (N) and total phosphorus (P) in three measured floods during January, July, and October 2020. Molar N:P ratios differed between floods and increased with distance from levee in all floods, indicating that relative amounts of N and P delivery were not consistent across floods, but more P was consistently retained than N. Variation in  $\text{NH}_4$  and  $\text{NO}_3$  spatial trends during the July flood suggested the floodplain's internal N cycling dynamics influenced the degree to which the floodplain was a net sink for total N, while  $\text{PO}_4$  concentrations were relatively consistent with total P retention patterns. However, soil N:P ratios that do not match water export patterns indicate potential for unmeasured P export from the floodplain. Soil core incubation results generally agreed with floodwater patterns of  $\text{NH}_4$  release and  $\text{PO}_4$  uptake, but spatial patterns of  $\text{PO}_4$  uptake were different between floodwater monitoring and soil incubation measurements. Nitrate uptake was much higher for soil core

incubations, likely because of high NO<sub>3</sub> concentrations in flow-through source water relative to natural floodwater. Greenhouse gas flux (N<sub>2</sub>O and CH<sub>4</sub>) was generally low compared with literature values, indicating that nutrient retention in this floodplain is possible without substantial greenhouse gas emissions. Both floodwater monitoring and flow-through soil incubations provide valuable information about nutrient retention capacity. Future studies should focus on how departures from ambient conditions drive differences between flow-through incubations and *in situ* floodwater monitoring.

## Introduction

Stream channelization has historically disconnected rivers from their floodplains (Nunnally, 1978), exacerbating downstream effects of nutrient pollution from urban and agricultural runoff (Carpenter et al., 1998; Vitousek et al., 1997). Creation of levees constrains complex nitrogen (N) and phosphorus (P) cycling processes (Galloway, 1998; Ready et al., 1999) to the river channel except in rare overbank flows (Junk et al., 1989; Shrestha et al., 2014). Retention of nutrients and sediment is minimal in channelized stream reaches with short residence times (Booman & Laterra, 2019) but can be improved through stream restoration practices that facilitate frequent overbank flows (McMillan & Noe, 2017). Levee breaks can help to restore variable floodplain topography (Florsheim & Mount, 2002) which helps trap sediment and nutrients and mitigates negative downstream impacts of non-point source pollution (Carpenter et al., 1998; White et al., 2014).

Nutrient retention capacity of floodplain wetlands has been studied in various ways including sediment deposition studies (Gillespie et al., 2018), development of *in*

*situ* nutrient budgets (Mitsch et al., 2005), soil slurry nutrient assays (Richardson et al., 2019), intact soil core incubations (Hurst et al., 2016; Poe et al., 2003), and nutrient additions in the field (Forshay & Stanley, 2005). Nutrient budgets are useful for quantifying floodplain contribution to riverine nutrient load reductions (Hopkins et al., 2018) but give little information on biogeochemical mechanisms that influence nutrient transformations (Argiroff et al., 2017; Hurst et al., 2016; Olde Venterink et al., 2003; Poe et al., 2003). Conversely, mechanistic studies of soil nutrient processes introduce experimental artifacts that can influence localized processing rates and systematic errors can be magnified when scaled across a landscape. While it is not possible to measure all aspects of floodplain complexity in a single study (Appling et al., 2014; Wohl, 2021), investigations of floodplain nutrient retention capacity should strive to incorporate complementary methods and evaluate differences between them.

Delivery of nutrients to floodplains depends on watershed-scale processes that influence riverine nutrient transport (Czuba et al., 2018; Tong & Chen, 2002; Wollheim et al., 2018). Patterns of nutrient delivery and retention can affect floodplain biogeochemistry over time (Baldwin & Mitchell, 2000) and influence patterns of floodplain succession (Mitsch et al., 2005). Further, not all nutrients can be maximally retained under the same conditions. Anoxic conditions necessary for  $\text{NO}_3$  reduction to  $\text{N}_2$  (Knowles, 1982) can also facilitate  $\text{PO}_4$  release under certain conditions (Aldous et al., 2005; Kinsman-Costello et al., 2014). Interactions of carbon (C), N and P cycling can lead to nutrient retention tradeoffs (Ardón et al., 2010), downstream nutrient export (Kroeze et al., 2012), and greenhouse gas (GHG) emissions (Burgin et al., 2013; Hefting et al., 2013; Kang et al., 2022). Such complexities require complementary methods of

evaluating floodplain biogeochemistry to understand ecological benefits and costs of floodplain restoration.

The United States Department of Agriculture (USDA) has implemented the Wetlands Reserve Program (WRP) through the Natural Resources Conservation Service (NRCS). Landowners are compensated for allowing ecological restoration on frequently flooded WRP easements to facilitate ecosystem services of nutrient retention, flood mitigation, and biodiversity enhancement (Brinson & Eckles, 2011; Faulkner et al., 2011b; King et al., 2006). One forested WRP easement adjacent to Mayfield Creek in western Kentucky, USA, was selected for construction of five levee breaks in 2016, allowing water from Mayfield Creek to enter the floodplain more readily. Pre-restoration data from this site is not available. However, post-restoration nutrient retention capacity of this floodplain was evaluated as a function of inflowing nutrient concentrations. This evaluation provides a case study of floodplain nutrient retention capacity intended to encourage pre-restoration monitoring of floodplain reconnection sites so that expected post-restoration benefits can be more precisely valued over time.

Objectives of this study were: (1) quantify seasonal differences in total N and P delivery and relative retention rates between floods, (2) describe locations of sources and sinks of dissolved inorganic N and P fractions within the floodplain in a single summer flood, and (3) determine maximum nutrient uptake capacity of the floodplain by simulating a summer flood with elevated nutrient concentration using flow-through incubation of intact soil cores. I hypothesized that (1) the floodplain would act as a net sink for floodwater total N and P across seasons, (2) dissolved N and P would be released from the floodplain during the summer flood, and (3) dissolved N and P flux rates from

flow-through soil core incubations would show capacity of the floodplain as a net sink for dissolved nutrients.

## **Methods**

### **Study site**

The study site was in Carlisle County, Kentucky, USA, approximately 14 km from the confluence of Mayfield Creek with the Mississippi River. Much of Mayfield Creek has been channelized, but remnants of the original channel remain as backwater areas a few hundred meters from the levee (i.e. the current study site). The Mayfield Creek watershed drains a 735 km<sup>2</sup> area upstream of the study site with heavy agricultural and some developed land cover. Watershed land cover was summarized from NLCD19 values accessed through Model My Watershed® (Stroud Water Research Center, 2021) and is approximately 67.7% agricultural, 18.9% forested, 8.5% developed, and 4.7% wetland (Fig. 4.1). Floodwater sample collection for this study occurred in January, July, and October 2020. Discharge data was not available for Mayfield Creek across all three floods. However, a water level sensor was deployed for July and October floods. Shapes of the hydrographs for July and October floods in Mayfield Ditch were similar to hydrographs from a nearby USGS gauge station in an adjacent watershed (Bayou de Chien, monitoring location 07024000) over the same time period. This station was also recording data during the January 2020 flood where water level data was missing for Mayfield Ditch. Hydrographs from the Bayou de Chien gauging station are likely the best available means to compare relative flood sizes in the region from January – October 2020.

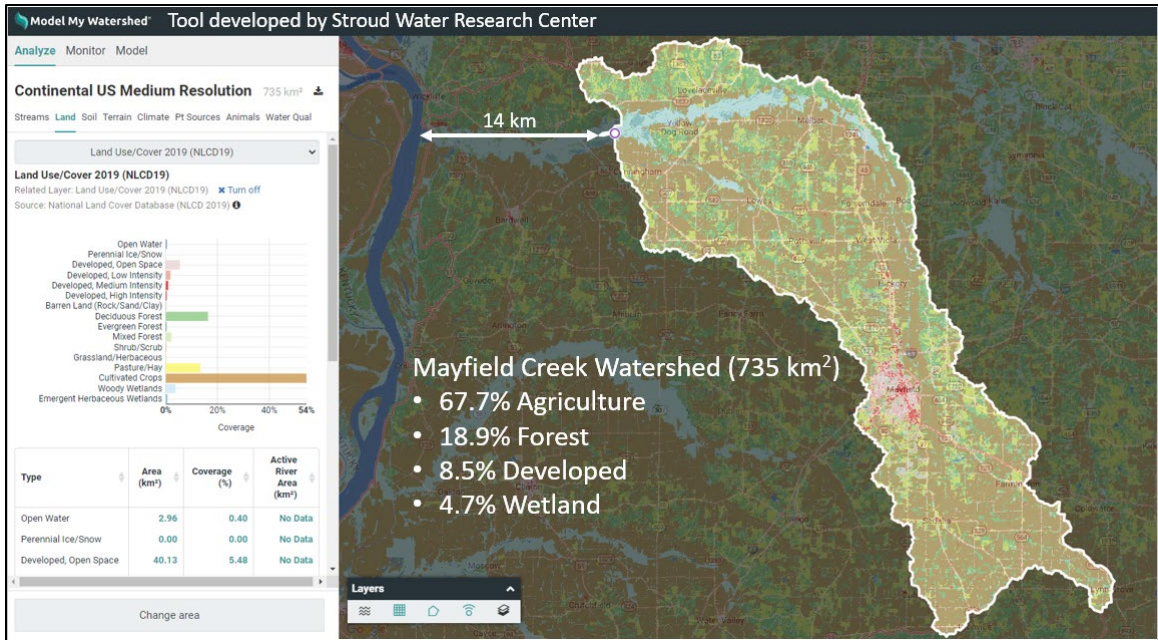


Figure 4.1. Mayfield Creek watershed landcover and proximity to Mississippi River. Screenshot modified from Stroud Water Research Center “Model My Watershed” tool.

### Floodwater sampling

Automated floodwater samplers (ISCOs) were deployed in four locations representative of flood flow paths across the easement. The most upstream ISCO was located at a levee break where floodwater first enters the floodplain from the channelized main flow path of Mayfield Ditch. The second ISCO was located along a flow path in the forest approximately 240 m downstream from the levee ISCO. The third ISCO was located at the intersection of a flow path draining the forest with the backwater remnant channel of Mayfield Creek, approximately 490 m downstream of the levee ISCO. The most downstream ISCO was located on the remnant channel approximately 950 m downstream of the levee ISCO (Fig. 4.2). These four locations were spatially representative of flow paths across the easement and sample collection during floods was

more consistent at these locations than other sites where floodwater collection was attempted across the easement.

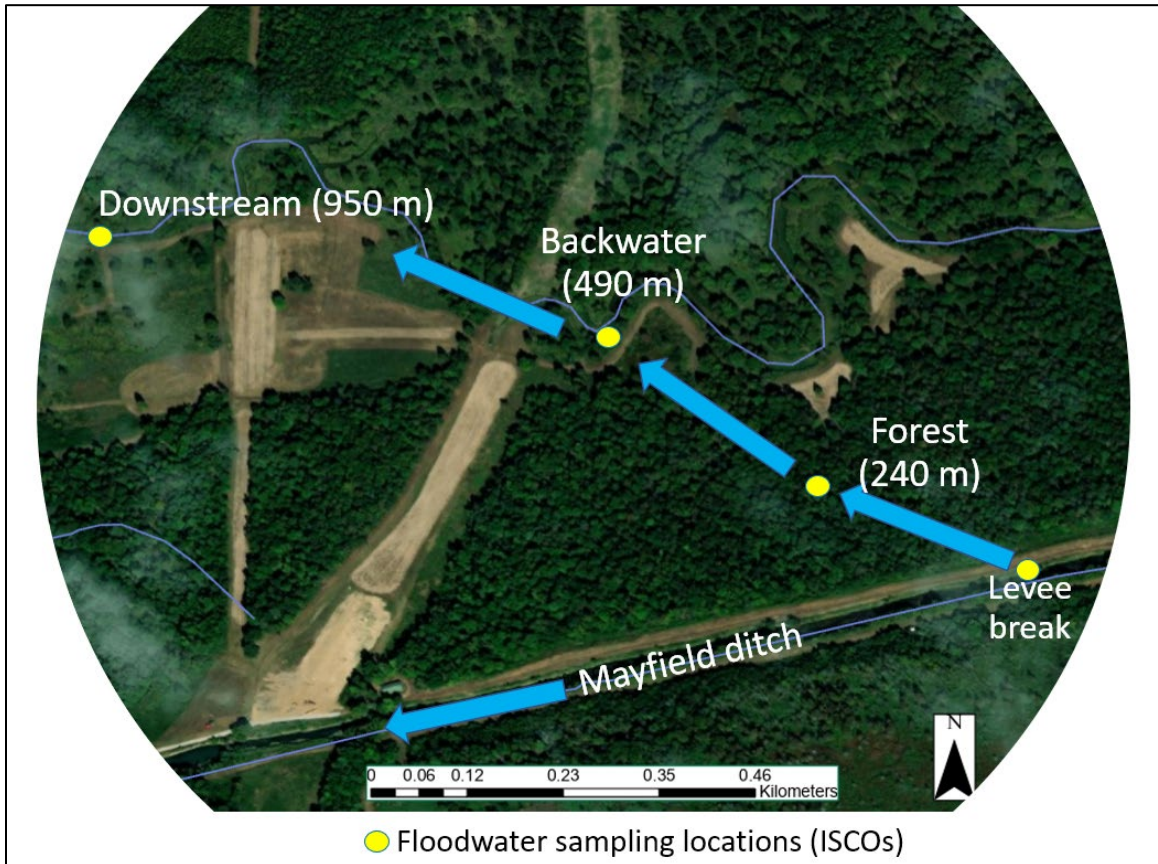


Figure 4.2. Floodwater flow direction (blue arrows), sampling locations (yellow ellipses) and distances from levee break.

Sample collection began when floodwater reached liquid level actuators connected to each ISCO. Actuators were positioned 10-30 cm above the soil surface and adjusted between floods to minimize sample collection in the floodplain before water overtopped levee breaks in each flood event. Intake hoses were positioned immediately below actuators and submerged before sampling began. Each ISCO was programmed to collect 800 mL of water every hour for 24 hours. Sample bottles each contained 0.5 mL 50% sulfuric acid which lowers pH below 2 to limit microbial activity until samples were

retrieved post-flood, transported to the laboratory on ice, and refrigerated until analysis of total nitrogen (TN), total phosphorus (TP), total suspended solids (TSS), and particulate organic matter (POM) within 30 days. Three floods were sampled in January, July, and October of 2020 to assess seasonal patterns in nutrient transport across the floodplain. Water samples for the July flood were analyzed for dissolved N and P fractions ( $\text{NH}_4$ ,  $\text{NO}_3 + \text{NO}_2$ , and  $\text{PO}_4$  concentrations).

## **Sample processing**

### ***Particulates***

Total suspended solids (TSS) were measured by weight after thoroughly shaking each sample bottle to homogenize particulates and pouring a known volume, measured via graduated cylinder, into a filter tower loaded with a pre-weighed  $0.7 \mu\text{m}$  glass fiber filter and connected to a vacuum pump. Filters were ashed at  $500^\circ\text{C}$  for at least 2 hours in a muffle furnace and stored in a desiccator before use. Particulates were rinsed with DI water from the graduated cylinder and sides of the filter tower cup onto the filter for each sample. Filters were dried at  $60^\circ\text{C}$  for 48 hours, cooled, and weighed again. Initial filter weight was subtracted from dried filter weight and divided by the volume of water filtered for each sample to give TSS concentration in  $\text{mg L}^{-1}$ . Filters were then ashed at  $500^\circ\text{C}$  for 3 hours, cooled and weighed again. The difference between dried and ashed weights for each filter gave particulate organic matter (POM) concentration in  $\text{mg L}^{-1}$ .

### ***Total nutrient concentrations***

Unfiltered water samples were digested at a 2:1 sample:reagent ratio using a potassium persulfate solution amended with 2.0 M sodium hydroxide to raise the starting pH of the reaction above 12 for samples acidified to pH 2. After digestion, total nitrogen concentrations were determined by combustion with a Shimadzu TOC/N liquid analyzer and total phosphorus was determined by colorimetric reaction with molybdate on a Seal AQ400 discrete nutrient autoanalyzer. A subset of undigested water samples was filtered through 0.7  $\mu\text{m}$  glass fiber filters and analyzed for  $\text{NH}_4$ ,  $\text{NO}_3 + \text{NO}_2$ , and  $\text{PO}_4$  concentrations as described below.

### **Soil core collection and processing**

Thirty pairs of soil cores were collected in 7.6 x 30 cm acrylic tubes across the floodplain between levee breaks and the most downstream ISCO on the remnant channel in July 2022. Core pairs were collected to represent a 30  $\text{cm}^2$  area by hammering an acrylic tube housed in a steel coring device into the soil. Twenty-two core pairs were collected inside the floodplain forest, six core pairs were collected from an impounded area of shallow water near the most downstream ISCO, and two core pairs were collected from dry area of mowed grass next to the impounded area. Core depth ranged from 10-16 cm. All cores were transported to the laboratory on ice. One of each pair was analyzed for soil pH, soil moisture, soil bulk density, extractable  $\text{NH}_4$  and extractable  $\text{NO}_3$  in the top 10 cm of soil at Tennessee Tech. Analyses of soil moisture, bulk density, and pH are described in chapter 3. Soil  $\text{NH}_4$  and  $\text{NO}_3$  was extracted by adding 125 mL 0.5M  $\text{K}_2\text{SO}_4$  to each sample, shaken for one hour on an orbital shaker, centrifuged and filtered for each sample using a 0.45  $\mu\text{m}$  nylon filter. Additional samples dried and homogenized from

each core were shipped to the Kansas State University Soil Testing Laboratory for analysis of total carbon (C), total nitrogen (N), and extractable phosphorus (P) as described in chapter 3. Soil iron (Fe) content was also measured from the same samples as extractable P following Mehlich III extraction at Kansas State. The second core from each pair was used in flow-through incubation.

### **Soil core incubation**

The flow-through core incubation was conducted according to methods detailed in chapter 2. Briefly, synthetic water with elevated  $\text{NO}_3$  (~10 mg  $\text{NO}_3\text{-N/L}$ ) and  $\text{PO}_4$  (~1 mg  $\text{PO}_4\text{-P/L}$ ) concentrations was supplied to soil cores at approximately 1.8 mL/min via peristaltic pump to saturate nutrient uptake rates. Incubations were conducted at 24°C. Outflow rates were measured for each core at the time of sample collection. Approximately 15 mL water was collected from inflowing source water and outflowing water from each core as soon as cores filled with water (approximately 6 hours after flow-through system was initiated). Water samples were filtered via 0.7  $\mu\text{m}$  glass fiber filters and frozen until analysis of  $\text{NO}_3$ ,  $\text{NO}_2$ ,  $\text{NH}_4$ , and  $\text{PO}_4$  (see nutrient analyses below). Additional samples were collected after 24- and 48-h incubation for dissolved nutrient analyses as described above.

Triplicate dissolved gas samples were collected at 12-, 24-, and 48-h incubation time and analyzed for  $\text{N}_2$ ,  $\text{O}_2$ ,  $\text{N}_2\text{O}$ , and  $\text{CH}_4$  concentrations using membrane inlet mass spectrometry (MIMS) and the Ar ratio method (Kana et al., 1994). Inflow and outflow water samples were collected from each core by placing each tube fed by peristaltic pump in 12 mL exetainers and allowing each to overflow at least 3 times, reducing potential for contamination by atmospheric gases. A preservative was added ( $\text{ZnCl}_2$ , 180  $\mu\text{L}$ ) to stop

microbial activity, and NaOH (180  $\mu$ L) was added to precipitate CO<sub>2</sub> as bicarbonate. Removal of CO<sub>2</sub> was an essential step because CO<sub>2</sub> and N<sub>2</sub>O both have molecular weights of 44 and cannot be measured simultaneously via MIMS. Carbon dioxide was not measured in this study. Exetainers were immediately capped without any headspace after addition of ZnCl<sub>2</sub> and NaOH, checked for presence of bubbles, and stored underwater at 4°C until analysis.

### **Nutrient analyses**

Nutrient concentrations were analyzed from filtered floodwater and incubation water using a Seal AQ400 autoanalyzer and standard colorimetric methods provided by Seal, equivalent to EPA method detection limits. Nitrate was measured using cadmium reduction to NO<sub>2</sub>. Nitrite concentrations were subtracted from NO<sub>3</sub> + NO<sub>2</sub> concentrations to yield NO<sub>3</sub> only concentrations for soil core incubations in July 2022. Combined NO<sub>3</sub> + NO<sub>2</sub> concentrations were used in analyses of July 2020 floodwater. Nitrite concentrations were measured by color development after addition of sulfanilamide with *N*-(1-naphthyl)-ethylenediamine dihydrochloride (NEDD) to each sample. Absorbance was measured at 520 nm. Phosphate was measured via reaction of acid molybdate with antimony and reduced by ascorbic acid for color development. Absorbance was measured at 880 nm. Ammonia was measured at alkaline pH by reaction with hypochlorite derived from dichloroisocyanurate and further reaction with salicylate to form a dye measured colorimetrically at 660 nm. Coefficients of variation (standard deviation divided by mean) were calculated for each triplicate set of inflow nutrient concentrations. Outlier concentrations of NO<sub>3</sub> and PO<sub>4</sub> were identified and removed from flux calculations if CVs were greater than 10 percent.

## Dissolved gas analyses

The MIMS system was modified for detection of trace gases, specifically N<sub>2</sub>O (Speir et al. In review). The liquid nitrogen cold trap traditionally used for measurement of N<sub>2</sub> and O<sub>2</sub> is below the freezing point of N<sub>2</sub>O (-91°C) and was replaced with a mixture of crushed dry ice and methanol to maintain a temperature of approximately -79°C, slightly below the freezing point of CO<sub>2</sub>. However, CO<sub>2</sub> is not immediately frozen at this temperature, thus, precipitation to bicarbonate via NaOH addition is essential for all samples intended for N<sub>2</sub>O measurements. Standards were prepared from DI water held in a constantly stirred flask maintained at the incubation temperature (24°C) so that aqueous gas concentrations were maintained at equilibrium with the atmosphere. Water was pumped from the flask into 12 mL gas exetainers via peristaltic pump. Exetainers were triple filled with atmospherically equilibrated DI water and amended with ZnCl<sub>2</sub> and NaOH as previously described. Six standards were made at a time during MIMS warm-up and daily sample analysis. Standards were stored in ice water and analyzed every six samples to account for drift in MIMS signal. Dissolved gases were measured via MIMS at the following channels: N<sub>2</sub> at  $m/z$  28, O<sub>2</sub> at  $m/z$  32, N<sub>2</sub>O at  $m/z$  44, CH<sub>4</sub> at  $m/z$  15 and Ar at  $m/z$  40, corresponding to their molecular weights. Methane was measured at 15  $m/z$  because singlet oxygen atoms can interfere with signal at  $m/z$  16 ( Zhao et al., 2021). All measurements were made with the secondary electron multiplier (SEM) activated to improve detection of trace gases.

Triplicate gas concentrations for each core were screened for outliers for each gas. Outliers were identified and removed if one triplicate concentration of N<sub>2</sub> was > 0.5% from the triplicate mean, if one triplicate concentration of O<sub>2</sub> was > 10% from the

triplicate mean, or if one triplicate of N<sub>2</sub>O or CH<sub>4</sub> was > 5% from the triplicate mean. Differences in concentration thresholds for outlier identification reflect relatively higher concentration of N<sub>2</sub> and less variability across samples compared with O<sub>2</sub>. Similarly, N<sub>2</sub>O and CH<sub>4</sub> concentrations were much lower than N<sub>2</sub> or O<sub>2</sub> with high variability relative to concentrations.

### **Flux rate calculations**

Flux rates were calculated using Eq. 3 from chapter 2 shown below:

$$F_{i,nc} = \frac{([Core]_{out} - [IN]) Q_{core}}{A}$$

Where  $F_{i,nc}$  is the flux rate (mg m<sup>-2</sup> h<sup>-1</sup>) accounting for individual flow rates for each core.  $[Core]_{out}$  is the dissolved nutrient or gas concentration (mg L<sup>-1</sup>) in the core outflow.  $[IN]$  is the inflow concentration of dissolved nutrient or gas averaged from three inflow lines pumped from source water via peristaltic pump.  $Q_{core}$  is the outflow rate (L h<sup>-1</sup>) measured for each core.  $A$  is the core surface area (0.0045604 m<sup>2</sup>). All calculated flux rates were averaged over three sampling time points for each core during the 48h incubation before statistical analyses.

### **Data processing and analyses**

#### ***Nutrient concentrations***

Paired nonparametric Wilcoxon t-tests were conducted to compare median differences in floodwater TN and TP between each ISCO sampling station downstream of the levee in each flood. Samples were paired for comparison so that each downstream

sample was collected after each upstream sample (between 7 and 42 minutes). Sixteen paired samples were available from the January flood, 14 from the July flood, and 7 from the October flood. Sampling the same parcel of water across the floodplain was not possible. However, these pairings provide the best possible estimate of nutrient concentration differences between sampling locations given variability in flood flow paths. Results are visually presented as percent median difference in TN or TP concentration relative to concentration at the more upstream sampling location for each comparison in each flood.

Relationships between floodwater N:P ratios and distance from levee were directly assessed by regression with ANCOVA, accounting for different N:P ratios at the levee break between floods. Floodwater molar N:P ratios were regressed against flood duration for each ISCO sampling station in each flood. Flood duration is represented by the number of hours that all ISCOs were collecting water samples so that temporally paired comparisons could be made between upstream and downstream sampling stations. Regression slopes represent changing N:P ratios over the duration of flooding at each sampling location. Comparison of regression intercepts between each sampling station enables inference of changing N:P ratios across floodplain locations (i.e. distance from levee).

Floodwater  $\text{NH}_4$ ,  $\text{NO}_3+\text{NO}_2$ , and  $\text{PO}_4$  concentrations in July were assessed using Welch's t-tests for samples with unequal variances. Mean differences were assessed between ISCO sampling stations in reference to nutrient concentrations measured at the levee ISCO. Dissolved inorganic nitrogen (DIN) was calculated from the sum of  $\text{NH}_4+\text{NO}_3+\text{NO}_2$  to generate DIN: $\text{PO}_4$  ratios for each sample. Dissolved inorganic

nitrogen:PO<sub>4</sub> ratios were regressed against distance from levee to assess relative changes in floodwater inorganic dissolved N and P compared with TN:TP ratios. Ammonium concentration was regressed against POM to assess links between organic matter mineralization and NH<sub>4</sub> concentration.

Relationships between floodwater TN and particulates (TSS and POM) and TP and particulates were assessed by regression with ANCOVA, pooling all samples within floods and accounting for concentration differences between floods. Each nutrient was regressed against TSS and POM separately because POM and TSS were colinear. The more parsimonious predictor (TSS or POM) for each nutrient was identified by choosing the model with a lower AICc.

Soil molar N:P ratios were calculated from soil TN and extractable phosphorus (eP) concentrations at 0-10 cm depth. Additional soil molar N:P ratios were calculated from dissolved inorganic nitrogen (DIN) and eP concentrations. Each measurement of molar N:P ratios was regressed against distance from levee to compare patterns of soil N:P with floodwater N:P across the floodplain. These regressions provide an opportunity to observe trends in soil N:P ratios where we lack soil TP data to make direct comparisons between floodwater TN:TP and soil TN:TP molar ratios. Results were considered significant with  $\alpha < 0.05$  and marginally significant with  $\alpha$  between 0.05 and 0.10.

### ***Nutrient flux at the soil-water interface***

Flux rates derived from flow-through soil core incubations were assessed visually with boxplots. Negative flux is indicative of nutrient or gas uptake and positive flux is indicative of nutrient or gas release at the soil-water interface. Negative median values

indicate that uptake was more prevalent for a particular nutrient (i.e. more than 15 of 30 cores with negative flux). Negative mean values indicate that the floodplain was a net sink for a given nutrient.

Redundancy analysis (RDA) was conducted to model relationships between flux rate responses to soil structural characteristics and distance from levee. Constrained ordination through RDA allows variation in flux rate responses to be correlated with soil structural characteristics as explanatory variables, along with distance from levee sampling station. In essence, RDA allows soil functions potentially influenced by nutrient and particulate deposition during floods to be directly associated with flux rates where inferences can be made to describe C, N, and P cycling processes.

## **Results**

### **Floodwater nutrients and hydrology**

Total nitrogen concentrations ranged from 3.154 to 9.575 mg N L<sup>-1</sup> across floods and sampling locations. Total phosphorus concentrations ranged from 0.314 to 1.970 mg P L<sup>-1</sup> across floods and sampling locations. Maximum, minimum, and median TN and TP concentrations are shown for each ISCO sampling location in each month (Table 4.1) and visualized via boxplots in Fig. 4.3. Total nitrogen concentrations appear lower in January, compared with July and October floods. Total phosphorus concentrations were relatively similar across the three floods. Visual comparison of hydrographs show January and July floods were similar in size (i.e. maximum gauge height) and duration. The October flood was relatively small by comparison (Fig. 4.3).

Table 4.1. Minimum, median, and maximum TN (mg N L<sup>-1</sup>) and TP (mg P L<sup>-1</sup>) concentrations for each sampling location (as meters downstream of levee break) in each month.

Month	Distance from levee	Min TN	Med TN	Max TN	Min TP	Med TP	Max TP
January	0 m	4.091	4.303	6.795	0.838	1.183	1.524
	240 m	3.154	3.354	4.264	0.56	0.779	1.404
	490 m	3.514	3.647	4.627	0.422	0.546	0.848
	950 m	3.106	3.233	4.367	0.314	0.367	0.901
July	0 m	7.038	7.63	8.501	0.975	1.24	1.449
	240 m	7.859	8.181	9.325	0.782	0.969	1.199
	490 m	5.831	6.524	8.379	0.415	0.779	1.063
	950 m	6.14	6.675	7.179	0.555	0.736	0.785
October	0 m	7.346	7.644	9.199	1.323	1.692	1.97
	240 m	6.305	7.912	9.575	0.913	1.121	1.305
	490 m	6.485	6.992	8.759	0.739	0.907	0.969
	950 m	6.002	7.314	8.174	0.724	0.777	0.857

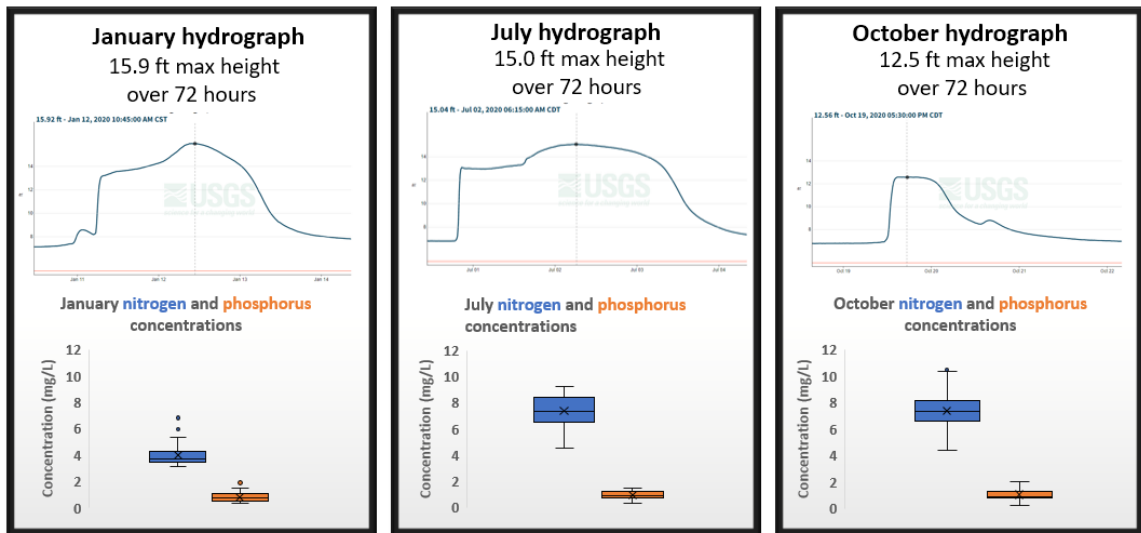


Figure 4.3. Hydrographs from USGS gauge (# 07024000) on Bayou de Chien, Kentucky, comparing relative size and duration of three floods between January 11-14th, July 1-4th, and October 19-22nd 2020. The y-axis scale is identical for each hydrograph and ranges from approximately 6 feet to 16 feet, including the minimum and maximum water levels during the 72-hour window (x-axis) shown for each flood. Boxplots below hydrographs summarize the range of TN (blue) and TP (orange) concentrations over the duration of sample collection (24 h) for each flood.

## **Longitudinal comparisons of TN and TP concentrations**

### ***240 m from levee***

Differences in relative TN and TP retention were observed between floods within 240 m from the levee (Fig. 4.4). Retention patterns of TN and TP near the levee were most similar in January. Total N retention in January was 22.9%, and 22.2% of TP was retained within 240 m of the levee (Fig. 4.4, Table 4.2, both  $p < 0.001$ ). Total N concentrations increased 8.8% in July within 240 m of the levee, indicating a potential N source in that area of the floodplain (Fig. 4.4, Table 4.2,  $p < 0.001$ ). Total P retention in July was 19.9% within 240 m of the levee (Fig. 4.4, Table 4.2,  $p < 0.001$ ). There was no statistically significant change in October TN concentrations within 240 m of the levee (Fig. 4.4, Table 4.2,  $p = 0.938$ ). Total P retention in October was 35.4% within 240 m of the levee (Fig. 4.4, Table 4.2,  $p = 0.016$ ).

### ***490 m from levee***

Total P retention between the levee and backwater sampling stations (490 m downstream) was consistently higher than TN retention among the three floods. Median TP retention was 48.9% in January, 38.8% in July (both  $p < 0.001$ ), and 47.1% in October (Fig. 4.5, Table 4.2,  $p = 0.016$ ) within 490 m of the levee. Median TN retention was 16.7% in January ( $p < 0.001$ ) and 14.4% in July (Fig. 4.5, Table 4.2,  $p = 0.001$ ). Median TN retention in October was not statistically different from zero within 490 m of the levee (Fig. 4.5, Table 4.2,  $p = 0.219$ ).

**950 m from levee**

Total P retention across the floodplain (950 m from levee) was consistently higher than TN retention among the three floods. Nutrient retention patterns were similar to those observed at the backwater sampling station (490 m downstream of levee), but TP retention estimates were slightly higher. Median TP retention estimates over the whole floodplain were 61.1% in January ( $p < 0.001$ ), 41.8% in July ( $p = 0.001$ ), and 54.3% in October (Fig. 4.6, Table 4.2,  $p = 0.016$ ). January TN retention over the whole floodplain was 24.5% ( $p < 0.001$ ), 13.5% in July ( $p < 0.001$ ) and not statistically different from zero in October (Fig. 4.6, Table 4.2,  $p = 0.109$ ).

Table 4.2. Results of Wilcoxon non-parametric paired t-tests. Difference of medians is reported in units of  $\text{mg L}^{-1}$ . Percent decrease refers to change in each downstream median estimate compared with median estimates at the levee; essentially, a measure of relative TN or TP retention between sampling stations.

<b>Flood</b>	<b>Nutrient</b>	<b>Comparison between sampling stations</b>	<b>difference of medians</b>	<b>95 % CI</b>	<b>% (decrease) from upstream</b>	<b>p-value</b>
January	TN	levee - 240m	0.986	0.884, 1.329	22.9	< 0.001
		levee - 490m	0.717	0.577, 0.951	16.7	< 0.001
		levee - 950m	1.055	0.974, 1.510	24.5	< 0.001
	TP	levee - 240m	0.263	0.181, 0.340	22.2	< 0.001
		levee - 490m	0.578	0.492, 0.639	48.9	< 0.001
		levee - 950m	0.723	0.650, 0.804	61.1	< 0.001
July	TN	levee - 240m	-0.674	-0.983, -0.523	-8.8	< 0.001
		levee - 490m	1.101	0.512, 1.606	14.4	0.001
		levee - 950m	1.029	0.592, 1.426	13.5	< 0.001
	TP	levee - 240m	0.248	0.154, 0.328	19.9	< 0.001
		levee - 490m	0.482	0.365, 0.666	38.8	< 0.001
		levee - 950m	0.520	0.443, 0.644	41.8	0.001
October	TN	levee - 240m	-0.086	-1.066, 0.873	-1.1	0.938
		levee - 490m	0.917	-0.143, 1.609	12.0	0.219
		levee - 950m	0.783	-0.111, 1.952	10.2	0.109
	TP	levee - 240m	0.599	0.388, 0.660	35.4	0.016
		levee - 490m	0.797	0.646, 0.968	47.1	0.016

levee - 950m	0.918	0.741, 1.093	54.3	0.016
--------------	-------	--------------	------	-------

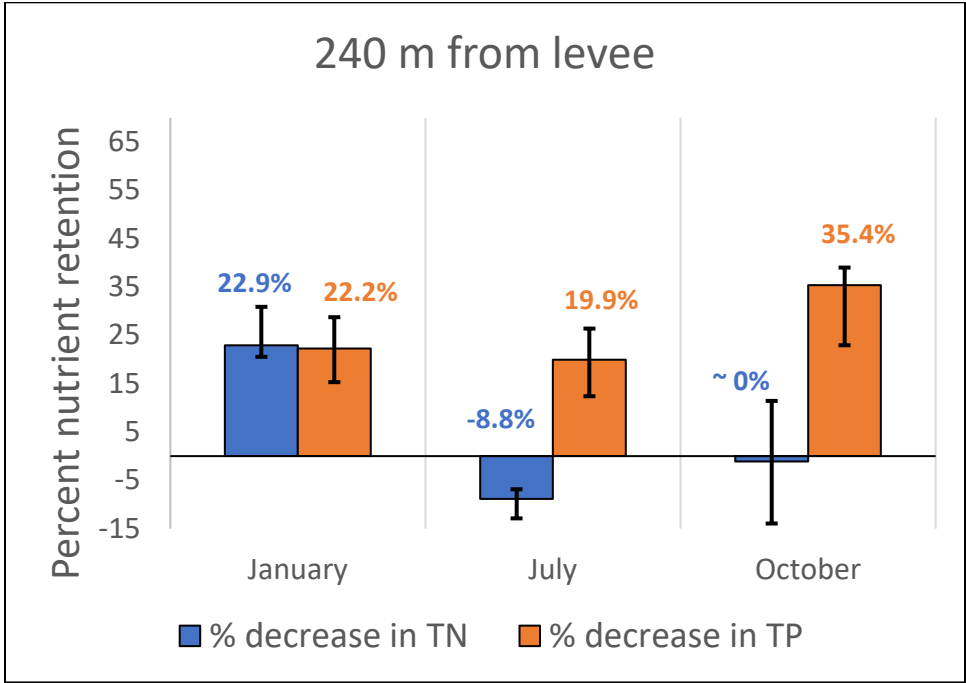


Figure 4.4. Percentage decrease in total nitrogen and total phosphorus concentrations between the levee sampling station and the forest sampling station 240 m downstream. Error bars represent 95 % confidence intervals calculated by Wilcoxon non-parametric paired t-tests.

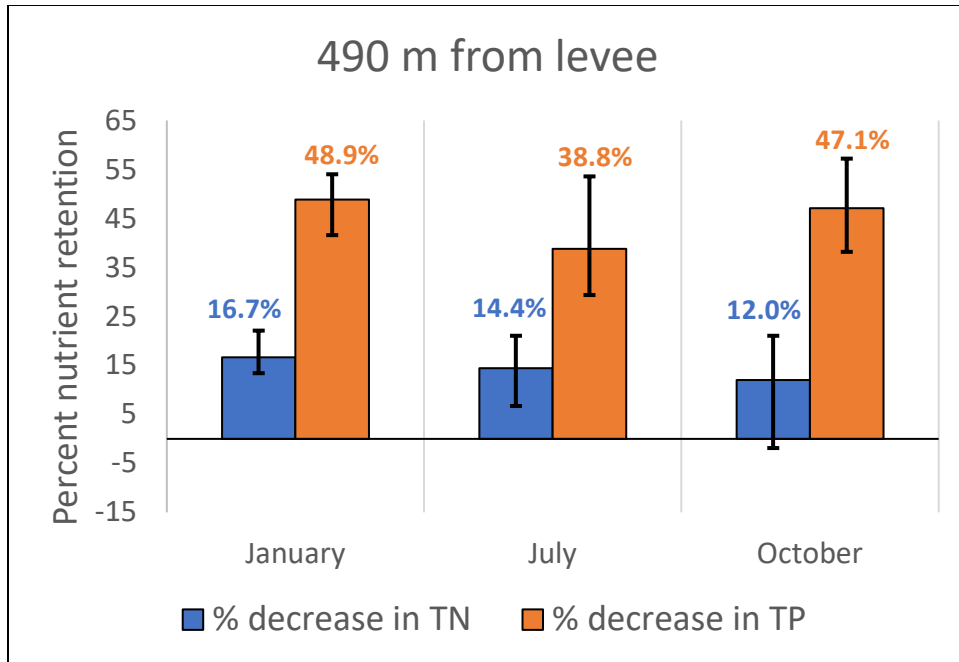


Figure 4.5. Percentage decrease in total nitrogen and total phosphorus concentrations between the levee sampling station and the backwater sampling station 490 m downstream. Error bars represent 95 % confidence intervals calculated by Wilcoxon non-parametric paired t-tests.

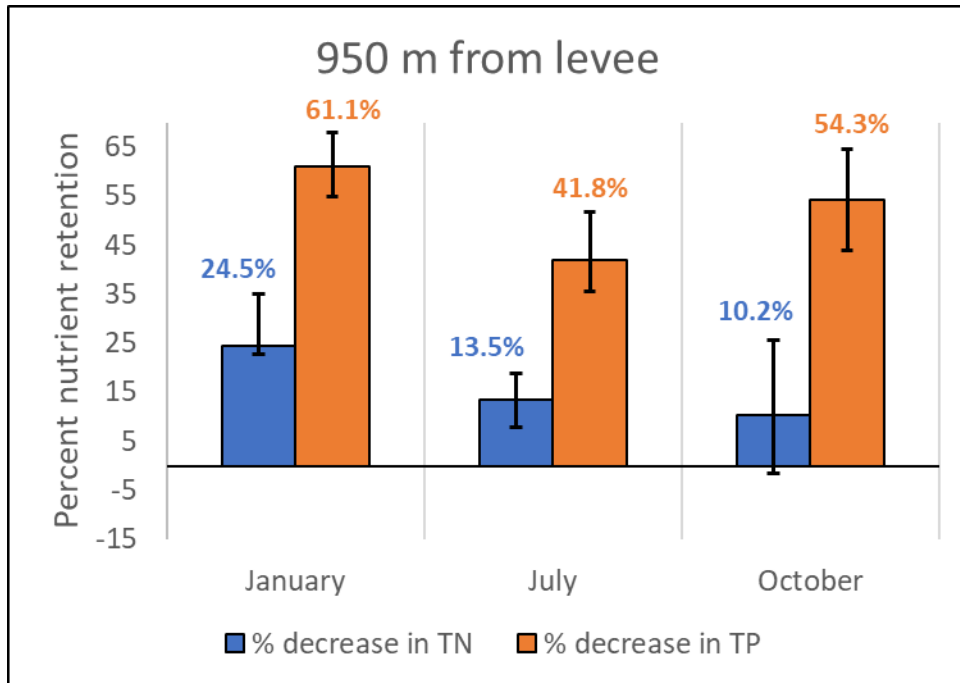


Figure 4.6. Percentage decrease in total nitrogen and total phosphorus concentrations between the levee sampling station and the furthest sampling station 950 m downstream. Error bars represent 95 % confidence intervals calculated by Wilcoxon non-parametric paired t-tests.

## Floodwater N:P stoichiometry

### *Longitudinal changes among floods*

Floodwater TN:TP ratios increased with distance from levee in all three floods. The slope of the relationship was 0.009, roughly equivalent to a 1 unit increase in floodwater TN:TP for every 110 m increase in distance from levee (Fig 4.7. Table 4.3,  $F_{(3, 143)} = 91.53$ ,  $R^2 = 0.65$ ). The intercept showed an estimated TN:TP ratio of approximately 8.4 at the start of the January flood ( $p < 0.001$ ). Relatively more N was delivered to the floodplain via levee breaks in July (TN:TP  $\sim 14.8$ ) and October (TN:TP  $\sim 12.6$ ) floods (Fig. 4.7, Table 4.3, both  $p < 0.001$ ).

Table 4.3. Results of regression with ANCOVA for the relationship of floodwater TN:TP ratio with distance from levee, controlling for starting concentrations of TN and TP in each flood. The estimate for the intercept shows predicted TN:TP ratio as water first entered the levee break in January. Estimates for July and October floods show predicted differences in TN:TP ratios as water first entered levee breaks in each flood compared with the January (intercept) estimate.

Predictor	estimate	Std. error	t-value	p-value	F-value	R <sup>2</sup>
intercept (January flood)	8.446	0.535	15.788	< 0.001	91.53 (3, 143)	0.65
distance from levee (m)	0.009	0.001	12.767	< 0.001		
July flood	6.388	0.599	10.673	< 0.001		
October flood	4.198	0.639	6.574	< 0.001		

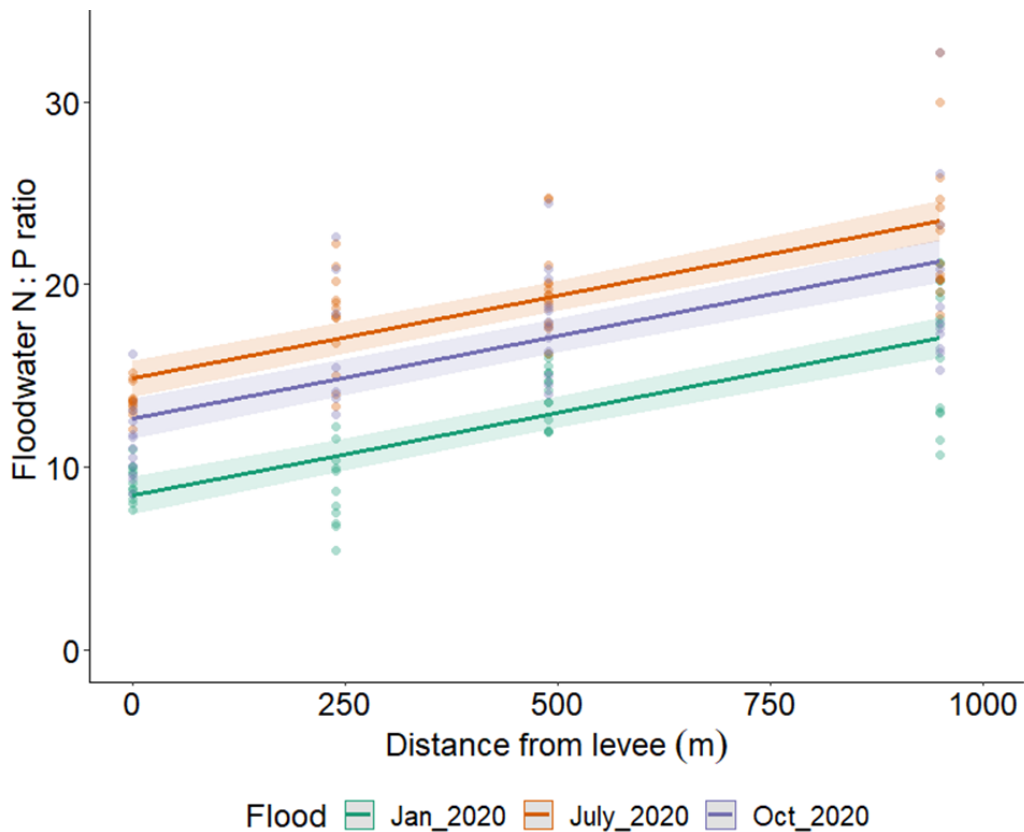


Figure 4.7. Relationships between floodwater TN:TP ratios and distance from levee. Interaction between distance from levee and flood was not statistically significant, so an additive model was used. Non-overlapping 95% confidence intervals for each regression line at the intercept indicate that the ratio of N:P delivery to the floodplain differed between floods, with the July flood delivering the most N relative to P.

### *Temporal changes during floods*

Molar TN:TP ratios tended to increase over the duration of the January flood at all four sampling stations (Fig. 4.8, Table 4.4). The slope of the relationship was lowest at the levee sampling station and statistical support for this relationship was weak (Table 4.4,  $R^2 = 0.17$ ,  $p = 0.062$ ), but slope increased at the sampling station 240 m from the levee, indicating a slightly positive relationship between floodwater TN:TP and flood duration (Fig. 4.8, Table 4.4,  $R^2 = 0.49$ ,  $p = 0.002$ ). Slope and intercept increased 490 m and 950 m downstream of the levee, indicating that January floodwater TN:TP ratios increased with flood duration and distance from levee (Fig. 4.8, Table 4.4, both  $R^2 > 0.6$ , both  $p < 0.001$ ).

There was no statistically significant change in TN:TP ratios over the duration of the July flood at any of the four sampling stations (Fig. 4.9, Table 4.4, all  $p > 0.2$ , all  $R^2 < 0.06$ ). However, intercepts for each model (Fig. 4.9) were statistically significant (Table 4.4, all  $p < 0.001$ ) and increased with distance from levee, providing additional evidence for an increase in TN:TP ratios with distance from levee at the beginning of the flood.

Molar N:P ratios tended to decrease over the duration of the October flood (Fig. 4.10, Table 4.4) at all sampling stations but statistical support for these trends was generally weaker than for the opposite (positive relationships) observed for all sampling stations in the January flood (Fig. 4.8, Table 4.4). However, there was strong statistical support for decreasing TN:TP ratios with flood duration 950 m downstream of the levee in the October flood (Fig. 4.10, Table 4.4,  $p = 0.004$ ,  $R^2 = 0.80$ ). Negative trending relationships between flood duration and TN:TP are more likely in October than July, relative to the flat slopes, high p-values, and low  $R^2$  observed in July (Table 4.4).

Table 4.4. Simple linear regression results of molar N:P ratios against flood duration. Flood duration (hours) is representative of the length of time that all ISCOs were simultaneously collecting floodwater. Sampling stations are demoted by distance (m) downstream from levee.

Month	Sampling station	Predictor	estimate	Std. error	t-value	p-value	F-value	R <sup>2</sup>
January	levee	intercept	8.030	0.492	16.320	< 0.001	4.122 (1, 14)	0.17
		Flood duration	0.103	0.035	2.030	0.062		
	240 m	intercept	6.841	0.644	10.615	< 0.001	15.31 (1, 14)	0.49
		Flood duration	0.261	0.067	3.912	0.002		
	490 m	intercept	11.592	0.603	19.216	< 0.001	30.91 (1, 14)	0.67
		Flood duration	0.347	0.062	5.559	< 0.001		
950 m	intercept	13.395	1.116	12.004	< 0.001	24.86 (1, 14)	0.61	
	Flood duration	0.575	0.115	4.986	< 0.001			
July	levee	intercept	14.086	0.734	19.202	< 0.001	0.21(1, 12)	-0.07
		Flood duration	-0.039	0.086	-0.453	0.658		
	240 m	intercept	18.732	1.352	13.856	< 0.001	0.02 (1, 12)	-0.08
		Flood duration	0.021	0.159	0.132	0.897		
	490 m	intercept	20.673	2.361	8.757	< 0.001	0.02 (1, 12)	-0.08
		Flood duration	0.039	0.277	0.140	0.891		
950 m	intercept	22.408	1.011	22.164	< 0.001	1.70 (1, 12)	0.05	
	Flood duration	-0.155	0.119	-1.303	0.217			
October	levee	intercept	13.146	1.404	9.365	< 0.001	4.05 (1, 5)	0.34
		Flood duration	-0.631	0.314	-2.011	0.100		
	240 m	intercept	19.543	2.621	7.458	< 0.001	2.45 (1, 5)	0.19
		Flood duration	-0.917	0.586	-1.565	0.178		
	490 m	intercept	20.953	2.392	8.761	< 0.001	1.76 (1, 5)	0.11
		Flood duration	-0.710	0.535	-1.328	0.241		
950 m	intercept	25.988	1.230	21.135	< 0.001	24.44 (1, 5)	0.80	
	Flood duration	-1.387	0.275	-5.044	0.004			

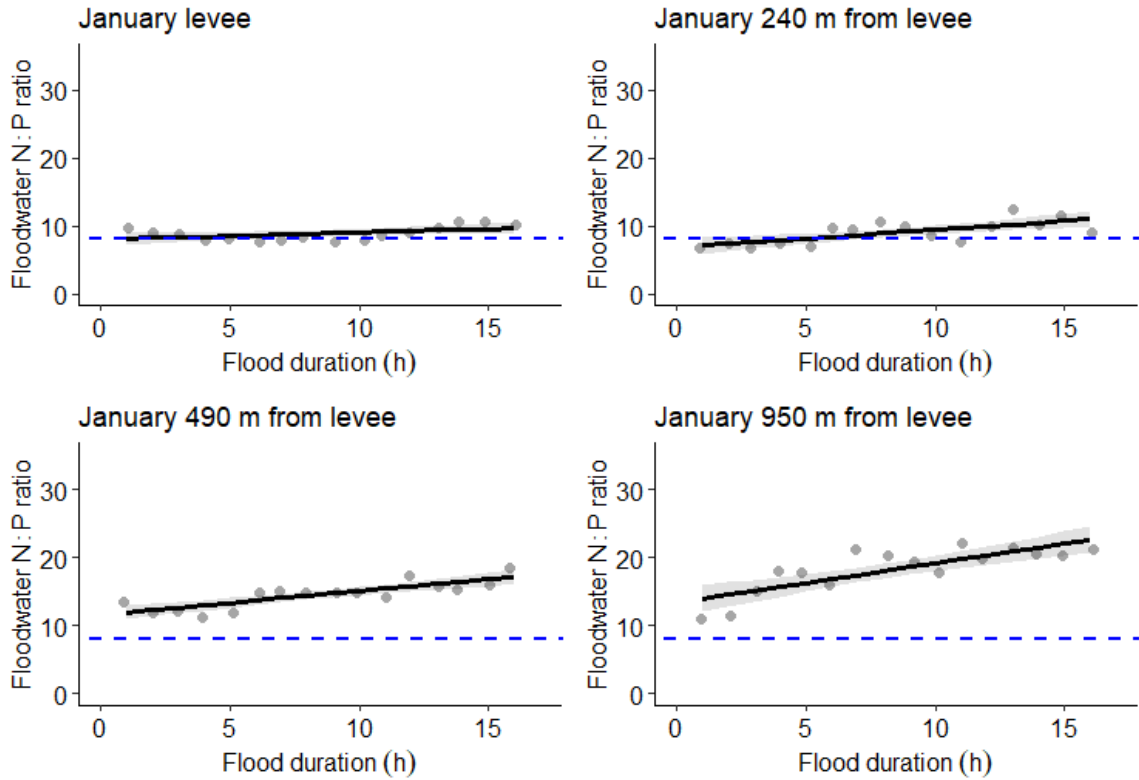


Figure 4.8. Simple linear regressions of January floodwater molar TN:TP ratios against flood duration for each sampling station. Relationships are regressed across the time that all four ISCOs were collecting samples ( $n = 16$ ). The dashed blue line represents the intercept (8.03), indicative of floodwater TN:TP ratio at the time when water first breached the levee. Corresponding statistics are in Table 4.4.

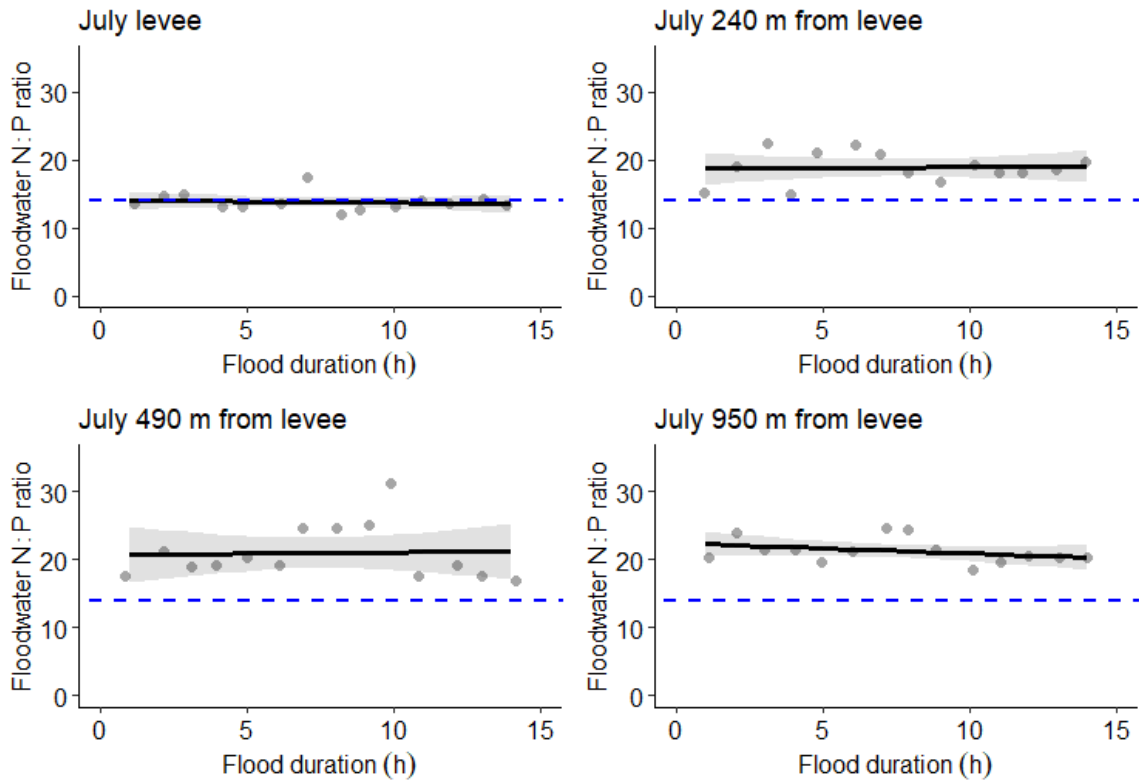


Figure 4.9. Simple linear regressions of July floodwater molar TN:TP ratios against flood duration for each sampling station. Relationships are regressed across the time that all four ISCOs were collecting samples ( $n = 14$ ). The dashed blue line represents the intercept (14.01), indicative of floodwater TN:TP ratio at the time when water first breached the levee. Corresponding statistics are in Table 4.4.

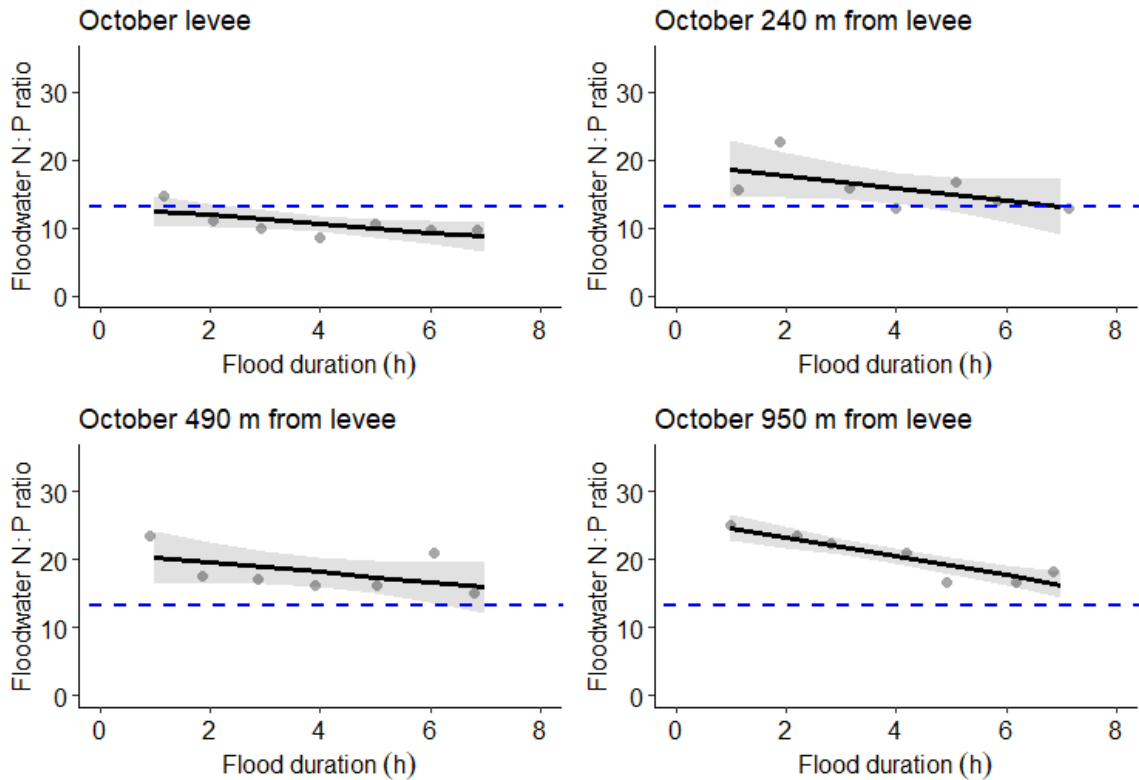


Figure 4.10. Simple linear regressions of October floodwater molar TN:TP ratios against flood duration for each sampling station. Relationships are regressed across the time that all four ISCOs were collecting samples ( $n = 7$ ). The dashed blue line represents the intercept (13.15), indicative of floodwater TN:TP ratio at the time when water first breached the levee. Corresponding statistics are in Table 4.4.

### ***Dissolved nutrients in the July flood***

Regression of DIN:PO<sub>4</sub> ratios in July floodwater against distance from levee showed a positive trend (Fig. 4.11  $p < 0.001$ ,  $R^2 = 0.83$ ), similar to TN:TP ratios across all floods (Fig. 4.7). Interestingly, the intercept of the July DIN:PO<sub>4</sub> – distance relationship is lower (7.8 vs. 14.8) and the slope was steeper (0.025 vs. 0.009) than the July TN:TP – distance relationship. This suggests that floodwater PO<sub>4</sub> may be retained in

the floodplain more readily than other fractions of TP, or that the floodplain may be a source of DIN more so than other fractions of TN.

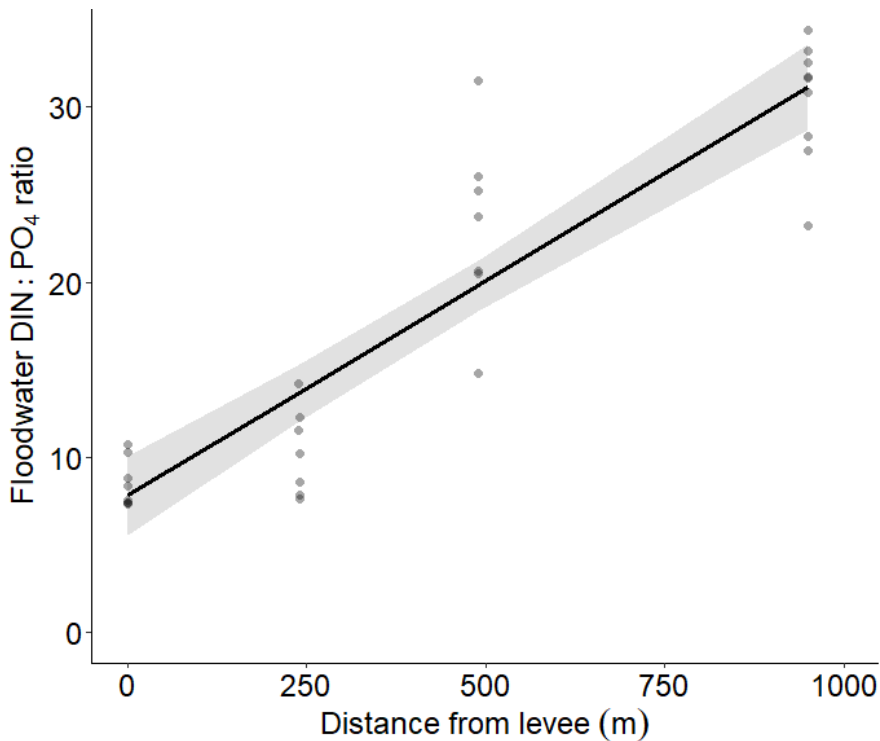


Figure 4.11. Relationship of July floodwater dissolved inorganic nitrogen DIN:PO<sub>4</sub> ratio with distance from levee. Intercept = 7.796, slope = 0.025,  $F_{(1,29)} = 152.4$ ,  $R^2 = 0.83$ ,  $p < 0.001$ ).

There was a parabolic relationship between July NH<sub>4</sub> concentrations and distance from levee. There was a 74.1% decrease in NH<sub>4</sub> within 240 m of the levee, a 53.7% increase within 490 m, and a 114.4% increase within 950 m (Fig. 4.12, all  $p < 0.004$ ), relative to inflowing NH<sub>4</sub> concentrations at the levee. July NO<sub>3</sub> concentrations increased 42.6% within 240 m of the levee (Fig. 4.12,  $p = 0.02$ ) but NO<sub>3</sub> at 490 and 950 m downstream was not statistically different from levee concentrations (Fig. 4.12, both  $p > 0.47$ ). July PO<sub>4</sub> concentrations decreased 27.7% within 240 m of the levee and 62.5% within 490 m from levee (Fig. 4.12, both  $p < 0.001$ ). These patterns indicate that both

increasing DIN and decreasing PO<sub>4</sub> concentrations contributed to the steep increase in DIN:PO<sub>4</sub> ratios with distance from levee (Fig. 4.11). The positive relationship between floodwater NH<sub>4</sub> and POM was only statistically significant 950 m from the levee (Fig. 4.13). Relationships between NH<sub>4</sub> and POM concentrations at all other floodplain locations were not statistically significant (all  $p > 0.1$ ).

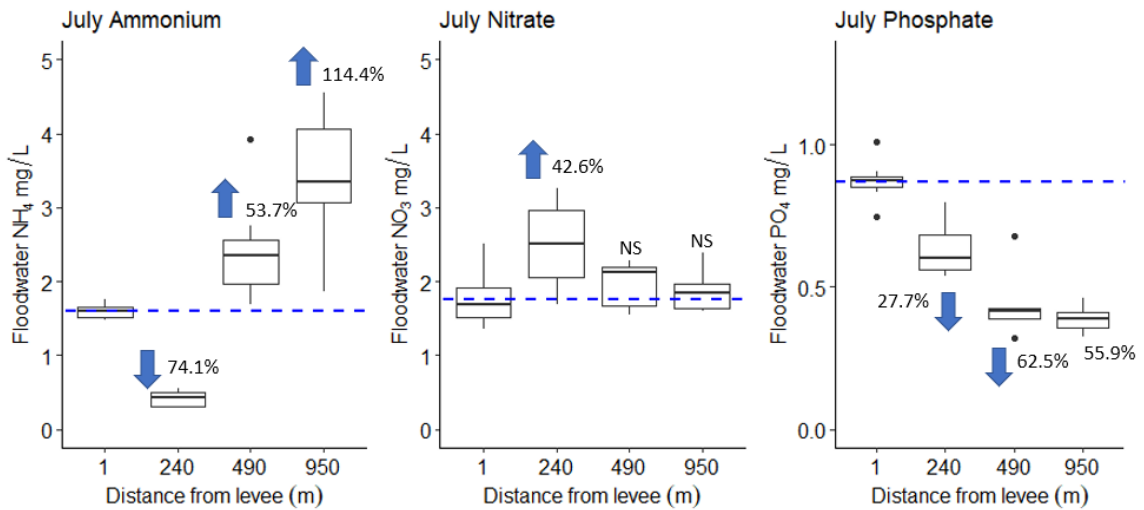


Figure 4.12. Boxplots comparing July NH<sub>4</sub>, NO<sub>3</sub>, and PO<sub>4</sub>, concentrations with distance from levee. Comparison of percent change in each nutrient concentration is relative to mean concentration at the levee (dashed line). Blue arrows indicate the direction of change. Comparisons were made by Welch t-test accounting for unequal variances in MS Excel. Non statistically significant differences from levee concentrations are shown by “NS”.

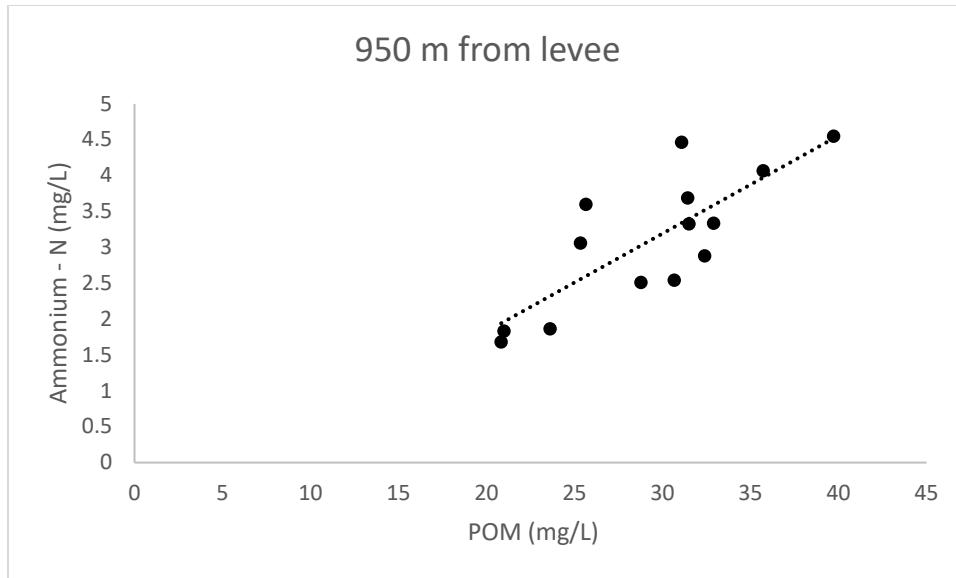


Figure 4.13. Regression of ammonium ( $\text{NH}_4$ ) concentration against particulate organic matter (POM) at 950 m from the levee in July 2020.  $R^2 = 0.60$ ,  $p < 0.001$ .

### Total nutrients and particulates

Total N and TP were both positively correlated with TSS and POM concentrations in all floods. Both TSS and POM were strong predictors for both nutrients, but these relationships were non-linear and differed between floods (Fig. 4.14). Particulate OM was a more parsimonious predictor of TN concentration (Fig. 4.14,  $p < 0.001$ ,  $R^2 = 0.85$ ,  $\text{AICc} = 349.3$ ) than TSS (Fig. 4.14,  $p < 0.001$ ,  $R^2 = 0.84$ ,  $\text{AICc} = 364.4$ ). Total SS were a more parsimonious predictor of TP (Fig. 4.14,  $p < 0.001$ ,  $R^2 = 0.81$ ,  $\text{AICc} = -105.2$ ) than POM (Fig. 4.14,  $p < 0.001$ ,  $R^2 = 0.73$ ,  $\text{AICc} = -53.8$ ). Interestingly, there was a negative quadratic relationship of TN and TP with POM in July and October floods and positive quadratic relationship of both nutrients with POM in the January flood.

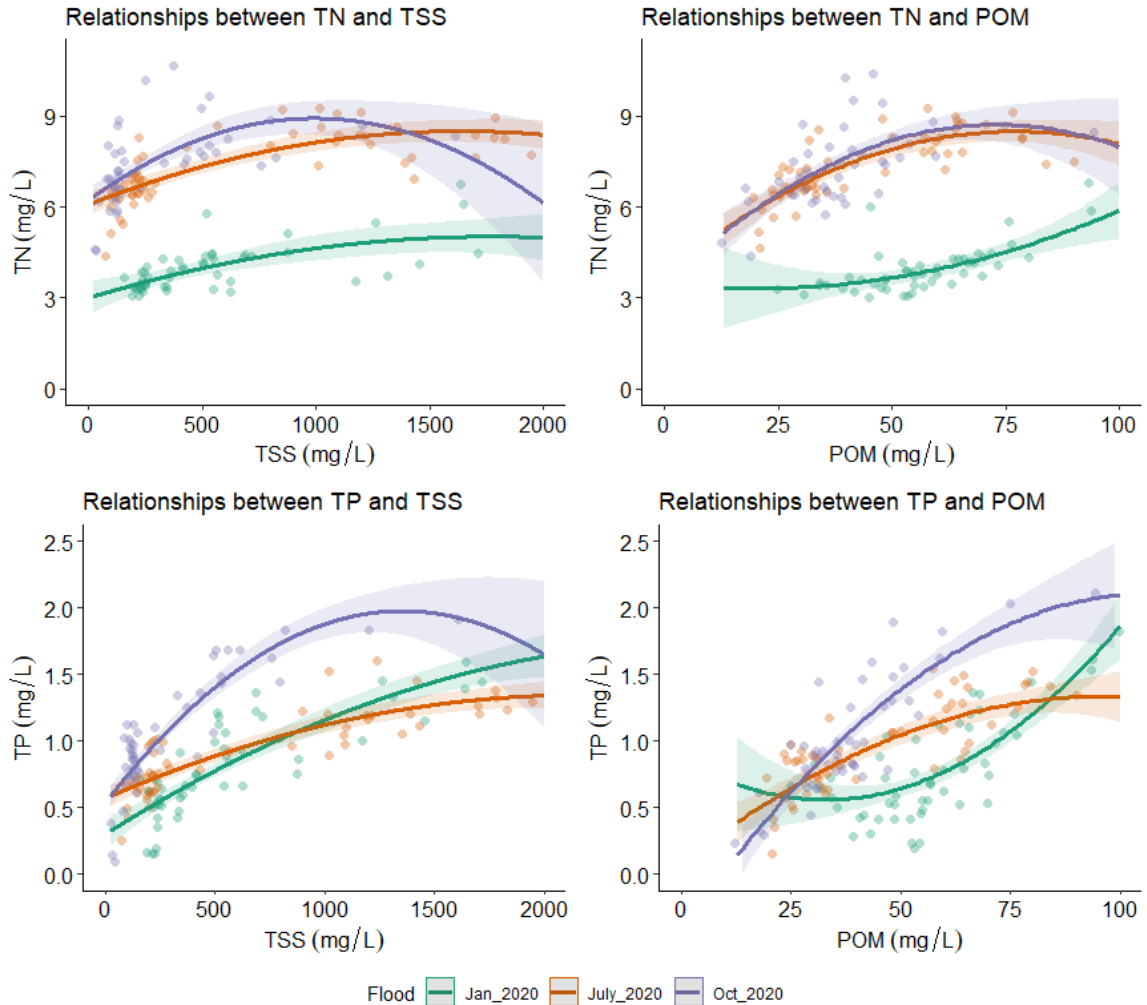


Figure 4.14. Regression with ANCOVA results of TN and TP concentrations regressed against TSS and POM, accounting for differences in TN and TP concentrations between floods.

### Soil N:P stoichiometry

There was a positive relationship between soil N:P ratios and distance from levee. The relationship was stronger for TN:eP ratios in the top 10 cm of soil and relatively weak for DIN:eP ratios in the top 10 cm of soil (Table 4.5, Fig. 4.15). Lack of soil TP data precludes direct comparison of soil and floodwater N:P ratios. Soil N:P ratios

presented here are much higher (TN:eP) and lower (DIN:eP) than floodwater N:P ratios. However, trends presented in Fig. 4.15 suggest that soil N:P ratios tend to increase with distance from the levee.

Table 4.5. Simple linear regression results of soil N:P ratios of 30 soil cores against distance (m) from levee. Soil total nitrogen to extractable phosphorus ratio (TN:eP) and dissolved inorganic nitrogen to extractable phosphorus ratios (DIN:eP) at 0-10 cm soil depth.

Response	Predictor	estimate	Std. error	t-value	p-value	F-value	R <sup>2</sup>
TN:eP 10 cm	intercept	23.0257	7.8917	2.92	0.007		
	distance to levee	0.0877	0.0146	6.03	< 0.001	36.3 (1, 28)	0.55
DIN:eP 10 cm	intercept	0.1904	0.0613	3.11	0.004		
	distance to levee	0.0002	0.0001	1.98	0.058	3.913 (1, 28)	0.09

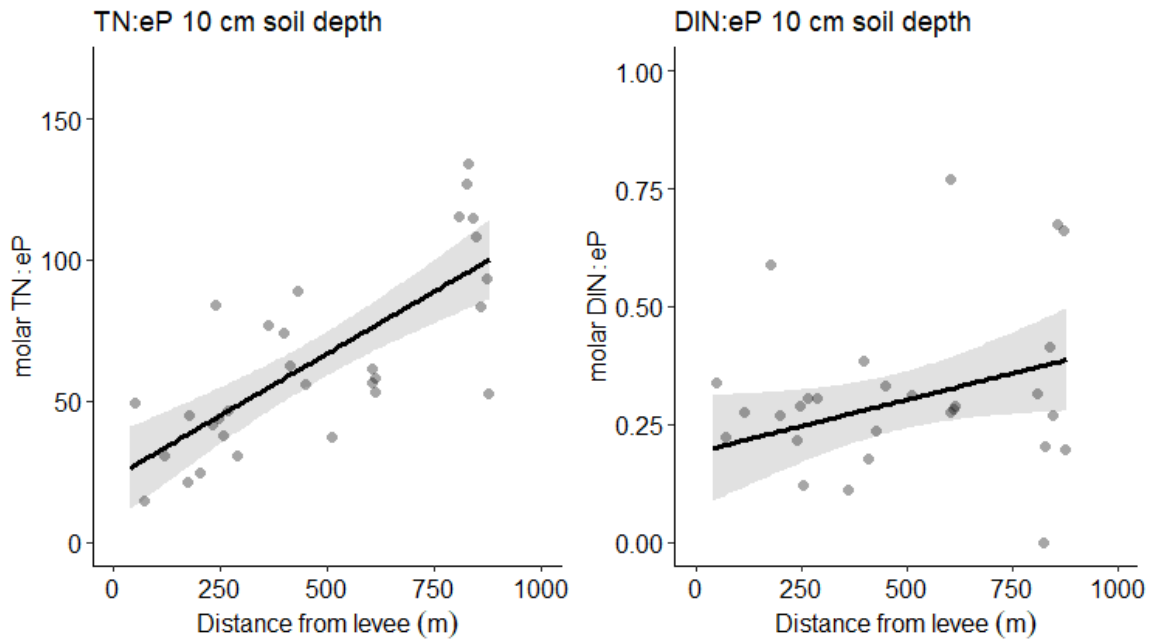


Figure 4.15. Molar ratios of soil total nitrogen to extractable phosphorus (TN:eP) and dissolved inorganic nitrogen to extractable phosphorus ratios (DIN:eP) in the top 10 cm of soil regressed against distance (m) from levee. Molar soil TN:eP ratios are inflated compared with ISCO TN:TP ratios due to lack of soil TP data. Molar DIN:eP ratios are compressed because eP makes up a larger proportion of TP than DIN does for TN.

### **Nutrient flux at the soil-water interface**

Mean flux rates derived from flow-through incubation of soil cores indicate this floodplain was a net sink for dissolved fractions of N and P in July (Table 4.6, Fig. 4.16). However, this trend was not ubiquitous for all N species, or all sampled locations. Variation in flux rates was greater than means for  $\text{NH}_4$ ,  $\text{NO}_2$ , and  $\text{N}_2\text{O}$  (CVs > 100) but  $\text{NO}_3$  and  $\text{N}_2$  fluxes were relatively less variable (Table 4.6). Negative median flux rates for  $\text{NH}_4$ ,  $\text{NO}_3$ , and  $\text{PO}_4$  indicate that uptake of these nutrients was more prevalent than release across 30 sampled locations. This relationship held with negative mean flux of  $\text{NO}_3$  and  $\text{PO}_4$ , suggesting net uptake of these nutrients across the floodplain. Mean  $\text{NH}_4$  flux was positive, indicating net release of  $\text{NH}_4$  from the floodplain even though uptake was measured at more locations than release. All 30 cores had positive  $\text{NO}_2$  flux rates, making this floodplain a likely source of  $\text{NO}_2$  to downstream environments. All  $\text{N}_2$  flux rates were positive, indicating that N removal processes outpace N-fixation across the floodplain. Positive median and mean  $\text{N}_2\text{O}$  flux rates indicate prevalence of  $\text{N}_2\text{O}$  production and net release across the floodplain. However,  $\text{N}_2\text{O}$  accounted for less than 0.05% of gaseous N removal. High CVs and maximum  $\text{N}_2\text{O}$  and  $\text{CH}_4$  flux rates suggest that hotspots are likely, especially for  $\text{CH}_4$  production (Table 4.6, Fig 4.17).

Table 4.6. Summary statistics for NH<sub>4</sub>, NO<sub>2</sub>, NO<sub>3</sub>, and N<sub>2</sub> (mg N L<sup>-1</sup>) PO<sub>4</sub> (mg P L<sup>-1</sup>), O<sub>2</sub> (mg O L<sup>-1</sup>), N<sub>2</sub>O (μg N L<sup>-1</sup>), and CH<sub>4</sub> (μg C L<sup>-1</sup>) for 30 soil cores incubated in a flow-through system simulating a 48 h flood. Coefficient of variation (CV) is the ratio of standard deviation of the mean. Negative median and mean values represent uptake from the water column by the soil. Positive values represent release from the soil to the water column.

Flux rate	median	mean	st. dev.	CV %	minimum	maximum
NH <sub>4</sub>	-0.083	0.371	1.116	300.9	-0.341	3.735
NO <sub>2</sub>	0.563	1.031	1.089	105.6	0.124	4.552
NO <sub>3</sub>	-11.793	-11.937	8.519	71.4	-29.865	5.817
PO <sub>4</sub>	-0.557	-0.506	1.580	311.9	-3.785	1.823
N <sub>2</sub>	3.025	3.467	2.106	60.8	0.702	9.570
N <sub>2</sub> O	0.542	1.759	3.288	186.9	-0.007	16.337
CH <sub>4</sub>	-0.008	0.906	3.592	396.3	-0.026	18.086
O <sub>2</sub>	-41.044	-43.957	3.592	8.2	-70.376	-24.385

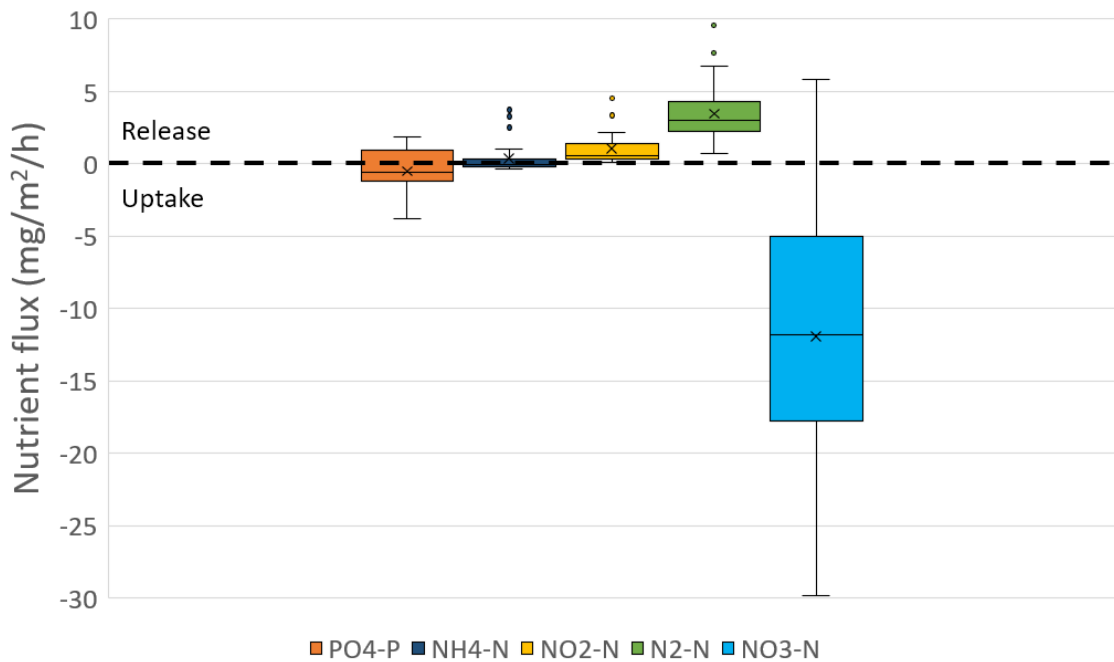


Figure 4.16. Variation in PO<sub>4</sub>, NH<sub>4</sub>, NO<sub>2</sub>, N<sub>2</sub>, and NO<sub>3</sub> flux rates for 30 soil cores collected across the floodplain and incubated in a flow-through system. The dashed line represents zero flux. Means are indicated by x and medians by horizontal line in boxplots. Boxes represent one standard deviation from the mean and whiskers represent two standard deviations.

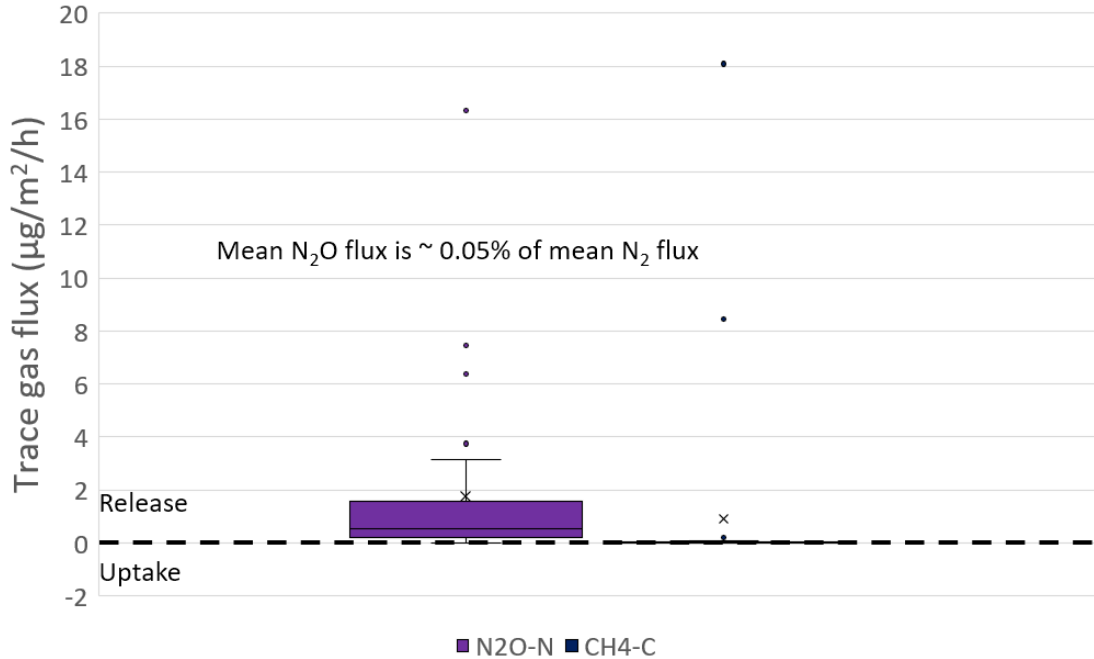


Figure 4.17. Variation in N<sub>2</sub>O and CH<sub>4</sub> flux rates for 30 soil cores collected across the floodplain and incubated in a flow-through system. The dashed line represents zero flux. Means are indicated by x and medians by horizontal line in boxplots. Boxes represent one standard deviation from the mean and whiskers represent two standard deviations. Methane flux was < 1 µg/m<sup>2</sup>/h in 28 of 30 soil cores.

### ***Redundancy analysis***

Constrained ordination through redundancy analysis explained 51.50% of the variation in flux responses as a function of soil properties and distance from the levee ISCO. Unconstrained residual relationships between explanatory variables accounted for 14.02% of the variation. ANOVA results testing statistical significance of relationships described by the seven RDA axes generated by the model showed that RDA1 ( $F_{(1,22)} = 48.27, p < 0.001$ ), RDA2 ( $F_{(1,22)} = 18.05, p = 0.002$ ), and RDA3 ( $F_{(1,22)} = 10.41, p = 0.024$ ) were strong predictors of flux rate responses over 48 h incubations. Remaining RDA axes had little predictive value (all  $p > 0.88$ ) and are not discussed further.

The first axis (RDA1) explained 30.76% of the variation in flux responses. The second axis (RDA2) explained 11.50% of the variation (Fig. 4.18). The third axis (RDA3) explained 6.58% of the variation. The first residual axis (PC1) explained 6.22% of the variation. All other axes explained less than 5% of the variation. Soil bulk density, soil extractable P, and soil NO<sub>3</sub> concentration loaded positively on RDA1 and were negatively correlated with PO<sub>4</sub> uptake and NO<sub>3</sub> uptake. Soil NH<sub>4</sub>, SOD, and distance from levee loaded negatively on RDA1 and RDA2 and were positively correlated with N<sub>2</sub> removal and NO<sub>3</sub> uptake. Soil TN, TC, moisture, Fe, and pH loaded negatively on RDA1 and positively on RDA2 and were positively correlated with PO<sub>4</sub> uptake and release of N<sub>2</sub>O, and CH<sub>4</sub> (Fig. 4.18).

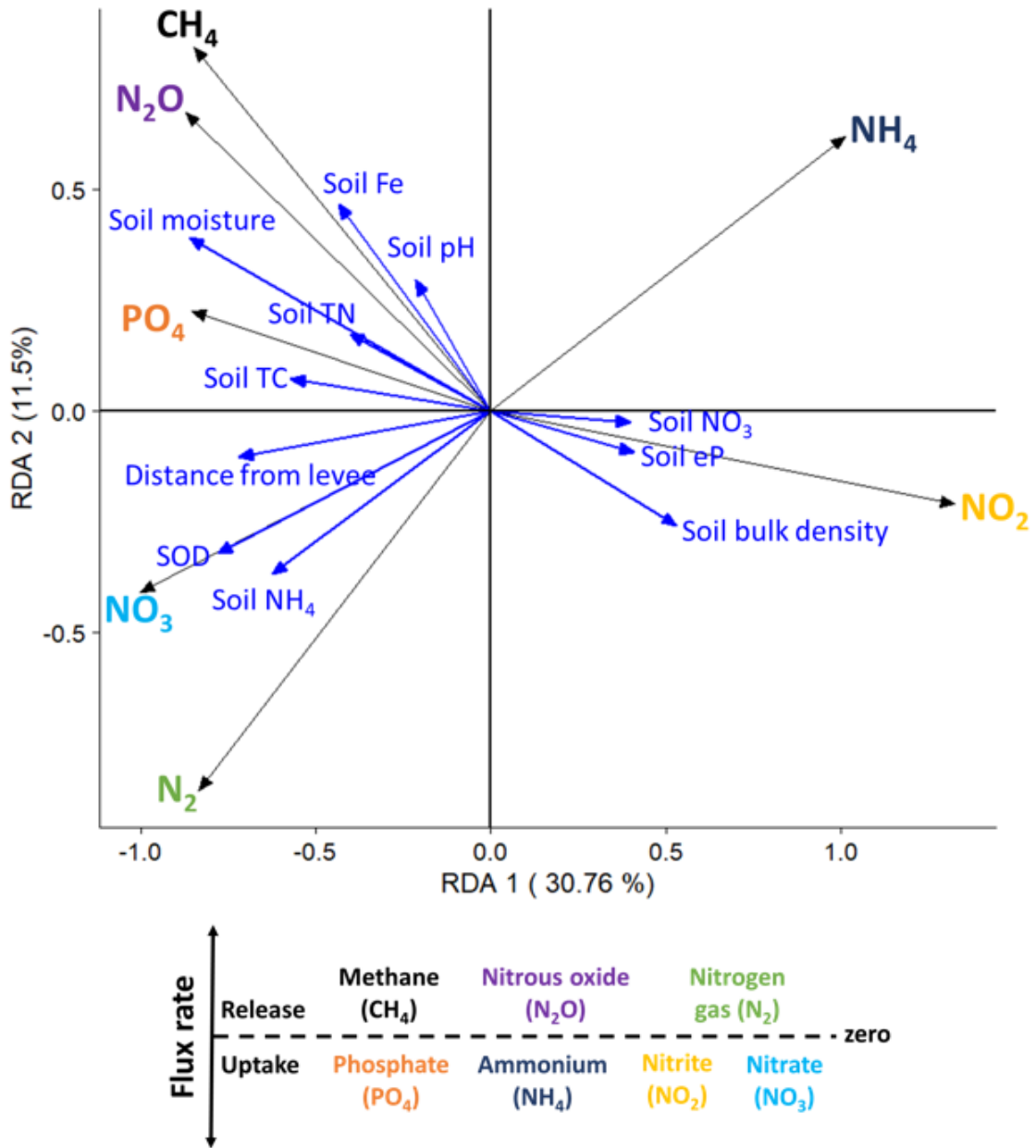


Figure 4.18. Redundancy analysis of flux rate responses to soil structural properties and distance from levee. Explanatory variables are shown with blue rays. Soil total nitrogen is represented by Soil TN, soil total carbon by Soil TC. And soil extractable phosphorus by Soil eP. Flux rate responses for each nutrient/gas species are color coded as in Fig. 4.16. Rays are pointed in the direction of release for CH<sub>4</sub>, N<sub>2</sub>O and N<sub>2</sub>; and uptake for PO<sub>4</sub>, NH<sub>4</sub>, NO<sub>2</sub>, and NO<sub>3</sub>. Smaller acute angles between rays represent positive correlations between variables; 90 ° angles between variables indicate no relationship; 180 ° angles between variables represent negative correlations.

## Discussion

### Floodplain nutrient retention capacity

The floodplain was a net sink for N and P among the three floods. A greater percentage of P was retained compared with N. Proportionally higher P retention in this study is consistent with previous studies in European (Olde Venterink et al., 2006; Olde Venterink, Wiegman, et al., 2003) and North American floodplains (Noe & Hupp, 2005, 2009), likely due to deposition of P sorbed to sediment in the water column (Bridgham et al., 2001; Ready et al., 1999). Retention rates were highest for N (25%) and P (61%) during the January flood, relative to inflowing concentrations at the levee break. Most studies report relative retention rates directly measured through depositional studies (Gillespie et al., 2018) as a function of riverine nutrient loads (Gordon et al., 2020). Comparison of TN and TP concentrations across the floodplain relative to concentrations entering the levee during each flood provides a more direct comparison of nutrient retention as a function of delivery to this floodplain via levee breaks. However, floodwater measurements of nutrient retention from this study cannot be represented as a function of watershed nutrient budgets without hydrologic data for Mayfield Creek.

Phosphorus retention showed a roughly linear increase across the floodplain in all seasons, but there was an apparent source of N between 240 and 490 m downstream of the levee in January. Nitrogen was released between the levee and 240 m downstream and retained between 240 m and 490 m downstream in July. This indicates that source-sink dynamics of N may shift seasonally within the floodplain while maintaining a net N sink within 1 km of levee breaks. Variable source-sink dynamics were reported for another short hydroperiod floodplain across seasons and locations within the floodplain

(Noe & Hupp, 2007). The authors suggest the idea of floodplains as universal nutrient sinks may not necessarily apply to small river systems with relatively short flood duration. More recent work has shown net nutrient retention across a temperate floodplain despite increased N and P mineralization rates at high nutrient loadings (Noe et al., 2013). This finding agrees with the present study, where total N and P retention relative to delivery from the channelized flow-path generally outpace mineralization within the floodplain and delivery from upland sources. The floodplain adjacent to levee breaks on Mayfield Creek appeared to retain N during the October flood but low sample size ( $n = 7$ ) likely contributed to wider 95% confidence intervals overlapping with zero compared with January ( $n = 16$ ) and July floods ( $n = 14$ ). Smaller paired sample sizes for the October flood were probably due to lower water levels or shorter duration of high-water levels, given the relatively small hydrograph in comparison with January and July floods. If smaller sample size was a result of a smaller October flood, further distinction between ecologically real source-sink variability (i.e. Noe & Hupp 2007) and statistical limitations is not possible for the October flood. However, the fact that this floodplain acted as a statistically significant sink for P in the October flood suggests consistency as a nutrient sink among floods, at least for P.

### **N:P stoichiometry**

#### ***Spatial patterns in floodwater***

Among flood differences in molar TN:TP ratios at the levee break represent relative changes in N and P concentrations delivered to the floodplain. Phosphorus limitation of oceanic biological growth predominantly occurs at N:P molar ratios  $> 15$

and N limitation occurs at lower ratios (Redfield, 1958). Nutrient limitation is similar across marine, freshwater, and terrestrial ecosystems in that either or both nutrients could be limiting (Elser et al., 2007) in the context of Redfield ratios. Molar TN:TP ratios for floodwater entering the levee were less than 15 for all floods, indicating potential N limitation of nutrient cycling processes within floodwater in January (N:P = 8.4), July (N:P = 14.8), and October (N:P = 12.6). Phosphorus limitation is more likely to occur further from the levee, evidenced by increasing N:P ratios with distance from the levee in all three measured floods. The change in floodwater TN:TP, likely due to higher P deposition in the floodplain (i.e. retention), appears to be consistent across seasons. However, N:P delivered to further downstream ecosystems (i.e. Mississippi River) is likely to vary among floods, given variable ratios of N:P delivery to the floodplain (from 8.4 in January to 14.8 in July). Variation in N:P delivery is likely due to cumulative watershed influences (i.e. land use, position in the watershed, antecedent soil moisture, precipitation intensity) on a given flood (Kroeze et al., 2012) not necessarily attributable to nutrient retention patterns at individual restoration sites.

### ***Flood duration***

The influence of flood duration on floodwater N:P ratios across each flood was more variable than the influence of floodplain position (as distance from levee). Increasing TN:TP ratios over the duration of the January flood across all sampling stations suggests potential increase of N delivery over time. Increased N delivery could have resulted from a later flood pulse from upstream tributaries with high N loading (Royer et al., 2006) where the distribution of landcover types (Dupas et al., 2019) within differently structured sub watersheds (Helton et al., 2018) influences nutrient export and

retention dynamics (Speir et al., 2021). Conversely, P delivery could have decreased over time due to similar processes, resulting in a higher N:P ratio. In fact, both TN and TP concentrations decreased over the duration of the January flood but TP concentration decreased more. This is likely due to deposition of TP with suspended sediment in transport to the floodplain (Kiedrzyńska et al., 2008; Olde Venterink et al., 2006), which increases in winter when vegetation plays a less active role in upland sediment-bound P retention (Withers & Jarvie, 2008). Phosphorus can then be more readily transported to the river via runoff and settle out where flow decreases. Strong positive correlation observed in this study between January TP and TSS concentrations supports this hypothesis.

The negative relationships between floodwater N:P ratios and October flood duration appears to have been driven by temporally decreasing TN concentrations at all sampling stations and increasing TP concentrations at the levee and 490 m downstream at the backwater site. Decreasing TN concentrations could be driven by water column denitrification, which can occur in rivers at similar rates to headwater streams (Reisinger et al., 2016) and wetlands (Forshay & Stanley, 2005) with high N loads (Richardson et al., 2019). Organic carbon from senescent leaves may have been a source of C facilitating denitrification in the floodwater column, reducing floodwater N concentrations over the duration of the October flood. Particulate organic matter concentration explained 85% of the variation in TN concentration among the three floods measured here and may indicate a source of organic N which could have been mineralized, nitrified, and denitrified over the course of a flood in conjunction with anoxic microsites on suspended sediments (Xia et al., 2017).

There is a growing need to understand how aquatic and terrestrial biogeochemical processes interact to influence the stoichiometry of cross-ecosystem subsidies and local nutrient cycling rates (Sitters et al., 2015). These processes are especially important to consider in agroecosystems where nutrient cycling processes are often driven by high internal nutrient loading that reduce an ecosystem's capacity to process additional nutrients delivered from upstream (Nifong & Taylor, 2022). Leaf litter may be a source of C that directly promotes denitrification in floodplain wetland soils (Stoler & Relyea, 2020) or influence floodplain nutrient retention indirectly by enhancing water column denitrification (Reisinger et al., 2016; Ritz et al., 2018) during floods thereby reducing the amount of N delivered to floodplains (Schindler & Smits, 2017). Water column denitrification during floods could be further enhanced by formation of anoxic microsites on suspended sediments (Xia et al., 2017) but floodplain soils likely become more important denitrification sites as sediment is deposited in overbank flow (Olde Venterink et al., 2006). Disentangling sources of variability in nutrient delivery to and processing within floodplains will benefit from more extensive monitoring and modeling of river networks (Helton et al., 2011, 2018) as river-floodplain connections improve with restoration activities.

### ***Soil N:P stoichiometry***

Inferences from soil N:P ratios are limited in this study because measurement of soil extractable P using the Mehlich III method and measurement of soil TN through combustion are not quantitatively comparable to floodwater N:P ratios derived from persulfate digestion of each sample for TN and TP analysis. Total P measurements can be 800% higher than Mehlich III measurements of extractable P in agricultural soils (Zbiral

& Němec, 2002) but differences in total vs. extractable P are not necessarily consistent across soil types with differing P contents (Ivanov et al., 2012). Unfortunately, variability among soil types precludes correction of Mehlich III measurements to represent TP metrics. While soil TN:eP and DIN:eP ratios are stoichiometrically flawed and should not be interpreted as indicators of nutrient limitation in this study, positive correlation of these soil N:P ratios with distance from levee indicates that a negative relationship between soil N:P and distance from levee is unlikely. This begs the question of where floodwater P goes if it is removed from the water column as indicated by floodwater TN:TP ratios.

Deposition of particulate nutrients from floodwater may have a stronger influence on floodplain plant growth than dissolved nutrients (Keizer et al., 2018). Interestingly, Keizer et al. 2018 found that particulate N and P deposition were equally positively correlated with aboveground plant biomass in a herbaceous natural floodplain, indicating potential colimitation of plant growth by both N and P availability. The growth rate hypothesis (Elser et al., 2000; Sterner and Elser, 2002) predicts positive correlation between growth rate, RNA content, and P content of organisms. Essentially, P-rich RNA fuels protein synthesis required for rapid growth (Elser et al., 2000). More frequent inundation of the forest near the levee break in the current study appears to have increased tree mortality, opening the canopy and facilitating herbaceous plant growth (personal observation). Rapid growth of herbaceous plants in spring and summer likely assimilate soil P deposited during floods but herbaceous plants may release P after senescence in fall and winter floods (Mitsch et al., 1995). Quantifying transient storage and release of P resulting from floodplain restoration requires more detailed

measurements of P assimilation and mineralization (Ready et al., 1999) in conjunction with monitoring of floodplain succession before and after restoration (Skinner, 2022).

### **Nutrient fractions in floodwater**

Dissolved N dynamics within the floodplain were more complicated than P in July 2020. Results from the July 2020 flood show that the floodplain was a net sink for  $\text{PO}_4$ , net source of  $\text{NH}_4$ , and neutral in terms of net changes in  $\text{NO}_3$  concentration. Export of  $\text{NH}_4$  has been measured for at least one other short-hydroperiod floodplain (Noe & Hupp, 2007). The authors hypothesize hyporheic flushing of  $\text{NH}_4$  by floodwater as a mechanism of  $\text{NH}_4$  export, and nitrification of  $\text{NH}_4$  as a mechanism of  $\text{NO}_3$  export. Similar mechanisms likely play a role in the current study. Ammonium uptake near the levee coincided with  $\text{NO}_3$  release, indicating potential nitrification in the floodwater within 240 m of the levee. Ammonium was released further from the levee without apparent nitrification. Hyporheic flushing is more likely to contribute to  $\text{NH}_4$  export than alternative upstream  $\text{NH}_4$  sources because concentrations in the remnant channel of Mayfield Creek upstream of levee breaks were relatively low in the July flood ( $< 1 \text{ mg NH}_4\text{-N/L}$ ) compared with  $\text{NH}_4$  concentrations in the remnant channel 490 and 950 m downstream of the levee break (Fig. 4.12). Alternatively,  $\text{NH}_4$  may have been mineralized from particulate organic matter in floodwater. Given the significant positive correlation between  $\text{NH}_4$  and POM at 950 m downstream of the levee (Fig. 4.13) and lack of correlation between  $\text{NH}_4$  and POM at all other measured locations, it appears that N mineralization from organic matter was more likely further from the levee breaks. A combination of hyporheic flushing of  $\text{NH}_4$  and N mineralization from floodwater organic matter most likely contributed to  $\text{NH}_4$  export from this floodplain in July 2020. Although

not explicitly measured in this study, N mineralization and DIN export from this floodplain is plausible during other floods given the strong predictive power of POM for TN concentration across the three floods measured here.

Export of  $\text{NH}_4$  associated with particulate organic matter delivery in this study highlights potential commonalities between short-hydroperiod floodplains in terms of organic nutrient import and inorganic nutrient export (Noe & Hupp, 2007). Mineralization rates increase with nutrient delivery to floodplains (Gillespie et al., 2018; Noe et al., 2013) and may be responsible for localized inorganic N export despite net TN retention. Essentially, some forms of N may be retained within the floodplain while some leaks downstream as  $\text{NH}_4$ , but not all floodplains leak in the same way. A recent study showed that swampy wetlands within a watershed retain particulate matter and inorganic nutrients while releasing recalcitrant dissolved organic matter (Atkinson et al., 2019). Both Noe and Hupp 2007 (Maryland, USA) and Atkinson et al 2019 (Alabama, USA) studied floodplains with less agricultural impact and lower nutrient concentrations than the current study in Kentucky, yet both studies found contrasting results in terms of dissolved inorganic nutrient retention. Results of the current study align more with Noe and Hupp in terms of summer  $\text{NH}_4$  export and Atkinson et al. in terms of  $\text{PO}_4$  retention. Differences may be due to geographic variation between sites in the eastern USA, temporal variation between floods, or methodological decisions in study design at different scales. Dissolved organic matter quality and organic fractions of dissolved N and P should be explicitly considered in further studies of floodplain nutrient retention to understand how nutrient transformations contribute to floodplain source-sink capacity.

## Soil nutrient processing

### *Comparing flow-through incubation with flooding in July*

Nutrient processing rates derived from the 48h flow-through core incubation agreed with floodwater results discussed above in that the floodplain was a net sink for  $\text{PO}_4$  and a net source of  $\text{NH}_4$ . Contrary to apparent floodwater  $\text{PO}_4$  uptake near the levee in July 2020,  $\text{PO}_4$  uptake during 2022 soil incubations increased with distance from levee and was higher for soils with lower extractable P concentrations and lower bulk density. Sorption of  $\text{PO}_4$  to soil particles was likely promoted in soil cores with low P concentrations due to more available binding sites (Bridgham et al., 2001). The spatial mismatch between apparent  $\text{PO}_4$  uptake from July 2020 floodwater and soil  $\text{PO}_4$  uptake from July 2022 highlight differences between field-scale measurements and flow-through incubations. Sheet flow across soil during floods likely results in much shorter residence time compared to flow-through core incubation ( $\sim 0.12 \text{ L h}^{-1}$ ), lowering potential for  $\text{PO}_4$  uptake vis less contact with the soil (Lu et al., 2009).

Uptake of  $\text{NH}_4$  by soil cores was higher for cores collected closer to the levee and was negatively correlated with soil  $\text{NH}_4$  content, distance from levee and soil oxygen demand (SOD). Soil incubation results corroborate spatial patterns of floodwater  $\text{NH}_4$  concentrations in July 2020 and support the hypothesis that hyporheic flushing of soil  $\text{NH}_4$  contributes to  $\text{NH}_4$  release from the floodplain (Noe & Hupp, 2007) with increasing distance from levee. Dissimilatory nitrate reduction to ammonium (DNRA) can produce  $\text{NH}_4$  in floodplain soils (Burgin & Hamilton, 2007) but rates are often low relative to  $\text{NO}_3$  reduction (Hoagland et al., 2019; Welti et al., 2012). Mineralization of organic N is

another potential source of soil  $\text{NH}_4$  in the current study, but further experiments are needed to identify  $\text{NH}_4$  production mechanisms.

Nitrate uptake far exceeded all other N fluxes measured from soil core incubations, likely because of high N loadings designed to saturate soil  $\text{NO}_3$  uptake rates throughout the incubation. In contrast, there was no  $\text{NO}_3$  uptake apparent from changing floodwater concentrations in the July 2020 flood. Relative change in July 2020 floodwater  $\text{NO}_3$  concentrations tended toward release within 240 m of the levee. Nitrate uptake increases with concentration in aquatic systems (Forshay & Stanley, 2005; Kemp & Dodds, 2002; Speir et al., 2017) so higher uptake rates for core incubations with  $\sim 10$  mg  $\text{NO}_3\text{-N/L}$  were expected, compared to mean  $\text{NO}_3\text{-N}$  concentration near  $1.75$  mg  $\text{L}^{-1}$  delivered to the levee in July 2020. The lack of net  $\text{NO}_3$  uptake observed in the July 2020 flood could be due to nitrification within floodwater where  $\text{NH}_4$  is converted to  $\text{NO}_3$  (Delaune et al., 1996; Hoagland et al., 2019). Nitrification was most likely within 240 m of the levee where  $\text{NH}_4$  concentrations decreased and  $\text{NO}_3$  concentrations increased. Increasing  $\text{NH}_4$  concentrations further from the levee may have provided an N source for nitrification, potentially explaining the lack of change in  $\text{NO}_3$  concentrations further from the levee if  $\text{NO}_3$  uptake and nitrification rates were similar. Alternatively, shorter residence time of *in situ* floodwater measurements may have suppressed ambient  $\text{NO}_3$  uptake via less contact time with the soil (James et al., 2008), similar to  $\text{PO}_4$  uptake trends resulting from sheet flow of floodwater.

Residence times of floodwater within the floodplain were not measured in this study but were certainly lower (i.e. faster sheet flow across soil surface) than flow-through soil core incubations. Thus, ambient rates of  $\text{NO}_3$  and  $\text{PO}_4$  uptake were likely

enhanced due to longer (~ 6 hour) residence time within flow-through cores (James et al., 2008; Lu et al., 2009) and elevated nutrient supply. Measured differences in  $\text{NO}_3$  and  $\text{PO}_4$  concentrations across the floodplain did not account for interacting flow paths throughout the forest that likely influenced  $\text{NO}_3$  and  $\text{PO}_4$  concentrations at individual sampling stations. The relatively closed flow-through incubation system explicitly accounts for flow and allows changes in concentration to be attributed directly to the soil. Measurement of multiple N flux rates ( $\text{NO}_3$ ,  $\text{NO}_2$ ,  $\text{NH}_4$ ,  $\text{N}_2$ , and  $\text{N}_2\text{O}$ ) from the flow-through system allows more targeted development of hypotheses explaining N cycling processes and  $\text{NO}_3$  reduction mechanisms.

### ***Fates of nitrate and $\text{N}_2$ production***

Nitrification during soil core incubations was unlikely given high levels of water column  $\text{NO}_3$  and low  $\text{NH}_4$  concentrations. The strong correlation between  $\text{NO}_3$  uptake and SOD suggests  $\text{NO}_3$  was used as an alternative electron acceptor following oxygen depletion. Positive correlation between  $\text{NO}_3$  uptake and  $\text{N}_2$  production indicates denitrification was a dominant dissimilatory pathway and accounted for about 30% of  $\text{NO}_3$  uptake. Negative correlation between  $\text{N}_2$  production and  $\text{NH}_4$  uptake suggests anammox plays a relatively small role in N removal for this floodplain, although, floodplains can have anammox rates that account for more than half of  $\text{N}_2$  production (Hoagland et al., 2019). Historically, removal of N via denitrification has been ubiquitous in occurrence and extremely variable in magnitude, ranging from 0 – 100% across aquatic systems (Seitzinger, 1988; Seitzinger et al., 2006). Biotic assimilation may have accounted for a large portion of  $\text{NO}_3$  uptake in core incubations (Welti et al., 2012) but was not directly measured in this study. Future studies of floodplain  $\text{NO}_3$  reduction

capacity should consider autotrophic and heterotrophic assimilation of  $\text{NO}_3$  (Dodds & Cole, 2007).

Additionally,  $\text{NO}_3$  uptake may have been influenced by sulfide oxidation and DNRA (Burgin & Hamilton, 2008). Burgin & Hamilton (2008) concluded sulfur driven DNRA potentially contributed up to 90% of  $\text{NO}_3$  reduction. However, the range of DNRA contribution to N reduction across wetlands was extremely wide, validating low DNRA rates measured by Welti et al. 2012 and Hoagland et al. 2019. Nitrite ( $\text{NO}_2$ ) production is rarely quantified in floodplains but has been measured in coastal wetlands (Zhao et al., 2019). Nitrite is an intermediate in many N cycling processes (Quick et al., 2019; Tao, 2018) and is typically present at low concentrations. Nitrite production measured at all 30 core locations, along with net  $\text{NH}_4$  production across the floodplain indicates leakiness of the system (Elrys et al., 2022) in terms of buildup of unwanted N products under high  $\text{NO}_3$  loading that could be exported downstream.

### **Greenhouse gas production**

High concentrations of  $\text{NO}_3$ ,  $\text{NO}_2$ , and  $\text{NH}_4$  can stimulate  $\text{N}_2\text{O}$  production as an intermediate step of various N cycling processes in aquatic systems (Parton et al., 1996; Quick et al., 2019; X. Zhu et al., 2013). However, high  $\text{NO}_3$  loading does not appear to increase  $\text{N}_2\text{O}$  production in the current study. Nitrous oxide yield ( $\text{N}_2\text{O}/(\text{N}_2 + \text{N}_2\text{O}) * 100$ ) in the current study (0.05%) was comparable to the lowest measurements made in a riparian wetland (Burgin & Groffman, 2012; Hefting et al., 2013) and stream sediments (Burgin et al., 2013). Hefting et al. (2013) found a negative correlation between soil pH (range: 4-7) and  $\text{N}_2\text{O}$  emissions. There was a positive correlation between  $\text{N}_2\text{O}$  flux and pH (range 5.0 – 6.2) in the current study, highlighting variability among drivers of N

cycling processes across different environments. Nitrification and denitrification both contribute to  $\text{N}_2\text{O}$  production but the degree of contribution by either process is widely variable (Parton et al., 1996) and requires isotopic labeling and molecular analyses to trace N atoms through various forms and microbially mediated transformations (Masta et al., 2022). A recent synthesis of  $\text{N}_2\text{O}$  production in streams and rivers (Quick et al., 2019) and denitrification in terrestrial landscapes (Almaraz et al., 2020) demonstrate valuable progress in N cycling research in relation to tradeoffs with greenhouse gas emissions. These separate reviews also highlight the need to synthesize N cycling research across ecosystem boundaries.

Methane production is stimulated under reducing conditions normally promoted for  $\text{NO}_3$  reduction, but  $\text{CH}_4$  flux was extremely low from soil core incubations in the current study. Low  $\text{CH}_4$  flux was likely due to high  $\text{NO}_3$  supply for soil core incubations which created redox conditions favorable to denitrifiers, allowing them to outcompete methanogens which are favored at lower redox states (Bodelier & Steenbergh, 2014). However,  $\text{CH}_4$  production has been shown to increase with  $\text{NO}_3$  addition in beaver ponds (Burgin et al., 2013). Simultaneous N and P additions can increase competitive advantage of methanogens against denitrifiers relative to N addition alone (Kim et al., 2015) by enhancing microbial growth rates (Elser et al., 2000; Isanta-Navarro et al., 2022). Nutrient enriched water used for flow-through incubations had a molar N:P ratio of  $\sim 23$  (as  $\text{NO}_3\text{-N}:\text{PO}_4\text{-P}$ ), higher than  $\text{NO}_3\text{-N}:\text{PO}_4\text{-P}$  ratios in July 2020 floodwater ( $\sim 12$ ). This may have caused P limitation in core incubations and enabled denitrifiers to outcompete methanogens for electron donors (Bodelier, 2011).

Low net production rates of  $\text{N}_2\text{O}$  and  $\text{CH}_4$  alongside high  $\text{NO}_3$  uptake and  $\text{N}_2$  production suggest N reduction within this floodplain is possible while limiting GHG emissions. However, hotspots of GHG flux did occur (McClain et al., 2003; Vidon et al., 2010) and should be considered when designing an ecosystem to enhance nutrient retention (Bernhardt et al., 2017). While  $\text{CH}_4$  flux may have been limited by competition with denitrifiers for P and the floodplain was a net sink for  $\text{PO}_4$ ,  $\text{PO}_4$  uptake was not ubiquitous in all soil cores, indicating that  $\text{PO}_4$  was not limiting biotic uptake in all cases. Further mechanistic studies are needed across ecosystem boundaries to elucidate GHG dynamics associated with C, N, and P cycling (Kang et al., 2022; Kim et al., 2015) and floodplain nutrient storage (Wohl, 2021).

## **Conclusion**

This case study provides evidence that floodplains reconnected to their rivers via levee breaks have potential to retain N and P from transport to downstream ecosystems. Effects of levee breaks, in terms of nutrient load reductions, were not quantifiable in this study because there was no pre-restoration monitoring of floodwater entering the floodplain. Hydrologic modeling of the Mayfield Creek system can potentially provide estimates of flow through levee breaks, allowing future studies of this restored floodplain to estimate nutrient load reductions.

The widespread idea of reconnected floodplains as nutrient sinks was generally supported in this study. However, relatively low N retention compared to P, and sources of  $\text{NH}_4$  and  $\text{NO}_3$  within the floodplain point to nutrient cycling idiosyncrasies that influenced the degree to which the floodplain was a net sink for N. Additionally, qualitative comparison of floodwater and soil N:P ratios suggest some fraction of soil P is

missing, either due to laboratory extraction methods, storage in vegetative biomass, or unmeasured export from the floodplain. Finally, disagreement between flood monitoring results and flow-through core incubations are most likely driven by differences in residence time and nutrient concentrations between field-scale and laboratory incubation measurements. Both methods provide insights into floodplain nutrient retention. Focused studies of nutrient processing rates under ambient conditions are likely to improve agreement between field and laboratory results.

## CHAPTER 5: SUMMARY AND FUTURE WORK

My dissertation research draws attention to the utility of flow-through soil core incubations for evaluation of nutrient retention capacity of restored floodplain wetland soils. Inferences of WRP nutrient retention capacity must be made within the context of fieldwork and laboratory constraints (chapter 2) that explain up to 16% of variation in nutrient flux rates derived from flow-through soil core incubations. Further, I show in chapter 2 that core incubation materials appear to influence nutrient flux rates, highlighting the need for additional experimentation to identify mechanisms of these effects. Quantitatively rigorous interpolation methods are not suitable for our dataset because of our relatively small geostatistical sample size ( $n = 30$ ) within each easement. Therefore, extrapolation across represented management areas/restoration practices provide more informative results (chapter 3) where WRP nutrient retention capacity can be modeled in relation to influential soil characteristics at local and regional scales. Flow-through incubation results of each WRP easement could be analyzed as case studies of local-scale relationships between soil structure and nutrient retention patterns. I demonstrate utility of a case study approach using one easement in conjunction with *in situ* floodwater nutrient dynamics (chapter 4). Both floodwater monitoring and flow-through core incubations qualified this easement as a net sink for N and P. However, floodwater data suggested the easement had greater P retention capacity than N, while flow-through soil core incubations suggested the opposite pattern. Further study of experimental artifacts associated with flow-through incubations representative of ambient

environmental conditions should improve agreement between field and laboratory studies.

Regional-scale patterns of WRP restoration trajectories inferred from our flow-through soil incubations are dependent on the space-for-time sampling design employed throughout the monitoring project. Space for time substitution utilizing WRP easements of different restoration ages to represent temporal trends of bottomland hardwood forest succession after cropland restoration can facilitate understanding of nutrient cycling trends and lead to development of hypotheses that can guide development of future studies (Pickett, 1989). However, it is important to note that inferences made from space-for-time studies of secondary succession are confounded by spatial variability of past ecosystem dynamics and management practices that occurred before succession (i.e. wetland restoration) began (Johnson & Miyanishi, 2008). Continued evaluation of WRP nutrient retention capacity should consider a Lagrangian approach (Doyle & Ensign, 2009), where a few specific areas could be monitored over time as they transition from cropland to bottomland hardwood forest. This would complement our regional-scale space-for-time approach by providing additional insights into successional patterns that may have influenced results of the current WRP monitoring program.

Future work investigating mechanisms of nutrient retention capacity and greenhouse gas production in WRP easements would benefit from the use of stable isotope tracers to understand nutrient transformation pathways. Addition of isotopic tracers (i.e.  $^{15}\text{N-NO}_3$  and/or  $^{15}\text{N-NH}_4$ ) to flow-through source water in soil core incubations enables quantification of specific N removal rates as dissolved  $\text{NO}_3$  and  $\text{NH}_4$  are transformed to gaseous  $\text{N}_2\text{O}$ , and  $\text{N}_2$  end products through dissimilatory pathways

used by microbes to gain energy (Kuypers et al., 2018; Robertson et al., 2019). Biomass assimilation of N via wetland plants and soils can also be evaluated through isotopic labeling studies (Hong et al., 2019). Phosphorus does not have a stable isotopic form, but P transformations can still be traced through ecosystems using  $^{18}\text{O}$ - $\text{PO}_4$  isotopes (Davies et al., 2014; Wang et al., 2022). Addition of  $^{15}\text{N}$  isotopic tracers to flow-through soil incubations has already been applied to gain informative mechanistic explanations of wetland N cycling (Scott et al., 2008) but research involving addition of  $^{18}\text{O}$  for examination of P cycling in flow-through wetland soil core incubations is absent from the literature. Nutrient flux measurements derived from isotopic labeling additions are based on fractionation rates of the heavy isotope (i.e.  $^{15}\text{N}$ ) compared with the light isotope (i.e.  $^{14}\text{N}$ ) and must be accounted for using mathematical models representative of the system (Spott & Stange, 2007). Essentially,  $^{14}\text{N}$  is used more readily in biological processes than  $^{15}\text{N}$  because it is thermodynamically favorable to use the lighter element. Therefore, the fractional isotopic composition of an end product (i.e.  $\text{N}_2$  gas) changes predictably with the addition of  $^{15}\text{N}$ - $\text{NO}_3$  if  $\text{NO}_3$ -N is converted to  $\text{N}_2$ -N through a denitrification pathway. Combination of isotopic labeling experiments with flow-through soil core incubations complicates an already labor-intensive process because the chance for isotopic contamination of incubation materials is high. I recommend small pilot studies and single use of new incubation materials for future students combining isotope pairing techniques (Robertson et al., 2019) with flow-through incubations.

Coupled biogeochemical cycles (Schlesinger et al., 2011) and their cascading influences through wetland food webs are another essential part of understanding tradeoffs between nutrient retention and greenhouse gas emissions. For example,  $\text{CH}_4$

emissions could be reduced, and N removal enhanced where methanotrophic denitrifiers use CH<sub>4</sub>-C as an energy source to fuel the reduction of NO<sub>3</sub>-N to N<sub>2</sub>-N gas (Raghoebarsing et al., 2006; Zhu et al., 2010). Recent progress in methanotrophic denitrification research has focused on waste-water treatment systems (Costa et al., 2022) but measurement of gene abundances associated with microbes capable of the methanotrophic denitrification process (Ettwig et al., 2008) could shed light on the prevalence of such beneficial microbial food webs in restored wetland soils. In addition to methanotrophic denitrification, entrainment of methane-derived carbon (MDC) within wetland food webs can contribute to wetland C storage patterns (Grey, 2016; Hart et al., 2019). Essentially, MDC measured through studies of ambient <sup>13</sup>C-CH<sub>4</sub> in wetland food web compartments can contribute to long-term C accumulation in wetland soils where methanotrophic microbes contribute substantially to the base of food webs.

Finally, my dissertation research and our larger WRP monitoring project relied on flow-through incubation results of soil nutrient uptake capacity with elevated “floodwater” NO<sub>3</sub>-N and PO<sub>4</sub>-P. Future studies of WRP nutrient retention should consider measuring ambient nutrient flux rates by adjusting nutrient supply for incubations to approximate *in situ* concentrations of nutrient delivered to floodplains. This approach should constrain some of the variability I report in my dissertation results where nutrient processing rates were intentionally maximized by constantly high nutrient supply.

## BIBLIOGRAPHY

- Aldous, A., McCormick, P., Ferguson, C., Graham, S., & Craft, C. (2005). Hydrologic regime controls soil phosphorus fluxes in restoration and undisturbed wetlands. *Restoration Ecology*, *13*(2), 341–347. <https://doi.org/10.1111/j.1526-100X.2005.00043.x>
- Alexander, R. B., Smith, R. A., Schwarz, G. E., Boyer, E. W., Nolan, J. V., & Brakebill, J. W. (2008). Differences in phosphorus and nitrogen delivery to the Gulf of Mexico from the Mississippi River Basin. *Environmental Science and Technology*, *42*(3), 822–830. <https://doi.org/10.1021/es0716103>
- Almaraz, M., Wong, M. Y., & Yang, W. H. (2020). Looking back to look ahead: a vision for soil denitrification research. *Ecology*, *101*(1), 1–10. <https://doi.org/10.1002/ecy.2917>
- An, S., & Gardner, W. S. (2002). Dissimilatory nitrate reduction to ammonium (DNRA) as a nitrogen link, versus denitrification as a sink in a shallow estuary (Laguna Madre/Baffin Bay, Texas). *Marine Ecology Progress Series*, *237*, 41–50. <https://doi.org/10.3354/meps237041>
- An, S., Gardner, W. S., & Kana, T. (2001). Simultaneous Measurement of Denitrification and Nitrogen Fixation Using Isotope Pairing with Membrane Inlet Mass Spectrometry Analysis. *Applied and Environmental Microbiology*, *67*(3), 1171–1178. <https://doi.org/10.1128/AEM.67.3.1171-1178.2001>
- Appling, A. P., Bernhardt, E. S., & Stanford, J. A. (2014). Floodplain biogeochemical mosaics: A multidimensional view of alluvial soils. *Journal of Geophysical Research: Biogeosciences*, *119*(8), 1538–1553. <https://doi.org/10.1002/2013JG002543>
- Ardón, M., Morse, J. L., Doyle, M. W., & Bernhardt, E. S. (2010). The Water Quality Consequences of Restoring Wetland Hydrology to a Large Agricultural Watershed in the Southeastern Coastal Plain. *Ecosystems*, *13*(7), 1060–1078. <https://doi.org/10.1007/s10021-010-9374-x>
- Argiroff, W. A., Zak, D. R., Lanser, C. M., & Wiley, M. J. (2017). Microbial Community Functional Potential and Composition Are Shaped by Hydrologic Connectivity in Riverine Floodplain Soils. *Microbial Ecology*, *73*(3), 630–644. <https://doi.org/10.1007/s00248-016-0883-9>
- Atkinson, C. L., van Ee, B. C., Lu, Y. H., & Zhong, W. (2019). Wetland floodplain flux: temporal and spatial availability of organic matter and dissolved nutrients in an unmodified river. *Biogeochemistry*, *142*(3), 395–411. <https://doi.org/10.1007/s10533-019-00542-z>

- Baldwin, D. S., & Mitchell, A. M. (2000). The effects of drying and re-flooding on the sediment and soil nutrient dynamics of lowland river-floodplain systems: A synthesis. *River Research and Applications*, 16(5), 457–467. [https://doi.org/10.1002/1099-1646\(200009/10\)16:5<457::aid-rrr597>3.0.co;2-b](https://doi.org/10.1002/1099-1646(200009/10)16:5<457::aid-rrr597>3.0.co;2-b)
- Bannister, J. M., Herbert, E. R., & Craft, C. B. (2015). Spatial variability in sedimentation, carbon sequestration, and nutrient accumulation in an alluvial floodplain forest. In *The Role of Natural and Constructed Wetlands in Nutrient Cycling and Retention on the Landscape* (pp. 41–55). Springer International Publishing. [https://doi.org/10.1007/978-3-319-08177-9\\_4](https://doi.org/10.1007/978-3-319-08177-9_4)
- Bernhardt, E. S., Blaszczyk, J. R., Ficken, C. D., Fork, M. L., Kaiser, K. E., & Seybold, E. C. (2017). Control Points in Ecosystems: Moving Beyond the Hot Spot Hot Moment Concept. *Ecosystems*, 20(4), 665–682. <https://doi.org/10.1007/s10021-016-0103-y>
- Błońska, E., & Lasota, J. (2017). Soil organic matter accumulation and carbon fractions along a moisture gradient of forest soils. *Forests*, 8(11). <https://doi.org/10.3390/f8110448>
- Bodelier, P. L. E. (2011). Interactions between nitrogenous fertilizers and methane cycling in wetland and upland soils. *Current Opinion in Environmental Sustainability*, 3(5), 379–388. <https://doi.org/10.1016/j.cosust.2011.06.002>
- Bodelier, P. L. E., & Steenbergh, A. K. (2014). Interactions between methane and the nitrogen cycle in light of climate change. *Current Opinion in Environmental Sustainability*, 9–10, 26–36. <https://doi.org/10.1016/j.cosust.2014.07.004>
- Booman, G. C., & Laterra, P. (2019). Channelizing Streams for Agricultural Drainage Impairs their Nutrient Removal Capacity. *Journal of Environmental Quality*, 48(2), 459–468. <https://doi.org/10.2134/jeq2018.07.0264>
- Bridgham, S. D., Johnston, C. A., Schubauer-berigan, J. P., & Weishampel, P. (2001). Phosphorus Sorption Dynamics in Soils and Coupling with Surface and Pore Water in Riverine Wetlands. *Soil Sci. Soc. Am. J.*, 65, 577–588.
- Brinson, M. M., & Eckles, S. D. (2011). U.S. Department of Agriculture conservation program and practice effects on wetland ecosystem services: A synthesis. *Ecological Applications*, 21(3 SUPPL.), S116–S127. <https://doi.org/10.1890/09-0627.1>
- Bruland, G. L., & Richardson, C. J. (2004). Wetlands and Aquatic Processes A Spatially Explicit Investigation of Phosphorus Sorption and Related Soil Properties in Two Riparian Wetlands. *Journal of Environmental Quality*, 33, 785–794.
- Burgin, A. J., & Groffman, P. M. (2012). Soil O<sub>2</sub> controls denitrification rates and N<sub>2</sub>O yield in a riparian wetland. *Journal of Geophysical Research: Biogeosciences*, 117(1), 1–10. <https://doi.org/10.1029/2011JG001799>

- Burgin, A. J., Groffman, P. M., & Lewis, D. N. (2010). Factors Regulating Denitrification in a Riparian Wetland. *Soil Science Society of America Journal*, 74(5), 1826–1833. <https://doi.org/10.2136/sssaj2009.0463>
- Burgin, A. J., & Hamilton, S. K. (2007). Have we overemphasized the role of denitrification in aquatic ecosystems? A review of nitrate removal pathways. *Frontiers in Ecology and the Environment*, 5(2), 89–96. [https://doi.org/10.1890/1540-9295\(2007\)5\[89:HWOTRO\]2.0.CO;2](https://doi.org/10.1890/1540-9295(2007)5[89:HWOTRO]2.0.CO;2)
- Burgin, A. J., & Hamilton, S. K. (2008). NO<sub>3</sub>--driven SO<sub>4</sub><sup>2-</sup> production in freshwater ecosystems: Implications for N and S cycling. *Ecosystems*, 11(6), 908–922. <https://doi.org/10.1007/s10021-008-9169-5>
- Burgin, A. J., Lazar, J. G., Groffman, P. M., Gold, A. J., & Kellogg, D. Q. (2013). Balancing nitrogen retention ecosystem services and greenhouse gas disservices at the landscape scale. *Ecological Engineering*, 56, 26–35. <https://doi.org/10.1016/j.ecoleng.2012.05.003>
- Carpenter, S. R., Caraco, N. F., Correll, D. L., Howarth, R. W., Sharpley, A. N., & Smith, V. H. (1998). Nonpoint Pollution of Surface Waters with Phosphorus and Nitrogen. *Ecological Applications*, 8(3), 559–568. <https://doi.org/10.1017/CBO9781107415324.004>
- Chave, J. (2013). The problem of pattern and scale in ecology: What have we learned in 20 years? *Ecology Letters*, 16(SUPPL.1), 4–16. <https://doi.org/10.1111/ele.12048>
- Cheng, F. Y., Van Meter, K. J., Byrnes, D. K., & Basu, N. B. (2020). Maximizing US nitrate removal through wetland protection and restoration. *Nature, March*. <https://doi.org/10.1038/s41586-020-03042-5>
- Costa, R. B., Lens, P. N. L., & Foresti, E. (2022). Methanotrophic denitrification in wastewater treatment: microbial aspects and engineering strategies. In *Critical Reviews in Biotechnology* (Vol. 42, Issue 1, pp. 145–161). Taylor and Francis Ltd. <https://doi.org/10.1080/07388551.2021.1931014>
- Cotner, J. B., Sada, R. H., Bootsma, H., Johengen, T., Cavaletto, J. F., & Gardner, W. S. (2000). Nutrient Limitation of Heterotrophic Bacteria in Florida Bay. *Source: Estuaries*, 23(5), 611–620. <https://www.jstor.org/stable/1352888>
- Cross, W. F., Hood, J. M., Benstead, J. P., Hury, A. D., & Nelson, D. (2015). Interactions between temperature and nutrients across levels of ecological organization. *Global Change Biology*, 21(3), 1025–1040. <https://doi.org/10.1111/gcb.12809>
- Czuba, J. A., Hansen, A. T., Foufoula-Georgiou, E., & Finlay, J. C. (2018). Contextualizing Wetlands Within a River Network to Assess Nitrate Removal and Inform Watershed Management. *Water Resources Research*, 54(2), 1312–1337. <https://doi.org/10.1002/2017WR021859>

- Davies, C. L., Surridge, B. W. J., & Goody, D. C. (2014). Phosphate oxygen isotopes within aquatic ecosystems: Global data synthesis and future research priorities. *Science of the Total Environment*, *496*, 563–575. <https://doi.org/10.1016/j.scitotenv.2014.07.057>
- Dee, M. M., & Tank, J. L. (2020). Inundation time mediates denitrification end products and carbon limitation in constructed floodplains of an agricultural stream. *Biogeochemistry*, *0123456789*. <https://doi.org/10.1007/s10533-020-00670-x>
- Deek, A., Emeis, K., & Van Beusekom, J. (2012). Nitrogen removal in coastal sediments of the German Wadden Sea. *Biogeochemistry*, *108*(1), 467–483. <https://doi.org/10.1007/S10533-01>
- Delaune, R. D., Boar, R. R., Lindau, C. W., & Kleiss, B. A. (1996). Denitrification in Bottomland Hardwood Wetland Soils of the Cache River. In *WETLANDS* (Vol. 16, Issue 3).
- Diaz, R. J., & Rosenberg, R. (2008). Spreading Dead Zones and Consequences for Marine Ecosystems. In *New Series* (Vol. 321, Issue 5891).
- Dodds, W. K. (2006). Nutrients and the “Dead Zone”: The Link between Nutrient Ratios and Dissolved Oxygen in the Northern Gulf of Mexico. *Frontiers in Ecology and the Environment*, *4*(4), 211–217. <https://doi.org/10.1017/CBO9781107415324.004>
- Dodds, W. K., & Cole, J. J. (2007). Expanding the concept of trophic state in aquatic ecosystems: It’s not just the autotrophs. *Aquatic Sciences*, *69*(4), 427–439. <https://doi.org/10.1007/s00027-007-0922-1>
- Dolph, C., Finlay, J. C., Hansen, A. T., & Dalzell, B. (2022). *Predicting high resolution total phosphorus concentrations for soils of the Upper Mississippi River Basin using machine learning*. <https://doi.org/10.21203/rs.3.rs-2285751/v1>
- Doyle, M. W., & Ensign, S. H. (2009). Alternative reference frames in river system science. *BioScience*, *59*(6), 499–510. <https://doi.org/10.1525/bio.2009.59.6.8>
- Drouin, A., Diane, S. L., Lavoie, L., & Ouellet, C. (2011). High-precision elevation model to evaluate the spatial distribution of soil organic carbon in active floodplains ariane drouin1. *Wetlands*, *31*(6), 1151–1164. <https://doi.org/10.1007/s13157-011-0226-z>
- Duncan, J. M., Groffman, P. M., & Band, L. E. (2013). Towards closing the watershed nitrogen budget: Spatial and temporal scaling of denitrification. *Journal of Geophysical Research: Biogeosciences*, *118*(3), 1105–1119. <https://doi.org/10.1002/jgrg.20090>
- Dupas, R., Abbott, B. W., Minaudo, C., & Fovet, O. (2019). Distribution of landscape units within catchments influences nutrient export dynamics. *Frontiers in Environmental Science*, *7*(APR), 1–8. <https://doi.org/10.3389/fenvs.2019.00043>

- Elrys, A. S., Uwiragiye, Y., Zhang, Y., Abdel-Fattah, M. K., Chen, Z. xiong, Zhang, H. min, Meng, L., Wang, J., Zhu, T. bin, Cheng, Y., Zhang, J. bo, Cai, Z. cong, Chang, S. X., & Müller, C. (2022). Expanding agroforestry can increase nitrate retention and mitigate the global impact of a leaky nitrogen cycle in croplands. *Nature Food*. <https://doi.org/10.1038/s43016-022-00657-x>
- Elser, J. J., Bracken, M. E. S., Cleland, E. E., Gruner, D. S., Harpole, W. S., Hillebrand, H., Ngai, J. T., Seabloom, E. W., Shurin, J. B., & Smith, J. E. (2007). Global analysis of nitrogen and phosphorus limitation of primary producers in freshwater, marine and terrestrial ecosystems. *Ecology Letters*, *10*(12), 1135–1142. <https://doi.org/10.1111/j.1461-0248.2007.01113.x>
- Elser, J. J., Sterner, R. W., Gorokhova, E., Fagan, W. F., Markow, T. A., Cotner, J. B., Harrison, J. F., Hobbie, S. E., Odell, G. M., & Weider, L. W. (2000). Biological stoichiometry from genes to ecosystems. *Ecology Letters*, *3*(6), 540–550. <https://doi.org/10.1046/j.1461-0248.2000.00185.x>
- Ettwig, K. F., Shima, S., Van De Pas-Schoonen, K. T., Kahnt, J., Medema, M. H., Op Den Camp, H. J. M., Jetten, M. S. M., & Strous, M. (2008). Denitrifying bacteria anaerobically oxidize methane in the absence of Archaea. *Environmental Microbiology*, *10*(11), 3164–3173. <https://doi.org/10.1111/j.1462-2920.2008.01724.x>
- Evans, J. L., Murdock, J. N., Taylor, J. M., & Lizotte, R. E. (2021). Sediment nutrient flux rates in a shallow, turbid lake are more dependent on water quality than lake depth. *Water (Switzerland)*, *13*(10). <https://doi.org/10.3390/w13101344>
- Evelt, S. R., Schwartz, R. C., Tolk, J. A., & Howell, T. A. (2009). Soil Profile Water Content Determination: Spatiotemporal Variability of Electromagnetic and Neutron Probe Sensors in Access Tubes. *Vadose Zone Journal*, *8*(4), 926–941. <https://doi.org/10.2136/vzj2008.0146>
- Faulkner, S., Barrow, W., Keeland, B., Walls, S., & Telesco, D. (2011a). Effects of conservation practices on wetland ecosystem services in the Mississippi Alluvial Valley. *Ecological Applications*, *21*(3), S31–S48. <http://www.jstor.org/stable/23021649>
- Faulkner, S., Barrow, W., Keeland, B., Walls, S., & Telesco, D. (2011b). *Effects of conservation practices on wetland ecosystem services in the Mississippi Alluvial Valley Authors ( s ): Stephen Faulkner , Wylie Barrow Jr ., Bob Keeland , Susan Walls and David Telesco Source : Ecological Applications , Vol . 21 , No . 3 , Supp. 21*(3).
- Fernald, A. G., Wigington, P. J., & Landers, D. H. (2001). Transient storage and hyporheic flow along the Willamette River, Oregon: Field measurements and model estimates. *Water Resources Research*, *37*(6), 1681–1694. <https://doi.org/10.1029/2000WR900338>

- Florsheim, J. L., & Mount, J. F. (2002). Restoration of floodplain topography by sand-splay complex formation in response to intentional levee breaches, Lower Cosumnes River, California. *Geomorphology*, *44*, 67–94. [www.elsevier.com/locate/geomorph](http://www.elsevier.com/locate/geomorph)
- Forshay, K. J., & Stanley, E. H. (2005). Rapid Nitrate Loss and Denitrification in a Temperate River Floodplain. *Biogeochemistry*, *75*(1), 43–64. <http://www.jstor.org/stable/20055257>
- Gallardo, A. (2003). Spatial Variability of Soil Properties in a Floodplain Forest in Northwest Spain. *Ecosystems*, *6*(6), 564–576. <https://doi.org/10.1007/s10021-003-0198-9>
- Galloway, J. N. (1998). The global nitrogen cycle: changes and consequences. *Environmental Pollution*, *102*, 15–24. [www.archive.org](http://www.archive.org)
- Gardner, W. S., McCarthy, M. J., An, S., Sobolev, D., Sell, K. S., & Brock, D. (2006). Nitrogen fixation and dissimilatory nitrate reduction to ammonium (DNRA) support nitrogen dynamics in Texas estuaries. *Limnology and Oceanography*, *51*(1 II), 558–568. [https://doi.org/10.4319/lo.2006.51.1\\_part\\_2.0558](https://doi.org/10.4319/lo.2006.51.1_part_2.0558)
- Garten, C. T., & Hanson, P. J. (2006). Measured forest soil C stocks and estimated turnover times along an elevation gradient. *Geoderma*, *136*(1–2), 342–352. <https://doi.org/10.1016/j.geoderma.2006.03.049>
- Gibbs, M., & Özkundakci, D. (2011). Effects of a modified zeolite on P and N processes and fluxes across the lake sediment-water interface using core incubations. *Hydrobiologia*, *661*(1), 21–35. <https://doi.org/10.1007/s10750-009-0071-8>
- Gillespie, J. L., Noe, G. B., Hupp, C. R., Gellis, A. C., & Schenk, E. R. (2018). Floodplain Trapping and Cycling Compared to Streambank Erosion of Sediment and Nutrients in an Agricultural Watershed. *Journal of the American Water Resources Association*, *54*(2), 565–582. <https://doi.org/10.1111/1752-1688.12624>
- Glibert, P. M. (2017). Eutrophication, harmful algae and biodiversity — Challenging paradigms in a world of complex nutrient changes. *Marine Pollution Bulletin*, *124*(2), 591–606. <https://doi.org/10.1016/j.marpolbul.2017.04.027>
- Glibert, P. M. (2020). From hogs to HABs : impacts of industrial farming in the US on nitrogen and phosphorus and greenhouse gas pollution. In *Biogeochemistry* (Vol. 150, Issue 2). Springer International Publishing. <https://doi.org/10.1007/s10533-020-00691-6>
- Glibert, P. M., Maranger, R., Sobota, D. J., & Bouwman, L. (2014). The Haber Bosch-harmful algal bloom (HB-HAB) link. *Environmental Research Letters*, *9*(10). <https://doi.org/10.1088/1748-9326/9/10/105001>
- Glibert, P. M., Middelburg, J. J., McClelland, J. W., & Jake Vander Zanden, M. (2019). Stable isotope tracers: Enriching our perspectives and questions on sources, fates,

- rates, and pathways of major elements in aquatic systems. *Limnology and Oceanography*, 64(3), 950–981. <https://doi.org/10.1002/lno.11087>
- Gonzalez, A., Germain, R. M., Srivastava, D. S., Filotas, E., Dee, L. E., Gravel, D., Thompson, P. L., Isbell, F., Wang, S., Kéfi, S., Montoya, J., Zelnik, Y. R., & Loreau, M. (2020). Scaling-up biodiversity-ecosystem functioning research. *Ecology Letters*, 23(4), 757–776. <https://doi.org/10.1111/ele.13456>
- Gordon, B. A., Dorothy, O., & Lenhart, C. F. (2020). Nutrient retention in ecologically functional floodplains: A review. In *Water (Switzerland)* (Vol. 12, Issue 10). MDPI AG. <https://doi.org/10.3390/w12102762>
- Grantz, E. M., Kogo, A., & Thad Scott, J. (2012). Partitioning whole-lake denitrification using in situ dinitrogen gas accumulation and intact sediment core experiments. *Limnology and Oceanography*, 57(4), 925–935. <https://doi.org/10.4319/lo.2012.57.4.0925>
- Grey, J. (2016). The incredible lightness of being methane-fuelled: Stable isotopes reveal alternative energy pathways in aquatic ecosystems and beyond. *Frontiers in Ecology and Evolution*, 4(FEB). <https://doi.org/10.3389/fevo.2016.00008>
- Griffiths, R. P., Madritch, M. D., & Swanson, A. K. (2009). The effects of topography on forest soil characteristics in the Oregon Cascade Mountains (USA): Implications for the effects of climate change on soil properties. *Forest Ecology and Management*, 257(1), 1–7. <https://doi.org/10.1016/j.foreco.2008.08.010>
- Groffman, P. M., Altabet, M. A., Böhlke, J. K., Butterbach-Bahl, K., David, M. B., Firestone, M. K., Giblin, A. E., Kana, T. M., Nielsen, L. P., & Voytek, M. A. (2006). Methods for measuring denitrification: Diverse approaches to a difficult problem. *Ecological Applications*, 16(6), 2091–2122. [https://doi.org/10.1890/1051-0761\(2006\)016\[2091:MFMDDA\]2.0.CO;2](https://doi.org/10.1890/1051-0761(2006)016[2091:MFMDDA]2.0.CO;2)
- Groffman, P. M., Butterbach-Bahl, K., Fulweiler, R. W., Gold, A. J., Morse, J. L., Stander, E. K., Tague, C., Tonitto, C., & Vidon, P. (2009). Challenges to incorporating spatially and temporally explicit phenomena (hotspots and hot moments) in denitrification models. *Biogeochemistry*, 93(1–2), 49–77. <https://doi.org/10.1007/s10533-008-9277-5>
- Groffman, P. M., & Tiedje, J. M. (1988). Denitrification Hysteresis During Wetting and Drying Cycles in Soil. *Soil Science Society of America Journal*, 52(6), 1626–1629. <https://doi.org/10.2136/sssaj1988.03615995005200060022x>
- Grzebisz, W., Zielewicz, W., & Przygocka-Cyna, K. (2023). Deficiencies of Secondary Nutrients in Crop Plants—A Real Challenge to Improve Nitrogen Management. *Agronomy*, 13(1). <https://doi.org/10.3390/agronomy13010066>

- Hall, R. O., & Madinger, H. L. (2018). Use of argon to measure gas exchange in turbulent mountain streams. *Biogeosciences*, *15*(10), 3085–3092. <https://doi.org/10.5194/bg-15-3085-2018>
- Hall, R. O., Mulholland, P. J., Sobota, D. J., Dodds, W. K., Findlay, S. E. G., Grimm, N. B., Hamilton, S. K., McDowell, W. H., O'Brien, J. M., Tank, J. L., Ashkenas, L. R., Cooper, L. W., Dahm, C. N., Gregory, S. V., Johnson, S. L., Meyer, J. L., Peterson, B. J., Poole, G. C., Valett, H. M., ... Thomasn, S. M. (2009). Nitrate removal in stream ecosystems measured by <sup>15</sup>N addition experiments: Total uptake. *Limnology and Oceanography*, *54*(3), 653–665. <https://doi.org/10.4319/lo.2009.54.3.0666>
- Hamdan, T. A., Scott, T. A., Wolf, T., & Haggard, D. E. (2010). Sediment phosphorus flux in Beaver Lake in Northwest Arkansas. *Discovery, The Student Journal of Dale Bumpers College of Agricultural, Food and Life Sciences*, *11*(1), 3–12.
- Hansen, A. T., Dolph, C. L., Foufoula-Georgiou, E., & Finlay, J. C. (2018). Contribution of wetlands to nitrate removal at the watershed scale. *Nature Geoscience*, *11*(2), 127–132. <https://doi.org/10.1038/s41561-017-0056-6>
- Hansson, L. A., Brönmark, C., Nilsson, P. A., & Åbjörnsson, K. (2005). Conflicting demands on wetland ecosystem services: Nutrient retention, biodiversity or both? *Freshwater Biology*, *50*(4), 705–714. <https://doi.org/10.1111/j.1365-2427.2005.01352.x>
- Hart, J. A., Vizza, C., West, W. E., Chaloner, D. T., Jones, S. E., & Lamberti, G. A. (2019). Methane Cycling Contributes to Distinct Patterns in Carbon Stable Isotopes of Wetland Detritus. *Wetlands*, *39*(2), 361–370. <https://doi.org/10.1007/s13157-018-1119-1>
- Hefting, M. M., van den Heuvel, R. N., & Verhoeven, J. T. A. (2013). Wetlands in agricultural landscapes for nitrogen attenuation and biodiversity enhancement: Opportunities and limitations. *Ecological Engineering*, *56*(September 2011), 5–13. <https://doi.org/10.1016/j.ecoleng.2012.05.001>
- Helton, A. M., Hall, R. O., & Bertuzzo, E. (2018). How network structure can affect nitrogen removal by streams. *Freshwater Biology*, *63*(1), 128–140. <https://doi.org/10.1111/fwb.12990>
- Helton, A. M., Poole, G. C., Meyer, J. L., Wollheim, W. M., Peterson, B. J., Mulholland, P. J., Bernhardt, E. S., Stanford, J. A., Arango, C., Ashkenas, L. R., Cooper, L. W., Dodds, W. K., Gregory, S. v., Hall, R. O., Hamilton, S. K., Johnson, S. L., McDowell, W. H., Potter, J. D., Tank, J. L., ... Zeglin, L. (2011). Thinking outside the channel: Modeling nitrogen cycling in networked river ecosystems. *Frontiers in Ecology and the Environment*, *9*(4), 229–238. <https://doi.org/10.1890/080211>
- Hoagland, B., Schmidt, C., Russo, T. A., Adams, R., & Kaye, J. (2019). Controls on nitrogen transformation rates on restored floodplains along the Cosumnes River,

- California. *Science of the Total Environment*, 649, 979–994.  
<https://doi.org/10.1016/j.scitotenv.2018.08.379>
- Hohman, S. P., Smyth, A. R., Bean, E. Z., & Reisinger, A. J. (2021). Internal nitrogen dynamics in stormwater pond sediments are influenced by pond age and inorganic nitrogen availability. *Biogeochemistry*, 156(2), 255–278.  
<https://doi.org/10.1007/s10533-021-00843-2>
- Hong, J., Zhang, J., Ma, Y., Gu, B., & Lee, R. (2019). The Fates of Nitrogen in an Experimental Wetland Food Web: a Stable Isotope Study. *Wetlands*, 39(2), 303–310. <https://doi.org/10.1007/s13157-018-1085-7>
- Hopkins, K. G., Noe, G. B., Franco, F., Pindilli, E. J., Gordon, S., Metes, M. J., Claggett, P. R., Gellis, A. C., Hupp, C. R., & Hogan, D. M. (2018). A method to quantify and value floodplain sediment and nutrient retention ecosystem services. *Journal of Environmental Management*, 220, 65–76.  
<https://doi.org/10.1016/j.jenvman.2018.05.013>
- Hurst, N., White, J. R., & Baustian, J. (2016). Nitrate Reduction in a Hydrologically Restored Bottomland Hardwood Forest in the Mississippi River Watershed, Northern Louisiana. *Soil Science Society of America Journal*, 80(6), 1698–1705.  
<https://doi.org/10.2136/sssaj2016.08.0250>
- Isanta-Navarro, J., Prater, C., Peoples, L. M., Loladze, I., Phan, T., Jeyasingh, P. D., Church, M. J., Kuang, Y., & Elser, J. J. (2022). Revisiting the growth rate hypothesis: Towards a holistic stoichiometric understanding of growth. *Ecology Letters*, 25(10), 2324–2339. <https://doi.org/10.1111/ele.14096>
- Ivanov, K., Zapryanova, P., Petkova, M., Stefanova, V., Kmetov, V., Georgieva, D., & Angelova, V. (2012). Comparison of inductively coupled plasma mass spectrometry and colorimetric determination of total and extractable phosphorus in soils. *Spectrochimica Acta - Part B Atomic Spectroscopy*, 71–72, 117–122.  
<https://doi.org/10.1016/j.sab.2012.05.013>
- James, W. F., Richardson, W. B., & Soballe, D. M. (2008). Effects of residence time on summer nitrate uptake in Mississippi River flow-regulated backwaters. *River Research and Applications*, 24(9), 1206–1217. <https://doi.org/10.1002/rra.1150>
- Johnson, E. A., & Miyanishi, K. (2008). Testing the assumptions of chronosequences in succession. In *Ecology Letters* (Vol. 11, Issue 5, pp. 419–431).  
<https://doi.org/10.1111/j.1461-0248.2008.01173.x>
- Junk, J. J., Bayley, P. B., & Sparks, R. E. (1989). *The flood pulse concept in river-floodplain systems. March*, 110–127.
- Kana, T. M., Darkangelo, C., Hunt, M. D., Oldham, J. B., Bennett, G. E., & Cornwell, J. C. (1994). Membrane Inlet Mass Spectrometer for Rapid High-Precision

- Determination of N<sub>2</sub>, O<sub>2</sub>, and Ar in Environmental Water Samples. *Analytical Chemistry*, 66(23), 4166–4170. <https://doi.org/10.1021/ac00095a009>
- Kana, T. M., Sullivan, M. B., Cornwell, J. C., & Groszkowski, K. M. (1998). Denitrification in estuarine sediments determined by membrane inlet mass spectrometry. *Limnology and Oceanography*, 43(2), 334–339. <https://doi.org/10.4319/lo.1998.43.2.0334>
- Kang, H., Lee, J., Zhou, X., Kim, J., & Yang, Y. (2022). The Effects of N Enrichment on Microbial Cycling of Non-CO<sub>2</sub> Greenhouse Gases in Soils—a Review and a Meta-analysis. In *Microbial Ecology* (Vol. 84, Issue 4, pp. 945–957). Springer. <https://doi.org/10.1007/s00248-021-01911-8>
- Keizer, F. M., van der Lee, G. H., Schot, P. P., Kardel, I., Barendregt, A., & Wassen, M. J. (2018). Floodplain plant productivity is better predicted by particulate nutrients than by dissolved nutrients in floodwater. *Ecological Engineering*, 119, 54–63. <https://doi.org/10.1016/j.ecoleng.2018.05.024>
- Kemp, M. J., & Dodds, W. K. (2002). The influence of ammonium, nitrate, and dissolved oxygen concentrations on uptake, nitrification, and denitrification rates associated with prairie stream substrata. *Limnology and Oceanography*, 47(5), 1380–1393. <https://doi.org/10.4319/lo.2002.47.5.1380>
- Kiedrzyńska, E., Kiedrzyński, M., & Zalewski, M. (2008). Flood sediment deposition and phosphorus retention in a lowland river floodplain: Impact on water quality of a reservoir, Sulejów, Poland. *Ecohydrology and Hydrobiology*, 8(2–4), 281–289. <https://doi.org/10.2478/v10104-009-0022-z>
- Kim, S. Y., Veraart, A. J., Meima-Franke, M., & Bodelier, P. L. E. (2015). Combined effects of carbon, nitrogen and phosphorus on CH<sub>4</sub> production and denitrification in wetland sediments. *Geoderma*, 259–260, 354–361. <https://doi.org/10.1016/j.geoderma.2015.03.015>
- King, S. L., Twedt, D. J., & Wilson, R. R. (2006). The Role of the Wetland Reserve Program in Conservation Efforts in the Mississippi River Alluvial Valley. *Wildlife Society Bulletin*, 34(4), 914–920.
- Kinsman-Costello, L. E., O'Brien, J., & Hamilton, S. K. (2014). Re-flooding a Historically Drained Wetland Leads to Rapid Sediment Phosphorus Release. *Ecosystems*, 17(4), 641–656. <http://www.jstor.org/stable/43677621>
- Knowles, R. (1982). Denitrification. *Microbiological Reviews*, 46(1), 43–70. <https://doi.org/10.1016/B978-008045405-4.00264-0>
- Kreiling, R. M., Thoms, M. C., Bartsch, L. A., Larson, J. H., & Christensen, V. G. (2020). Land Use Effects on Sediment Nutrient Processes in a Heavily Modified Watershed Using Structural Equation Models. *Water Resources Research*, 56(7). <https://doi.org/10.1029/2019WR026655>

- Krivoruchko, K., & Gribov, A. (2019). Evaluation of empirical Bayesian kriging. *Spatial Statistics*, 32. <https://doi.org/10.1016/j.spasta.2019.100368>
- Kroeze, C., Bouwman, L., & Seitzinger, S. (2012). Modeling global nutrient export from watersheds. *Current Opinion in Environmental Sustainability*, 4(2), 195–202. <https://doi.org/10.1016/j.cosust.2012.01.009>
- Kröger, R., Lizotte, R. E., Douglas Shields, F., & Usborne, E. (2012). Inundation influences on bioavailability of phosphorus in managed wetland sediments in agricultural landscapes. *Journal of Environmental Quality*, 41(2), 604–614. <https://doi.org/10.2134/jeq2011.0251>
- Kröger, R., Scott, J. T., & Czarnecki, J. M. P. (2014). Denitrification potential of low-grade weirs and agricultural drainage ditch sediments in the Lower Mississippi Alluvial Valley. *Ecological Engineering*, 73, 168–175. <https://doi.org/10.1016/j.ecoleng.2014.09.019>
- Kuypers, M. M. M., Marchant, H. K., & Kartal, B. (2018). The microbial nitrogen-cycling network. *Nature Reviews Microbiology*, 16(5), 263–276. <https://doi.org/10.1038/nrmicro.2018.9>
- Kuzyakov, Y., & Blagodatskaya, E. (2015). Microbial hotspots and hot moments in soil: Concept & review. *Soil Biology and Biochemistry*, 83, 184–199. <https://doi.org/10.1016/j.soilbio.2015.01.025>
- Land, M., Granéli, W., Grimvall, A., Hoffmann, C. C., Mitsch, W. J., Tonderski, K. S., & Verhoeven, J. T. A. (2016). How effective are created or restored freshwater wetlands for nitrogen and phosphorus removal? A systematic review. *Environmental Evidence*, 5(1). <https://doi.org/10.1186/s13750-016-0060-0>
- Li. (2021). An enhanced dual IDW method for high-quality geospatial interpolation. *Scientific Reports*, 11(1). <https://doi.org/10.1038/s41598-021-89172-w>
- Li, G.-Y., & Koenig, J. L. (2005). A review of rubber oxidation. *Rubber Chemistry and Technology*, 78, 355–390.
- Li, & Heap, A. D. (2014). Spatial interpolation methods applied in the environmental sciences: A review. In *Environmental Modelling and Software* (Vol. 53, pp. 173–189). <https://doi.org/10.1016/j.envsoft.2013.12.008>
- Li, Zhang, X., Zhu, R., Zhang, Z., & Weng, Z. (2020). Integrating data-to-data correlation into inverse distance weighting. *Computational Geosciences*, 24(1), 203–216. <https://doi.org/10.1007/s10596-019-09913-9>
- Lowrance, R., Todd, R., Fail, J., Hendrickson, O., Leonard, R., & Asmussen, L. (1984). Riparian Forests as Nutrient Filters in Agricultural Watersheds. *BioScience*, 34(6), 374–377.

- Lu, G. Y., & Wong, D. W. (2008). An adaptive inverse-distance weighting spatial interpolation technique. *Computers and Geosciences*, 34(9), 1044–1055. <https://doi.org/10.1016/j.cageo.2007.07.010>
- Lu, S. Y., Wu, F. C., Lu, Y. F., Xiang, C. S., Zhang, P. Y., & Jin, C. X. (2009). Phosphorus removal from agricultural runoff by constructed wetland. *Ecological Engineering*, 35(3), 402–409. <https://doi.org/10.1016/j.ecoleng.2008.10.002>
- Masta, M., Espenberg, M., Gadegaonkar, S. S., Pärn, J., Sepp, H., Kirsimäe, K., Sgouridis, F., Müller, C., & Mander, Ü. (2022). Integrated isotope and microbiome analysis indicates dominance of denitrification in N<sub>2</sub>O production after rewetting of drained fen peat. *Biogeochemistry*, 161(2), 119–136. <https://doi.org/10.1007/s10533-022-00971-3>
- McCarthy, M. J., Lavrentyev, P. J., Yang, L., Zhang, L., Chen, Y., Qin, B., & Gardner, W. S. (2007). Nitrogen dynamics and microbial food web structure during a summer cyanobacterial bloom in a subtropical, shallow, well-mixed, eutrophic lake (Lake Taihu, China). *Hydrobiologia*, 581(1), 195–207. <https://doi.org/10.1007/s10750-006-0496-2>
- McClain, M. E., Boyer, E. W., Dent, C. L., Gergel, S. E., Grimm, N. B., Groffman, P. M., Hart, S. C., Harvey, J. W., Johnston, C. A., Mayorga, E., McDowell, W. H., & Pinay, G. (2003). Biogeochemical Hot Spots and Hot Moments at the Interface of Terrestrial and Aquatic Ecosystems. *Ecosystems*, 6(4), 301–312. <https://doi.org/10.1007/s10021-003-0161-9>
- McMillan, S. K., & Noe, G. B. (2017). Increasing floodplain connectivity through urban stream restoration increases nutrient and sediment retention. *Ecological Engineering*, 108, 284–295. <https://doi.org/10.1016/J.ECOLENG.2017.08.006>
- Michael, M. (2021). Spatial Variation of Nutrient Uptake in a Restored West Tennessee Agricultural Wetland. MS Thesis. Tennessee Technological University.
- Miller-Way, T., & Twilley, R. R. (1996). Theory and operation of continuous flow systems for the study of benthic-pelagic coupling. *Marine Ecology Progress Series*, 140, 257–269.
- Mitsch, J. M., Day, J. W., Gilliam, J. W., Groffman, P. M., Hey, D. L., Randall, G. W., & Wang, N. (2001). Reducing Nitrogen Loading to the Gulf of Mexico from the Mississippi River Basin: Strategies to Counter a Persistent Ecological Problem. *BioScience*, 51(5), 373–388.
- Mitsch, W. J., Cronk, J. K., Wu, X., Nairn, R. W., & Hey, D. L. (1995). Phosphorus Retention in Constructed Freshwater Riparian Marshes. *Ecological Applications*, 5(3), 830–845.

- Mitsch, W. J., & Day, J. W. (2006). Restoration of wetlands in the Mississippi-Ohio-Missouri (MOM) River Basin: Experience and needed research. *Ecological Engineering*, 26(1), 55–69. <https://doi.org/10.1016/j.ecoleng.2005.09.005>
- Mitsch, W. J., & Gosselink, J. G. (2000). The value of wetlands: importance of scale and landscape setting. *Ecological Economics*, 35, 25–33. [www.elsevier.com/locate/ecolecon](http://www.elsevier.com/locate/ecolecon)
- Mitsch, W. J., Zhang, L., Anderson, C. J., Altor, A. E., & Hernández, M. E. (2005). Creating riverine wetlands: Ecological succession, nutrient retention, and pulsing effects. *Ecological Engineering*, 25(5), 510–527. <https://doi.org/10.1016/j.ecoleng.2005.04.014>
- Mostovoy, G. V., & Anantharaj, V. G. (2008). Observed and simulated soil moisture variability over the lower Mississippi Delta Region. *Journal of Hydrometeorology*, 9(6), 1125–1150. <https://doi.org/10.1175/2008JHM999.1>
- Myers, D. E. (1994). Spatial interpolation: an overview. In *Geoderma* (Vol. 62).
- Nifong, R. L., & Taylor, J. M. (2021). Vegetation and residence time interact to influence metabolism and net nutrient uptake in experimental agricultural drainage systems. *Water (Switzerland)*, 13(10). <https://doi.org/10.3390/w13101416>
- Nifong, R. L., & Taylor, J. M. (2022). Spatial and temporal patterns of benthic nutrient cycling define the extensive role of internal loading in an agriculturally influenced oxbow lake. *Biogeochemistry*, 0123456789. <https://doi.org/10.1007/s10533-022-00935-7>
- Nifong, R. L., Taylor, J. M., & Moore, M. T. (2019). Mulch-derived organic carbon stimulates high denitrification fluxes from agricultural ditch sediments. *Journal of Environmental Quality*, 48(2), 476–484. <https://doi.org/10.2134/jeq2018.09.0341>
- Niswander, S. F., & Mitsch, W. J. (1995). FUNCTIONAL ANALYSIS OF A TWO-YEAR-OLD CREATED IN-STREAM WETLAND: HYDROLOGY, PHOSPHORUS RETENTION, AND VEGETATION SURVIVAL AND GROWTH. *WETLANDS*, 15(3), 212–225.
- Noe, G. B. (2011). Measurement of Net Nitrogen and Phosphorus Mineralization in Wetland Soils Using a Modification of the Resin-Core Technique. *Soil Science Society of America Journal*, 75(2), 760–770. <https://doi.org/10.2136/sssaj2010.0289>
- Noe, G. B., & Hupp, C. R. (2005). Carbon, Nitrogen, and Phosphorus Accumulation in Floodplains of Atlantic Coastal Plain Rivers, USA. *Ecological Applications*, 15(4), 1178–1190. <http://www.jstor.org/stable/4543428>
- Noe, G. B., & Hupp, C. R. (2007). Seasonal variation in nutrient retention during inundation of a short-hydroperiod floodplain. *River Research and Applications*, 23(10), 1088–1101. <https://doi.org/10.1002/rra.1035>

- Noe, G. B., & Hupp, C. R. (2009). Retention of Riverine Sediment and Nutrient Loads by Coastal Plain Floodplains. *Ecosystems*, *12*(5), 728–746.  
<https://doi.org/10.1007/s10021-009-9253-5>
- Noe, G. B., Hupp, C. R., & Rybicki, N. B. (2013). Hydrogeomorphology Influences Soil Nitrogen and Phosphorus Mineralization in Floodplain Wetlands. *Ecosystems*, *16*(1), 75–94. <https://doi.org/10.1007/s10021-012-9597-0>
- Nunnally, N. R. (1978). Stream Renovation" An Alternative to Channelization. *Environmental Management*, *2*(5), 403–411.
- Ohio Departments of Natural Resources, Agriculture, and Environmental Protection (2023). H2Ohio: Ohio's Plan for Clean Water. <https://h2.ohio.gov/>
- Olde Venterink, H., Davidsson, T. E., Kiehl, K., & Leonardson, L. (2002). Impact of drying and re-wetting on N, P and K dynamics in a wetland soil. *Plant and Soil*, *243*(1), 119–130. <https://about.jstor.org/terms>
- Olde Venterink, H., Hummelink, E., Van, M. W., & Hoorn, D. (2003). Denitrification Potential of a River Floodplain during Flooding with Nitrate-Rich Water: Grasslands versus Reedbeds. *Biogeochemistry*, *65*(2), 233–244.  
<https://www.jstor.org/stable/1469854?seq=1&cid=pdf->
- Olde Venterink, H., Vermaat, J. E., Pronk, M., Wiegman, F., Lee, G. E. M. van der, Hoorn, M. W. van den, Higler, L. W. G. (Bert), & Verhoeven, J. T. A. (2006). Importance of Sediment Deposition and Denitrification for Nutrient Retention in Floodplain Wetlands. *Applied Vegetation Science*, *9*(2), 163–174.  
<http://www.jstor.org/stable/4620475>
- Olde Venterink, H., Wiegman, F., van der Lee, G. E. M., & Vermaat, J. E. (2003). Role of active floodplains for nutrient retention in the River Rhine. *Journal of Environmental Quality*, *32*, 1430–1435.
- Oliver, M. A., & Webster, R. (2014). A tutorial guide to geostatistics: Computing and modelling variograms and kriging. In *Catena* (Vol. 113, pp. 56–69).  
<https://doi.org/10.1016/j.catena.2013.09.006>
- Orr, C. H., Predick, K. I., Stanley, E. H., & Rogers, K. L. (2014). Spatial autocorrelation of denitrification in a restored and a natural floodplain. *Wetlands*, *34*(1), 89–100.  
<https://doi.org/10.1007/s13157-013-0488-8>
- Parton, W. J., Mosier, A. R., Ojima, D. S., Valentine, D. W., Schime, D. S., Weier, K., & Kulmala, A. E. (1996). Generalized model for N<sub>2</sub> and N<sub>2</sub>O production from nitrification and denitrification. *Global Biogeochemical Cycles*, *10*(3), 401–412.  
<https://doi.org/10.1029/96GB01455>
- Peng, C., Zhang, Y., Huang, S., Li, X., Wang, Z., & Li, D. (2019). Sediment phosphorus release in response to flood event across different land covers in a restored wetland.

- Environmental Science and Pollution Research*, 26(9), 9113–9122.  
<https://doi.org/10.1007/s11356-019-04398-6>
- Peñuelas, J., & Sardans, J. (2022). The global nitrogen-phosphorus imbalance. *Science*, 375(6578), 266–267. <https://doi.org/10.1126/science.abl4827>
- Petersen, R. J., Liang, Z., Prinds, C., Jéglot, A., Thamdrup, B., Kjaergaard, C., & Elsgaard, L. (2020). Nitrate reduction pathways and interactions with iron in the drainage water infiltration zone of a riparian wetland soil. *Biogeochemistry*, 2, 235–255. <https://doi.org/10.1007/s10533-020-00695-2>
- Pickett, S. T. A. (1989). Space for time substitution in ecology. In *Long-Term Studies in Ecology* (pp. 110–135).
- Poe, A. C., Piehler, M. F., Thompson, S. P., & Paerl, H. W. (2003). Denitrification in a constructed wetland receiving agricultural runoff. *Wetlands*, 23(4), 817–826. [https://doi.org/10.1672/0277-5212\(2003\)023\[0817:DIACWR\]2.0.CO;2](https://doi.org/10.1672/0277-5212(2003)023[0817:DIACWR]2.0.CO;2)
- Pollard, P. C. (2022). Globally, Freshwater Ecosystems Emit More CO<sub>2</sub> Than the Burning of Fossil Fuels. *Frontiers in Environmental Science*, 10(June), 1–12. <https://doi.org/10.3389/fenvs.2022.904955>
- Quick, A. M., Reeder, W. J., Farrell, T. B., Tonina, D., Feris, K. P., & Benner, S. G. (2019). Nitrous oxide from streams and rivers: A review of primary biogeochemical pathways and environmental variables. *Earth-Science Reviews*, 191(February), 224–262. <https://doi.org/10.1016/j.earscirev.2019.02.021>
- Raghoebarsing, A. A., Pol, A., Van De Pas-Schoonen, K. T., Smolders, A. J. P., Ettwig, K. F., Rijpstra, W. I. C., Schouten, S., Sinninghe Damsté, J. S., Op Den Camp, H. J. M., Jetten, M. S. M., & Strous, M. (2006). A microbial consortium couples anaerobic methane oxidation to denitrification. *Nature*, 440(7086), 918–921. <https://doi.org/10.1038/nature04617>
- Ready, K. R., Kadlec, R. H., Flaig, E., & Gale, P. M. (1999). Phosphorus retention in streams and wetlands: A review. In *Critical Reviews in Environmental Science and Technology* (Vol. 29, Issue 1, pp. 83–146). <https://doi.org/10.1080/10643389991259182>
- Redfield, A. C. (1958). *The biological control of chemical factors in the the environment* (Vol. 46, Issue 3). <https://about.jstor.org/terms>
- Reisinger, A. J., Tank, J. L., Hoellein, T. J., & Hall, R. O. (2016). Sediment, water column, and open-channel denitrification in rivers measured using membrane-inlet mass spectrometry. *Journal of Geophysical Research: Biogeosciences*, 121(5), 1258–1274. <https://doi.org/10.1002/2015JG003261>
- Richardson, C. J., & Reddy, K. R. (2013). Methods for Soil Phosphorus Characterization and Analysis of Wetland Soils. In R. D. DeLaune, K. R. Reddy, C. J. Richardson, &

- J. P. Megonigal (Eds.), *Methods in Biogeochemistry of Wetlands* (pp. 603–638).  
<https://doi.org/10.2136/sssabookser10.c32>
- Richardson, W. B., Bartsch, L. A., Bartsch, M. R., Kiesling, R., & Lafrancois, B. M. (2019). Nitrogen cycling in large temperate floodplain rivers of contrasting nutrient regimes and management. *River Research and Applications*, *35*(5), 529–539. <https://doi.org/10.1002/rra.3267>
- Ritz, S., Dähnke, K., & Fischer, H. (2018). Open-channel measurement of denitrification in a large lowland river. *Aquatic Sciences*, *80*(1), 0. <https://doi.org/10.1007/s00027-017-0560-1>
- Robertson, E. K., Bartoli, M., Brüchert, V., Dalsgaard, T., Hall, P. O. J., Hellemann, D., Hietanen, S., Zilius, M., & Conley, D. J. (2019). Application of the isotope pairing technique in sediments: Use, challenges, and new directions. *Limnology and Oceanography: Methods*, *17*(2), 112–136. <https://doi.org/10.1002/lom3.10303>
- Robertson, G. P. (1987). Geostatistics in Ecology: Interpolating With Known Variance. *Ecology*, *68*(3), 744–748.
- Royer, T. v., David, M. B., & Gentry, L. E. (2006). Timing of riverine export of nitrate and phosphorus from agricultural watersheds in Illinois: Implications for reducing nutrient loading to the Mississippi River. *Environmental Science and Technology*, *40*(13), 4126–4131. <https://doi.org/10.1021/es052573n>
- Ruser, R., Flessa, H., Russow, R., Schmidt, G., Buegger, F., & Munch, J. C. (2006). Emission of N<sub>2</sub>O, N<sub>2</sub> and CO<sub>2</sub> from soil fertilized with nitrate: Effect of compaction, soil moisture and rewetting. *Soil Biology and Biochemistry*, *38*(2), 263–274. <https://doi.org/10.1016/j.soilbio.2005.05.005>
- Rutherford, J. C., & Nguyen, M. L. (2004). Nitrate Removal in Riparian Wetlands: Interactions between Surface Flow and Soils. *Journal of Environmental Quality*, *33*(3), 1133–1143.
- Rysgaard, S., Risgaard-Petersen, N., Nielsen, L. P., & Revsbech, N. P. (1993). Nitrification and denitrification in lake and estuarine sediments measured by the <sup>15</sup>N dilution technique and isotope pairing. *Applied and Environmental Microbiology*, *59*(7), 2093–2098.
- Schindler, D. E., & Smits, A. P. (2017). Subsidies of Aquatic Resources in Terrestrial Ecosystems. *Ecosystems*, *20*(1), 78–93. <https://doi.org/10.1007/s10021-016-0050-7>
- Schlesinger, W. H., Cole, J. J., Finzi, A. C., & Holland, E. A. (2011). Introduction to coupled biogeochemical cycles. *Frontiers in Ecology and the Environment*, *9*(1), 5–8. <https://doi.org/10.1890/090235>

- Schramm, H. L., Cox, M. S., Tietjen, T. E., & Ezell, A. W. (2009). Nutrient dynamics in the lower Mississippi River floodplain: comparing present and historic hydrologic conditions. *Wetlands*, 29(2), 476–487.
- Scott, J. T., McCarthy, M. J., Gardner, W. S., & Doyle, R. D. (2008). Denitrification, dissimilatory nitrate reduction to ammonium, and nitrogen fixation along a nitrate concentration gradient in a created freshwater wetland. *Biogeochemistry*, 87(1), 99–111. <https://doi.org/10.1007/s10533-007-9171-6>
- Seitzinger, S. P. (1988). Denitrification in freshwater and coastal marine ecosystems: Ecological and geochemical significance. *Limnology and Oceanography*, 33(4part2), 702–724. <https://doi.org/10.4319/lo.1988.33.4part2.0702>
- Seitzinger, S. P., Harrison, J. A., Böhlke, J. K., Bouwman, A. F., Lowrance, R., Tobias, C., & Drecht, G. van. (2006). Denitrification across Landscapes and Waterscapes : A Synthesis. *Ecological Applications*, 16(6), 2064–2090.
- Sekulić, A., Kilibarda, M., Heuvelink, G. B. M., Nikolić, M., & Bajat, B. (2020). Random forest spatial interpolation. *Remote Sensing*, 12(10). <https://doi.org/10.3390/rs12101687>
- Shrestha, J., Niklaus, P. A., Pasquale, N., Huber, B., Barnard, R. L., Frossard, E., Schleppe, P., Tockner, K., & Luster, J. (2014). Flood pulses control soil nitrogen cycling in a dynamic river floodplain. *Geoderma*, 228–229, 14–24. <https://doi.org/10.1016/j.geoderma.2013.09.018>
- Sitters, J., Atkinson, C. L., Guelzow, N., Kelly, P., & Sullivan, L. L. (2015). Spatial stoichiometry: Cross-ecosystem material flows and their impact on recipient ecosystems and organisms. *Oikos*, 124(7), 920–930. <https://doi.org/10.1111/oik.02392>
- Skinner, M. (2022). Wetland phosphorus dynamics and phosphorus removal potential. *Water Environment Research*, 94(10). <https://doi.org/10.1002/wer.10799>
- Smith, L. K., Sartoris, J. J., Thullen, J. S., & Andersen, D. C. (2000). Investigation of denitrification rates in and ammonia-dominated constructed wastewater-treatment wetland. *WETLANDS*, 20(4), 684–696.
- Smith, L. K., Voytek, M. A., Böhlke, J. K., & Harvey, J. W. (2006). Denitrification in nitrate-rich streams: Application of N<sub>2</sub>:Ar and <sup>15</sup>N-tracer methods in intact cores. *Ecological Applications*, 16(6), 2191–2207. [https://doi.org/10.1890/1051-0761\(2006\)016\[2191:DINSAO\]2.0.CO;2](https://doi.org/10.1890/1051-0761(2006)016[2191:DINSAO]2.0.CO;2)
- Smyth, A. R., Thompson, S. P., Siporin, K. N., Gardner, W. S., McCarthy, M. J., & Piehler, M. F. (2013). Assessing Nitrogen Dynamics Throughout the Estuarine Landscape. *Estuaries and Coasts*, 36(1), 44–55. <https://doi.org/10.1007/s12237-012-9554-3>

- Speir, S. L., Tank, J. L., Bieroza, M., Mahl, U. H., & Royer, T. v. (2021). Storm size and hydrologic modification influence nitrate mobilization and transport in agricultural watersheds. *Biogeochemistry*, *156*(3), 319–334. <https://doi.org/10.1007/s10533-021-00847-y>
- Speir, S. L., Taylor, J. M., & Scott, T. J. (2017). Seasonal differences in relationships between nitrate concentration and denitrification rates in ditch sediments vegetated with rice cutgrass. *Journal of Environmental Quality*, *46*(6), 1500–1509. <https://doi.org/10.2134/jeq2016.11.0450>
- Spott, O., & Stange, C. F. (2007). A new mathematical approach for calculating the contribution of anammox, denitrification and atmosphere to an N<sub>2</sub> mixture based on a <sup>15</sup>N tracer technique. *Rapid Communications in Mass Spectrometry*, *21*(14), 2398–2406. <https://doi.org/10.1002/rcm.3098>
- Sturner, Robert and Elser, J. (2002). *Ecological Stoichiometry*. Princeton University Press.
- Stoler, A. B., & Relyea, R. A. (2020). Reviewing the role of plant litter inputs to forested wetland ecosystems. *90*(2), 1–23. <https://doi.org/10.2307/27081018>
- Stroud Water Research Center (2021). Model My Watershed [Software]. Available from <https://modelmywatershed.org/>
- Tao, W. (2018). Microbial removal and plant uptake of nitrogen in constructed wetlands: mesocosm tests on influencing factors. *Environmental Science and Pollution Research*, *25*(36), 36425–36437. <https://doi.org/10.1007/s11356-018-3543-4>
- Tong, S. T. Y., & Chen, W. (2002). Modeling the relationship between land use and surface water quality. *Journal of Environmental Management*, *66*(4), 377–393. <https://doi.org/10.1006/jema.2002.0593>
- Urakawa, H., & Bernhard, A. E. (2017). Wetland management using microbial indicators. *Ecological Engineering*, *108*, 456–476.
- Vidon, P., Allan, C., Burns, D., Duval, T. P., Gurwick, N., Inamdar, S., Lowrance, R., Okay, J., Scott, D., & Sebestyen, S. (2010). Hot spots and hot moments in riparian zones: Potential for improved water quality management. *Journal of the American Water Resources Association*, *46*(2), 278–298. <https://doi.org/10.1111/j.1752-1688.2010.00420.x>
- Vitousek, P. M., Aber, J. D., Howarth, R. W., Likens, G. E., Matson, P. A., Schindler, D. W., Schlesinger, W. H., & Tilman, D. G. (1997). Technical Report: Human Alteration of the Global Nitrogen Cycle: Sources and Consequences. *Ecological Applications*, *7*(3), 737. <https://doi.org/10.2307/2269431>
- Wang, R., Zou, R., Liu, J., Liu, L., & Hu, Y. (2021). Spatial distribution of soil nutrients in farmland in a hilly region of the pearl river delta in China based on geostatistics

- and the inverse distance weighting method. *Agriculture (Switzerland)*, *11*(1), 1–12. <https://doi.org/10.3390/agriculture11010050>
- Wang, X., Xu, L., Wan, R., & Chen, Y. (2016). Seasonal variations of soil microbial biomass within two typical wetland areas along the vegetation gradient of Poyang Lake, China. *Catena*, *137*, 483–493. <https://doi.org/10.1016/j.catena.2015.10.020>
- Wang, Z., Guo, Q., & Tian, L. (2022). Tracing phosphorus cycle in global watershed using phosphate oxygen isotopes. *Science of The Total Environment*, *829*, 154611. <https://doi.org/10.1016/j.scitotenv.2022.154611>
- Weiss, R. F. (1970). The solubility of nitrogen, oxygen and argon in water and seawater. *Deep-Sea Research and Oceanographic Abstracts*, *17*(4), 721–735. [https://doi.org/10.1016/0011-7471\(70\)90037-9](https://doi.org/10.1016/0011-7471(70)90037-9)
- Welti, N., Bondar-Kunze, E., Mair, M., Bonin, P., Wanek, W., Pinay, G., & Hein, T. (2012). Mimicking floodplain reconnection and disconnection using <sup>15</sup>N mesocosm incubations. *Biogeosciences*, *9*(11), 4263–4278. <https://doi.org/10.5194/bg-9-4263-2012>
- Welti, N., Bondar-Kunze, E., Singer, G., Tritthart, M., Zechmeister-Boltenstern, S., Hein, T., & Pinay, G. (2012). Large-scale controls on potential respiration and denitrification in riverine floodplains. *Ecological Engineering*, *42*, 73–84. <https://doi.org/10.1016/j.ecoleng.2012.02.005>
- White, M. J., Santhi, C., Kannan, N., Arnold, J. G., Harmel, D., Norfleet, L., Allen, P., DiLuzio, M., Wang, X., Atwood, J., Haney, E., & Johnson, M. V. (2014). Nutrient delivery from the Mississippi River to the Gulf of Mexico and effects of cropland conservation. *Journal of Soil and Water Conservation*, *69*(1), 26–40. <https://doi.org/10.2489/jswc.69.1.26>
- Wiens, J. A. (1989). Spatial Scaling in Ecology. In *Ecology* (Vol. 3, Issue 4).
- Winikoff, S. G., & Finlay, J. (2023). Water quality outcomes of wetland restoration depend on hydroperiod rather than restoration strategy. *Freshwater Science*. <https://doi.org/10.1086/724014>
- Withers, P. J. A., & Jarvie, H. P. (2008). Delivery and cycling of phosphorus in rivers: A review. *Science of the Total Environment*, *400*(1–3), 379–395. <https://doi.org/10.1016/j.scitotenv.2008.08.002>
- Wohl, E. (2021). An Integrative Conceptualization of Floodplain Storage. *Reviews of Geophysics*, *59*(2). <https://doi.org/10.1029/2020RG000724>
- Wollheim, W. M., Bernal, S., Burns, D. A., Czuba, J. A., Driscoll, C. T., Hansen, A. T., Hensley, R. T., Hosen, J. D., Inamdar, S., Kaushal, S. S., Koenig, L. E., Lu, Y. H., Marzadri, A., Raymond, P. A., Scott, D., Stewart, R. J., Vidon, P. G., & Wohl, E. (2018). River network saturation concept: factors influencing the balance of

- biogeochemical supply and demand of river networks. *Biogeochemistry*, 141(3), 503–521. <https://doi.org/10.1007/s10533-018-0488-0>
- Wollheim, W. M., Harms, T. K., Peterson, B. J., Morkeski, K., Hopkinson, C. S., Stewart, R. J., Gooseff, M. N., & Briggs, M. A. (2014). Nitrate uptake dynamics of surface transient storage in stream channels and fluvial wetlands. *Biogeochemistry*, 120, 239–257. <https://doi.org/10.1007/s10533-014-9993-y>
- Woltemade, C. J. (2000). Ability of restored wetlands to reduced nitrogen and phosphorus concentrations in agricultural drainage water. *Journal of Soil and Water Conservation*, 55(3), 303–308.
- Xia, X., Liu, T., Yang, Z., Michalski, G., Liu, S., Jia, Z., & Zhang, S. (2017). Enhanced nitrogen loss from rivers through coupled nitrification-denitrification caused by suspended sediment. *Science of the Total Environment*, 579, 47–59. <https://doi.org/10.1016/j.scitotenv.2016.10.181>
- Zbiral, J., & Némec, P. (2002). Comparison of Mehlich 2, Mehlich 3, CAL, Egner, Olsen, and 0.01 M CaCl<sub>2</sub> extractants for determination of phosphorus in soils. *Communications in Soil Science and Plant Analysis*, 33(15–18), 3405–3417. <https://doi.org/10.1081/CSS-120014534>
- Zedler, J. B. (2003). Wetlands at Your Service: Reducing Impacts of Agriculture at the Watershed Scale. *Frontiers in Ecology and the Environment*, 1(2), 65. <https://doi.org/10.2307/3868032>
- Zhao, C., Liu, S., Jiang, Z., Wu, Y., Cui, L., Huang, X., & Macreadie, P. I. (2019). Nitrogen purification potential limited by nitrite reduction process in coastal eutrophic wetlands. *Science of the Total Environment*, 694. <https://doi.org/10.1016/j.scitotenv.2019.133702>
- Zhao, F., Xu, H., Kana, T., Zhu, G., Zhan, X., Zou, W., Zhu, M., Kang, L., & Zhao, X. (2021). Improved membrane inlet mass spectrometer method for measuring dissolved methane concentration and methane production rate in a large shallow lake. *Water (Switzerland)*, 13(19), 1–14. <https://doi.org/10.3390/w13192699>
- Zhu, G., Jetten, M. S. M., Kusch, P., Ettwig, K. F., & Yin, C. (2010). Potential roles of anaerobic ammonium and methane oxidation in the nitrogen cycle of wetland ecosystems. *Applied Microbiology and Biotechnology*, 86(4), 1043–1055. <https://doi.org/10.1007/s00253-010-2451-4>
- Zhu, X., Burger, M., Doane, T. A., & Horwath, W. R. (2013). Ammonia oxidation pathways and nitrifier denitrification are significant sources of N<sub>2</sub>O and NO under low oxygen availability. *Proceedings of the National Academy of Sciences of the United States of America*, 110(16), 6328–6333. <https://doi.org/10.1073/pnas.1219993110>

Zimmerman, D., Pavlik, C., Ruggles, A., & Armstrong, M. P. (1999). An experimental comparison of ordinary and universal kriging and inverse distance weighting. *Mathematical Geology*, 31(4), 375–390. <https://doi.org/10.1023/A:1007586507433>